Stripes and Cuprate High-T_C Superconductors

Marco Bosch

Stripes and Cuprate High-T_c Superconductors

PROEFSCHRIFT

TER VERKRIJGING VAN
DE GRAAD VAN DOCTOR AAN DE UNIVERSITEIT LEIDEN,
OP GEZAG VAN DE RECTOR MAGNIFICUS DR. D.D. BREIMER,
HOOGLERAAR IN DE FACULTEIT DER WISKUNDE EN
NATUURWETENSCHAPPEN EN DIE DER GENEESKUNDE,
VOLGENS BESLUIT VAN HET COLLEGE VOOR PROMOTIES
TE VERDEDIGEN OP WOENSDAG 10 DECEMBER 2003
KLOKKE 14.15 UUR

DOOR

MARCO BOSCH

geboren te Eindhoven in 1972

Promotiecommissie:

Promotor:	Prof. dr. ir. W. van Saarloos
Referent:	Prof. dr. J. Zaanen
Overige Leden:	Dr. J. van den Brink
	Dr. H.B. Brom
	Dr. P.J.H. Denteneer
	Prof. dr. P.H. Kes
	Prof. dr. J.M.J. van Leeuwen
	Prof. dr. C.J.M. Schoutens (UvA)

Het onderzoek beschreven in dit proefschrift is uitgevoerd als onderdeel van het wetenschappelijke programma van de Nederlandse Organisatie voor Wetenschappelijk Onderzoek (NWO) en de Stichting voor Fundamenteel Onderzoek der Materie (FOM).

The research described in this thesis has been carried out as part of the scientific program of the Netherlands Organization for Scientific Research (NWO) and the Foundation for Fundamental Research on Matter (FOM).

About the cover

This thesis reflects that solving the problem of high-T_c superconductivity is analogous to trying to predict the outcome of a chess game. The antiferromagnetic background forms a chessboard like pattern in which the pieces (the holes and hole-pairs) have to move.

"*There will be a glorious theory of physics at the end of the journey*"

Jan Zaanen, Nature, 4 January 2001, p. 8

Contents

Chapter 1

Introduction

Superconductors are materials that become perfect conductors of electricity when cooled to very low temperatures [87, 139, 142]. Almost all substances have some resistance to electrical currents. Even copper, which is used for most electrical wiring, has a resistance. So much so that a significant fraction of all the electrical power generated is lost as heat in copper wires. Only a superconducting wire can prevent such losses, because a current that is started in a superconductor can flow forever. In 1911 superconductivity was observed for the first time by the Dutch physicist Heike Kamerlingh Onnes of Leiden University. He measured the resistance of liquid mercury as he lowered the temperature and found that at a critical temperature of 2.4 Kelvin, the resistance suddenly became exactly zero. There was no theoretical explanation for this effect until 1957. Between 1911 and 1986, superconductivity was strictly a low-temperature phenomenon. Nb_3Ge with a critical temperature T_c of approximately 23K held the record for the highest value of T_c. The only useful refrigerants were liquid helium and liquid hydrogen.

Theoretical advances

In 1933, Meissner and Ochsenfeld discovered that a magnetic field is expelled by going into the superconducting phase. This perfect diamagnetism is called the Meissner effect and is together with the zero resistance the defining property of a superconductor. Superconductivity was theoretically explained by Bardeen, Cooper and Schrieffer in 1957 [19], when they showed that crystal vibrations called phonons cause an attractive interaction between two conduction electrons with opposite spin and momentum close to the Fermi surface. Below the critical temperature, these electrons form a bound state, and the resulting pairs immediately establish long range phase coherence. Another significant theoretical advancement came in 1962 when Josephson [11, 97] predicted that electrical current would flow between two superconducting materials, even when they

are separated by a non-superconductor or insulator. This tunneling phenomenon is today known as the "*Josephson effect*". It explains why cracks, holes and dirt in samples do not destroy the superconductivity.

Applications

The phenomenon of superconductivity was confined to scientific laboratories until the late 1950s, when the first technological applications became feasible. Unlike the transistor and the laser, which were invented before most applications had been conceived, high-temperature superconductors have been a dream of physicists for years. Powerful and efficient lightweight magnets and motors, compact computers using Josephson junctions, magnetically levitated trains able to travel hundreds of miles per hour, money-saving power transmission cables linked to safe remote nuclear and solar generators, long-term energy storage systems, and a multitude of other devices are all possible in theory. All that was missing was a compound that would transform these dreams into reality. But for everyday applications, it has been simply too difficult and too expensive to refrigerate any of the known superconducting devices to the required low temperatures. One successful application of superconductivity is the SQUID, the superconducting quantum interference device, which has become an unrivaled instrument for the detection of extremely small variations in magnetic fields, electric voltages and resistance. Another successful area, where the cost of cooling is offset by the benefits, are the powerful superconducting magnets used in Magnetic Resonance Imaging devices.

Discovery of the cuprates

One important step towards turning some of these conceived applications into reality was reached when the high-T_c superconductors were discovered in 1986 by Georg Bednorz and Alex Müller [24]. They discovered that La-Ba-Cu-O, a mix of lanthanum, barium, copper and oxygen, becomes superconducting at a temperature of 35 K. Aside from the high critical temperature, this result was also surprising because previous experience had shown that one should avoid magnetic and oxide materials to get good superconductors. Soon hereafter, Wu *et al.* [210] found that suitably doped $YBa_2Cu_3O_7$ has a T_c of 92 K, well above the boiling point of liquid nitrogen. In the years that have passed since 1987, several other classes of high temperature superconductors have been found. The maximum value of T_c has increased steadily to its present value of 133 K for the compound $HgBa_2Ca_2Cu_3O_8$. When it is subjected to a high pressure, the onset T_c increases to 164 K, more than halfway to room temperature. While this material cannot be used for applications because of the high pressures needed and the fact that Hg is poisonous, this result suggests that values of T_c in the neighborhood of 160 K, or even higher, are attainable in cuprates.

But there is one big problem for engineers waiting to use these superconductors in applications. The new class of superconductors differs not only in transition temperature from the old superconductors. The new materials are ceramic materials, not metals, which means that they are very brittle and that the production of cables is very complicated. While it is relatively easy to make small samples, making large continuous wires of high temperature superconducting materials has therefore proved to be quite difficult.

1.1 Stripes

From a theoretical perspective, the fact that the critical temperature for the superconducting state is high, is not the main reason for interest in these new superconductors. What is much more interesting is the fact that the standard BCS theory of superconductivity does not seem to apply (see chapter 6). There is no evidence for a phonon based mechanism. Furthermore, the normal state above T_c is a very peculiar one, with very strong anisotropy, an absence of quasi-particles and strange phenomena such as a pseudogap state, a neutron resonance and a peak-dip-hump structure in photo-emission experiments.

One of the reasons for some of the strange experimental results is that the electrons in the cuprates form a two-dimensional antiferromagnet. This is caused by the strong Coulomb interaction which leads to a Mott-Hubbard electronic insulator. The physics of the superconducting state is related to the doping of this Mott-Hubbard insulator.

Neutron scattering has shown that there are **incommensurate peaks** in the Fourier transform of the spin-spin correlation function, which points to an extra periodicity in the magnetic structure. These results indicate that the holes in the two-dimensional antiferromagnet order into one-dimensional lines of charge. These are called **STRIPES** and are the subject of this thesis.

There have been many attempts to describe both the normal state and the superconducting state properties of the high-T_c superconductors with many ingenious and fundamentally different theories. Some of these theories are the resonating valence bond theory, interlayer tunneling mechanism, marginal Fermi liquids, anyon theory, hot spots, cold spots, $SO(5)$ theory, spin-bag mechanism, nearly antiferromagnetic Fermi liquid, bipolarons, preformed pairs, d-wave BCS, etc. See section 1.10 for a short description of a number of these theories. However, not withstanding the enormous efforts put into them, none of them is generally considered to be *the* explanation of the strange normal state properties and the high-T_c superconducting state. **STRIPES** are a relatively new attempt at describing these properties. In the stripe theory, one focuses on the positions and dynamics of the charges in real space and the consequences this has on the surrounding antiferromagnetic regions.

The existence of stripes has by now been experimentally established by a large number of different experiments, like neutron scattering, nuclear magnetic resonance,

X-ray scattering and features such as the 'holy cross' in photo-emission experiments. An overview of the theoretical reasons for the existence of stripes and the experimental evidence is given in chapter 2.

1.2 Structure of this thesis

The main goal for the stripe theory is an explanation for most of the strange properties of the high-T_c superconductors, both in the normal and in the superconducting state. Therefore, this thesis starts with an introduction to some of these properties.

After this, two lines of approach concerning stripes are presented. The main original ideas of this thesis are described in chapters 5, 8 and 9, and concerns the possible formation of kinks when the doping increases (chapter 5), and the development of a simple physical insight into the formation and properties of stripes in an antiferromagnetic background (chapters 8 and 9). This work was done together with Z. Nussinov. The second contribution of this thesis to the understanding of stripes is an extensive review of the relevant experimental and theoretical findings for stripes (chapter 2) and of superconductivity in correlated models with short-range interactions (chapter 6). The latter chapter is also necessary to prepare for the discussion in chapters 8 and 9. In the remainder of this introductory chapter a more general introduction to the structure and physics of the cuprate superconductors is given.

1.3 Structure of the Cuprates

A large number of different compounds has been found in the last fifteen years that become superconducting at high temperatures. All of these materials have several properties in common, the most important of them being that they all contain copper and oxygen atoms in two-dimensional layers inside the crystal. Because of this, they are collectively called the cuprates. The three most commonly studied materials are $La_{2-x}Sr_xCuO_4$, $YBa_2Cu_3O_{6+x}$ and $Bi_2Sr_2CaCu_2O_8$. On account of the relative simplicity of its structure, the La_2CuO_4 structure is considered to be the archetype of the cuprates. At the same time, the behavior of this compound typifies that of the whole class of cuprates. At high temperature, La_2CuO_4 has a crystal structure that is called the perovskite structure. The structure alternates along the c axis between a square planar CuO_2 layer and two buckled La-O layers. The mobile charge carriers in the doped system reside primarily within the CuO_2 planes, therefore the CuO_2 plane is the layer in which the relevant physics takes place. The intermediate layers function as charge reservoirs and control the doping of the CuO_2 planes with charge carriers.

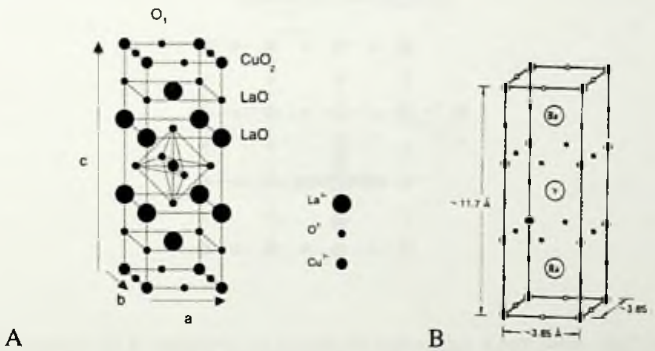

Figure 1.1: Figure A shows the crystal structure unit cell of La_2CuO_4. One can see the octahedral surrounding of Cu by six O atoms. In the LTO and LTT phases these octahedra rotate around the (110) *and* $(1\bar{1}0)$*-axis. figure B shows the crystal structure of* $YBa_2Cu_3O_{6+x}$.

LTO and LTT

As can be seen in figure 1.1A, the Cu atoms lie at the center of a cube, the La atoms occupy the cube corners and oxygen atoms are positioned halfway along all cube edges. A consequence of this atomic structure is that every copper atom is surrounded by six oxygens in an octahedral arrangement. Each of those octahedral units shares all six oxygen atoms at its corners with six others, giving the perovskite structure an infinite framework of corner-sharing octahedra. At high temperature the CuO_6 octahedron is perfect in position and the *a* and *b* axis of the crystal are identical. Therefore at high temperature the crystal structure is tetragonal (the HTT phase). However, the CuO length is slightly too long to fit directly to the LaO charge reservoir layers. To release the strain, the octahedron starts to tilt, leading to a buckling of the LaO planes and as a consequence an orthorhombic distortion exists at a lower temperature, in the LTO phase. Through doping, the CuO bond becomes smaller, thus a smaller tilt is needed and therefore the octahedron distortions become smaller.

The new *a* and *b* axes differ by less than 1%. Lowering the temperature even more leads to a tetragonal deformation, the low-temperature tetragonal or LTT phase. The LTT phase can be thought of as a coherent superposition of the twin-related orthogonal structures, in which the tilt axes of the octahedra are rotated to lie along [100] axes of the HTT phase. The magnitudes of the octahedra tilts are little affected by the transformation, only the tilt direction changes.

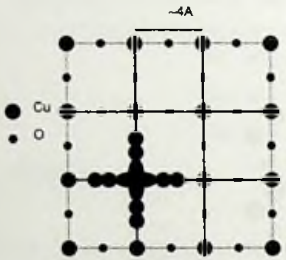

Figure 1.2: The CuO_2 plane that is responsible for most of the properties of the cuprates. Every Cu atom is surrounded by four oxygen atoms. The electronic properties of the cuprates are the result of holes in anti-bonding combinations of oxygen $2p_x$ and $2p_y$ orbitals that overlap with copper $3d_{x^2-y^2}$ orbitals.

Structure of other cuprates

The structure of other high-T_c materials differs only in ways which do not affect the central issues. For example it is oxygen doping in $YBa_2Cu_3O_{6+x}$ that provides planar holes instead of Sr and Ba doping. Normally, it has the stoichiometry $Y_1Ba_2Cu_3O_7$ and the crystal structure shown in figure 1.1B. This structure is also based on the simple cubic perovskite, consisting of three such cells stacked one upon the other. However, the yttrium and barium are on the corner sites and alternate in a Ba-Y-Ba-Ba-Y-Ba sequence. The complete absence of O from the Y layers separates the material into $Y/CuO_2/BaO/CuO/BaO/CuO_2/Y$ slabs. There are strategic oxygen vacancies: no oxygens in the yttrium plane and two oxygens missing from the Cu-O layer between the barium planes. These latter missing oxygens are ordered, leading to chains so that the structure is not tetragonal, but is orthorhombic. It is slightly larger in the direction of the chains (the *b* direction) than in the perpendicular direction. It was found that nearly all of the rare-earth elements, including the magnetic rare earths, could be substituted for Y without having a significant effect on the transition temperature. O_6 is an insulator and $O > 6.64$ is metallic. $YBa_2Cu_3O_{7-\delta}$ and $Bi_2Sr_2Ca_1Cu_2O_x$ have two CuO_2 layers per unit cell and are therefore called bilayer materials.

Electronic structure of CuO_2 planes

The superconductivity is usually assumed to originate in the CuO_2 planes since this is the only structural element common to all high-T_c materials. The layered nature of the structure is also responsible for the highly anisotropic electrical and magnetic properties. As will be discussed in chapter 2, the tilting of the structure can have a profound influence on the charge dynamics of stripes. However, for most properties the tilting of

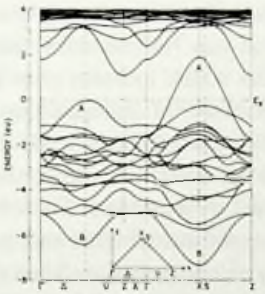

Figure 1.3: Calculated Local Density Approximation energy bands for La_2CuO_4 along high symmetry directions in body-centered tetragonal Brillouin zone according to Mattheiss [123]. The bands around the Fermi energy are related to Cu 3d and O 2p orbitals. Notice that the band labeled "A" crosses the Fermi energy: this incorrectly predicts a metallic state.

the CuO_6 octahedron and the small octahedral distortions are not very important. The perovskite planes have little interaction with each other. Therefore, all the physics of the problem is contained in the two-dimensional CuO_2 plane as illustrated in figure 1.2. These are nothing but simple two-dimensional square lattices with a unit cell consisting of one Cu and two O atoms. The crystal is tetragonal, in the sense that x and y direction in the square lattice are equivalent, while the z-direction is inequivalent.

The fact that only the CuO_2 layers are important for the fundamental properties of the material follows for instance from electronic band structure calculations. To prepare the reader for some of the work in this thesis, it is useful to review this here briefly. Early on, Mattheiss ([123], see also [86]) showed using the local density approximation that the electronic structure of La_2CuO_4 around the Fermi energy is a spaghetti of one-electron bands (see figure 1.3). All the bands close to the Fermi surface are composed primarily of strongly hybridized planar Cu $3d$ and O $2p$ states. The electronic band structure has a two-dimensional character — there is very little dispersion perpendicular to the plane of the CuO octahedra. There is one strongly dispersing band which is the one derived from Cu $3d_{x^2-y^2}$ and the oxygen $2p_x$ and $2p_y$ states. The Cu-O band structure is nearly filled: for the 22 bands (including spin), there are 21 electrons available. Since the density is one hole per unit cell, the top-most band becomes half-filled. These calculations confirm that it is sufficient to look at the planes only.

1.4 Mott insulator

Contrary to experiments, these calculations predict metallic behavior in La_2CuO_4. The calculation shows that the Fermi level lies near the top of the Cu d-O p complex in figure

1.3 and is crossed by a single half-filled anti-bonding band labeled "A". Mattheiss [123] has demonstrated that this band can be reasonably described within a simple two-dimensional tight-binding model which includes only the Cu $3d_{x^2-y^2}$ orbital and the $2p_\sigma$ orbital on the O atoms. Because for undoped La_2CuO_4 there is one electron per copper orbital, the local density approximation leads to cosine band that crosses the Fermi surface. This theoretical calculation would predict metallic behavior, while experimentally the undoped systems are insulators. Therefore, band structure calculations do not correctly reproduce the experimental electronic properties of the cuprates. Similar problems with local density calculations have been observed earlier in the classical transition-metal oxides such as FeO, CoO, and NiO. The reason is that the local density approximation is not capable of including the strong interaction between electrons in the strongly correlated oxygen systems. The physics in the cuprates is dominated by correlated electronic behavior resulting from a large intra-atomic Coulomb repulsion U between Cu $3d$ electrons. The cuprates are insulators because of this Mott-Hubbard correlation gap between occupied and unoccupied Cu $3d$ states. The strong Coulomb interaction blocks the band motion, and each orbital is occupied by a single localized electron.

A Mott insulator is fundamentally different from a conventional insulator. In the latter system, conductivity is blocked by the Pauli exclusion principle. When the highest occupied band contains two electrons per unit cell, electrons cannot move because all orbitals are filled. In a Mott insulator, charge conduction is blocked instead by electron-electron repulsion. When the highest occupied band contains one electron per unit cell, electron motion requires creation of a doubly occupied site. If the electron-electron repulsion is strong enough, this motion is blocked. Because electrons repel one another quite strongly, the energy needed to force a second electron onto a copper atom that has not already lost its loosely bound electron, is prohibitive. So with one loosely bound electron on every copper atom, the resulting electronic traffic jam makes the material a poor conductor. Therefore, the ground state of the cuprates is that of a Mott insulator, in which each electron is localized on a lattice site due to strong electron-electron interactions.

1.5 The Hubbard model

The essential physics of the cuprates is thus contained in the two-dimensional CuO_2 planes. The unit cell of this system consists of one Cu atom and two oxygen atoms. Zhang and Rice [224] have shown that this CuO_2 unit can be replaced by one effective electron with spin $\frac{1}{2}$. If a hole is created in a CuO_2 unit, the hole resides primarily on the oxygen sites. However, the Cu-O hybridization strongly binds the hole to the central Cu^{2+} ion to form a local singlet. This singlet moves through the lattice in a similar way as a hole would in the single-band effective Hamiltonian. Furthermore, two holes

feel a strong repulsion against being on the same square. Therefore, the CuO_2 unit can effectively be replaced by a single lattice point.

Anderson [9, 10] was the first to propose the two-dimensional one-band Hubbard model close to half-filling as a starting point to model the correlations in the cuprates. He argued that a single-band effective Hamiltonian with moderately large repulsion energy U is adequate as far as low-energy properties is concerned. The basic interaction between these electrons is repulsive, opening up a "Hubbard gap" U between states containing, respectively, two holes or one hole per Cu.

One therefore has to study models with explicit repulsive interactions between the electrons. The essential simplification of the Hubbard model is to only look at electrons that repel each other when they are at the same position in space. The argument is that if they are further apart in space, the other electrons and the positive cores of the atomic nuclei will shield the two charges from noticing each other.

The Hubbard model is in second-quantization notation given by

$$H_{\text{Hubbard}} = \sum_{i,\delta,\sigma=\{\uparrow,\downarrow\}} \left(-t c^{\dagger}_{i\sigma} c_{i+\delta,\sigma} + h.c.\right) + U \sum_i n_i^{\uparrow} n_i^{\downarrow}. \tag{1.1}$$

Here $c^{\dagger}_{i\sigma}$ creates an electron at position i with spin σ, which can be $\uparrow$ or $\downarrow$. The $c_{i\sigma}$ term removes an electron with spin σ at position i. The first term in the Hubbard Hamiltonian is thus the kinetic term. It lets electrons move from one position i to the nearest neighbor position $i+\delta$. The second term is the repulsion term; it is the product of the number of electrons with spin $\uparrow$ and spin $\downarrow$ at the same position in space. Because electrons are fermions, according to the Pauli exclusion principle there can only be zero or one electrons with spin $\uparrow$ at the same site. Thus the product is always zero unless there is both a spin $\uparrow$ and a spin $\downarrow$ on the same site.

This Hubbard model is the simplest model one can write down that includes the repulsion between electrons. It cannot be reduced to a single-particle theory. Various spectroscopic studies have confirmed that U is indeed sufficiently large to cause strong correlations in the cuprates.

1.6 Antiferromagnetism

In a half-filled Mott insulator, the amount of charge per Cu atom becomes fixed, leaving only the electron spin of the nearly filled Cu^{2+} $3d^9$ shell on each site to fluctuate. Virtual hopping of the electrons between neighboring metal sites lowers their kinetic energy in second order perturbation theory. When combined with the Pauli exclusion principle, this leads to a anti-parallel alignment of neighboring spins. Therefore, the low-energy properties of the cuprates are related to that of a two-dimensional square

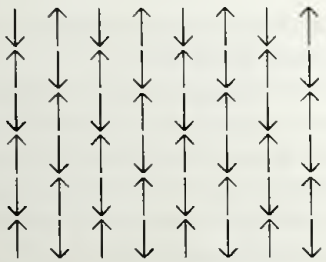

Figure 1.4: A simplistic representation of a perfect two-dimensional antiferromagnet. This is the classical Néel state. In the quantum-mechanical groundstate, a large number of spins will have been temporarily flipped by quantum fluctuations. The arrows represent the Zhang-Rice singlets that are localized on a CuO_2 unit.

spin-$\frac{1}{2}$ Heisenberg antiferromagnet described by

$$H_{\text{Heisenberg}} = J \sum_{\langle ij \rangle} \mathbf{S}_i \cdot \mathbf{S}_j. \tag{1.2}$$

In this equation $\mathbf{S}_i$ is a spin-$\frac{1}{2}$ located at position i and J is the effective interaction strength between the spins. This model can be derived from the Hubbard model at half-filling with $J = t^2/U$. The material is a strong antiferromagnet because of the strong super-exchange path between Cu^{2+} ions via the planar O. This leads to very large values of J, of the order of 1200 K, making the cuprates the strongest known antiferromagnets. La_2CuO_4 is an excellent realization of a two-dimensional square lattice Heisenberg antiferromagnet.

The classical solution to the Heisenberg model is called the Néel state (see figure 1.4). Although the Heisenberg model has not been solved exactly in two dimensions, it has been shown numerically that the ground state is ordered. Quantum fluctuations do not destroy this classical state in two or more dimensions. Quantum fluctuations in one dimensions always destroy any continuous order at a finite temperature. The ordered moment corresponds to $0.4\mu_B$ per Cu atom.

Spin wave theory describes the excitations of this model very well. This is related to the fact that the Heisenberg Hamiltonian is $O(3)$ symmetric and in the low temperature ordered phase, this continuous symmetry is broken, leading to Goldstone bosons which in this case are called spin waves. The predictions of spin wave theory have been thoroughly investigated using neutron scattering, which measures the spin-spin correlation function. Neutron scattering provides detailed information about the energy and momentum dependence of the magnetic dynamics of materials, provided sufficiently large single crystals are available [119]. The results show that both the static susceptibility and spin excitations are well described by the classical spin wave model. Quantum ef-

fects introduce small modifications of the numerical parameters, but they do not lead to quantum frustration or other qualitatively new dynamics. For instance, Coldea *et al.* [44] used high resolution neutron scattering to measure the dispersion of the spin waves in La_2CuO_4. They found sharp spin waves with absolute amplitudes in agreement with the theory including quantum corrections throughout the Brillouin zone. They did see deviations related to higher order Hubbard terms that lead to a cyclic or ring exchange. The detailed energy dependence of the spin waves follows directly from the Hubbard model in order t^4 if one uses $t = 0.32 \pm 0.02$ eV and $U = 2.6 \pm 0.3$ eV and thus $U \approx 8t$. This shows that the relevant regime for the Hubbard model is the large but not infinite U region.

These results demonstrate that a one-band Hubbard model with large U is an excellent starting point for describing the magnetic interactions of the underdoped cuprates. A weak interlayer coupling of approximately $10^{-5}J$ even leads to long-range three-dimensional antiferromagnetic ordering at non-zero temperatures (but much lower than the in-plane exchange energy). For undoped La_2CuO_4, this Néel temperature is about 330K. The antiferromagnetic structure explains the fact that the NMR has different magnitude and temperature dependence for the Cu and O atoms. For an overview of the magnetic, transport and optical properties of mono-layer copper oxides see the reviews by Kastner *et al.* [98] and Maple [116].

Finite temperature properties

The spin-wave theory starts from the assumption that there is long range ordering of the spins. The Mermin-Wagner theorem proves that for a purely two-dimensional system at any finite temperature the order is broken because of the spin waves. Even though locally the antiferromagnet is still strongly ordered, the long-range properties have to be described by a different model. Chakraverty, Halperin and Nelson [37] showed that the low temperature behavior of the two-dimensional Heisenberg model can be mapped onto a non-linear σ model in two space dimensions. The non-linear σ model is the simplest continuum model that contains all the essential low-energy physics. It has a linear spectrum and models the interaction between the spin-waves. They use a $(d+1)$-dimensional non-linear σ model, where the thickness in the extra dimension is the quantum or imaginary time direction; it is proportional to the inverse temperature of the system.

Using parameters consistent with the spin-wave theory for the nearest neighbor spin-$\frac{1}{2}$ Heisenberg antiferromagnet on a square lattice, they calculate using renormalization group the reduction of the $T = 0$ staggered order parameter due to the quantum fluctuations, as well as the spin-spin correlation length and the susceptibility. Renormalization of the Hamiltonian as a function of temperature can be used to obtain the correlation length ξ. They predicted the correct exponential temperature dependence of the corre-

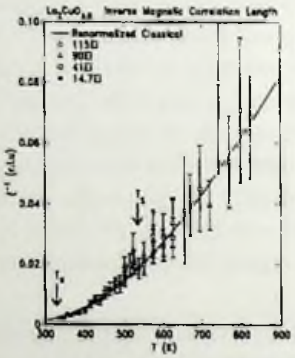

Figure 1.5: Inverse magnetic correlation length extracted from fits to neutron scattering data at the (π,π) position of La_2CuO_4 from Birgeneau et al. *[25]. The solid line is the result of a fit to the renormalized classical theory prediction of equation 1.3 with $J = 135$ meV. The Néel and structural transition temperatures are indicated by arrows.*

lation length using perturbative renormalization group arguments. The low-temperature properties of these systems obey renormalized classical scaling. Hasenfratz and Niedermayer [85] go beyond their work by predicting the exact prefactor and the first $O(T)$ correction in $\xi(T)$, leading to

$$\xi = \frac{e}{8}\frac{c}{2\pi\rho_s} e^{\frac{2\pi\rho_s}{k_B T}} \left(1 - \frac{T}{4\pi\rho_s} + O\left(\frac{k_B T}{2\pi\rho_s}\right)^2\right). \tag{1.3}$$

The spin wave velocity c and the $T = 0$ spin stiffness parameter ρ_s control the low-energy behavior of the model. The predictions can be compared above $T_N \approx 200K$ to the renormalized classical theory. Below T_N there is an infinite correlation length because of the very weak coupling between the planes.

Typically, the Fourier transform of the instantaneous spin-spin correlation function is a Lorentzian centered on (π,π) with a width proportional to the inverse correlation length. From this, one can determine the correlation length as a function of temperature.

The neutron scattering measurements of $\xi(T)$ in $S = \frac{1}{2}$ layered Heisenberg antiferromagnets such as La_2CuO_4 [76] and $Sr_2CuO_2Cl_2$ reveal a remarkable agreement with the theoretical prediction 1.3. This is shown in figure 1.5. Aside from a region of temperature extremely close to the three-dimensional phase transition, the antiferromagnetic correlations in La_2CuO_4 are essentially two-dimensional in character due to the very large anisotropy in the magnetic interactions in the Hamiltonian. The fit with the experimental data from neutron-scattering is extremely good with $J = 1200$ K. The only effect of the quantum fluctuations is to renormalize the coupling constants. Beard *et al.* [22]

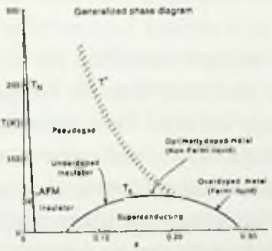

Figure 1.6: Generic temperature versus carrier concentration phase diagram for the cuprates from the review by Maple [116]. It shows the regions of superconductivity and antiferromagnetic ordering for the hole doped $La_{2-x}Sr_xCuO_4$ system. At low carrier concentrations x, electron repulsion causes an exchange interaction leading to an antiferromagnetic ordering. At higher doping, a superconducting region is created. The hatched line corresponds to a crossover temperature T^* below which most physical properties exhibit a pseudogap behavior. The solid lines labeled T_N and T_c delineate the antiferromagnetic and superconducting regions, respectively.

have argued that the mapping is only strictly valid for $\xi > 10^5$ and that the apparent agreement for higher T is perhaps coincidental.

The important conclusion from these considerations is that a simple one-band Hubbard model in two-dimensions, focusing on the relatively large U case, is the appropriate model to study.

1.7 Doping and phase diagram

The properties of the Mott insulating parent compounds are very well studied and understood. For the undoped system, the electrons cannot move because of the large Coulomb repulsion and the only physics left is that describing the orientation and dynamics of the spins of these electrons. However, if there are holes in the system, the electrons can start to move again and the situation becomes more complicated. Now both the charge and spin degrees of freedom are important. One must use as carriers the same electrons that are participating in making an antiferromagnetically correlated spin structure. Doping restores electrical conductivity by creating sites to which electrons can jump without incurring a cost in Coulomb repulsion energy. All the copper-oxide high-T_c materials come from an insulating antiferromagnetic "parent" compound which becomes superconducting upon either electron or hole doping. The generic phase diagram of the high-T_c superconductors is indicated in figure 1.6. The phase-diagram is quite complicated with a large number of different physical phenomena.

By chemically altering the so-called charge reservoir layers, the CuO layers can be

doped with holes; the net hole concentration is indicated with x in figure 1.6. If one introduces Sr, Ba or Ca into $La_2Cu_4O_8$ to replace La, one effectively takes out one electron from the two-dimensional plane because strontium has a greater affinity for electrons and so attracts the loosely bound electrons from the copper atoms. With some copper sites now vacant, electrons can hop between the copper atoms and so carry electricity. When the material is doped with strontium, and x increases from zero, $La_{2-x}Sr_xCuO_4$ first turns from an antiferromagnetic insulator into a reasonable conductor. At larger values of x, the material gains the ability to be superconducting when cooled. The transition temperature T_c at which superconductivity arises depends on the value of x, reaching a peak at around $x = 0.17$.

With increasing Sr doping the Néel temperature T_N is reduced, it vanished beyond $x \approx 0.02$. There is a small region of spin glass behavior beyond this value. For doping levels in the range $0.07 - 0.25$, superconductivity occurs with a maximum T_c of 39K for $x = 0.15$. It produces superconductivity in $La_{2-x}Sr_xCuO_4$ with a maximum T_c of approximately 40 K at $x \approx 0.17$.

For very small dopings, the system stays non-metallic and spin-glass like, but around $x \approx 0.05$ superconductivity sets in (*underdoped regime*). Upon further doping, T_c increases to reach a maximum around $x = 0.15$ (*optimal doping*); beyond this value, it decreases (*overdoped regime*). The unconventional aspects most clearly manifest themselves in the underdoped regime $x \leq 0.15$: sufficiently deep inside the overdoped regime a more normal Fermi-liquid type of behavior is restored.

In $YBa_2Cu_3O_{6+x}$, doping is achieved by changing the oxygen concentration. The conducting properties are strongly dependent on the degree of oxidation of the chain layer. Maximum conduction of the planes corresponds to an oxygen stoichiometry of seven. As oxygen is removed from the layers containing the chains, the conductivity of the planes decreases, the chains become partially disordered, and T_c decreases.

The strangest phase is the **pseudogap phase**. In the pseudogap phase the systems show insulating behavior as a function of temperature. Above the pseudogap temperature (indicated by the dashed line), the system can be characterized as a Fermi-liquid.

Magnetism and high-T_c superconductivity are thus closely related. The electrons which exhibit magnetism are the same as the charge carriers. While the superconducting compositions no longer show long-range magnetic ordering, strong antiferromagnetic correlations between the fluctuating magnetic moments still remain. The proximity of antiferromagnetism suggests that superconducting electron pairing in the cuprates may be mediated by the antiferromagnetism. Thus the problem to solve is that of doping a single Mott-Hubbard band.

1.8 Physical Properties

The normal-state properties of the CuO superconductors are as strange as their high transition temperatures. Since all the cuprates have similar normal metal properties and since close to optimum doping, they have very similar resistivity per plane, spin susceptibility, nuclear magnetic relaxation, Hall effects, photoelectronic and infrared spectra and tunneling curves, it is generally agreed that the electronic properties are crucially determined by the CuO_2 planes. A nice description of these properties can be found in [116], Anderson's book [10], or various review articles.

It was realized at the outset that the normal state properties of the high-T_c cuprate superconductors are unusual and appear to violate the Landau Fermi liquid paradigm. It will be necessary to develop an understanding of the normal state before the superconducting state can be understood.

As one might expect from the crystal structure, the electrical properties of the layered cuprates are highly anisotropic. The electrical resistivity of $Bi_2Sr_2CaCu_2O_8$, for example, can be up to 10^5 times larger in the c direction (perpendicular to the CuO_2 layers) than it is in the a and b directions (along the layers). The degree of anisotropy is specific to a compound family and reflects how effectively the charge reservoir layers block the coherent motion of electrons between the CuO_2 layers. This demonstrates that for the most part the carriers are confined to the planes and that interlayer transitions are less favorable.

The in-plane resistivity ρ_{ab} behaves like that of a metal, increasing as the temperature is raised, while the perpendicular resistivity ρ_c is reminiscent of semiconductor behavior, decreasing upon heating. The resistivities are all close in magnitude; they increase approximately linearly with temperature over wide temperature ranges (from T_c up to 7000 K) and they are quite small when extrapolated to zero temperature. The striking similarity of the $\rho_{ab}(T)$ curves for optimized compositions is evidence that the common CuO_2 layers are the electronically active building blocks in otherwise very different crystal structures. The mean-free path at 100 K is estimated to be $100 - 200$ Å for $YBa_2Cu_3O_7$, which is long compared to the lattice parameter of 3.8 Å.

The electrical resistance displays a linear temperature dependence up to very high temperatures with an extrapolated residual resistivity $\rho_{ab}(0)$ that is very small. This property has attracted considerable attention. There are also strong experimental indications of short-range magnetic fluctuations. There is little effect of random scattering by the doping ions. This resistivity due to the off-stoichiometric doping is never seen, nor is there any resistivity visible that is clearly caused by conventional phonon scattering. The absence of a residual resistivity of the dopant ions and of phonon resistivity means that Fermi Liquid theory does not apply.

A consistent description of the observed frequency dependent conductivity $\sigma(\omega)$, within a model of carriers scattering from excitations (such as phonons) requires that

the scattering time τ depends on both temperature and frequency. The peculiarity of the cuprate charge dynamics is reflected in the form of this rate: $\hbar/\tau(\omega, T)$ is given by the greater of $k_B T$ or $\hbar\omega$. A proposed functional form in the Marginal Fermi Liquid approach of section 1.10.3 is $(\hbar/\tau)^2 = (\alpha k_B T^2 + (\beta\hbar\omega)^2$, with α and β of order unity, or simply

$$\frac{1}{\tau} \approx max(\frac{\omega}{\frac{kT}{\hbar}}). \tag{1.4}$$

An important conclusion from the transport and light-scattering experiments is that there is no scale for low-energy excitations other than the temperature itself.

1.9 Superconducting properties

The cuprates display a number of superconducting properties, when doped with holes, that are in many ways similar to those of conventional BCS superconductors. First of all, flux quantization and Josephson tunneling experiments have demonstrated that the superconducting state is made up of paired carriers. Another important property of conventional superconductors is the presence of an energy gap. A number of investigations, most notably photo-emission spectroscopy, have shown that the cuprates also exhibit an energy gap in the superconducting state.

On the other hand, the cuprates also possess many surprising properties. For example, the superconducting coherence length is extremely short: conventional superconductors have coherence lengths of approximately 10^{-6} m, whereas the cuprate superconductors have coherence lengths of the order of 10^{-9} m. For instance, magnetic measurements indicate that in the La-Sr-Cu-O compound, $\xi_0 \approx 29$ Å. The short coherence length increases the significance of fluctuation effects in the vicinity of the superconducting transition. Because of their short coherence length and large penetration depths, the cuprates are extreme type *II* superconductors. Therefore, for low magnetic fields they can enter a mixed state with a vortex structure (see [46]).

An important question, having direct bearing on the problem of the origin of high-T_c, is that of the symmetry of the pair wave function. In conventional superconductors, the pair wave function has *s*-wave symmetry. However, the cuprate superconductors have a *d*-wave gap. See chapter 6 for a more detailed look at the superconducting properties.

1.10 Theoretical approaches

The purpose of the above introduction is to show the reasons why theory has to focus on the Hubbard model on a square lattice in two dimensions. The *t-J* model is a limit of

the Hubbard model. Not withstanding its apparent simplicity, the understanding of the physics of the Hubbard model is still limited.

1.10.1 Hubbard model in one dimension

Even in the one-dimensional case, where the exact groundstate wavefunction has been found by a Bethe Ansatz solution (Lieb and Wu [108] and Yang [213]) the knowledge is far from complete. The ground state correlations and excitations have been investigated by bosonization, field theoretical methods, the Luttinger and Tomonaga models, and the perturbative renormalization group (see Auerbach [15]).

Analysis of the Bethe Ansatz solutions has shown that the low-energy excitations in a one-dimensional correlated electron system are not quasi-particles with charge e and spin $\frac{1}{2}$ as in a Fermi liquid. Instead, electrons are decoupled into collective modes of spin and charge excitations called *spinons* and *holons*. Probably the most important feature arising is the Luttinger liquid like behavior, characterized by non-universal power laws, together with the separation of the charge and spin dynamics.

Another important result has been obtained by Ogata and Shiba [141]. They found that in the large repulsive U limit, the Bethe Ansatz wave function has a simple form for any electron density. They determined the momentum distribution function $n(k)$ and spin-correlation function $S(k)$ for the one-dimensional large-U Hubbard model with various electron densities. Its charge degrees of freedom are expressed as a Slater determinant of spinless fermions, while its spin degrees of freedom are equivalent to the one-dimensional $S = \frac{1}{2}$ Heisenberg model. Therefore, the holes are effectively squeezed out of the system. Kruis has shown that this is a general phenomenon, that takes place for all positive values of U [105].

Unfortunately, the methods listed above are specialized to one dimension and their application to two and three dimensions has yet to produce conclusive results. Anderson has suggested that Luttinger liquid behavior might also occur in two dimensions. The separation of spin and charge degrees of freedom for an electron in strongly correlated two-dimensional systems has received much attention.

1.10.2 RVB and Interlayer tunneling

The first alternative theory for high-T_c superconductivity was introduced immediately after the discovery of high-T_c superconductivity by Anderson [9]. He focused on the electronic and spin structure in the CuO_2 planes. Anderson's suggestion was that the ground state of a two-dimensional square lattice is not the classical Néel state, but rather a quantum spin-liquid or "resonating valence bond" (RVB) state. A single valence bond in this picture is defined as a singlet state constructed from any pair of spins. The RVB ground state then corresponds to a coherent superposition of all possible configurations

of valence bonds. Such a state is itself a precise singlet and has no long-range order and no fixed spin direction at each site.

When this system is doped, it contains a non-Fermi liquid state within the planes [38], with separate spin and charge excitations. An unpaired spin acts as an uncharged spin-$\frac{1}{2}$ fermion known as a spin soliton or spinon. The hole produced by removing such a spin acts as a charge e, spin-zero, boson, or "holon". There is a separation of spin and charge because there are two different Fermi velocities for charge and spin fluctuations. A physical hole is a combination of a spinon and a holon. Anderson called the extension of these ideas to two dimensions a Luttinger liquid.

Superconductivity is in this model caused by deconfinement by interlayer Josephson tunneling. The only objects that can move coherently from one plane to another are real electrons, but these do not exist in the ground state and they break up incoherently into holons and spinons. Therefore single electrons can not hop coherently between copper-oxide layers so that second order hopping processes such as pair tunneling become important. Pairs of electrons *can* tunnel coherently from plane to plane. There is no coherent three-dimensional motion along the c-axis, as is experimentally observed. The superconducting T_c in this picture is thus a crossover from two- to three-dimensional behavior. In the interlayer tunneling theory the interlayer pair tunneling energy is the motivation for superconductivity. The interlayer hypothesis is that electron pairing in the superconducting state makes this transport coherent and is responsible for the Josephson-like superconducting coupling between the layers.

Although this is a nice mechanism, there are two objections. It is now known that both the 214 and 123 system do exhibit true antiferromagnetic long-range order thus the groundstate of the undoped parents is not an RVB state. Even more importantly, Van der Marel *et al.* [187] have shown that their optical conductivity data do not fit these theoretical predictions.

1.10.3 Marginal Fermi Liquid theory

A lot of the strange normal state properties of the cuprates can be explained by one single phenomenological hypothesis about the excitation spectrum. The absence of quasi-particles in the normal state and the fact that the resistance is linear in the temperature led Varma *et al.* [194] to propose the Marginal Fermi Liquid theory. From the linear resistivity, one learns that the scattering-rate $\frac{1}{\tau}$ is proportional to T. Frequency dependent conductivity has also shown that $\frac{1}{\tau}$ is proportional to ω. Because the scattering rate is equal to the imaginary part of the self-energy, the real part of the self-energy can be constructed by a Kramers-Kronig transformation, which leads to: $\mathrm{Re}\Sigma \propto \omega \log \frac{x}{\omega_c}$ and $\frac{1}{\tau} \approx \mathrm{Im}\Sigma(\omega, T) = \frac{\lambda\pi}{2}\max(\omega, T)$ independent of q.

If the normal state were accessible at zero temperatures, it would be described by a "marginal" Fermi liquid where the quasi-particles have an infinite lifetime, but a (loga-

rithmically) vanishing spectral weight. This agrees with the fact that well-defined quasi-particles have not been observed in the *normal state* of any of the cuprates.

Varma *et al.* found that if they modified the Green's function slightly, they could reproduce a lot of experimental data on the normal state of the new high-T_c superconductors. However, it is not a first-principles microscopic theory, only a phenomenological approach that shows that the various anomalous properties can all be captured by a single Ansatz. This modification of the Green functions has to be caused by something, and they did not know by what.

Lately, Varma has proposed a new microscopic theory to give a microscopic underpinning to the Marginal Fermi Liquid theory [1]. Recent angular-resolved photoemission experiment on high-temperature superconductors are consistent with a phenomenological description of the normal state of these materials as Marginal Fermi Liquids. Especially the data in the nodal direction agrees with the Marginal Fermi Liquid theory. The magnetic excitations spectrum is momentum k independent over most of the Brillouin zone and it has a scale-invariant form, as a function of frequency ω and temperature T. For a Marginal Fermi Liquid the width should be proportional to $x = \max(|\omega|, T)$ where ω is measured form the chemical potential. Their hypothesis predicted that the width of the quasi-particle peak varies linearly with its energy separation from the Fermi surface, consistent with data from photo-emission.

1.10.4 Quantum critical point

In $La_{2-x}Sr_xCuO_4$ with $x = 0.14$, where no static stripe order is observed at finite temperature, the dynamics of the magnetic fluctuations might exhibit quantum critical behavior. In fact, evidence for such behavior is reported by Aeppli *et al.* [2]. Polarized and unpolarized neutron scattering was used to measure the wave vector- and frequency dependent magnetic fluctuations in the normal state (from the superconducting transition temperature $T_c = 35$K, up to 350K) of single crystals of $La_{1.86}Sr_{0.14}CuO_4$. The peaks which dominate the fluctuations have amplitudes that decrease as T^{-2} and widths that increase in proportion to the thermal energy, k_BT and energy transfer added in quadrature. The nearly singular fluctuations are consistent with a nearby quantum critical point. Infrared reflectivity shows also that $\sigma \propto T$, therefore only the temperature sets the scale. These data are clearly consistent with the nearness of a quantum critical point, but the precise interpretation or the nature of this point is still under discussion.

1.10.5 Hot spots

Another example of a non-Fermi liquid theories are the cold- and hot-spot theories, in which the basic entities are more exotic objects, for example spinons and holons. In Fermi-liquid based approaches one must invoke an anomalous scattering mechanism.

Various models have been proposed. A central concept is the 'hot spot', a small region on the Fermi surface (typically taken to be near the $(\pi, 0)$ and $(0, \pi)$ points) where the electron lifetime is unusually short and has an anomalous temperature dependence. Hot spots arise for example in models involving antiferromagnetic fluctuations that are strongly peaked at a particular momentum transfer. There is a strong doping dependent anisotropy, which affects states near the zone corners more strongly than those near the zone diagonals. All the available normal state NMR and NQR measurements in the $YBa_2Cu_3O_7$ system can be accounted for by a model susceptibility strongly peaked at the zone corner according to Millis, Monien and Pines [127]. Models involving hot spots have had some successes, but have not led to complete and generally accepted descriptions of cuprate physics.

1.10.6 Cold spots

Ioffe and Millis [95] have come with a description of the data in terms of cold spots. These are small regions near the zone diagonal in which the lifetime is assumed to be much longer than elsewhere on the Fermi surface. It is based on the characteristic feature of a d-wave superconductor: the existence of four nodal points where the order parameter vanishes. Since low-energy excitations are concentrated around these nodes, low temperature behavior is dominated by the details of the node structure and in particular the ratio of the Fermi velocity to the gap velocity. They used a Boltzmann equation analysis of the transport properties of a model of electrons with a lifetime which is short everywhere except near the Brillouin zone diagonals. This is a Fermi liquid approach.

1.10.7 $SO(5)$

The $SO(5)$ theory of high-T_c superconductors, proposed by Zhang [226] in 1997, is different from the approach of microscopic theories like the Hubbard and t-J models. It is based on the well established existence of the antiferromagnetic and d-wave superconducting ordered phases and the close proximity between them. The $SO(5)$ theory does not view these two states as competing orders, but treats them on equal footing. Just as in Landau-Ginzburg theory, $SO(5)$ theory is only concerned with equations for the order-parameter. The $SO(5)$ theory groups the antiferromagnetic order parameter (three components) together with the real and imaginary part of the superconducting order parameter into one new order-parameter with five components: the superspin. In order to go from the antiferromagnetic state to the superconducting state it defines transformation operators π. The general strategy is to look at what kind of Hamiltonians can give phase diagrams with antiferromagnetic and superconducting order, by formulating a general model with a small number of phenomenological constants which captures all the qualitative physics of the special models and can be fitted quantitatively to experiments. One important ingredient of the $SO(5)$ theory is that the π resonance in the

t-J model is assumed to correspond to the neutron resonance peak in the $YBa_2Cu_3O_{6+x}$ superconductor [56]. Using the $SO(5)$ symmetry, one can construct an effective low-energy theory. In a sense it resembles the Ginzburg-Landau kind of equation for the evolution of these order parameters.

The big question is if these special model Hamiltonians are connected to the cuprates. For the Hubbard model to be $SO(5)$ symmetric, the Hamiltonian needs to commute with the generators of the symmetry. The problem is that $\pi_\alpha^\dagger$ does not commute with the Hubbard Hamiltonian, so the $SO(5)$ symmetry is not exact. Although the Hubbard model is not explicitly $SO(5)$ symmetric, it is claimed that exact diagonalization studies on Hubbard and t-J clusters show evidence that the low-energy states agree with the level structure anticipated from $SO(5)$ symmetry. Numerical tests by Meixner *et al.* [125] on a small Hubbard cluster show that dynamical correlation functions are consistent with $SO(5)$ for low-energy. Similar results have been found for the spin correlations in the t-J model (Demler *et al.* [55]) and for ladders (Eder *et al.* [68]). Therefore, the π-operator seems to be an approximate eigenoperator of the Hubbard model. A different approach is to explicitly create microscopic theories that are $SO(5)$ symmetric [190]. The problem with this approach is that these models are equivalent to extended Hubbard models with non-physical long range interactions and hoppings.

The conjecture of an approximate $SO(5)$ symmetry has been used to derive a number of new results. It has for instance been predicted that the cores of the non-superconducting vortices which occur in a type-*II* superconductor in a magnetic field should be antiferromagnetic (Alama *et al.* [3]). An *"$SO(5)$ proximity"* effect is predicted at the interface of an antiferromagnet and a superconductor by Demler *et al.* [54]. And recently, a mechanism for superconductivity has been proposed based on the energy-gain due to the π-fluctuations in the superconducting phase (Zhang [227]).

1.11 Summary

This introductory chapter has introduced the concept of superconductivity and that of the cuprates. The physical properties of the cuprates were discussed. The relevant physics of the cuprates is confined within the CuO_2 planes. Therefore, this thesis will focus on two-dimensional lattice model. The Hamiltonian that is relevant to this system is that of the Hubbard model. The last section has also reviewed a number of theories that have been used to describe the physics of the cuprates. In the next chapter it will be shown that doping holes into the Hubbard model leads to the formation of stripes.

Chapter 2

Stripes

The introduction has shown that large parts of the problem of high-T_c cuprates can be understood if one knows what happens when holes are doped into a two-dimensional Mott-Hubbard antiferromagnet. The idea of stripes is that those holes do not move individually (spin-polarons) or as pairs (spin-bags). Instead it is assumed that they form one-dimensional lines of charge in this two-dimensional antiferromagnet. The formation of stripes is related to the difficulty of moving single holes through an antiferromagnet. The charge of the holes also rules out complete phase separation. These competing interactions lead the holes to form a periodic magnetic and charge structure: STRIPES. The earliest evidence for stripes came from observing this additional periodicity in neutron- and X-ray scattering. Later, local probes such as NMR and NQR resonances, one-dimensional conductivity and one-dimensional features in photo-emission experiments have given additional evidence that stripes do exist. There is also strong evidence for stripes in related systems, such as the nickelates and manganites and even in some Quantum Hall Effect systems. This chapter gives an overview of the experimental evidence for stripes.

2.1 Doping an antiferromagnet

Chapter 1 has shown that the parent compounds of the cuprates are two-dimensional antiferromagnetic insulators. They only become superconductors when one introduces holes in the CuO_2 planes. Therefore, the starting configuration for this discussion is a two-dimensional Heisenberg antiferromagnet. The question now is what happens to holes in an antiferromagnet. The most natural assumption would be that if a finite concentration of holes is introduced into an antiferromagnet, the result would be a uniform distribution of holes: a hole gas. The essence of 'stripes' is that this is not the case and that the holes want to come together in one-dimensional lines. It explains one of

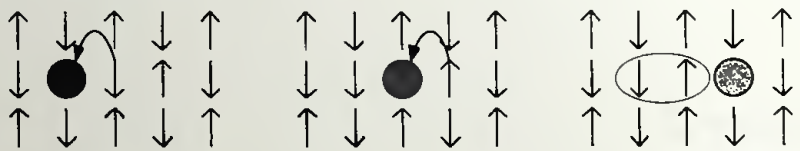

Figure 2.1: Hopping of one hole in an antiferromagnet creates ferromagnetic bonds between neighboring spins that cost a lot of energy. Therefore, movement of single holes through an antiferromagnet is frustrated. The arrows indicate the spins of the electrons and the circles the charge density associated with the excess holes.

the striking features of the cuprates, namely the coexistence of local antiferromagnetism with homogeneous superconductivity. The simplest way to understand the survival of the correlations is in terms of spatial segregation of the doped holes and the spins.

Single hole motion

Stripes were predicted by Zaanen and Gunnarson [215] in 1988, right after the discovery of the high-T_c cuprates by Bednorz and Müller [24]. Zaanen and Gunnarson showed that half-filled stripes are a stable solution of the mean-field approximation to the three-band Hubbard model in two-dimensions. However, the reason for the stability of stripes can already be understood using a simple discussion assuming a classical Néel state for the surround antiferromagnet. In order to understand why stripe formation would take place, first look at the motion of a single hole in such a system. The problem with a single hole is that it disrupts the background antiferromagnet as is shown in figure 2.1. A single hole has four neighboring electrons, all having the same spin. The hole can move if one of these neighboring electrons jumps onto the hole site, which is empty. Now the hole has effectively moved one site. However, because the electron has gone from one sublattice to another, it now has 3 ferromagnetic bonds. This costs an energy of approximately $3J$, a lot of energy (recall that J is very large for the cuprates). If another electron would again move onto the hole position, letting the hole continue to the right, there will again be another two wrong ferromagnetic bonds. Therefore, a single hole that is moving through an antiferromagnetic will create a string of wrongly aligned spins. Consequently, a single hole does not really want to move through an antiferromagnet. It is effectively localized. In chapter 7 it will be shown that there are additional second order processes that gives a hole a finite probability to move. However, this probability is small compared to the normal hopping amplitude t.

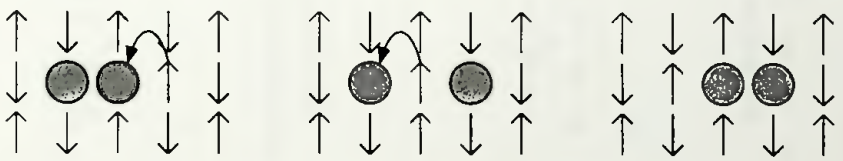

Figure 2.2: Two holes can move through an antiferromagnet without creating strings, by forming pairs. The second hole will undo the damage of the first hole.

Pair formation

The problem can be overcome when two holes are next to each other (see figure 2.2). The basic problem is that because of the antiferromagnetic ordering, the electrons belong on one of two sublattices. By moving one site, they end up on the wrong sublattice. By letting the holes move in pairs, the electron can move twice and end up on the same sublattice as it started. It only has an intermediate state with two ferromagnetic couplings. The second hole can undo the damage of the first hole as long as both holes move together. This is the physical reason why two holes in an antiferromagnet want to stay together.

2.2 What are stripes?

What happens if more holes are put into the system? Of course, it is possible that this would result in a gas of real-space pairs. This would be an interesting result. However this does not seem to happen in reality. Instead it seems that the pairs want to form lines, as proposed by Zaanen and Gunnarson [215]. Physically, stripes or domain walls result from the balance between two competing effects, namely the fact that holes lower their quantum mechanical energy by hopping and the fact that a moving hole destroys an antiferromagnetically ordered spin background. In figure 2.3A there is a single stripe in an antiferromagnet. This stripe was created by removing a finite number of holes out of the antiferromagnet. The result is that the coupling between spins over the stripe is ferromagnetic. However, this is not the configuration for real stripes. In order to understand this, imagine that an electron next to the stripe, on the left of it, hops onto the stripe. Effectively, the hole moves one position to the left and as a result there is a kink in the stripe as shown in figure 2.3B. The hopping electron has now ended up on the other side of the stripe. However, because of the ferromagnetic coupling over the stripe, it now has the same spin direction as the electron to the right of it, which again will cost

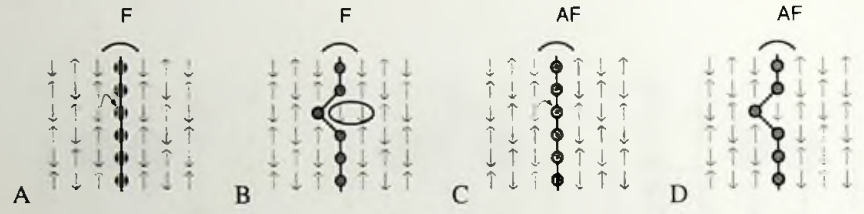

Figure 2.3: Even when holes have spontaneously condensed into a stripe configuration, they still have some freedom to move without breaking up a stripe. If there is a ferromagnetic coupling over the stripe, the hopping process creates a high energy ferromagnetic bond. However, if the coupling over a stripe is antiferromagnetic, a fluctuating stripe does not lead to any ferromagnetic bonds. In this picture, stripes are completely empty.

a lot of energy. Fluctuations of this stripe are therefore not low-energy excitations.

A situation that does allow the fluctuation of stripes is obtained for a stripe which has an antiferromagnetic coupling over the stripes as shown in figure 2.3C. All holes on the stripe can hop to the left and to the right, without creating ferromagnetic bonds. To create this situation, the magnetization for half the spins in the starting antiferromagnetic state will have to be flipped. This has to be done during the formation of the antiferromagnet at high temperature. For this reason, it is called topological doping.

Because a stripe with an antiferromagnetic coupling over a stripe does not create ferromagnetic bonds for electrons jumping on and off it, this antiferromagnetic coupling is the most likely configuration. This is in essence the result of the calculation by Zaanen and Gunnarson. These simple arguments have been validated by many different types of calculations, such as Variational Monte Carlo, Density Matrix Renormalization Groups *etc.* as will be discussed in chapter 3.

Frustrated phase separation

Another, more indirect way, of explaining the existence of stripes is the idea of frustrated phase separation, as advanced by Emery and Kivelson [71]. They start by noting that an interacting system would like to split up with one part being a perfect antiferromagnet and the other part being completely filled with holes. However, because of the Coulomb repulsion between the charged electrons, complete phase separation would cost an enormous amount of electrostatic energy. Therefore only small regions with a higher hole density would be created. Why this would lead to one-dimensional lines and why there would be an antiferromagnetic coupling over a stripe cannot be explained with this idea. However, it does explain why the idea of stripes is a very general one. Every time when there are competing attractive and repulsive interactions, there is the possibility of a non-homogeneous system. Therefore, stripe-like features have been observed in other

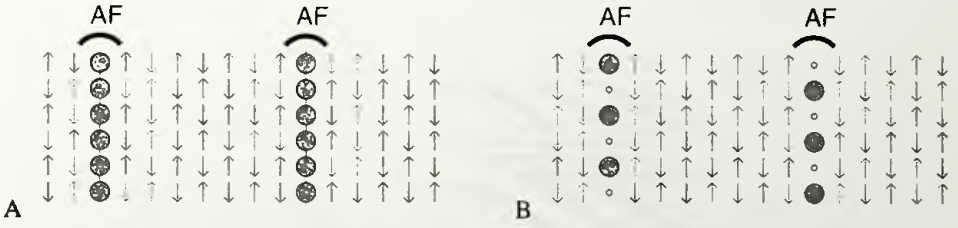

Figure 2.4: Figure A shows a schematic drawing of a half-filled *static striped phase with* $x = \frac{1}{8}$. *This system has a unit cell of* 16×2. *Figure B shows the same system, but now with a* quarter-filled *stripe. It has one hole for every two stripe sites. This stripe is the relevant stripe for the cuprates.*

highly correlated electron systems such as the nickelates, manganites and Quantum Hall Effect samples.

2.3 Half-filled and quarter-filled stripes

The segregation of the holes into charge stripes leaves narrow intervening regions that are essentially undoped. Effectively, there is a separation between charge and spins. The magnetic moments of the Cu ions in the intervening regions are correlated antiferromagnetically. Because of the antiferromagnetic coupling over the stripe, the charge stripes act as anti-phase domain walls.

If the stripes are regularly spaced this leads to a change in the magnetic and charge unit cells. Not only is the charge density modulated, the walls also induce a modulation in the spin density. Because the staggered magnetic order parameter change sign across a wall the period of the magnetic order is twice that of the charge order. In figure 2.4, the charge unit cell is equal to 8×2 and the spin unit cell is equal to 16×2. The extra periodicity in the x-direction can be measured with neutron-diffraction. Without the stripes, there is a doubling of the unit-cell because of the antiferromagnetism, so there should be a magnetic peak in neutron-scattering at $(\pi/a, \pi/a)$ or $(0.5, 0.5)$ in units of $2\pi/a$. Here a is the CuO lattice constant. However because of the extra periodicity introduced by the stripes, this peak should disappear and there should be some slightly shifted incommensurate peaks. The peaks that are no longer exactly at (π, π), are called incommensurate peaks (see figure 2.5). They signify a magnetic structure whose period is different from that of the underlying lattice. Evidence for incommensurate magnetic fluctuations in $La_{2-x}Sr_xCuO_4$ was first provided by the inelastic neutron-scattering measurements of Cheong *et al.* [42].

They experimental fact that the (π, π) peaks splits in four separate points has two

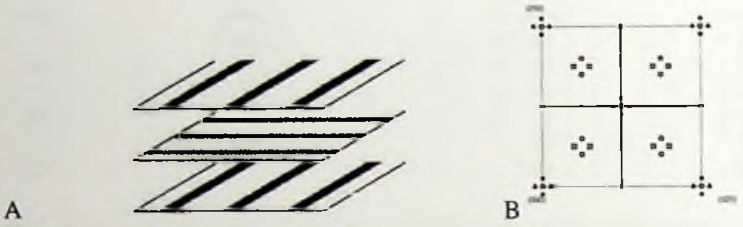

Figure 2.5: Figure A shows a sketch of the relative orientation of stripe patterns in neighboring CuO_2 planes of the LTT phase. Stripes in one layer are all oriented in the same direction. The displacement pattern in one layer is exactly opposite to that in the layer just above and below it. Figure B shows a diagram of the Brillouin zone in reciprocal space, with the splitting of the peaks, caused by stripes.

possible interpretations: either the neutron-scattering is averaging over domains, each of which has a single modulation direction as in 2.5A, or the two modulations are superimposed in each region of the sample. The simple stripe picture is based on the former model. Finite repulsive Coulomb interaction will favor a stacking of charge stripe layers in such a way as to minimize the Coulomb interaction.

The incommensuration δ is the distance in k-space from $(\pi/a, \pi/a)$ to the incommensurate peak in terms of reciprocal lattice units $(2\pi/a)$ and is related to the distance between the stripes. The experimental observation that the incommensuration δ is equal to the doping concentration x, means that on a stripe, there is on average only $\frac{1}{2}$ a charge per site (as shown in figure 2.4B). Because the total possible number of charges on a site can be two (one up- and one down-electron), these stripes are therefore called *quarter-filled stripes*.

2.4 The Barium $x = \frac{1}{8}$ dip

In retrospect, the above picture of a stripe at $x = \frac{1}{8}$ doping can be used to explain a long standing mystery about the doping concentration of $x = \frac{1}{8}$. It has been known since 1988 that the superconducting transition temperature T_c is dramatically suppressed in systems like $La_{2-x}Ba_xCuO_4$ [128] and $La_{2-x-y}Nd_ySr_xCuO_4$ for compositions around $x = \frac{1}{8}$. Because of this, the superconducting transition temperature as a function of doping has two maxima separated by a local minimum for $x = \frac{1}{8}$ (see figure 2.6). Even in plain $La_{2-x}Sr_xCuO_4$, there is evidence (by Takagi and Ido *et al.* [174]) that the superconductivity is suppressed somewhat in $La_{2-x}Sr_xCuO_4$ for x near 0.115 though not to the same extent as in the above mentioned materials. Radaelli *et al.* [151] have shown the presence of a shallow cusp at the same doping level.

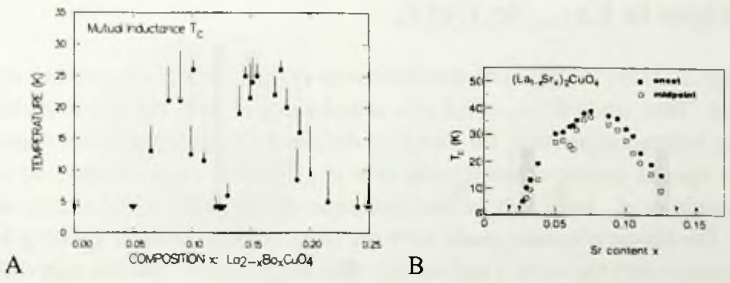

Figure 2.6: Figure A shows the superconducting transition temperature T_c versus the doping concentration for $La_{2-x}Ba_xCuO_4$ according to Moodenbaugh et al. *[128]. Solid lines are drawn between T_c and the "bulk onset" temperature. Dotted lines are drawn between bulk onset and highest onset temperature. Figure B shows the doping dependence of the superconducting transition temperature T_c for $La_{2-x}Sr_xCuO_4$ from Takaji* et al. *[174]. Here the effect is less noticeable but still visible.*

Why does the addition of Nd or Ba reduce the superconducting temperature in a narrow range of x around 0.125 only? The idea of *pinned stripes* in the low temperature tetragonal phase provides a possible explanation for this anomaly. The main effect of the Nd, which has the same valence as La, is associated with its smaller ionic radius relative to Sr. Its presence induces a change from the usual low-temperature orthorhombic phase to the low-temperature tetragonal (LTT) phase below about $70K$. This structural transition is caused by a subtle change in orientation of the low-temperature tilt pattern of the CuO_6 octahedra. This effect was first observed in $La_{1.88}Ba_{0.12}CuO_4$ by Axe *et al.* [16] using X-ray and neutron-diffraction measurements. For $x < \frac{1}{8}$ there is a correlation between the fraction of LTT phase present in low temperature and the suppression of the bulk T_c.

The tilting of the oxygen octahedra along the [100] and [010] directions (parallel to the Cu-O bonds) in the LTT phase introduces a pinning potential for horizontal and vertical stripes, whereas in the low temperature orthorhombic phase it is absent due to the rotation of the tilting axis into the diagonal [110] direction. The horizontal tilt pattern in the LTT phase rotates by 90° on going from one layer to the next. The lattice-distortion is oriented in the same direction as the proposed charge stripes. If the period of the charge stripes is commensurate with the lattice distortion, as happens at $x = \frac{1}{8}$, then the stripes can be pinned by the crystal structure modification in the LTT phase. The fact that this seems to lead to a reduction in superconducting behavior indicates that stripes are related to superconductivity.

2.5 Stripes in $La_{2-x}Sr_xCuO_4$

Tranquada *et al.* [183] are generally credited with experimentally discovering stripes in the cuprates. They studied $La_{2-x}Sr_xCuO_4$ samples doped with Nd at a hole doping of $x = \frac{1}{8}$ using neutron-scattering. As shown in the preceding paragraph, the doping with Nd and the special doping concentration of $x = \frac{1}{8}$ leads to *static* stripes. Because of this, Tranquada *et al.* were able to find incommensurate peaks using *elastic* neutron-scattering. The elastic magnetic peaks have the same incommensurate splitting δ as that found in crystals with the same x and no Nd . The suggestion is that the only difference between the charge and spin correlations in these various compounds is that they can become pinned to the lattice in the LTT structure, whereas they remain purely dynamical in the LTO phase. Without Nd doping there still are stripes, but they are fluctuating and therefore more difficult to detect.

Next to a set of four incommensurate peaks around (π, π) they also discovered peaks related to the charge periodicity. Neutrons do not scatter from charge directly, but instead are sensitive to the atomic displacements induced by the charge-density modulation. This second set of peaks occurs about nuclear Bragg peaks, split by 2δ. The charge-order peaks appear at a higher temperature than the magnetic peaks, as has recently been confirmed by X-ray scattering measurements with 100 keV X-rays [198].

Later Tranquada *et al.* showed [178] that similar order also occurs in crystals with $x = 0.15$ and 0.20. Zero-field-cooled magnetization measurements show that all three compositions are also superconducting. The results strongly suggest a local coexistence of superconductivity and stripe order. Static stripes are not restricted to Sr-doped La_2CuO_4. Lee *et al.* [106] have demonstrated that incommensurate magnetic order occurs, with an onset very close to T_c ($42K$), in an oxygen-doped sample with a net hole concentration of ~ 0.15.

2.6 Stripes in $YBa_2Cu_3O_{6+x}$

If charged stripes are supposed to be connected to the cuprate superconductors, they should not only exist in $La_{2-x}Sr_xCuO_4$, but also in the other cuprate superconductors. The problem with $YBa_2Cu_3O_{6+x}$ and $Bi_2Sr_2CaCu_2O_8$ is that the magnetic correlation length in these systems is smaller than in $La_{2-x}Sr_xCuO_4$. This means that the width of the peaks in Fourier space is larger. Therefore, the two incommensurate peaks at $\pi - \delta$ and $\pi + \delta$ will start to overlap and it will look as if there is a single broad, flat topped peak around (π,π) with steep sides. Tranquada *et al.* [181] and Sternlieb *et al.* [170] noted that the q dependence of the line shape of $\chi''(q, \omega)$ for $YBa_2Cu_3O_{6.6}$ is more complex than a simple commensurately centered Gaussian. From this they inferred the possibility of incommensuration. However, this is indirect evidence.

For this reason, the direct observations of incommensurate magnetic scattering in

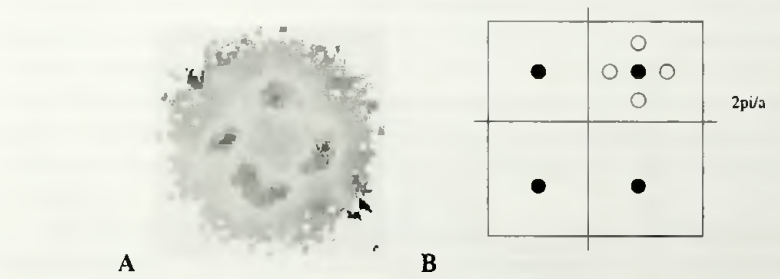

Figure 2.7: A: *Inelastic neutron-scattering data around the (π,π) reciprocal position in $YBa_2Cu_3O_{6.6}$ taken on the HET spectrometer of ISIS (Mook* et al. *[129]). The scattering took place in the superconducting state at $T = 13$ K with an energy transfer of 24.5 meV. The experimental result clearly shows the four peaks in Fourier-space caused by the stripes.* B: *Two-dimensional reciprocal space for the CuO_2 planes in the cuprates. The dots mark the $(\frac{1}{2},\frac{1}{2})$ and equivalent points at which magnetic Bragg scattering appears in the parent insulating compounds. The quartet of circles indicates the expected position of the peaks when there are stripes.*

$YBa_2Cu_3O_{6.6}$ is very important. Direct inelastic neutron-scattering measurements have been done by Dai *et al.* [51] and Mook *et al.* [129] on underdoped $YBa_2Cu_3O_{6.6}$. Dai, Mook and Dogan [51] reported low temperature q-scans at $\hbar\omega = 24$ meV that display well-defined double peaks. Low-frequency magnetic fluctuations in $YBa_2Cu_3O_{6.6}$ ($T_c = 62.7K$) change from commensurate to incommensurate on cooling, with the incommensurability first appearing at temperatures above T_c.

Measurements with improved q-resolution by Mook *et al.* [129] confirm this observation. The Mook data are one of the most accurate neutron-scattering results to date. They used the recently installed position sensitive detectors on the HET spectrometer at ISIS. This allowed images of the fluctuations to be recorded in the Cu-O planes of YBa_2CuO_{6+x}. In their case, $\delta = 0.21$ reciprocal lattice units. The orientation of the pattern is the same as in $La_{2-x}Sr_xCuO_4$. Furthermore the magnitudes of the incommensurability δ is indistinguishable for the same doping level in $La_{2-x}Sr_xCuO_4$, revealing a unifying feature in the magnetic fluctuations.

Neutron resonance

Because of the neutron-resonance in $YBa_2Cu_3O_{6+x}$, which does not seem to be present in $La_{2-x}Sr_xCuO_4$, the situation for $YBa_2Cu_3O_{6+x}$ is a little bit more complex according to Dai *et al.* [52]. At low-energy there are the above mentioned incommensurate peaks. However, for $YBa_2Cu_3O_{6.6}$ there is a sharp commensurate resonance at 34 meV . The incommensurability decreases with increasing energy close to the resonance (Arai *et al.* [14]). Therefore, underdoped $YBa_2Cu_3O_{6.7}$ has an incommensurate wave vector

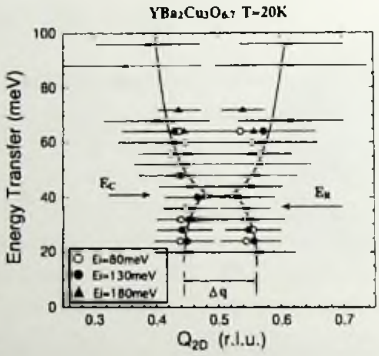

Figure 2.8: The energy dependence of the peak position of the incommensurate peaks projected along Q_{2d} in $YBa_2Cu_3O_{6+x}$ from Arai et al. *[14]. The separation (Δq) is about 0.16 reciprocal lattice unit in the Q_{2d} unit in the low-energy region, it shrinks around the energy E_c of the neutronresonance and then gradually increases above E_c. The solid line is just a guide to the eye. The horizontal bars stand for the FWHM of the peaks.*

dependence with "pillars" in the dispersion relation at the positions $(\frac{1}{2} \pm d, \frac{1}{2}, 0)$ and $(\frac{1}{2}, \frac{1}{2} \pm d)$. The pillar appears above an energy of 10 meV and has two legs centered on 0.4 and 0.6 reciprocal lattice units. The two incommensurate peaks merge at E_c. Even well above the superconducting transition temperature $T_c = 67K$, the magnetic response for the incommensurate peaks still exists.

Mook *et al.* [132] report that in the $Bi_2Sr_2CaCu_2O_8$ system, there are also indications of small incommensurate peaks. $Bi_2Sr_2CaCu_2O_8$ shows a peak at (π,π) in energy about 10 meV wide, which is equal to the energy resolution of the experiment at $10K$, while it has disappeared at $100K$.

2.7 X-ray diffraction

Just as for neutron-scattering, also for X-ray diffraction static pinned stripe order is needed for a diffraction pattern to be visible. X-ray diffraction is complementary to neutron-scattering. X-ray scattering has confirmed the existence of superlattice peaks due to charge order [198]. Zimmermann *et al.* [198] used high energy (120 keV) photon diffraction X-ray studies to see the stripe charge-order superlattice peaks in an $x = 0.12$ $La_{1.48}Nd_{0.4}Sr_{0.12}CuO_4$ sample. A similar $T_{\text{charge}} \approx 70K$ was found. Using the same method, charge-order superlattice peaks have also been found for $x = 0.15$ by Niemöller *et al.* [137]. The charge peaks vanish at a slightly lower temperature of $62K$, whereas the magnetic signal from neutrons is already suppressed at $45K$. Consistent with the idea

of pinning by the LTT lattice modulation, static stripe ordering within the CuO_2 planes appears at the transition temperature from the LTO to the LTT phase which is at $68K$. This is an important result, because high-field magnetization and muon-spin-rotation studies have indicated that bulk superconductivity exists in this sample below $10K$. Another conclusion of the μSR study is that static magnetic order is present throughout the entire sample volume. Thus it appears that stripe order and superconductivity coexist at $x = 0.15$.

At both Sr concentrations, charge ordering appears at a higher temperature than magnetic order. This seems to indicate that the ordering of spins and holes is driven by the charges. One might conclude that fluctuations of stripes set in if the pinning potential in the LTT phase is destroyed at the structural transition from LTT to LTO, as observed in the $x = 0.12$ sample. However, the idea that the LTT structure is required for charge-stripe order is challenged by the interpretation of the Cu NQR results in $La_{2-x}Sr_xCuO_4$ by Hunt *et al.* [93]. That work suggests that static stripes can occur even within the LTO phase, and that the ordering temperature continues to increase as x decreases below 0.12.

2.8 NQR wipeout

Diffraction experiments like neutron- and X-ray scattering only give good results if the system has long-range static order. For fluctuating stripes the signal will disappear. Indeed away from the robust $\frac{1}{8}$ region, detection of charge stripes by bulk scattering has proved difficult and up to now, no direct observation of charge-stripe order has been reported other than for $La_{1.48}Nd_{0.4}Sr_{0.12}CuO_4$ and $La_{1.45}Nd_{0.4}Sr_{0.15}CuO_4$. In order to see non-static stripes, a local probe is needed. One such local probe is Cu nuclear quadrupole resonance (NQR), which gives unique information about the charge environment at a Cu nuclear site. The resonance frequency is proportional to the electric field gradient at the Cu nuclear site, which is very sensitive to the charge environment. Therefore any change in the charge distribution within the CuO_2 plane directly affects the Cu NQR and hence Cu NQR is very sensitive to charge-stripes, even with short or poorly defined correlation lengths.

The integrated intensity of ^{63}Cu NQR in $La_{1.6-x}Nd_{0.4}Sr_xCuO_4$ decreases dramatically below the charge-stripe ordering temperature T_{charge}. The group of Imai [93, 169] claims that the missing fraction of the integrated intensity of the NQR signal represents the charge-stripe order parameter. They come to this claim by comparing this wipeout fraction with neutron- and X-ray scattering data about the stripe order parameter that are available. The wipeout fraction has identical temperature dependence for $x = 0.12$ and 0.15. Assuming that this relationship also holds for other doping levels, they extend the detection of charge-stripe order in $La_{1.6-x}Nd_{0.4}Sr_xCuO_4$ to the whole range $0.07 \leq x \leq 0.25$. They also establish that the transition is sharpest at $x = 0.12$. The

charge-stripe order continues to hold up to $x = 0.25$, where no static hyperfine fields have been reported by μSR. This implies that completely static spin-ordering is not a necessity for charge-ordering.

2.9 Coexistence of superconductivity and stripes

Tranquada *et al.* [178] observed stripes and superconductivity in the same sample. In their $x = 0.12$, 0.15 and 0.20 samples they reported the coexistence of static stripes and superconductivity, albeit with T_c's below $15K$. The inelastic neutron-scattering by Cheong *et al.* [42] and Thurston *et al.* [176] showed incommensurate peak splitting around the position of the antiferromagnetic peak of the undoped La_2CuO_4in the whole range of the superconducting phase ($0.05 < x < 0.25$).

Suzuki *et al.* [173] and Kimura *et al.* [100] performed neutron-scattering measurements on $La_{1.88}Sr_{0.12}CuO_4$ and found sharp *elastic* incommensurate magnetic peaks, without the use of Nd-doping. They also found that the magnetic transition temperature T_m, at which the magnetic peaks develop, is equal to T_c. The elastic magnetic peaks are observed at the same incommensurate positions as those of the magnetic inelastic peaks. Suzuki *et al.* [173] looked at $La_{2-x}Sr_xCuO_4$ with doping level $x = 0.12$ as well as for oxygen-doped $La_2CuO_{4+\delta}$ with a relatively high value of T_c ($42K$). It should be noted that both compounds do not show any indication of the LTT tilt modulation.

A question remains however, whether the samples might have had mixed phases, with some regions being superconducting and other manifesting stripe order. A natural question to ask is whether the stripe instabilities and superconductivity compete. In overdoped $La_{2-x}Sr_xCuO_4$ samples with $x > \frac{1}{8}$, static-stripe ordering is suppressed and superconductivity is robust. In that case one may conclude that they compete with each other. However, inelastic neutron-scattering measurements do indicate that low-energy dynamic stripe fluctuations extend beyond $x = \frac{1}{8}$. Furthermore, neutron-scattering on $La_2CuO_{4+\delta}$ by Lee *et al.* [106] report that the elastic spin-order intensity appears at the same temperature as the superconductivity, suggesting that the two phenomena are strongly correlated.

μSR

Doping holes into the Mott-Hubbard parent compound destroys the long-range antiferromagnetic order. However, short-range antiferromagnetic order over a few lattice spacings persists up to high doping levels. Muon spin rotation studies on $La_{2-x}Sr_xCuO_4$ have indicated that this short range antiferromagnetic correlated state coexists with superconductivity in the strongly underdoped regime for $0.05 < x < 0.1$ (Niedermayer *et al.* [136]). The μSR experiments suggests that in the ordered phase more than 95% of sample volume is antiferromagnetically ordered. The measured size of the Cu magnetic

moment is 0.2-0.3 μ_B, comparable with that in the undoped AF insulators. Therefore, local antiferromagnetism coexists with superconductivity in the same sample volume. Charge segregation into stripes provides an interesting way to reconcile these properties. Identical magnetic behavior is observed for both the single layer $La_{2-x}Sr_xCuO_4$ system and the bilayer $YBa_2Cu_3O_{6+x}$ compound. The consistency of these results suggests that the coexistence of superconductivity and antiferromagnetic order is an intrinsic property of the CuO_2 planes and not an artifact of chemical or structural impurities. The strength of the antiferromagnetic correlation is determined solely by the hole content of the CuO_2 planes and does not depend on the concentration of dopant atoms. Superconducting quantum interference device measurements by Ostenson *et al.* [144] suggest that superconductivity and stripe magnetic order coexist in these materials.

These observations directly reveal the persistent influence of the antiferromagnetic order as the doping level increases from the insulator to the superconductor. These modulated spin fluctuations persist in both the normal and superconducting state, with a suppression of their intensity occurring below T_c.

In $La_{2-x}Sr_xCuO_4$, long-range antiferromagnetic order is destroyed at $x \geq 0.02$. However, a recent muon-spin-rotation study by Niedermayer *et al.* [136] shows that the change in local magnetic order is much more gradual. At $T \leq 1K$, the average local hyperfine field remains unchanged even as long-range order disappears, and it decreases only gradually as x increases to ~ 0.07. In particular, local magnetic order is observed to coexist with bulk superconductivity.

Coexistence

The inference from the work of Suzuki and Kimura is that there is magnetic order at low temperatures in the superconducting state in $La_{1.88}Sr_{0.12}CuO_4$. The onset temperature T_m for the spin density wave order coincides with the superconducting transition temperature T_c in some cases. At a minimum, this demonstrates that the spin density wave and superconducting states are not mutually exclusive. Secondly, it is found that $La_{1.88}Sr_{0.12}CuO_4$ remains in the LTO phase down to the lowest temperatures measured and that any LTT phase, either short or long-range ordered, must be present in concentrations below the 1% level. This shows that magnetic order may occur whether the material is orthorhombic or tetragonal. However, it seems that having a hole concentration near $x = \frac{1}{8}$ is indeed fundamental for the static magnetic ordering. This also follows from the work of Yamada *et al.* [212], who showed that the low-energy dynamical coherence length is at a maximum for $x = \frac{1}{8}$.

As mentioned before, Suzuki *et al.* [173] and Kimura *et al.* [99] have observed elastic incommensurate peaks in $La_{0.188}Sr_{0.12}CuO_4$ in the LTO phase with an onset temperature of approximately T_c. Subsequently, incommensurate elastic peaks have also been observed in electrochemically-oxidized stage-4 $La_2CuO_{4+\delta}$ by Lee *et al.* [106], with the

onset also at T_c.

A final remark on where in the phase-diagram stripes can be found is that Borsa *et al.* [29] have been able to describe the low-temperature magnetization for doped antiferromagnetic $x < 0.02$ samples with a phenomenological spin-wave model where the magnetic domains are finite in one planar direction and bounded by segregated "charge rivers". This suggests that stripes exist in the phase-diagram of the cuprates essentially from $x = 0$ until $x = 0.25$.

2.10 One-dimensional conductivity

One would assume that the fact that stripes are one-dimensional systems would have an impact on the charge transport of striped cuprates. However, even if stripe order is present, the measured conductivity is likely to be isotropic because it averages over regions with different stripe orientations. Still, Noda *et al.* [138] have been able to show that charge transport in the underdoped samples is one-dimensional. To show this, they used the Hall effect. To measure the Hall effect, a sample is placed in a longitudinal electric field together with a transverse magnetic field. The magnetic field bends the conduction electrons aside, which leads to charge accumulation at one side of the sample. This can be measured as a transverse electric field. However, if the charges are confined on stripes, without the ability to hop to adjacent stripes, they cannot be bend by the magnetic field. Therefore there will be no Hall effect for one-dimensional transport, regardless of the orientation of the individual stripes.

Noda *et al.* [138] showed that the Hall voltage in $La_{1.6-x}Nd_{0.4}Sr_xCuO_4$ decreases sharply when the sample is cooled below the temperature where static stripes first appear. This is direct evidence that the electron motion indeed becomes one-dimensional in the presence of static stripes. The Hall effect is not suppressed in Nd-doped samples above the charge ordering temperature or in Nd-free samples at any temperature. For $x = \frac{1}{8}$ below the charge ordering temperature the Hall voltage decreases rapidly with T to become immeasurably small at temperatures $< 20K$. The decrease is sharpest around the $x = \frac{1}{8}$ doping where stripe order is believed to be most robust.

The interpretation seems unavoidable that the current flows as if the system is perfectly one-dimensional. Notice that in conventional quasi one-dimensional metals, the Hall voltage can become small but that it is usually still measurable. This perfect one-dimensionality also explains the complete lack of magneto-resistance in the non-superconducting state realized in large magnetic fields, as shown by Boebinger [26].

While the transversal current vanishes, the linear resistivity stays metallic-like. This is thus a state of two-dimensional electronic matter that is metallic in one direction and insulating in the other: a *quantum liquid crystal* is realized [103]. The charge dynamics is metallic despite the fact that nearly the entire sample is antiferromagnetically ordered, suggesting a spatial separation of the conduction paths from the spin domains. The

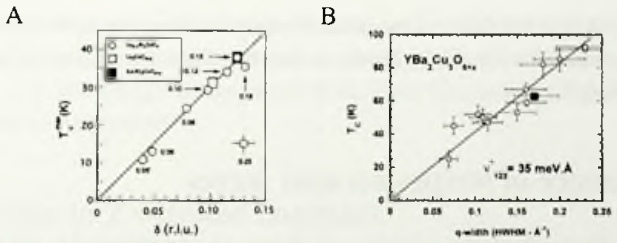

Figure 2.9: A: *The superconducting transition temperature T_c versus the incommensurate splitting δ for $La_{2-x}Sr_xCuO_4$ from Yamada* et al. *[212].* B: *Superconducting transition versus the half width at half maximum of the peak in the spin susceptibility for $YBa_2Cu_3O_{6+x}$ according to Balatsky and Bourges [17].*

charge dynamics also show a critical change upon increasing x across $\frac{1}{8}$, and in the highly doped materials the superconducting order seems to coexist with the static stripe order.

2.11 Linear relation between T_c and incommensurability

Another surprising result that indicates that there is a relationship between stripes and superconductivity is the linear relationship between the incommensurate peak splitting and T_c up to the optimal doping regime. Figure 2.9A shows the superconducting transition temperature versus the incommensuration δ for LaSrCuO superconductors by Yamada *et al.* [212]. The data plotted in this figure are completely free from any uncertainties connected with the doping level or oxygen stoichiometric in each sample. Furthermore, results from superconductors prepared by electrochemically oxygenation and heat treatment under high oxygen pressure fall on the same linear relation. This empirical result gives a direct relationship between incommensurate spin correlations and superconductivity in the underdoped samples. For the over-doped samples the T_c values deviate from the $\delta - T_c$ relation. This implies the existence of an inherent mechanism to degrade the superconductivity in the overdoped region.

For $YBa_2Cu_3O_{6+x}$ a similar linear dependence between T_c and the incommensuration has been found by Balatsky and Bourges [17]. A problem in this case is the fact that the distance between the stripes is not available experimentally, because the incommensurate peaks are not easily resolved in neutron-scattering. Therefore Balatsky and Bourges [17] looked at the q-width of the effectively commensurate peak at (π,π) under the implicit assumption that this must be related to the separation of the overlapping incommensurate peaks. They show that the q-width of the peak is linearly proportional to the superconducting T_c for the whole doping range as shown in figure 2.9B. Interestingly, the case where the incommensuration δ has been observed directly

by Mook *et al.* [129, 130] falls on the same linear plot. The only difference between the $La_{2-x}Sr_xCuO_4$ and $YBa_2Cu_3O_{6+x}$ results is that the slope for $La_{2-x}Sr_xCuO_4$ is smaller than for $YBa_2Cu_3O_{6+x}$.

2.12 Influence of stripes on spin waves

Another effect from which the existence of stripes can be inferred is the influence they have on the spin-wave velocity in the cuprates. The ordered charge stripes do not seem to affect the super-exchange energy within the antiferromagnetic domains. The picture that suggests itself is that of antiferromagnetic stripes interacting weakly across hole-rich domain walls. However, the stripes certainly will weaken the magnetic exchange coupling between neighboring magnetic domains. Castro Neto and Hone [35] have modeled this system in terms of a spatially anisotropic nonlinear sigma model, in which charged stripes cause the exchange coupling J to become anisotropic. For a large anisotropy, the velocity c for propagation parallel to the stripes is equal to $c_0/\sqrt{2}$. Inelastic neutron-scattering measurements on stripe-ordered $La_2NiO_{4.133}$ indicate that the low-energy spin excitations disperse away from the incommensurate peak positions with an effective spin-wave velocity that is 60% of that in undoped La_2NiO_4 for propagation parallel to the stripes. The dispersion is less well defined but comparable in the perpendicular direction. This is consistent with a reduction in the effective value of J due to relatively weak exchange coupling across domain walls. Inelastic measurements on $La_{2-x}Sr_xCuO_4$ [42] appear to be compatible with such a picture.

2.13 Charge- versus spin-driven stripe order

Stripe order is typically either "charge driven" or "spin driven". In the charge-driven case, spin order sets in at a temperature less than the charge ordering temperature. Both in the cuprates [183] and in the nickelates [41, 153] the holes order at a higher temperature than the spins and both transitions are second order, in agreement with a charge-driven scenario. Zachar *et al.* [223] conclude from this that the stripes which are found in these systems are formed by frustrated phase separation.

Fluctuations are not included in their mean field analysis, but they can change the picture drastically. Van Duin and Zaanen [191] argue that the difference between the charge- and spin-ordering temperatures is due entirely to the charge-ordering induced spatial anisotropy in the system. The reason for this is that the zero-temperature spin-system is three-dimensional, while the finite temperature spin-system is effectively two-dimensional because of the stripes in between. Because spins have a continuous symmetry, while charge is a discrete symmetry, the effect of the stripe induced anisotropy is much larger for the spin system than it is for the charge system. Also, the effect of

spatial anisotropy on the transversal spin fluctuations is much more drastic at finite temperatures than at zero temperature. Therefore, the Néel temperature is suppressed much more rapidly than the staggered magnetization. Thus fluctuations explain the different behavior of the two quantities.

2.14 Stripes in Zn-doped cuprates

The introduction of Nd leads to the LTT distortion which pins the stripe, resulting in incommensurate peaks in elastic neutron-scattering. There also is evidence for static stripes without introducing special modifications to the crystal structure. Light doping with Zn can also pin the charge and spin modulations. Zn substitutes for Cu in these systems. Because Zn hybridizes poorly with O atoms, it breaks local antiferromagnetic bonds. The holes can take advantage of the smaller number of bonds and localize close to the Zn sites. If the hole is part of a stripe, the whole stripe will get pinned, leading to static correlations. Measurements on Zn-doped $La_{1.86}Sr_{0.14}CuO_4$ have shown that the positions and widths of the incommensurate peaks are essentially unaffected by the presence of the Zn. Neutron-scattering results on a crystal of $La_{1.86}Sr_{0.14}Cu_{0.988}Zn_{0.012}O_{4-\delta}$ with $T_c = 19K$ by Hirota [92] showed elastic magnetic peaks in a superconducting crystal with $x = 0.14$, showing that the Zn doping does not modify the incommensurability of the magnetic scattering. In samples of $La_{2-x}Sr_xCuO_4$ with no static order, incommensurate splitting of the inelastic magnetic scattering is nearly identical to that of the elastic peaks in Nd-doped samples with the same Sr concentration. Zn-doped $YBa_2Cu_3O_{6+x}$ samples with a range of oxygen concentrations behave qualitatively similar to the $La_{2-x}Sr_xCuO_4$ case. It has been found by μSR and NMR studies that Zn suppresses superconductivity locally. This suggests that doping Zn into the CuO_2 planes destroys superconductivity by pinning the stripes.

2.15 Doping dependence

Stripes have now been observed essentially for all superconducting dopings in $La_{2-x}Sr_xCuO_4$. From these data, one can extract the doping dependence of the distance between the stripes. Yamada *et al.* [212] found incommensurate peaks for $x > 0.05$. For $0.06 \leq x \leq 0.12$ the incommensuration is approximately linearly proportional to x. A very similar trend is observed in hole-doped La_2NiO_4 [153]. This observation is easily explained by assuming that the density of holes on a stripe is a constant and that introducing more holes into the system by doping leads to a shorter distance between the stripes. From the slope of the distance against doping curve, one can see that the density of the holes on the stripe is equal to a $\frac{1}{2}$, leading to the picture of *quarter-filled* stripes, as shown in figure 2.4B. The fact that the charge density between 5% and 12% doping is

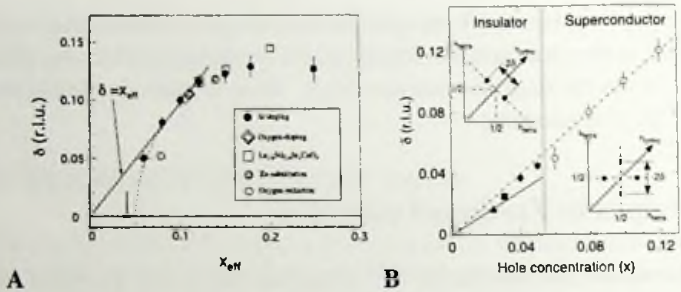

Figure 2.10: A: *The incommensurability* δ *versus the hole doping concentration x (the Yamada-plot, from Yamada* et al. *[212]).* B: *The same kind of measurements by Matsuda* et al. *[121] for smaller values of doping.*

constant means that in this region the density of holes on a stripe is constant. Therefore, stripes can not simply be regarded as a one-dimensional metal with an arbitrary density of charge carriers. Instead, the fact that the charge density is constant and commensurate with the lattice indicates that stripes are insulating.

For $x > \frac{1}{8}$, which corresponds to a distance of less than four atoms between two stripes, the incommensuration stays constant. The easiest interpretation of this experimental result is that the charge density on the stripe increases for these larger doping levels. It is difficult to imagine that stripes could be able to get closer together than four lattice sites, because the whole reason for the existence of stripes is the antiferromagnet surrounding them. If the stripes would have an average distance of only three sites, there would only be two sites between the holes, which probably is too small to maintain antiferromagnetic order between the stripes. Chapter 5 of this thesis proposes a different possibility to explain the experimental measurements. This explanation is based on the assumption that the hole density on the stripe will essentially stay constant, meaning that on large parts of the stripes the hole density will be exactly half. However, by introducing kinks into the stripes, locally a larger hole density can be created, which will be able to take up the extra introduced holes. In chapter 5 it is shown that if these kinks would all order in the same direction, they could be measurable as a small shift in the neutron-scattering peak positions. This shift, that can be measured experimentally, would as an extra bonus also give information about the charge ordering along the stripe.

Diagonal stripes

A surprising result has been found in neutron-scattering experiments by Matsuda *et al.* [121]: diagonal stripes in the cuprates. Their work is an extension of the Yamada plot down to 2%. They find that for $x < 5\%$ there are incommensurate peaks, related

to stripes, but the position of the peaks is rotated by 45°. This indicates that stripes in this doping range are diagonal. These results lead to the important conclusion that the static magnetic spin modulation changes from diagonal to vertical at $x = 0.05$. It shows that fundamental changes in the magnetic properties of $La_{2-x}Sr_xCuO_4$ take place at the insulator-to-superconductor doping transition.

Other neutron-scattering experiments on $La_{2-x}Sr_xCuO_4$ single crystals were performed by Wakimoto *et al.* [199] who found that elastic incommensurate magnetic peaks also appear at low temperatures in both insulating ($x = 0.02 - 0.05$) and superconducting ($x = 0.06$) samples. For $x = 0.06$, they found that the integrated intensity drastically changes across the low temperature insulator-superconductor boundary; the intensity of $x = 0.06$ is four times smaller than that of $x = 0.05$, while the intensity in the insulating region stays constant.

2.16 Are stripes conducting or insulating?

If the average hole concentration on each stripe is determined primarily by the competition between the Coulomb interaction and the local tendency to phase separation, the hole density per site along each stripe would be able to vary. In that case, stripes can be considered as one-dimensional Luttinger liquids, which may be intrinsically metallic, or even superconducting. However, if the stripes are a consequence of some sort of Fermi surface nesting, as is the case in the Hartree-Fock studies of stripe formation (see for instance Zaanen and Gunnarson [215]), the stripe period always adjusts precisely so as to maintain a gap or pseudogap at the Fermi surface: there is always one doped hole per two sites along each charge stripe.

Experimentally, there are indications that stripes are internally insulating. The stripes in the nickelates and the manganites are insulating, as we will see in the next section. The picture of exactly quarter-filled stripes also explains the insulating behavior of the cuprates at low temperatures (below T_c, when superconductivity is suppressed with a magnetic field) as found by Boebinger [26]. Charge commensuration is the only way for the lightly-doped antiferromagnet to insulate without impurity pinning.

The strongest evidence that charge stripes are incompressible, and therefore insulating, comes from the doping dependence of the incommensurate peak splitting. Because this relationship is strictly linear for doping levels smaller than $\frac{1}{8}$, this implies that the concentration of holes on a stripe does not change, but rather that the only effect of further doping is to change the concentration of stripes in a plane, bringing the stripes close together. The data for LaSrCuO are close to linear in the range $0.024 \leq x \leq 0.12$, despite the change in orientation from diagonal to vertical at $x = 0.05$.

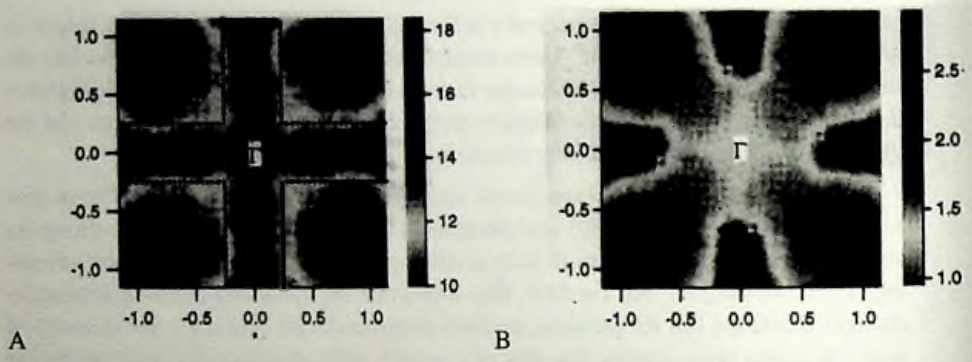

Figure 2.11: A: The ARPES 'holy cross' *from Zhou* et al. *[228]. It shows the integrated photo-emission intensity throughout the Brillouin zone. When integrating over the low energy excitations, two crossing one-dimensional bars are observed. B: Integrating over a larger energy window leads to a more two-dimensional structure.*

2.17 The *"Holy cross"*

The biggest problem of stripes is how to connect them to superconductivity. To make this connection, it is necessary to know more about the electronic structure of the systems. A direct way to look at the electronic structure is by using photo-emission spectroscopy. In Angle Resolved Photo-Emission (ARPES), light is used to eject electrons out of the system and the intensity of the ejected electrons as a function of energy and momentum is related to the underlying electronic structure.

ARPES is a direct way to see the occupation of the electronic states as a function of both momentum and energy. One can look at the intensity at a constant wavevector as a function of energy (EDC) or at constant energy as a function of momentum (MDC). However, one can also integrate over an energy range to obtain the electron occupation $n(k)$. This is what Zhou *et al.* [228] did in Nb doped $La_{2-x}Sr_xCuO_4$: the resulting plot, shown in figure 2.11A is often referred to as the "*holy cross*". The expectation from classical Fermi Liquid theory is that the occupied region will be a rotated square. The result of Zhou *et al.* [228], however, consist of two one-dimensional bars, indicating an underlying one-dimensional structure. The observed momentum distribution is strikingly consistent with the expectation for the quarter-filled one-dimensional bands associated with the quarter-filled stripes. However, by integrating over a smaller energy window, a strong dependence on the momentum perpendicular to the stripe direction is found (see figure 2.11B): a two dimensional structure appears. Concluding, ARPES yields evidence for one-dimensional structures in cuprates.

2.18 Other stripe systems

Nickelates

The first evidence for the existence of stripe correlations was not found in the cuprates, but instead in the closely related nickelates. Tranquada *et al.* [180] observed incommensurate magnetic ordering by neutron-scattering measurements in $La_{2-x}Sr_xNiO_{4+\delta}$. This was followed by electron diffraction measurements (Chen *et al.* [41]) showing indications of charge order. In the nickelates, nickel takes the place of copper. The nickelates have practically the same chemical structure as $La_{2-x}Sr_xCuO_4$. In contrast to the cuprates which become superconducting at more than 5% doping, the nickelates remain insulating up to very high Sr concentrations. Another difference is the effective spin in the planes. For the cuprates this is spin-$\frac{1}{2}$, while the nickelates have spin-1. The difference between the nickelates and the cuprates is probably caused by the larger effect of the electron-phonon coupling and the stronger magnetic localization (less important spin fluctuations) of a $S = 1$ system. As in the cuprates, the temperature dependence of the incommensurate peaks suggests that the magnetic order is driven by the charge order.

The nickelates have stripes that run diagonally with respect to the Ni-O bonds, as indicated by the positions of the charge-order and magnetic superlattice peaks observed by electron [41] and neutron-diffraction. The charge order peaks have also been observed by Vigliante *et al.* [196] by X-ray diffraction. Just as in the cuprates, the period of the spin structure in real space is twice that of the charge modulation. Experiments on a range of samples show that $\delta \approx n_h = x + 2\delta$ at low temperature.

Both in Sr and in oxygen doped samples, the incommensurate splitting is temperature dependent ([179] and [182]). This suggests that competing interactions are involved in the ordering. For $La_2NiO_{4+\delta}$ with $\delta = 0.125$ [180] and with $\delta = 0.1333$ [208] not only the magnetic first and third harmonic Bragg peaks were found, but also the second harmonic peaks associated with charge ordering. Analysis of the higher-order magnetic satellites provides evidence that the stripes are relatively narrow.

A single-band Hubbard model properly describes a spin-$\frac{1}{2}$ system. In order to describe a spin-1 system, Zaanen and Littlewood [217] did three-band Hubbard-model calculations at zero temperature using a mean-field approximation. The observed low-temperature hole density within the stripes is consistent with their work. They found that electron-phonon couplings tend to reinforce the stability of charged domain walls in an antiferromagnetic background. If the hole concentration in the nickelate stripes were precisely 1 hole per Ni site, then this would be equivalent to a half-filled one-dimensional system. The domain-wall states then form a half-filled one-dimensional band, which is unstable to a Peierls distortion. Such a distortion creates a gap at the Fermi level, explaining the insulating behavior. The experimental findings are consistent with the outcomes of this simple mean-field theory. The disproportionately large effect

of the rather small elemental electron-phonon couplings in the nickelates is explained in terms of a positive feedback between electron-phonon coupling and Zhang-Rice localization, as tuned by the splitting between the oxygen $2p$ and the lower Hubbard band. At large dopings, the residual interactions between the polarons leads to ordering into polaron lattices, but at low dopings the electronic localization proceeds better in domain wall textures.

Manganites

Besides the cuprates and the nickelates, manganites also manifest a spontaneous ordering of charges into lower dimensional structures. The manganite perovskites ($La_{1-x}Ca_xMnO_3$) exhibit charge ordering by forming *layers* of Mn^{3+} in between layers of Mn^{4+} (see for instance Hervieu *et al.* [91]). The transport and magnetic properties of these oxides are strongly correlated to the formation of this charge ordering. The manganites attracted attention because of the "colossal" magnetoresistance near the ferromagnetic spin-ordering transition. They can display over two orders of magnitude changes in electrical resistance when an applied magnetic field changes by a few Tesla. The reason for this is that the antiferromagnetic to ferromagnetic transition in the manganites is accompanied by a commensurate to incommensurate charge-ordering transition. The coexistence of ferromagnetism and charge ordering in $La_{0.5}Ca_{0.5}MnO_3$ results from an inhomogeneous spatial mixture of incommensurate charge-ordered and ferromagnetic charge-disordered micro domains. The manganese oxides turn out to be particularly good materials in which to explore stripe phases because any charge ordering produces comparatively large lattice distortions, which are more easily seen than those in the other transition metal oxides.

In the charge-ordered phase of the manganites with $x \geq 0.5$, the ordered Mn^{3+} stripes form pairs of Mn^{3+} stripes, which have large lattice contractions due to the Jahn-Teller effect. Those pairs of stripes are separated periodically by stripes of non-distorted $Mn^{4+}O_6$ octahedra. Because of the large Jahn-Teller effect leading to large crystal distortions and the two-dimensional structure of the bi-stripes, high-resolution transmission electron microscopy at low temperatures by Mori *et al.* [133] has been able to show real-space pictures of the charge localization. For $x \geq 0.5$ these pictures show pairing of charge stripes. Two stripes form a stable bi-pair and these pairs repeat periodically. A dark-field imaging technique has provided real-space images of the charge-ordered domains (Chen and Cheong [40]).

Quantum Hall systems

Another system that has unexpectedly shown stripe-like behavior are the quantum Hall devices. At low temperatures, the longitudinal resistivity of these devices spontaneously develop a very large anisotropy (Lilley *et al.* [109] and Du *et al.* [66]). When a high

mobility two-dimensional electron gas is subjected to perpendicular magnetic fields of intermediate strength, such that multiple Landau levels are occupied, the resultant transport properties are strongly anisotropic. Fradkin and Kivelson [80] have used a mean-field calculations for the two-dimensional electron gas in a large magnetic field with a partially filled Landau level to find "stripe-ordered" charge density wave ground-states.

2.19 Remaining experimental questions

There are a number of experimental questions that have not been answered yet, but for which the answer would give important input to the theoretical description of stripes. The first is whether stripes are bond-centered or site-centered. This is related to the fact whether one should think of a stripe as being one or two sites wide in the strong coupling limit.

Another important point is to know whether the current in a superconductor is flowing along the stripes or perpendicular to the stripes. This has not been determined yet because of the alternating horizontal and vertical layers of stripes. The experiment by Noda *et al.* [138] only shows that the conductivity is one-dimensional, not in what direction. To answer this question, one would probably have to create a sample for which all stripes would be oriented in the same direction. The perovskite structure and LTT deformations conspire to make the alternation of stripes in different layers energetically favorable. However, by making some modifications to the crystal structure, it might be possible to find a structure where all stripes want to be in the same direction. Mook *et al.* [131] showed data on partially de-twinned $YBa_2Cu_3O_{6+x}$ crystals, where two of the four incommensurate peaks become stronger and two weaker. The claim is that in totally de-twinned $YBa_2Cu_3O_{6+x}$ all stripes point in the same direction (no alternation between layers). One could determine this direction by doing neutron-scattering (there will be only two peaks instead of four peaks). And then one could try to measure the current along the a and b axis and determine the anisotropy.

There has been a suggestion by Ando [13] that applying a magnetic field would be able to orient the stripes. They measure the in-plane magnetoresistance and find an anisotropy upon rotating the magnetic field H within the CuO_2 plane. They claim this is caused by the rotation of the stripes forced by the external magnetic field. It is however difficult to imagine a process in which one has to simultaneously rotate all stripes in a layer by 90 degrees. However, if it is possible, this would really be a crucial experiment. Theories that assume that stripes are one-dimensional Luttinger liquids, naturally assume the current to be flowing along the stripes. However, a new theory by Zaanen concentrates on the end-points of stripes and defines these as new quasi-particles. These end-points would move perpendicular to stripes along glide planes and therefore the current would be perpendicular to stripes.

Another important experimental confirmation of stripes could come from real space

images of stripes. There are real-space images for manganites from Mori *et al.* [133]. De Lozanne has claimed to have obtained the first image of stripes in $YBa_2Cu_3O_{6+x}$ by Scanning Tunneling Microscopy. However, the problem is that it is more likely that what he has found are moving oxygen atoms in the $YBa_2Cu_3O_{6+x}$ chains. The problem for these sensitive surface probes is that the stripe layers are not directly at the surface.

2.20 Conclusion

This chapter has shown part of the evidence for the existence of stripes in the cuprates. The concept of stripes was found to be quite general: stripes do exist in cuprates, nickelates, manganites and Quantum Hall effect samples. The strong focus on stripes in the cuprates is caused by the fact that they compete and coexist with the superconducting state. In the cuprates, stripes are caused by the dynamics of holes moving in an antiferromagnet. Although most evidence for stripes is found in $La_{2-x}Sr_xCuO_4$, there are now also strong indications for their occurrence in YBa_2CuO_{6+x} and in $Bi_2Sr_2CaCu_2O_8$. There is also ample evidence for the coexistence of stripes and superconductivity in the same samples. Furthermore, T_c is inversely proportional to stripe spacing in both $La_{2-x}Sr_xCuO_4$ and $YBa_2Cu_3O_{6+x}$. This establishes an intimate relation between the magnetism and the transport properties in the high-temperature copper oxide superconductors. In order to look more closely at the properties of stripes, the next chapter will look at the results for half-filled and quarter-filled stripes that follow from a Hartree-Fock approximation to the Hubbard model.

Chapter 3

Stripes in the Hubbard model

Stripes were first predicted by Zaanen and Gunnarson using mean-field theory. For filled stripes, there are four different kind of stripes possible: bond-centered and site-centered, and horizontal or diagonal. Using mean-field theory, the properties of these stripes (their magnetic and charge width, their energy) can be investigated. Experimentally, quarter filled stripes are seen. These are local stable solutions in mean-field theory. Quarter filled stripes have more than one on-stripe possibility and are therefore more interesting than half-filled stripes. A number of people have criticized the use of mean-field theory in such a strongly correlated system. To investigate this, we compare in this chapter the results of Numerical solutions of the Hartree-Fock equations to Density Matrix Renormalization Group, Slave-Boson and Monte Carlo methods. This shows that although the detailed numerical results (the stripe widths, the energies, the value of the staggered magnetization) might differ, the general phenomena of stripe formation follows already from mean-field theory.

3.1 Hubbard model

The first evidence for stripes was coming from numerical work by Zaanen and Gunnarson in a three-band Hubbard model, treated in mean-field approximation [215]. Further investigation showed that stripes can theoretically also occur in one-band Hubbard models. Also, more extensive numerical methods, like Gutzwiller-projections, Monte-Carlo simulations and DMRG calculations have shown that numerically stripes indeed can exist in a one-band Hubbard model.

The Hubbard model is the simplest model that allows us to look at stripe formation. What is essential for the formation of stripes is the fact that the electrons are able to hop and that there is interaction between the electrons. The Hubbard model is the simplest model that contains both ingredients and so allows us to do some calculations. The

Hubbard model was introduced by Hubbard in 1957. It consists of a hopping part, which allows the electrons to hop from one site to a nearest neighbor site. The second term is the interaction term between electrons at the same site. Because electrons are fermions, there can not be two electrons with the same spin on the same site. However, electrons with opposite spin can be on the same site. This gives rise to the Hubbard interaction term. There is no long range Coulomb repulsion. So there is a kinetic term and a potential term in the Hubbard model:

$$H = -t\sum_{i\sigma\delta} c^{\dagger}_{i,\sigma}c_{i+\delta,\sigma} + U\sum_{i} n^{\uparrow}_{i}n^{\downarrow}_{i}, \tag{3.1}$$

were $n^{\uparrow}_{i} = c^{\dagger}_{i\uparrow}c_{i\uparrow}$. We have to sum over σ, the spin of the electrons, because both spin up and spin down electrons can hop. Furthermore, i is a site on the one-dimensional or two-dimensional lattice and δ are its nearest neighbors. There are two parameters in the model, t and U. t describes the strength of the hopping, U the strength of the interactions. Only the ratio U/t is important. Notice that there is no need for an interaction between electrons with the same spin on the same site, because this cannot happen because of the Pauli principle. The Hubbard U keeps electrons with opposite spin from occupying the same site. This leads to a antiferromagnetic groundstate.

Solving this problem means finding the eigenstates $\phi_n(x)$ that solve the Schrödinger equation $H\phi_n = \varepsilon_n\phi_n$. If the eigenstates are known, we can calculate the energies, the correlation functions, the Greens functions *etc.* However, this problem is impossible to solve analytically. This is because the interaction term couples all the electrons together. Or, put differently, the interaction term consists of four operators $(c^{\dagger}_{i\uparrow}c_{i\uparrow}c^{\dagger}_{i\downarrow}c_{i\downarrow})$.

For one dimension, there is a solution by Lieb and Wu using the Bethe Ansatz [108]. The Hubbard model has been impossible to solve in two dimensions. To be able to do a calculations in two dimensions, it is necessary to make some approximation. The hopping term is not the problem. If there is only hopping and no interaction between the electrons, than the model is almost trivial to solve through a Fourier transform. The complication is coming from the interaction term.

3.2 Mean-field approximation

Because an analytic solution is not possible, people have turned to numerical techniques to find answers to the questions about the Hubbard model. In essence there are three different numerical techniques: exact diagonalization, quantum Monte Carlo methods and approximate solutions like the new technique called DMRG.

A mean-field theory has a strong tendency to predict ordered phases, not a disordered or highly fluctuating fluid-like phase. At least in the so-called nickelates this mean-field picture of an ordered array of domain walls seems to apply quite well. Indeed, it can be argued that these systems are much closer to the classical or mean-field limit than

the cuprates, for which fluctuation effects appear to be much stronger (see Zaanen and Littlewood [217]).

Spin rotational invariance not important

Shraiman and Siggia [167, 168] look at the motion of holes in a locally Néel ordered antiferromagnet. It appears that beyond a critical value of the coupling of the holes to spin waves, the holes prefer to have their dipole moments aligned. This results in the formation of a "spiral" phase, characterized by a uniform planar rotation of the staggered magnetization with an incommensurability wave number scaling like the density of holes. Dombre [65] also looks at the modulated spiral phases in doped quantum antiferromagnets, in the regime of coupling constant where the effective spin wave stiffness is negative. For their work, it is important to take the rotational symmetry of the spin into account. However, numerous calculations with advanced methods have shown that in the regions of phase-space were stripes are found, that the rotational symmetry of the spin is not very important.

Mean field approximation

Mean field theory is a method of simplifying a model to be able to get some approximations to the physics of a model. In this case, we look at one electron as it moves through the lattice. In the Hubbard model it feels the influence of the other electrons if it is at a position in space were there is also another electron of the opposite spin. So, either there is a repulsion with energy U or there is no repulsion. In mean-field theory we assume that the electrons are moving so fast, that we can describe the interaction of an electron with all the other electrons by looking at the *average* occupation of a site instead of the actual occupation which varies discontinuously in time, either being one or zero. However, the average can be any number between zero and one.

A lot of people feel that mean-field theory does not give a valid description of a model. This feeling is based on the fact that for instance in statistical mechanical problems like the two-dimensional Ising model, mean field theory predicts wrong critical exponents. However, this difference between mean-field results and the exact results is only large right at the critical point. As soon as one is away from the critical point, where there are large fluctuations, mean-field theory gives a valid result. If one is far into the ordered state, the critical fluctuations can be neglected and mean-field theory is very good. Mean-field theory is very good at describing the collective degrees of freedom in a system of interacting, massive particles. If one (or more) modes acquire the status of order parameter, the system becomes classical. As long as this order parameter exists, semiclassics is qualitatively correct and the true ground state of the system may be reached by perturbative means. This theory underlies our understanding of the standard solid state, ranging from crystalline order to superconductivity.

In our mean-field approximation, we write $n = n^{\uparrow} + n^{\downarrow}$ and $m = n^{\uparrow} - n^{\downarrow}$. This way we can write $n^{\uparrow}n^{\downarrow} = \frac{1}{4}(n^2 - m^2)$. We now make the assumption that we are in a strongly ordered state (which stripes are). We assume that the charge density operator and the magnetic-density operator working on all wavefunctions gives approximately the same result everywhere. So, we can write $n = \langle n \rangle + \delta n$ and $m = \langle m \rangle + \delta m$. We than have

$$\frac{1}{4}(n^2 - m^2) = \frac{1}{4}(\langle n \rangle^2 + 2\langle n \rangle \delta n + \delta n^2 - \langle m \rangle^2 - 2\langle m \rangle \delta m - \delta m^2). \tag{3.2}$$

Neglecting $\delta n^2$and δm^2 leads to

$$n^{\uparrow}n^{\downarrow} \approx \frac{1}{4}(\langle n \rangle^2 + 2\langle n \rangle \delta n - \langle m \rangle^2 - 2\langle m \rangle \delta m). \tag{3.3}$$

Using $\delta n = n - \langle n \rangle$ and $\delta m = m - \langle m \rangle$, we can rewrite the last equation as

$$n^{\uparrow}n^{\downarrow} = \frac{1}{2}(\langle n \rangle - \langle m \rangle)n_i^{\uparrow} + \frac{1}{2}(\langle n \rangle + \langle m \rangle)n_i^{\downarrow} - \frac{1}{4}(\langle n \rangle^2 - \langle m \rangle^2). \tag{3.4}$$

Now, the Hubbard interaction depends on the two order parameters and linearly on $n_i^{\uparrow}$ and $n_i^{\downarrow}$.

In order to simplify the notation, from now on we will focus on a one-dimensional case with N_x lattice points. With the above Hartree-Fock approximation, we can write the Hubbard Hamiltonian as a sum of three terms: $H = H_{\uparrow} + H_{\downarrow} + H_{dc}$, with

$$\begin{aligned} H_{\uparrow} &= -t\sum_{x=1}^{N_x}(\hat{c}_{x\uparrow}^{\dagger}\hat{c}_{x+1\downarrow} + \hat{c}_{x\uparrow}^{\dagger}\hat{c}_{x-1\uparrow}) + \frac{U}{2}\sum_{x=1}^{N_x}(n_x - m_x)\hat{n}_{x\uparrow}, \\ H_{\downarrow} &= -t\sum_{x=1}^{N_x}(\hat{c}_{x\downarrow}c_{x+1\downarrow} + \hat{c}_{x\downarrow}\hat{c}_{x-1\downarrow}) + \frac{U}{2}\sum_{x=1}^{N_x}(n_x + m_x)\hat{n}_{x\downarrow}, \\ H_{dc} &= -\frac{U}{4}\sum_{x=1}^{N_x}(n_x^2 - m_x^2), \end{aligned} \tag{3.5}$$

Except for the labeling with up and down arrows and a change of - to +, $H_{\uparrow}$ and $H_{\downarrow}$ are equal and both are independent of each other. So, we have to diagonalize two independent problems. H_{dc} is usually called the 'double counting' term, because we have to subtract that energy. Although we succeeded in reducing the complexity of the problem, these Hamiltonians are still difficult to solve in general. In the next sections, we will look at results from numerical diagonalization of these Hamiltonians in real-space.

3.3 Numerical mean-field solutions

A homogeneous antiferromagnet in one dimension is one of the few problems that can be exactly solved. The reason it can be solved is that it is possible to do a Fourier transform, because the effective potentials in the interaction term do not depend on position. In general, this is not possible, especially with stripes, which are localized structures in real space. What one has to do then, is numerically diagonalize the $H_\uparrow$ and $H_\downarrow$ Hamiltonians and fill the energy levels with electrons. One has to construct the $H_\uparrow$ and $H_\downarrow$ Hamiltonians in a *real-space* basis. Those Hamiltonians have to be diagonalized and then the lowest eigenstates have to be filled with electrons. What one has to keep in mind though, is that the Hamiltonians depend on the average electron density and magnetization, which depend on the filled eigenstates. However, these have not yet been calculated. So, this is a kind of chicken and egg problem. One can solve this by doing a *self-consistent* calculation. We start with some initial profile for the electron-density n_e and magnetization m. Then the program calculates the eigenstates, fills the filled eigenstates and from this calculates the new electron-density and magnetization. These new values, combined with a certain fraction of the input values, are then again used to find the new eigenstates etc., until the difference between input and output is negligible. If the system is N_x times N_y sites, we have to diagonalize only a square matrix of dimension $N_x \times N_y$.

The numerical procedure consists of a few steps:

1. Take starting values for $n(i,j)$ and $m(i,j)$ and initialize them.
2. Calculate the hopping matrix by looking at which sites are connected to each other (being nearest neighbors), taking into account the boundary conditions.
3. Calculate the diagonal elements for the spin up and the spin down problem: $\frac{U}{2}(n(i,j) - \sigma(-1)^{i+j}m(i,j))$.
4. Calculate the eigenvectors and eigen-energies of the spin up and the spin down problem.
5. Use the eigenvectors of the filled eigenstates to find the average occupation numbers $n(i,j)$ and magnetization $m(i,j)$.
6. Calculate the total energy, magnetization, width of stripes etc.
7. Repeat step 3-6 until the total energy and n and m converge.

This process is repeated with increasing system size until the boundaries can be ignored. If $U \downarrow 0$, then large system sizes are needed. The most important parameters which can be varied for every calculation are the value of U/t, the dimension of the system, the

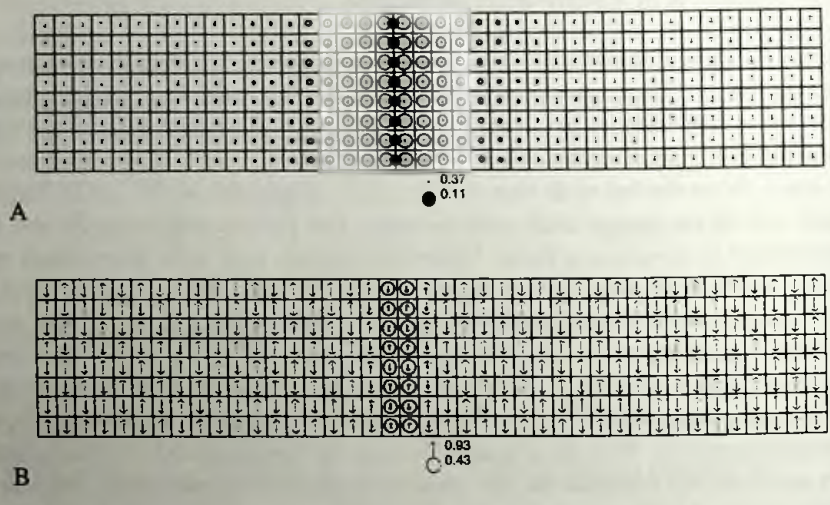

Figure 3.1: Vertical bond-centered stripes in a 41 by 8 system. Figure A has $U = 2t$ and figure B has $U = 10t$. The size of the holes and the arrows is proportional to the local charge and spin density.

boundary conditions and the initial magnetization and total electron density profile. The calculation is constrained in the sense that we demand that the number of spin up electrons is equal to the number of down electrons. So we always find an antiferromagnetic overall magnetization.

3.4 Half-filled stripes

Figure 3.1 shows the results from a mean-field calculation for two bond-centered vertical stripes. In this figure, the circles indicate the hole-density and the arrows indicate the magnetization. For small values of U, the stripe is very wide. For large values of U, the stripe is almost localized on two rows. The stripe does not disturb the surrounding antiferromagnet significantly. The same calculation can also be done for site-centered and for diagonal stripes.

In the Hartree-Fock Hubbard model, the total energy of a system with a stripe is always lower than that of a homogeneous antiferromagnet with the same number of holes (the binding energy is positive). Figure 3.2 shows the charge- and the staggered magnetization profile for a one-dimensional stripe.

For large values of U/t the change in the magnetization is almost a step function and the hole is basically localized on one site. However, if the value of U decreases, the

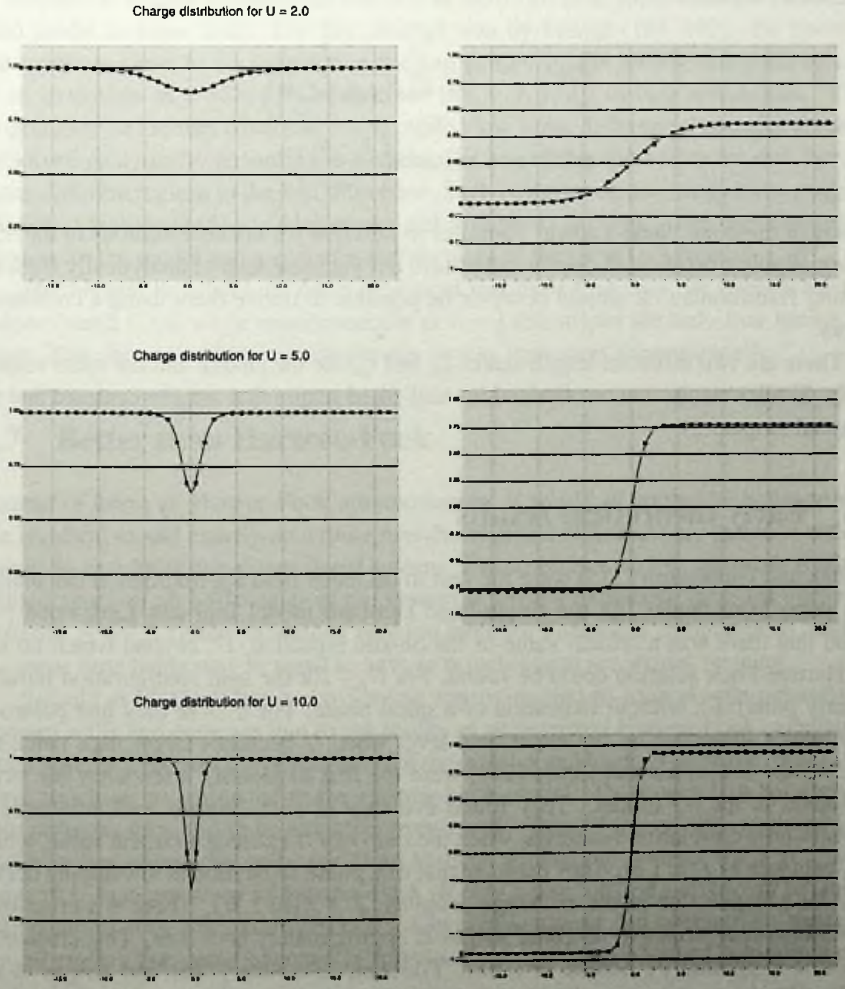

Figure 3.2: A cut-through through a vertical bond-centered stripe in a 41×8 *system for* $U = 2t$, $U = 5t$ *and* $U = 10t$. *Both the charge profile and the staggered magnetization profile are shown. The lines in the figure are fits to equation 3.6.*

step in the staggered magnetization becomes more gradual and the hole is not localized anymore on one site. For small values of U/t the profile for $n(x)$ and $m(x)$ can be described very well by

$$\begin{aligned} n(x) &= 1 - \frac{1}{\pi\xi_n}\frac{1}{\cosh\left(\frac{x-x_0}{\xi_n}\right)} \\ m(x) &= m_0 \tanh\left(\frac{x-x_0}{\xi_m}\right) \end{aligned} \tag{3.6}$$

Although these are "well-known" formulas to describe for instance solitons in the SSH theory of poly-acetylene, those formulas have not yet been derived analytically from the starting Hamiltonian. It should however be possible to derive them using a continuum theory.

There are two different length scales ξ_n and ξ_m for the charge and the spins respectively. Similar results can be obtained for half-filled stripes that are site-centered and for diagonal stripes.

3.5 Early theoretical results

Zaanen and Gunnarson [215] were the first to do mean-field approximation calculation in a three-band model. In the single-band Hubbard model Inui and Littlewood [94] found that there was a critical value of the on-site repulsion, U, beyond which no stable Hartree-Fock solution could be found. For $U \leq 20t$ the spin configuration remains linearly polarized, without indication of a spiral phase. For $U > 8t$ they find polarons, thus stripes disappear on the mean-field level when U becomes larger than twice the bandwidth. Prelovsek and Zotos [149] were the first to identify a tendency for stripe formation in the t-J model. They found evidence of such domain wall structures in the hole-hole correlation functions, when the ratio of J/t exceeds a critical value, which they estimate as $J_c \approx 1.5t$. They estimate that true phase separation at low doping occurs only for a large value of the exchange coupling, $J > J_s(\approx 2.5t)$. There is a cross-over from horizontal stripes to diagonal stripes at approximately $U = 3.6t$. This cross-over was first suggested by Schulz in [161]. Poilblanc and Rice [146] find stripes in the Hartree-Fock approximation to the Hubbard model with $U = 16t$.

3.6 Analytical theoretical results

Although the stripe instability has been thoroughly studied numerically, the qualitative understanding of the mechanism behind the instability is far from complete. The problem is that this instability has escaped an analytic treatment up to now. The existing

theoretical evidence for stripes is coming from numerical calculations of the one-band Hubbard model with intermediate U/t. Thus far, there have only been a small number of attempts at finding an analytical solution to the mean-field approximation of the Hubbard model in some limit. The first attempt was by Schulz [161, 162]. He linearized the spectrum close to E_F (neglecting the gap caused by the antiferromagnet) to arrive at an extension of a SSH-like model (see [88, 171, 172]) to two dimensions. These Bogoliubov-de Gennes equations (two coupled first order differential equations) can not be solved analytically according to Schulz. His reason for this claim are that there are many different regions in the Brillouin zone. Each of these regions needs its own approximation. Machida [115] and Matveenko and Mukhin [124] look at the one-dimensional version for the model and arrive at wavefunctions of the form $(a + b\tanh k_0 x)e^{ikx}$.

The biggest drawback of these analytical results is that they are correct for wide stripes (small U/t), while experimentally at $x = \frac{1}{8}$ the stripes are only four lattice sites apart. This shows that lattice scale physics is very important experimentally.

3.7 Better than Hartree-Fock

Instead of using an Hartree-Fock approximation, it would of course be better to solve the Hubbard model exactly on a finite two-dimensional lattice and try to extrapolate the results to an infinite two-dimensional system. The problem with this approach is that the Hilbert space of all basis-states of the system is already extremely large for very small systems. A 6×6 system is already way too large for numerical computations, while at the same time being way to small to have to possibility to see stripes forming.

Seibold *et al.* [164] use a slave-boson approximation to look at spin polarons and domain walls and compare that to the results of unrestricted Hartree-Fock calculations. Their approach reduces the polarization of these states and leads to increased delocalized wave functions as compared to the Hartree-Fock model. The interaction between two spin polarons turns out to be attractive over a wide range of the on-site repulsion U. In addition they obtain the crossover from vertical to diagonal domain walls at a higher value of U than predicted by Hartree-Fock ($U/t \simeq 3.6$ or 3.8 and a crossover to isolated spin polarons at $U \simeq 8t$). Hartree-Fock stripes are too narrow, but qualitatively the results are all right. The same conclusion follows from Quantum Monte Carlo simulations [6, 82, 149, 189].

Giamarchi and Lhuillier [81] use variational Monte Carlo on the two-dimensional Hubbard model. They find that the Hartree-Fock states are too high in energy. Hartree-Fock overestimates antiferromagnetic order to reduce the Hubbard repulsion. Within Hartree-Fock, the only mechanism avoiding double occupancy in order to reduce the Hubbard repulsion is to renormalize the spin-dependent on-site energy. Therefore the commensurate antiferromagnetic phase displays as an alternating shift of the spin-up and spin-down one-particle levels, respectively, which overestimates by far the polarization

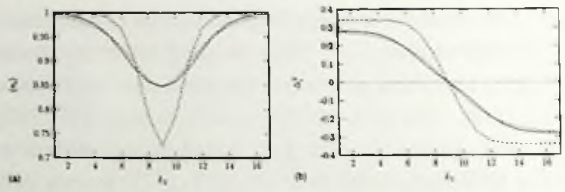

Figure 3.3: Charge- (a) and spin- (b) density profiles in the x direction for a vertical domain wall on a 17×4 *lattice. Solid lines are for the slave-boson approximation. Dashed lines: Hartree-Fock approximation; short dashed:* cosh *for charge and* tanh *for spin functional fit to the SB solution. (From [164]).*

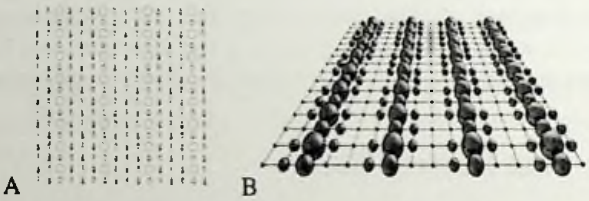

Figure 3.4: The results for a quarter-filled $4k_F$ *stripe from mean-field theory. Figure A shows the charge and magnetic structure, where the radius of the circles indicates the hole density and the size of the arrows the size of the magnetization. In figure B only the charge density is shown to illustrate the four-fold periodicity along the stripe.*

of the antiferromagnetic order.

Figure 3.3 shows the charge- and spin-density profile of a vertical domain wall calculated with unrestricted Hartree-Fock and Slave Boson approximations, respectively. The dip in the Hartree-Fock charge profile is nearly twice the value of the Slave Boson approximation. The Hartree-Fock theory only renormalizes the spin dependent on-site energies. Note that the Hartree-Fock method always leads to a very large spin polarization, since this is the only way within this approximation to minimize the on-site repulsion. From this we can conclude that the numbers for the energy, the width etc, that follow from Hartree-Fock, are not very accurate. However, the essence is still present in Hartree-Fock calculations.

3.8 Quarter-filled stripes

Experimentally, stripes in the cuprates are not half-filled, but quarter-filled. This means that there is one hole per two stripe sites. They therefore have an internal structure. Zaanen and Olés were the first to study stripes phases that were quarter-filled [219].

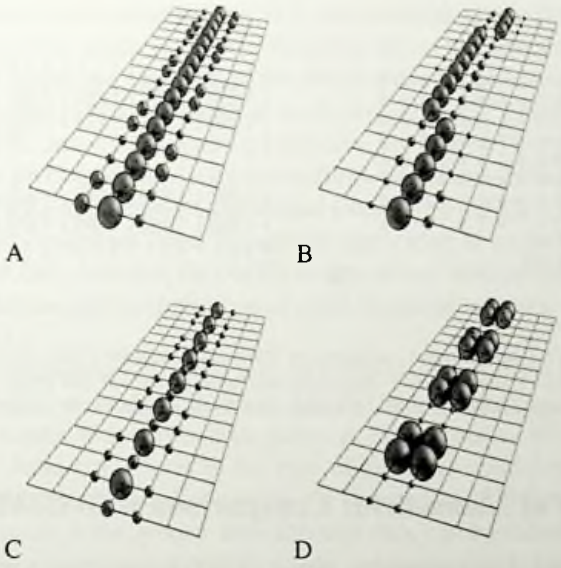

Figure 3.5: Possible configurations of completely filled stripes. Only the charges are shown.

The half-filled stripes are the ground state for the Hartree-Fock Hubbard model. The quarter-filled stripes are not the lowest energy states, but they are meta-stable.

Figure 3.5 illustrates four different kinds of half-filled stripes that are stabile in mean-field calculations of the extended Hubbard model. A lot of different extensions are possible, but these are the ones most frequently discussed in the literature. They all have an on-stripe periodicity of four lattice constants. They also have almost the same energy. Zaanen and Gunnarson were the first to find the A and D version of half-filled stripes. Seibold *et al.* found configurations B and C. Notice that there is always a periodicity of four along the stripe. The reason for the stability of stripes is that an additional symmetry breaking occurs, corresponding with a *quadrupling* of the period on the walls. They all have a period of four lattice constants along the stripe (if you also look at the spins). A has a homogeneous hole density along the stripe (not on the sides), B has two kinks, C and D have a charge modulation. D has units with a charge of two. All these configurations have almost the same energy. The difference in energy is in the order of $0.001t$ per hole, which is very small.

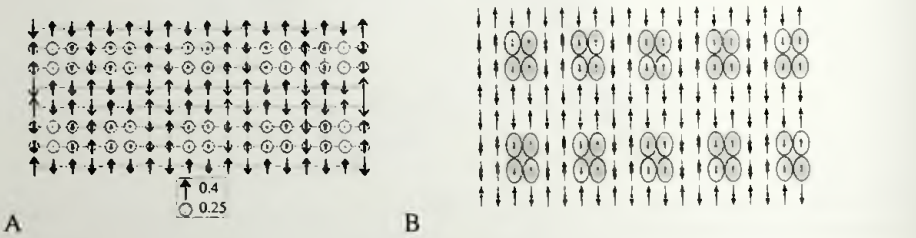

Figure 3.6: A: DMRG t-J model stripes calculated by White and Scalapino [203]. The 18×8 *system with* $J = 0.35t$ *has 20 holes. Open boundary conditions were used on the left and right. Figure B shows a mean-field Hubbard model stripe on a* 20×8 *system with 20 holes and* $U = 5t$*, using periodic boundary conditions.*

3.9 Validity of Mean-field: Comparison with DMRG

The Density Matrix Renormalization Group (DMRG) algorithm was introduced by White in 1992 [201] (see also White and Noack [202]). The algorithm is essentially a direct diagonalization of a truncated Hilbert space [67]. With this method, White and Scalapino [203] have found stripes in the t-J model. They used an 18×8 system with 20 holes and $J = 0.35t$, as shown in figure 3.6A. In the t-J model, one has to use open boundary conditions on the left and the right. However, focusing on the middle part of the picture, it can be seen that there are pairs of holes in this system (every circle has a charge of 0.5).

Almost exactly the same results follow immediately from a Hartree-Fock Hubbard model calculation. Because periodic boundary conditions had to be used, the calculation was done on a 20×8 system with 20 holes (see figure 3.6B). The charge and spin configuration in the middle part are almost the same as those from White and Scalapino. The overall features of the two figures are identical, except near the boundaries, because of the free boundary conditions used in the DMRG calculations. Notice that every cluster of four circles contains in total only *approximately* two holes, with a singlet orientation for the spins: real-space Cooper pairs. The agreement with DMRG is a very good indication that Hartree-Fock calculations have some validity for the properties of half-filled stripes.

3.10 Phase separation in t-J model

Hellberg and Manousakis [89] claim that the t-J model phase separates for all interaction strengths in two dimensions. This means that they do not believe the Hartree-Fock

and DMRG results concerning stripes. It is well established that for large values of J, the model completely phase separates. However, this is the non-physical regime. But according to Hellberg and Manousakis [89, 90] this also happens for $J < t$. They investigated the two-dimensional t-J model at a hole doping of $x = \frac{1}{8}$ using Green's function Monte Carlo. The low-energy states are uniform, not striped. They do find numerous excited states with charge density wave structures, which may be interpreted as striped phases, but they claim that without additional terms in the t-J Hamiltonian, stripes can be stabilized only as ground states through the application of artificial boundary conditions. Therefore they claim that the DMRG results are not valid because of the used open boundary conditions and the application of small staggered magnetic fields to accelerate the convergence.

[White and Scalapino [203, 204] also find striped ground states for $J/t = 0.35$ and $x = \frac{1}{8}$ using DMRG on ladders. However, Monte Carlo simulations on a torus by Hellberg and Manousakis [90] only exhibit stripes as excited states. Whether this discrepancy is due to finite size effects or the type of boundary conditions used is still not settled. The fixed node Monte Carlo studies of Becca *et al.* [23] likewise conclude that stripes do not occur in the ground state although they can be induced by the addition of rather modest anisotropy into the t-J model, suggesting that they are at least energetically competitive. While these conflicting conclusions may be difficult to resolve, it seems inescapable that stripes are important low energy configurations of the two dimensional t-J model for small doping and moderately small J/t.

3.11 Conclusions

This chapter has given an overview of the Hartree-Fock calculations that show that stripes do exist in the Hubbard model. This has been confirmed by Monte Carlo, Slave Boson and Monte Carlo methods. In quarter-filled stripes, there are a number of different stripes possible, with different on stripe charge distributions. One of these half-filled Hartree-Fock stripes is identical to the one that is obtained from Density Matrix Renormalization calculations.

Chapter 4

Kinks and Fluctuating Stripes

As shown in chapter 2, the main evidence for stripes comes from neutron scattering experiments which show an incommensurate splitting of the antiferromagnetic neutron peak. The fact that the neutron peaks in Nd-doped systems are elastic means that there is no energy loss during the interaction between the neutrons and the magnetic excitation in the material. This implies that the stripes which cause the incommensurate peaks are static: they do not move. At the same time, this system is non-superconducting. However, in most superconducting samples, inelastic incommensurate peaks are observed. So, there seems to be a relationship between static and dynamic stripes and superconductivity.

In order to investigate the difference between static and non-static stripes, this chapter looks at fluctuating stripes in two different limits: strong and weak coupling to the lattice. The mean-field theory of the previous chapter is used to do the calculations. For small values of U, the stripes are very broad and not much dependent on the underlying lattice. In this limit stripes can be described by an effective classical theory. For large values of U, the influence of the lattice is very important and an effective model, with local energies defined for different configurations, can be used. For realistic values of U/t the system is on the localized kink side of the phase diagram. Therefore, the existence of the lattice and of discrete kinks is essential for a theory of stripes.

4.1 Fluctuating stripes

When Nd is added to La_2CuO_4, the superconductivity disappears and at the same time the neutron-scattering peaks become elastic [183]. In general, anything that locks the stripes to the lattice (Zn or Nd doping, LTT deformations) leads to a destruction of superconductivity. This seems to suggest that fluctuations of stripes are needed in order to have a superconducting sample. Later experiments found that superconducting

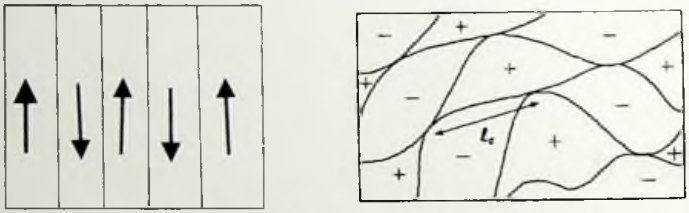

Figure 4.1: Figure A shows a static stripe. The spins show the staggered magnetization between the stripes and the lines denote the stripes. The ordered domain-wall state is realized in the nickelates, where the stripes run diagonally, and in $La_{2-x}Sr_xCuO_4$ with Nd-doping at $x = \frac{1}{8}$. The dynamic stripes in figure B (from Zaanen et al. *[216]) are a possibility in superconducting cuprates. This figure shows a snap shot of the domain-wall liquid as is conjectured to exist in the cuprate superconductors. The characteristic length l_c is indicated.*

$La_{2-x}Sr_xCuO_4$ samples have inelastic incommensurate neutron peaks. This is explained by assuming that without Nd there still are stripes, but they are dynamic and fluctuating in time. Figure 4.1 shows the difference between static and dynamic stripes.

In this chapter the assumption is made that a fluctuation means a distortion of a stripe. It is assumed that a stripe is physically changing its shape. A different assumption could be that the holes on a stripe are fast moving in the superconducting cuprates and that they are locked to the lattice in the non-superconducting samples. This would mean that the physical shape of a stripe would not change, only the internal degrees of freedom are fluctuating. However, this chapter will focus on physical changes of the stripes.

4.2 Sine-Gordon

There are broadly two different phases for non-straight stripes. If the coupling of stripes to the lattice is strong, localized kinks are expected. In the opposite limit of a negligible coupling to the lattice, the stripes will fluctuate freely. In the Hubbard model, the coupling to the lattice is related to the value of U. For large values of U, the stripes are very localized and therefore feel a strong influence of the lattice. For small values of U, the stripes are so wide, that they do not. These two limits can be described very well with the classical sine-Gordon Hamiltonian

$$H = \int dl \left(\frac{\sigma}{2} \left(\frac{\partial h(l)}{\partial l} \right)^2 - Y \cos 2\pi h(l) \right) \tag{4.1}$$

The first part of the Hamiltonian describes the freely fluctuating part of a string. The

string-tension σ determines the energy cost of fluctuations. The effect of the underlying lattice is taken into account by the commensuration energy Y in the second part of the Hamiltonian. It has a minimum energy when $h(l)$ is exactly localized on a lattice point. Every time the string is displaced by a lattice constant, the potential energy is at a minimum. This Hamiltonian contains both limits: the freely fluctuating string and the localized string. This model is also well understood.

When Y/σ is smaller than a critical value, the cosine term is irrelevant and scales to zero in a renormalization group analysis. And, although the dynamics is at least initially kink-like on microscopic scales, the string behaves as a free string at long wavelength. In the opposite limit, the lattice commensuration Y is relevant and the effect of the freely fluctuating part can be neglected. The excitation spectrum develops a gap and it is characterized by well-defined kink and anti-kink excitations.

A central result of the work of Osman *et al.* [143] and Eskes *et al.* [77] that will be described in the next sections is that equation 4.1 is not fully representative for the present lattice problem. For localized stripes, a number of additional localized phases is found, related to the sequence of kinks in a stripe. Furthermore, for realistic stripes in the cuprates, also attention has to be paid to the fact that stripes can be both site-centered and bond-centered, leading to additional kinks configurations.

4.3 Quantum Lattice String

The dynamic stripes have been investigated extensively by Osman *et al.* [143], using a strong-coupling model for a single filled stripe (see figure 4.2). These so-called quantum lattice strings are ordered chains of holes on the square lattice. The spin background within the domains is not taken into account. They used a general Hamiltonian consisting of a classical and a quantum hopping part. The classical part contains the interactions, using the nearest and next-nearest neighbor local discretized string-tensions. These energies depend on the distances between successive particles and the curvature, or the angle in the string, at a certain point. It is assumed that

1. the charge carriers are confined to domain walls.
2. the domain walls are not broken up, because this leads to strong spin frustration.
3. the lattice commensuration on the scale of the lattice constant has a dominant role. Configuration space is built up from strings which consist of "holes" which live on the sites of an underlying lattice. This implies that the microscopic dynamics is that of kinks along the string and this leads to major simplifications with regard to the long wavelength behavior of the string as a whole.
4. it is assumed that the strings do not carry other low lying internal degrees of freedom apart from the shape fluctuations, and that there are only filled stripes.

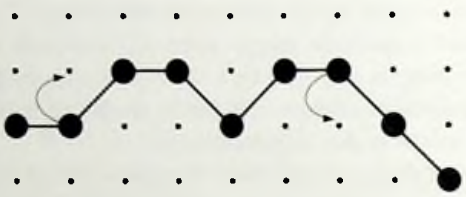

Figure 4.2: A directed quantum lattice string, where every hole is one position to the right of the preceding one. The holes can hop with an amplitude t.

The conclusion that Osman [143] draws from extensive Monte-Carlo studies of the behavior of this model is that apart from some extreme classical limits, the general lattice string model at zero temperatures is a *directed string*. He showed that the hopping of the holes leads to a remarkable *'garden hose'* effect: the stripe will automatically be directed in one direction. This means a stripe will not loop-back. The reason for this is that every hole on the stripe can move back and forth (because of the antiferromagnetic coupling over a stripe) and thus gain kinetic energy. However, if the stripe would loop-back, there would be holes that would not be able to move, leading to an increase in the total energy for such a stripe.

4.4 Directed strings and mapping to spin-1 model

This directed quantum lattice string model has been studied before by Eskes *et al.* [77]. Classical energies (discretized curvature energies) are associated with the various local lattice configurations. Quantum fluctuations result from local tunneling of holes to the neighboring sites, provided the new configuration satisfies the lattice string (next-) nearest neighbor constraint. As shown in figure 4.2 a directed lattice string consists of an ordered chain of holes occupying nearest and next-nearest neighbor sites on a square lattice. The spin background within the domains is thus not taken into account. There are a number of parameters that define a lattice model. First of all there is a difference in energy between diagonal and horizontal connections between two holes. Furthermore, one can make the energy of a configuration also dependent on second-nearest neighbor interactions. This leads to a model depending on four parameters, given by K, L_{12}, L_{22} and the hopping t as shown in figure 4.3. All these parameters can in principle have arbitrary values. As a function of the four parameters, there can be different realizations of stripes.

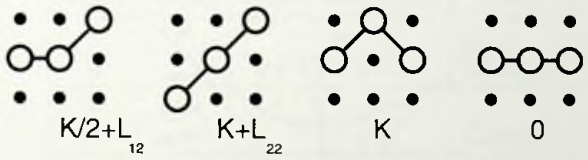

Figure 4.3: The energy for different local configurations of kinks in the quantum lattice string for large values of U .

The directedness of the stripe simplifies the model considerable. If the stripe is assumed to be directed along the x direction, it is still free to move along the y direction. Instead of labeling the positions in the $2D$ plane, the string is completely specified by the list of links, for which there are only three possibilities (in the $(1,1)$, $(1,0)$, or $(1,-1)$ direction). The classical energy of a stripe can thus be written in spin language as

$$H_{\text{spin}} = \sum_l \left[(K+2L_{12})(S_l^z)^2 + \frac{L_{22}}{2} S_l^z S_{l+1}^z + (\frac{L_{22}}{2} - 2L_{12})(S_l^z S_{l+1}^z)^2 \right]. \quad (4.2)$$

This directed model is specified by three parameters and the temperature. Following the spin-1 literature the following parameters are defined:

$$\begin{aligned} D &= K+2L_{12}, \\ J &= L_{12}/2, \\ E &= L_{22}/2-2L_{12}. \end{aligned} \quad (4.3)$$

When a hole hops up or down, one link goes up, and another link goes down. Therefore, the hopping term leads to terms of the form $t\left(S_l^+ S_l^- + S_l^- S_{l+1}^+\right)$. For the special choice $E=0$, the above Hamiltonian reduces to the familiar XXZ model with on-site anisotropy,

$$H_{XXZ} = \sum_l \left[D(S_l^z)^2 + J S_l^z S_{l+1}^z + \frac{t}{2}(S_l^+ S_{l+1}^- + S_l^- S_{l+1}^+) \right]. \quad (4.4)$$

The zero temperature phase diagram of the above spin-1 model has been discussed in detail in the literature, see e.g. Den Nijs and Rommelse [57]. In the next section we will briefly review the six phases found for this model from a perspective of directed strings.

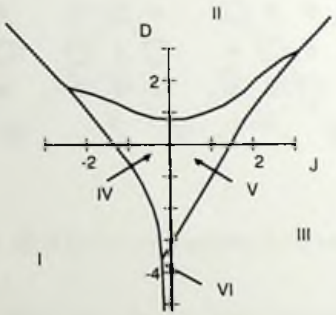

Figure 4.4: Phase diagram of the directed lattice-string problem for $L_{22} = 4L_{21}$ with $D = (K + 2L_{21})/t$ and $J = L_{22}/2t$. Phase IV is the Gaussian rough phase with gapless excitations. The other phases are gapped. Phase II is a straight, horizontal phase. Phase V is the Haldane phase.

4.5 Different phases

The zero-temperature phase diagram of the string problem has been found to be surprisingly rich, and even for the case $E = 0$ there are 6 phases and a large variety of phase transitions [77]. The phase diagram of the quantum string is shown in figure 4.4, as a function of D and J (assuming $t = 1$). Table 4.1 shows a representation of the possible phases.

As a function of the parameters, the zero temperature phase diagram of a single string exhibits many different phases. The phases can be classified in three groups: localized stripes, freely fluctuating stripes and a partly delocalized phase (the disordered flat phase). In addition to various gapped phases which correspond to flat strings, there is a massless phase whose long wavelength fluctuating properties are described by a free fluctuating Gaussian theory (phase IV). The phase transition between this phase and the gapped phase II (a vertical straight stripe), is in the Kosterlitz-Thouless universality class. The phases are further distinguished by the direction they take in the embedding space: they can be horizontal or vertical. Besides this, also a localized phase exists (phase V), which has a highly non-trivial internal structures: the "disordered flat" string, characterized by a proliferation of kinks, but where the kink flavors condense so that the strings as a whole remains localized. It is called a gapped 'Haldane' phase, because it is related to the Haldane phase of spin-1 spin-models. In this phase, the position of up and down steps is not ordered, but up steps are mostly followed by down steps.

Phase	String	Spin-1 description	Name
I		+++++++++	
II		0 0 0 0 0 0 0 0 0	Straight
III		+ - + - + - + -	
IV		+0-+0+0-+	Gaussian
V		-+0-0 0+-	Haldane
VI		+-++-+–	

Table 4.1: This table contains a description for the six possible phases for the directed lattice string. It also contains an example of the spin-1 notation for these phases.

4.6 Hubbard model calculations

The above calculations where done by mapping the directed string model onto the spin-1 model, and using Monte Carlo methods to explicitly calculate the complete phase diagram. The above discussion needed the values of the classical energies for the kinks as input values. It also neglected the surrounding spins and the fact that stripes can be both bond-centered and site-centered. In order to connect the model calculations of the spin-1 model to the Hubbard model, we have done simulations of kinks in stripes. We used the mean-field Hubbard model discussed in the preceding chapter to look at the shape of slightly mis-adjusted stripes in both the large and the small U limit.

4.6.1 Large U: localized kinks

In the large U limit, the classical energies are more important than the quantum mechanical kinetic energy t, which lets the holes jump. In that case it follows from the mapping to the spin-1 model that the sine-Gordon equation 4.1 no longer accurately describes all the possible phases of the model. For these kinds of stripes, the energy of a certain configuration is mostly determined by the local configuration of kinks.

Figure 4.5A shows the starting configuration for a slightly tilted vertical stripe in a 21×11 system. In order to simulate this system in the Hartree-Fock Hubbard model, shifted periodic boundary conditions in the y-direction are used. One must be careful that the spin system is also continued periodically: if the shift over the length of the stripe is one, then the length of the y-direction has to be odd. This system converges to a stripe with one abrupt kink as shown in figure 4.5B. The rest of the stripe is a perfect bond-centered stripe.

This is one of the many systems that is a meta-stable configuration in the mean-field Hubbard model. Starting with a diagonal stripe with a kink, or with a bond-centered or site-centered vertical stripe with a kink, the energies for these different meta-stable

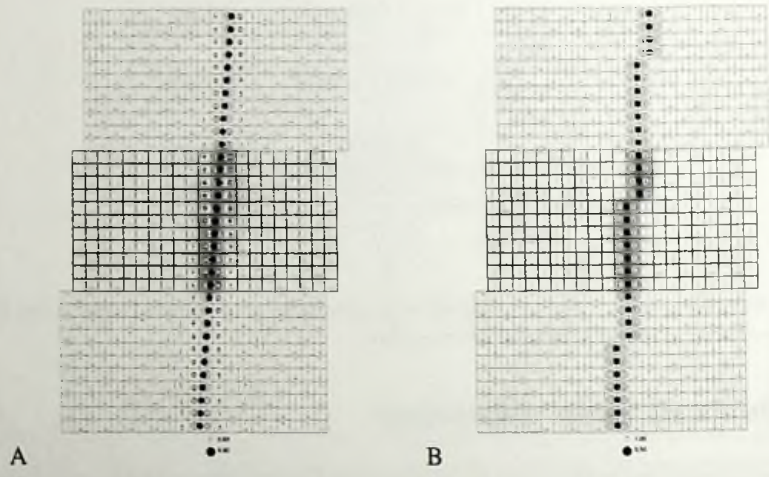

Figure 4.5: Figure A shows the starting configuration with a smooth almost vertical stripe in a 21×11 *system. Using the Hartree-Fock approximation to the Hubbard model with* $U = 100t$*, this system converges to a vertical stripe with sharp kinks as shown in figure B. The center 21x11 part of the system is used in the calculations, the blocks above and below are periodic continuations.*

configurations can be determined (see for instance figure 4.6). By comparing these energies, the energy values belonging to different kinds of kinks can be determined. These values can be used as input values to the spin-1 model.

Notice that in the Hubbard model there is an extra degree of freedom that was not included in the spin-1 model: the Hartree-Fock stripes can be both bond-centered and site-centered, and for instance two holes on the kink can be bond-centered, while another one is site-centered. However, by doing enough calculations with different kink configurations, the energy for every kind of kink can be determined. However, for very large values of U, the stripe only wants to exist at bond-centered positions, making it fit more closely with the work of Eskes *et al.* For $U = 100t$, this leads to the following configuration energies: $K = -0.204t$; $L_{22} = -0.049t$; $L_{21} = -0.011t$. L_{11} is almost infinite. Note that L_{22} is approximately equal to $4L_{21}$, therefore $E \approx 0$ in the effective spin-1 model. These values lead to $D = K + 2L_{21} = -0.226t$ and $J = L_{22}/2 = -0.024t$. Comparing this with the spin-1 phase-diagram shows that a stripe with $U = 100t$ is located in phase I, wanting to form a diagonal stripe.

Note that it is not always possible to find the kinks you want to find. For instance, if for large U one tries to construct kinks in vertical stripes, the system will automatically try to become diagonal, because for $U > 4t$ that is the most stable configuration.

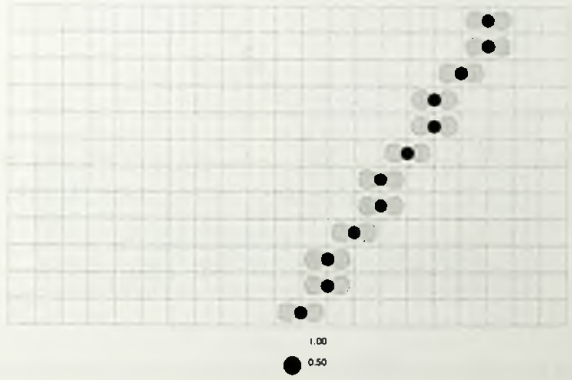

Figure 4.6: A $U = 100t$ diagonal bond-centered stripe with four kinks in an 21×12 system. To achieve the kinks, the boundary conditions in the y direction have been shifted by 8. The calculation started from a smooth diagonal stripe.

4.6.2 Small U: freely fluctuating

For small U, the stripes are less coupled to the lattice and at long wavelengths there is the possibility of fluctuating stripes (phase IV in the phase diagram above). In this case, the stripes become very wide. However, the midpoint of a stripe can still be defined. Figure 4.7 shows the step-profile for a stripe with $U = 4t$. For this value of U, the half-filled stripe wants to be diagonal in principle as was shown in the previous chapter. In figure 4.7, two kinks are introduced by using shifted boundary conditions. Because of the antiferromagnetic spin structure, two kinks are needed. With one kink it is not possible to create a diagonal stripe which also has a periodic antiferromagnetic spin structure. Because these two kinks have to be independent and because the stripes are wide, large systems are needed.

Because it is difficult to see the kink in the diagonal stripe, figure 4.8 shows the same kink, but now the stripe has been rotated over 45°. This shows that for small values of U the kink is very smooth.

Classical solution for kink

Because this kink is so smooth, it should be possible to find an analytic expression for its profile and energy. In this case, the stripe acts as a domain wall. It provides a transition between energetically equivalent minima of the free energy. At one end of the kink, the center position of the stripe has value ϕ_1, corresponding to one of the minima of the free

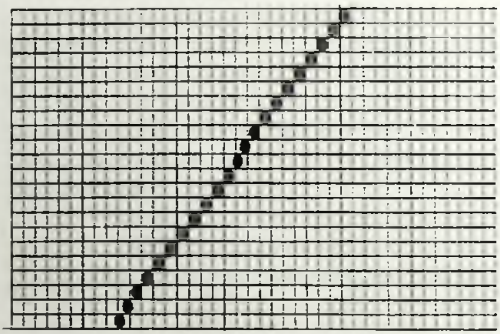

Figure 4.7: A diagonal stripe with $U = 4t$ with two kinks forced by boundary conditions.

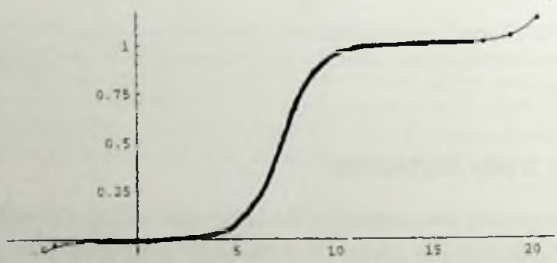

Figure 4.8: Profile of the kink in the stripe with $U = 4t$ stripe after rotation by 45°. For such small values of U/t, the kink is very smooth.

energy. At the other end of the kink, it takes on the value ϕ_2, corresponding to the other minimum. The position changes continuously in passing from one end to the other, and there is an increase in free energy relative to a spatially uniform equilibrium state both because of the energy cost associated with spatial variation and because the position must take on values for which the local free energy is higher than at its minimum.

In order to describe this situation, the sine-Gordon Hamiltonian 4.1 can be used. The minimum energy profile with a step follows from

$$\sigma \frac{\partial^2 h}{\partial x^2} + Y \frac{\partial}{\partial h} \cos 2\pi h = 0, \tag{4.5}$$

which can be rewritten as the following second order differential equation

$$\frac{\sigma}{Y} \frac{\partial^2 h}{\partial x^2} = -\frac{\partial}{\partial h} \cos 2\pi h. \tag{4.6}$$

This can be considered to be the equation of motion of a particle in a potential with mass $\frac{\sigma}{Y}$. Conservation of energy gives the following first order differential equation:

$$\frac{1}{2}\frac{\sigma}{Y}\left(\frac{\partial h}{\partial x}\right)^2 + \cos 2\pi h = \text{const.} \tag{4.7}$$

For the profile of a single step, $h(-\infty) = 0$, $h(\infty) = 1$ and $\frac{\partial h}{\partial x} = 0$ for $x = \pm\infty$. This implies that the constant has to be one. This leads to

$$\sqrt{\frac{\sigma}{2Y}}\left|\frac{\partial h}{\partial x}\right| = \sqrt{1-\cos 2\pi h} = \sqrt{2\sin^2 \pi h}. \tag{4.8}$$

or

$$\frac{1}{2}\sqrt{\frac{\sigma}{Y}}\left|\frac{\partial h}{\partial x}\right| = |\sin \pi h|. \tag{4.9}$$

For a step with $\frac{\partial h}{\partial x} > 0$:

$$\frac{1}{\sin \pi h}\frac{\partial h}{\partial x} = 2\sqrt{\frac{Y}{\sigma}}. \tag{4.10}$$

This first order differential equation can be integrated to give

$$\log \tan \frac{\pi h}{2} = 2\pi\sqrt{\frac{Y}{\sigma}}x \tag{4.11}$$

or

$$\tan \frac{\pi h}{2} = e^{2\pi\sqrt{\frac{Y}{\sigma}}x} \tag{4.12}$$

The profile of a kink in the sine-Gordon model is therefore given by

$$h(x) = \frac{2}{\pi}\arctan e^{2\pi\sqrt{\frac{Y}{\sigma}}x}. \tag{4.13}$$

Its width is determined by $\frac{Y}{\sigma}$. The smooth curve through the discrete profile in figure 4.8 is a fit to the above formula. As can be seen, the fit is extremely good. This shows that for a stripe with $U = 4t$ the classical description with the sine-Gordon theory is valid.

Energy of a kink

Using this profile, the energy of a kink can be found by substituting the profile back into the Hamiltonian. Using $\kappa = \sqrt{\frac{Y}{\sigma}}$, this leads to

$$\begin{aligned} H &= \int dx \left(\frac{\sigma}{2}\frac{Y}{\sigma}\frac{8e^{4\kappa\pi x}}{(1+e^{4\kappa\pi x})^2} - Y\cos\left(4\arctan(e^{2\pi\kappa x})\right)\right) \\ &= Y\int \left(dx\frac{4e^{4\kappa\pi x}}{(1+e^{4\kappa\pi x})^2} + \cos\left(4\arctan(e^{2\pi\kappa x})\right)\right). \end{aligned} \tag{4.14}$$

The $\cos(4 \arctan e^{\pi\kappa x})$ term can be rewritten as $1 - \cos = \frac{8e^{4\kappa\pi x}}{(1+e^{4\kappa\pi x})^2}$. Therefore the integral simplifies to

$$H = 12Y \int dx \frac{e^{4\kappa\pi x}}{(1+e^{4\pi\kappa x})^2}. \tag{4.15}$$

Using $y = 4\pi\kappa x$, this can be rewritten as

$$H = \frac{12Y}{4\pi\kappa} \int_{-\infty}^{+\infty} dy \frac{e^y}{(1+e^y)^2}. \tag{4.16}$$

This last integral is exactly equal to one, thus

$$\Delta E = \frac{3Y}{\pi} \sqrt{\frac{\sigma}{Y}} = \frac{3}{\pi} \sqrt{\sigma Y} \tag{4.17}$$

This is the energy of a kink in the sine-Gordon model. When calculating the energy of a kink in a diagonal stripe using the above formulas, an extra factor of $\frac{1}{2}\sqrt{2}$ has to be taken into account, related to the fact that the distance of one point to the next is equal to $\sqrt{2}a$.

For U in the range $3t$ to $5t$, stripes fit to this model very well and values of Y and σ can be calculated from the Hartree-Fock Hubbard model results for the energy and profile of a kink. The value of Y also directly follows from the commensuration energy. These bare values can be used as initial values for a renormalization group-flow. This can be used to determine whether the long-range properties of stripes are determined by the freely fluctuating Gaussian phase IV or by the straight phase II. Because the phase transition between these two phases is a Kosterlitz-Thouless transition, the stiffness takes on an universal value at the transition. For U larger than $5t$, this is no longer the case. In that case the kinks are localized on a single site. This shows that for the physical case of the cuprates ($U = 8t$), the stripes will have localized kinks.

4.7 Fluctuating stripes

As was shown before, there are two different limits for stripes: freely fluctuating or localized kinks. The spin-1 model and the above mean-field approximation to the Hubbard model are able to investigate most of the properties of single stripes. These properties can be used to discuss more general theories about how stripes might be related to superconductivity. For the freely fluctuating stripes, the interaction between the stripes is important and Zaanen and Van Saarloos [222] have come up with an effective theory for this: a stripe liquid. In the opposite limit of localized kinks, it is possible to think of these kinks or of the endpoint of stripes as charge carriers. Although it is not known at this time which of these theories is correct, they do illustrate the point that thinking about fluctuating stripes and local kinks can lead to physical proposals to explain the properties of the cuprate superconductors.

In the case of fluctuating stripes, the collection of stripes can form a quantum string liquid. One can then look at the dynamical stripe correlations and the resulting spin fluctuations. Zaanen, Horbach and Van Saarloos [216] conjecture that the anomalous spin dynamics observed in the normal state of the cuprate superconductors might find its origin in a nearly ordered spin-system, which is kept in motion by thermally meandering charged domain walls. In such systems, the phenomenon of entropic repulsions is common. For increasing temperature, the thermal meandering motions of individual domain walls increases, as well as the number of collisions between domain walls. Collisions cost entropy and the net effect is that the stiffness of the system as a whole increases. Due to these entropic repulsion effects, temperature becomes an important parameter in the dynamics. The standard theory of incommensurate fluids starts with the assumption that single domain walls behave like Gaussian strings. At finite temperatures, a domain wall will be subject to meandering motions. When the walls have an average distance d, they will on average collide when the typical distance between collision points is given by [216]

$$l_c \approx \frac{\Sigma d^2}{k_B T}. \tag{4.18}$$

This is the most important length scale in this problem. It sets (**a**) the crossover length where the system changes from single all dynamics to that of the domain wall fluid, (**b**) it determines the collision density and thereby the strength of the entropic repulsions, and (**c**) it corresponds to the shortest spin-spin disordering length in the special case of the striped fluid. In order to address the temporal aspects of the dynamics it is suggested that the single wall dynamics is coherent on length scales $\leq l_c$. If this is the case then both the characteristic length- and time scale vary as $1/T$, with the obviously important meaning that they both refer to the crossover from single wall to many wall behavior. These characteristic scales govern the spin dynamics as well. Every time a domain wall passes a particular site, the spin at this site is flipped and the spin dynamics is dominated by this dissipation source. Therefore, on length scales smaller than l_c, the single stripe properties are important. On scales much larger than $l_c$the single stripe properties are less important and the physics is determined by the interaction between the stripes. This would naturally explain why *'Temperature sets the scale'* . Both inelastic neutron-scattering and NMR have revealed that the fluctuations show a characteristic time and length-scale which are both precisely inversely proportional to temperature. The lack of an intrinsic scale is reminiscent of a (quantum) critical regime.

4.8 Sliding stripes

In the opposite limit of localized kinks, one can think about the movement of the kinks along the stripe. Because the kinks are charged, the kink excitations can play the role of current carriers. Dimashko *et al.* [60, 61] have studied the transversal dynamics of

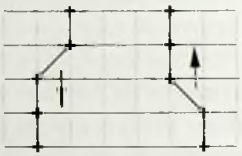

Figure 4.9: To move a stripe one position to the right, not the whole stripe has to move at once. If there is one kink, the whole stripe can move over, charge by charge, while the kinks propagate along the stripe.

a charged quantum stripe and have shown that zero temperature quantum fluctuations are able to de-pin it from the lattice. In their picture, at small hole concentrations the carriers remain localized at the domain walls, and there is no single-particle conduction. Conduction only happens because of a collective motion of the domain walls, tunneling through the Peierls barriers. To move a stripe one position to the right, not the whole stripe has to move at once. If there is one kink, the whole stripe can move over, charge by charge, while the kinks propagate along the stripe (see figure 4.9). By applying an external electrical field perpendicular to the stripe, a sliding behavior can arise, due to the competition between the pinning potential (produced by randomly distributed impurities) and the bias field. The first step costs energy, the rest follows automatically. If there is enough energy for one step, then there is automatically a current for up and down movement of kink and anti-kink pairs.

Dimashko *et al.* [60, 61] show that when the hopping amplitude t is much smaller than the string tension J, the string is pinned by the underlying lattice. At $t \gg J$, the string is de-pinned and allowed to move freely. By mapping the system onto a one-dimensional array of Josephson junctions, they show that the quantum de-pinning occurs at $\frac{t}{J} = \frac{2}{\pi^2}$. In the strong-tension limit $\frac{J}{t} \gg 1$ the ground state of the string is a kink-vacuum. In this case the string is flat, the excitation spectrum exhibits a gap $\Delta \approx J$ and the system is insulating. In the opposite weak-tension limit $J/t \ll 1$ the ground state of the system is a kink-condensate. Then, the string is rough and the excitation spectrum contains a gapless phonon-line node. In this case, the system is superconducting at $T = 0$.

The conductivity from a charge density wave was considered for the first time by Frohlich in 1954, who pointed out that due to the blocking of the scattering processes by the Landau criterion, the collective sliding mode displays perfect conductivity. However, pinning by the lattice or impurities destroys the perfect conductivity. Even extremely small inhomogeneities would pin the walls. Therefore, although this is a very nice connection between stripes, kinks and perfect conductivity, it is not relevant in practical samples.

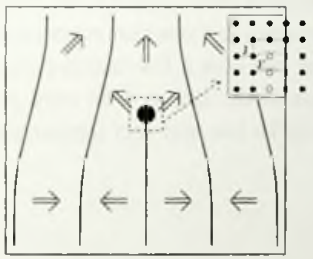

Figure 4.10: Sketch of the stripe dislocation from Zaanen and Nussinov [218]. The lines indicate the stripes and the arrows the direction of the Néel order parameter in the vicinity of the dislocation in the classical limit ('π-vortex'). The geometry of the 'curved' internal space seen by the spin system can be inferred from the exchange bonds indicated in the inset.

4.9 Moving endpoints of stripes

One other point of view based on the local picture of stripes is the recent research of Zaanen and Nussinov [218], in which they look at disconnected stripes: stripes that suddenly end in the surrounding antiferromagnet. These endpoints strongly perturb the surrounding antiferromagnet, because two antiferromagnets with opposite staggered order parameter must suddenly be joined. Zaanen and Nussinov argue that these topological excitations might be related to the BCS-like physics at large distances involving nodal fermions. Their argument is based on the hidden order of the spin-charge separation. According to Zaanen and Nussinov [218], stripes and nodal fermions are two sides of the same coin.

When the charge dislocations quantum proliferate, the sublattice parity turns into an Ising gauge field, and the confinement transition of the gauge theory describes the unbinding of charge dislocations into stripe dislocations. For small doping, the dislocations are suppressed and we are in the de-confined phase of the Z_2 gauge theory. For higher doping the dislocations have a finite density and proliferate, destroying the sublattice parity. This is the confining phase of the Z_2 gauge theory. It is suggested that this quantum phase transition might be the one responsible for the quantum criticality near optimal doping in the high temperature superconductors. However, since the order in this confinement-de-confinement transition is topological, one needs to consider non-local correlation functions to observe this [220]. But experimentally, it is very difficult to measure such correlation functions and therefore it is called hidden order.

Another important result that follows from this point of view is the possibility of charge transport perpendicular to the stripes. All other theories assume that the stripes itself can be viewed as one-dimensional conductors (Luttinger liquids). However the

endpoints of the stripes can fluctuate and connect to the next complete stripe. If then the original complete stripe breaks open and one part connects with the original endpoint, a new endpoint has been created, but now a few lattice constants away. Therefore, there can be a current perpendicular to the stripe. The only problem with this is that the number of charge carriers would be low and very temperature dependent.

4.10 Conclusions

We looked at fluctuating stripes and reviewed the work by Osman *et al.* Their Monte Carlo simulations showed that stripes want to form a directed line. Using this, a general stripe problem with nearest and next-nearest neighbor interactions can be formulated and mapped onto a spin-1 problem. The phase diagram for this system has a number of different phases. The three classes are: straight, Haldane like and freely fluctuating. All three phases can also be found using numerical simulations on the Hubbard Model. For small values of U, there are smooth kinks in the stripes. For large values of U the kinks are localized. There is a Kosterlitz-Thouless transition between those two regimes. For freely fluctuating stripes, one can think of a stripe liquid, which leads to a possible explanation of the reason why there is a energy scale in the system, given by the temperature. In the opposite limit of localized stripes and kinks, one can think of sliding stripes and the moving endpoints. Numerics has been used to show that the stripes in the cuprates are probably in the localized regime, in which the lattice commensuration energy is very important. It has been shown that Hartree-Fock numerics of the Hubbard model can be connected to the charge only model systems of Osman *et al.*

This chapter has also shown that the lattice scale physics has more interesting phases than the continuum physics, which is described very well by the classical sine-Gordon theory. It has shown that a microscopic theory (the Hubbard model in Hartree-Fock approximation) can be mapped onto two effective theories of stripes. In the low U limit, stripes are essentially freely fluctuating. In the large U limit, stripes can be described as a line of particles on a lattice with quantum hopping. The stripes in the mean-field Hartree-Fock Hubbard model can be forced to have kinks by using boundary conditions. The next chapter looks at evidence for kinks in stripes in the cuprates and how they can be used to determine the on-stripe charge ordering of quarter-filled stripes.

Chapter 5

Fractionally charged kinks

The previous chapter has looked at kinks in half-filled stripes. However, the stripes that are experimentally found in the cuprates are quarter-filled. This gives rise to an extra degree of freedom on the stripe. This chapter looks at the theoretical possibilities for kinks in these quarter-filled stripes. The most surprising result is that the kinks can have a charge of either e or of $\frac{1}{2}e$. Whether the stripe has an integer or fractional charge is determined by the on-stripe charge order. This is different for $4k_F$ and $2k_F$ stripes. If the kinks on all the stripes in a layer are oriented in the same direction, then this will be experimentally observable by neutron-scattering. The incommensurate peaks will move away from the directions of the crystal axes. This proposal can be tested experimentally by looking at shifts in the position of the incommensurate peaks in Fourier space. If these shifts are found, their magnitude gives the topological charge of these kinks. There already have been a number of experimental results that point in this direction. Another result is that kinks in stripes can explain the fact that after $x = \frac{1}{8}$ the distance between the stripes does not seem to become smaller.

5.1 Doping dependence of stripe distance

Important information about the microscopic origin of stripes is contained in the doping dependence of the inverse of the stripe spacing, shown in figure 5.1. This spacing can be obtained directly from the the distance δ between the four measured Fourier-peaks. It was experimentally found that δ is to a good approximation directly proportional to doping x for a variety of stripe systems like the nickelates [179] and manganites [91]. This is understandable by imagining that, because of the extra doping, more stripes are formed and they have to get closer together to fit in the sample. So for $x < \frac{1}{8}$, nothing changes to the stripes themselves, only the separation or distance between them changes. The stripes are **incompressible**. It is also found in cuprate stripe phases,

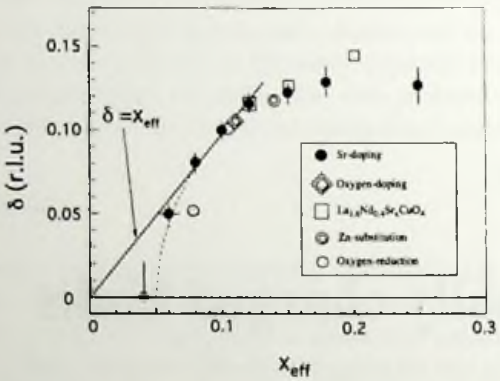

Figure 5.1: The inverse distance δ between the stripes as a function of doping x as measured by Yamada et al. *[212]. Below* $x = \frac{1}{8}$ *there is a linear relationship between the distance between the stripes and doping.*

but only in the doping regime where $x < \frac{1}{8}$, while for $x > \frac{1}{8}$, δ becomes roughly x independent [138,212].

The central assumption is that the cuprate stripe phase in the $x < \frac{1}{8}$ regime is insulating on the *microscopic* scale. Experimentally, the cuprate stripe phases are metallic-like and a popular viewpoint is that the electronic state on the stripes is metallic. However, the $\delta = x$ relation argues strongly against this internal metallicity. Its meaning, already suggested by earlier mean field calculations, is simply that every hole stabilizes a piece of charged stripe with a length which is an *integer multiple* of the lattice constant. This special stability when the electron charge and the lattice are commensurate, shows that the internal electronic state of a stripe is Mott-insulating on short length scales. At the same time, stripes which are internally insulating on microscopic scales are not necessarily inconsistent with metallic behavior on macroscopic scales. The stripe metal might be viewed as a quantum-disordered stripe insulator, characterized by a growth of the quantum fluctuations when length- and time scales are increasing. Although this issue will not be discussed in any further detail, the remainder should be read as a suggestion for a critical experimental test of this hypothesis.

5.2 Quarter-filled stripes

The nature of the reference insulator in the $x < \frac{1}{8}$ regime has been described in the literature before [134,219]. The slope of one of the δ versus x relationship for small x implies that one hole stabilizes two charge stripe unit cells. Accordingly, the dynamics asso-

ciated with the electrons along the stripe can be associated with that of a quarter-filled one-dimensional fermion system [228]. In recent photo-emission experiments evidence is found for an underlying one-dimensional band structure characterized by a Fermi momentum of a quarter-filled system: [228]. It is well known that such a system can become Mott-insulating by breaking translational symmetry with real space charge periods $2a$ and $4a$, or wavevectors $4k_F$ and $2k_F$ respectively, where $k_F = \pi/(4a)$ (a is the lattice constant). Schematically, the ordering pattern on the stripe is like $\cdots - 0 - \updownarrow - 0 - \updownarrow - \cdots$ and $\cdots - 0 - 0 - \updownarrow - \updownarrow - 0 - 0 - \updownarrow - \updownarrow - \cdots$ for the $4k_F$ and $2k_F$ stripes, respectively. Here 0 denotes the hole and $\updownarrow$ the presence of a spin, which is expected to be disordered due to quantum fluctuations. At present it is not known which type of density wave order is realized on the stripe. All that really matters for the remainder of the discussion is that the $4k_F$ stripe should be considered as the condensation of the charge e of one hole [134], while the $2k_F$ stripe is associated with the charge quantum of a *pair* of holes, $2e$ [219].

5.3 Minimum distance between stripes: $4a$

From the fact that the incommensuration stays at $\frac{1}{8}$ for $x > \frac{1}{8}$, it seems that stripes are not able to get closer together than shown in figure 5.2. The stripes seem to have a minimum distance of four lattice sites. Bringing the stripes closer together seems to cost energy. This stability is understandable. If the charges on the stripes are bond-centered, then there is a two-leg spin-ladder in between. This is a stable spin-configuration, with a spin-gap. If stripes would be forced closer together, there is no real antiferromagnet left anymore. So it seems impossible to dope the system with more holes than 12.5% doping. So it seems that above $x = \frac{1}{8}$, the stripes become **compressible**. The reason for this saturation of the incommensuration is unknown. This chapter shows a possible explanation of this in terms of kink-formation in the stripes. It will be shown that it is still possible to have **incompressible** stripes, and that doping is achieved by kink-formation in the stripes.

5.4 Doping through kink-formation

The (near) independence of $\delta(x)$ as function of doping for $x > \frac{1}{8}$ implies that a fraction of the holes $x' = x - \frac{1}{8}$ cannot be 'absorbed' by the $x < \frac{1}{8}$ insulator. These excess holes should dope the $x < \frac{1}{8}$ state and it is expected that these holes dope the 'soft' insulator associated with the density wave on the charge stripes instead of the magnetic domains, the remnants of the 'hard' insulator of half-filling. Doped charge density wave states are well understood in the context of conventional one-dimensional systems [83]. A key concept was introduced by Schrieffer [160] in the study of poly-acetylene: the elemen-

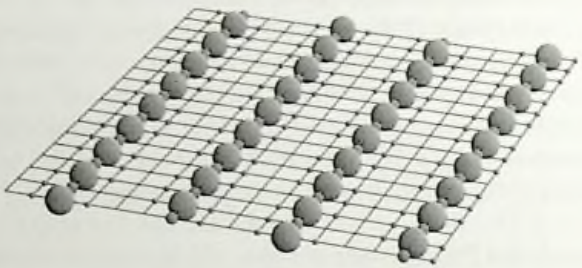

Figure 5.2: A system of quarter-filled site-centered $4k_F$ stripes with doping $x = \frac{1}{8}$ as calculated in the mean-field Hubbard model. The radius of the spheres denotes the hole-density at a site. The spin-density is not shown.

tary excitations in such a system are not electrons but in fact parts of an electron. The reason is that these excitations can be viewed as electrons bound to topological defects in the density wave order parameter. That the charge of the electron fractionalizes in doped $4k_F$ density wave systems is easily seen by considering the strong coupling limit [221]. The undoped state with one (static) hole added at the central site is indicated in figure 5.3A. After a couple of hops a configuration is reached where the bare hole has decayed into two propagating excitations carrying half the hole charge ($\frac{e}{2}$) which are at the same time domain walls (kinks) in the density wave (figure 5.3B). Such an $\frac{e}{2}$ domain wall corresponds with a region of enhanced charge density, and hence an increased Coulomb energy. In contrast to a one-dimensional crystal, a stripe has the additional freedom of moving sideways, thereby increasing the distance between the two holes associated with the domain wall [221], as sketched in figure 5.3C. Thus, the fractionally charged domain walls also cause the stripe to step sideways, modulating the position of the stripes in space, see figure 5.3D. If all the kinks are in the same direction, the net result is that the stripe takes on average an orientation in space which is tilted away from the lattice axis, very much like slanted phases that are found in lattice string models [77].

The schematic calculation from figure 5.3 can be repeated using the mean-field Hubbard model. Numerical calculations with the mean-field Hubbard model have shown that the situation where in addition to the extra hole, two extra kinks have been introduced, is more stable then a straight stripe without kinks and one extra hole. So it seems, that by introducing one extra hole, two kinks can be formed. What happens to the straight segments of the stripe is a shift in the periodicity. This way, the straight segments still are quarter-filled, while the system effectively has absorbed an extra hole. Locally, at the kink there is something that looks like a half-filled diagonal stripe. In the chapter

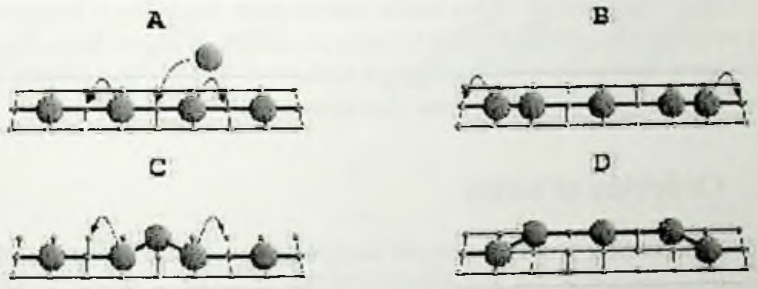

Figure 5.3: Soliton dynamics in a strongly coupled doped $4k_F$ stripe. The small spheres denote the lattice points with one electron, the large spheres are holes. The spins are not shown. Figure A shows a localized stripe with a $4k_F$ charge density wave, onto which an extra hole is added. If the stripe is rigid, the doped hole separates in a left- and right moving soliton, both carrying half the electron charge (figure B). However, when the curvature energy becomes less than the charge compressibility energy, the hole can escape 'sideways' (figure C). As a result, the stripe now has two kinks that can move independently of each other (figure D).

3 it was shown that there are many possibilities for the on-stripe charge distribution for half-filled stripes. At least four of them are meta-stable in Hartree-Fock theory. If two extra half holes are injected in situation C, this is a stable configuration in Hartree-Fock. However, it is more stable if also two extra kinks are introduced. So, injecting in total one hole leads to the creation of two kinks. So the topological charge of a kink is $\frac{e}{2}$.

The effective hole-doping can thus be increased by forming kinks, while the straight parts of the stripe stay incompressible. Therefore the stripes do not have to come closer: the average distance between the stripes in the x-direction stays $4a$. This can be seen as a possible explanation for the saturation of the incommensuration in figure 5.1.

The $x < \frac{1}{8}$ stripes might be viewed as the condensation of the topological defects associated with doping the half-filled Mott-insulator [102, 150, 215]. The $x > \frac{1}{8}$ state should be viewed in turn as the condensation of the topological defects associated with doping the stripe state itself. The stripes for $x > \frac{1}{8}$ are locally not different from the $x < \frac{1}{8}$ stripes sketched in figure 5.2, except that once in a while the stripe 'steps sideways': it forms kinks. These kinks carry half the fundamental charge quantum associated with the stripe-insulator of the $x < \frac{1}{8}$ regime and as they move a stripe always in the same direction they cause the orientation of the stripe phase to deviate from the lattice axis, explaining the Y-shift. Although not based on phase separation between two different types of stripe fillings, the proposal shares the essential idea, that the crossover around $x = \frac{1}{8}$ and the charge density and orientation of stripes are related, with a suggestion

of White and Scalapino [204]. This line of reasoning can explain the reason why the point $x = \frac{1}{8}$ is very special. It is a stable, special point, because it is a straight, quarter-filled stripe with a minimal distance between the stripes. With less holes, the stripes are further apart, with more holes there is kink-formation. This can also explain why stripes with $x < \frac{1}{8}$ are more one-dimensional than stripes with $x > \frac{1}{8}$ (see Uchida).

5.5 Ordering of kinks

Let us now consider a dense *system* of such 'slanted' stripes. In the presence of any stripe-stripe interaction this will condense at zero temperature in a stripe phase where all the stripes are tilted in the same direction: the explanation for the Y-shift. It is also expected that the kinks themselves order in a regular pattern at zero temperature. The argument is the usual one: the kink gas on a single stripe becomes at long wavelength a Luttinger liquid showing algebraic long range order. In the presence of any interaction between the Luttinger liquids on different stripes this will change into true long range order at zero temperature. Notice that the argument of Kivelson *et al.* [103] for the de-phasing of density correlations on different stripes by transversal stripe fluctuations does not apply here. Although valid in the continuum, the kinks that are considered here are tied to the presence of an underlying crystal lattice and it is easily seen that the de-phasing does not occur.

In principle, all the stripes could have a random distribution of kinks to the left and to the right. However, the stripes are so close together, that it seems logical that they all form the same sequence of kinks. The kink order from stripe to stripe is less easy to establish. On the one hand, the kinks carry charge and under the assumption that the screening length is of order or larger than the average kink separation the kinks would tend to maintain a maximum separation, thereby forming a Wigner crystal as indicated in figure 5.4B. However, one could imagine that elastic deformation energies are minimized when kinks line up as indicated in 5.4A. The precise realization of the kink superlattice is therefore a subtle, quantitative matter. Observation of this kink superlattice may therefore be a formidable experimental challenge. However, the existence of a superlattice would have so many conceptual implications that it is a goal worth hunting for.

If all the kinks are in one direction, there will be a slanted phase (see figure 5.4). If this is the case, then it should be possible to observe this in neutron-scattering. Because of the kinks, there has been a tilt in the unit-cell in real-space. As a consequence, there will be also a change in the position of the Fourier-peaks in reciprocal space. The periodicity in the x-direction stays the same. So, what happens is that the peaks in Fourier-space will shift up and down (see figure 5.5). The shift of the peaks is denoted by δk. This δk is predicted to linearly dependent on $x - \frac{1}{8}$ for x bigger than $\frac{1}{8}$ (see figure 5.6), because the more doping, the more kinks will be formed and this will lead to an

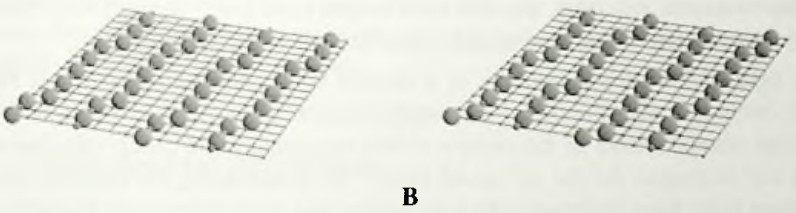

Figure 5.4: Both figures show the hole-concentration of a $4k_F$ striped-phase with a doping concentration of $x = 0.139$, thus with x bigger than $\frac{1}{8}$. There are four more holes than in the system shown in figure 5.2. The four extra holes are localized in eight kinks, so every kink has a fractional charge of $\frac{e}{2}$. The difference between the left and right figures is that the ordering of the kink positions is different. In the right figure, the Coulomb repulsion has been reduced by making a Wigner crystal.

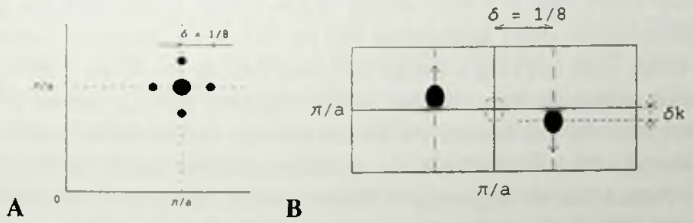

Figure 5.5: Figure A shows a sketch of the position of the incommensurate peaks in Fourier-space as measured by neutron-scattering. The large black circle shows where the peaks would have been if the system would have been a commensurate antiferromagnet. Because of the tilts in the stripes, the peaks will change position as shown in B. Here, only the peaks resulting from one layer are shown. The shift of the peaks δk is predicted to depend linearly on $x - \frac{1}{8}$ for $x > \frac{1}{8}$.

extra tilt in the unit-cell in real- and Fourier-space.

5.6 Numerical calculations

These general ideas can be illustrated with explicit calculations. Since we are considering fully ordered insulating states, mean-field theory is able to provide meaningful qualitative outcomes. The reference $2k_F$ and $4k_F$ stripe insulators actually both exist in the Hartree-Fock solutions of the Hubbard model as low lying, but weakly metastable states: the true mean-field ground state corresponds with filled stripes (one hole per stripe unit cell) [163, 219]. In Gutzwiller mean-field (qualitatively similar but more accurate than Hartree-Fock) half-filled stripes become the ground state of the Hubbard model with added long range Coulomb interaction: see [163]. But with increasing

neighbor Coulomb repulsion, the half-filled stripes have lower energy [163]. Some of the $4k_F$ site centered cases were already identified before [163, 215].

In figure 5.2 a typical example of a straight bond centered $2k_F$ stripe is shown. It was calculated with the mean-field approximation. The result strongly resembles the stripe patterns found in the density matrix renormalization group calculations by White and Scalapino for the t-J model [205]. By constraining the distance between the stripes to be fixed, increasing the hole density and using appropriate boundary conditions, doped stripes can also be investigated in mean-field theory. It was found that such doped stripes, if they exist as locally stable mean-field solutions, prefer localized fractionally charged kinks. In all cases where such doped stripes exist as locally stable mean-field solutions, they prefer localized fractionally charged kinks which tend to form an ordered pattern.

A typical example is shown in figure 5.4 where the density of excess holes is indicated for a $4k_F$ stripe state at a hole density of $x = 0.139$. In line with the qualitative arguments given above, every hole doped into the $4k_F$ $x = \frac{1}{8}$ reference insulator gives rise to two kinks, each carrying a charge of $\frac{e}{2}$ and moving the stripe sideways by one lattice constant. Although these 'slanted' stripes are quite stable solutions if the reference insulator is of the $4k_F$ variety, we did not manage to find stable solutions for the $2k_F$ stripes doped with additional holes — within mean field theory, such kinks tend to disintegrate. Notice that the argument of Kivelson *et al.* about stripe fluctuations does not apply here. Although valid in the continuum, the kinks we consider are tied to the presence of an underlying crystal lattice and it is easily seen that the de-phasing does not occur. In order to get some feeling of the relative stability of the $4k_F$ slanted phase we compared it with a straight stripe where an additional hole is simply inserted in the straight density wave ($\cdots - \updownarrow - 0 - 0 - 0 - \updownarrow \cdots$). On the Hartree-Fock level, a stripe with two kinks of charge $\frac{e}{2}$ always has significantly lower energy (of order $0.01t$). We also checked that the sidesteps can be further stabilized by including a nearest-neighbor Coulomb interaction. The energetics associated with the relative transversal orientation of the kinks is a more delicate matter which is strongly dependent on the distance between kinks. It is believed that collective fluctuation effects will promote long range slanted order over zig-zag type stripe patterns, in much the same way as quantum fluctuations make lattice strings directed [77].

Of course, these calculations merely serve to illustrate the principle — neither the question which possibility is realized in nature nor the question whether the 'topological' insulator is the proper reference state can be settled by these calculations. However, simple predictions follow which at least in principle can be checked by experiment. Most importantly, the charged kinks offer an explanation for the Y-shift which has already been observed in experiments. However, the kink notion implies that the super-lattice peaks of the slanted stripe phase are located along the straight lines crossing the super-lattice peaks associated with the $\frac{1}{8}$ phase as indicated in figure 5.5. The reason is that

the average distance between the stripes does not change when the stripes are making sidesteps, thereby leaving the distance between the peaks in reciprocal space along the horizontal axis in figure 5.5 unchanged.

5.7 Experimental prediction

Lattice commensuration effects make a transition to kinked stripes around $x = \frac{1}{8}$ most likely. At the moment, it is not known whether there should be a sharp transition or a rapid but smooth cross-over. However, due to complications associated with quenched disorder we have no prediction for whether there should be a sharp transition or a rapid but smooth cross-over. However, the scenario that there are no free holes, but that instead all holes go onto stripes, leads to an immediate relation between the $\delta(x)$ dependence and the Y-shift. The magnitude of the Y-shift is defined as δk and the fractional charge (in units of e) carried by the kink as q. Then $x' = x - \frac{1}{8}$ is the hole density associated with doping the stripes in the $x > \frac{1}{8}$ regime. It then follows that the Y-shift obeys $\delta k = \frac{x'}{2q}\frac{2\pi}{a}$ and that $\delta = (x - x')\frac{2\pi}{a}$ where a is the lattice constant. So we have $\delta + 2q\,\delta k = \frac{2\pi}{a}x$, independent of whether there is a crossover or sharp transition, and where it takes place. In figure 5.6 the prediction for the Y-shift as a function of x for the $2k_F$ and $4k_F$ cases is shown, both for the case of a sharp transition at $\frac{1}{8}$ and for the same smooth crossover as in figure 5.1. In this figure the two experimental results for the Y-shift have also been indicated, where the $x = 0.15$ point has been reported by Lee *et al.* [106] for an oxygen doped sample of La_2CuO_4 and the $x = 0.13$ point is measured in a $La_{2-x}Sr_xCuO_4$ sample by Matsushita *et al.* [122]. There is also one experimental indication of a Y-shift at dopings slightly less than $\frac{1}{8}$ by Kimura *et al.* [99, 100], which suggests that there is a smooth crossover.

Clearly an extensive experimental study is called for to establish whether the Y-shift is due to kinks and whether the predicted relationship between δk and $\delta(x)$ holds. The existing data seem to favor a kink charge of e over charge $\frac{e}{2}$, suggesting that the elementary charge quantum associated with the stripe phase is $2e$. Given the proximity of a superconductor characterized by charge quantum $2e$, such a stripe charge-quantization would obviously be quite interesting. Also notice that the $4k_F$ density wave is saturated with kinks already at $x = \frac{1}{4}$ with $\delta k = \frac{1}{8}\frac{\pi}{a}$. This corresponds with filled stripes oriented along the diagonals (like the $x = \frac{1}{4}$ stripes in nickelates). On the other hand, the $x = \frac{1}{4}$ kink saturated $2k_F$ stripes would show $\delta k = \frac{1}{16}\frac{\pi}{a}$. Despite the fact that the peaks are broadening rapidly as function of increasing $x > \frac{1}{8}$ it is expected that these gross differences should be observable.

Figure 5.6 shows the prediction for the shift δk of the Fourier-peaks as a function of doping for two different kind of kinks. Until now, it has only been possible to find the '$e/2$' kind of kinks in the mean-field Hubbard model calculations. It would be

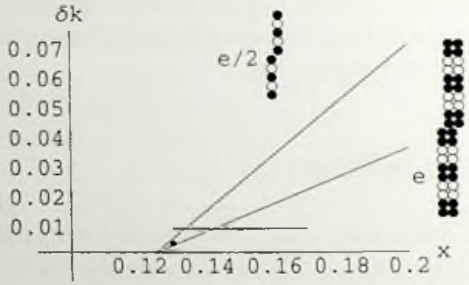

Figure 5.6: Prediction for the shift δk of the Fourier peaks, as a function of doping for two different kind of kinks: site-centered $4k_F$ stripes with kinks with fractional charge $\frac{e}{2}$ and bond-centered $2k_F$ stripes with charge e. Experimental points are from Matsushita et al. *[122] and Lee* et al. *[106].*

worthwhile to find the kind of kinks denoted by 'e'. However, until now they have not been found them in our mean-field Hubbard model calculations. The two circles are two experimental measurements of the shift of the Fourier-peaks. It would be very important to look for these rotations of peaks. First of all, it would prove that thinking of stripes as localized entities with kinks is a valid point of view. Further, if all rotations would be in the same direction, it will give information on both the fact if all stripes are oriented in the same direction in one layer, but also about the correlation of the stripes between layers.

Quite recently it was found [99,100,122] that in a number of cuprates the spin peaks tilt away from the $(1,0)$ or $(0,1)$ axis in reciprocal space. This puzzling behavior corresponds with a tilt of the stripe phase away from the main crystal axis of the perovskite planes in real space and seems characteristic for the $x > \frac{1}{8}$ regime. The scenario that is proposed here for the doping dependence of this so-called Y-shift, is independent of whether there is a crossover between the two regimes around doping $x = \frac{1}{8}$ or a sharp transition at this value. In either case, it leads to an explicit relation between the δ versus x dependence and the Y-shift, which, if confirmed experimentally, allows one to determine the topological charge of stripes. Although the measured tilt is a subtle effect (only a few degree), it is robust in certain samples. So far, there is no alternative explanation for the data and this aspect of the data has not been discussed much, probably because no intellectual significance has been attached to it. If the interpretation advanced here is correct, the data actually yields information about the elementary charge quantum numbers of the stripes.

5.8 Conclusion

This chapter continued to look at kinks in stripes, but now at some possible experimental properties in quarter-filled stripes. Because the charged kinks themselves should order, it should in principle be possible to observe the super-lattice reflections of this kink lattice in diffraction experiments. The kinks on single stripes will repel but the kink order from stripe to stripe is less easy to establish. On the one hand, the kinks carry charge and under the assumption that the screening length is of order or larger than the average kink separation the kinks would tend to maintain a maximum separation, thereby forming a Wigner crystal as indicated in figure 5.4B. However, one could imagine that elastic deformation energies are minimized when kinks line up as indicated in figure 5.4A. The precise realization of the kink super-lattice is therefore a subtle, quantitative matter. Observation of this kink super-lattice may be a formidable experimental challenge. However, given the conceptual implications implied by such an observation it should be given a high priority.

In conclusion, inspired by the tilting of the stripes seen at higher dopings we have proposed a scenario of stripe phases characterized by a proliferation of fractionally charged solitons. Remarkably, by studying merely the structural characteristics of this phase which is realized at higher dopings, the elementary charge quantum numbers of the stripes can be established.

Chapter 6

Superconductivity

This chapter explains what superconductivity is by reviewing the attractive Hubbard model and the BCS model. The behavior of the attractive Hubbard model is dominated by local pairs and it can be described by an effective pseudo-spin model. Looking at the influence of a magnetic field, it can be shown that the ordering of the pseudo-spins below a critical temperature is identical to a superconducting transition. The same kind of analysis in terms of a pseudo-spin model can also be applied to the BCS model. The mean field treatment of this model yields exactly the BCS gap equation. Experimental data is used to show that the BCS theory is not valid for the cuprate superconductors. Properties as the d-wave dependence of the energy gap, pseudogap behavior and indications of local superconducting behavior above T_c point to local superconducting pairs. It is pointed out that the existence of real-space pairs in an antiferromagnet does not automatically lead to superconducting behavior. However, one major obstacle is removed once the local pairs live on a one-dimensional system like a stripe.

6.1 Attractive U Hubbard model

The negative-U Hubbard model describes local *attractive* interactions between electrons. One should think of this model as an effective model with renormalized parameters, which applies at low frequencies and temperatures. When electrons polarize a collective degree of freedom, they can obtain a negative pair-binding energy $-U$ by sharing this polarization. There have been several polarization mechanism proposed for producing attraction between electrons. To list a few: lattice deformations (phonons), collective charge oscillations (plasmons), or spin fluctuations (paramagnons). The Hamiltonian is given by

$$H = -\sum_{ij\sigma} t_{ij} c^{\dagger}_{i\sigma} c_{j\sigma} - \frac{U}{2}\sum_{i}(n_i - 1)^2 + \frac{1}{2}\sum_{ij} V_{ij}(n_i - 1)(n_j - 1) - \mu \sum_{i} n_i. \qquad (6.1)$$

The attractive U term favors local pairs of $\uparrow$ and $\downarrow$ spins on the same site. However, the hopping term $t_{ij}c^{\dagger}_{i\sigma}c_{j\sigma}$ competes with this tendency since it delocalizes the electrons and unbinds the pairs. The inter-site interaction V_{ij} repel electrons at different sites. The influence of V_{ij} is important in selecting the ground state, especially near half-filling.

6.1.1 The pseudo-spin model and superconductivity

The fact that the attractive Hubbard model is superconducting is well known (see the review article by Micnas, Ranninger and Robaszkiewics [126]). Zaanen has given a very nice pedagogical explanation why this model is superconducting [214]. In order to understand the importance of local pairing and what it takes for models that lead to local pairing to be superconducting, his work is reviewed here.

Because of the assumed attraction between the electrons, the low-energy Hilbert space is built from real-space "Cooper pairs". For low-energy properties one can focus on only these new stable particles: this is called projective renormalization. Interestingly, this Hilbert space has precisely the same dimension as the Hilbert space of spins, and these Cooper pairs are also subject to a $SU(2)$ algebra, which is explicitly broken to $U(1)$ if the system is not electron-hole symmetric: attractive fermion systems are like XY spin systems. The importance for superconductivity is that these XY spins communicate with the vector potential of the electromagnetic field. Therefore the local gauge symmetry of the field is broken in the classical condensate. This aspect is the key to the unusual physics of the superconducting state (Zaanen [214]).

When $|U|$ becomes large the Hilbert space will be split up into different Hubbard sectors. Because the interactions are attractive, the lowest lying Hubbard sector is the one containing the maximum possible number of doubly occupied sties. The electrons have to be distributed on the lattice between empty and doubly occupied sites.

In addition to a lattice filled with only pairs, a 'first excited' Hubbard sector with energy $|U|$ also exists. This contains two singly occupied sites. There are sectors at higher multiplies of U, that contain more than one broken pair. At half-filling there are precisely as many doubly occupied as empty sites and the dimension of the ground state sector is 2^N. (Every site can be empty or double occupied). Therefore the Hilbert space has the same dimension as the Hilbert space of a $S = \frac{1}{2}$ problem. This hints at a spin-like character of the physics at low-energy. The crucial observation is, that the dynamics at energies $\ll |U|$ can be completely described in a set of operators, obeying a $SU(2)$ algebra. It is easy to deduce this algebra. In the projected Hilbert space it is only allowed to create a doubly occupied site from an empty site, or to annihilate the doubly

occupied site to end up with an empty site. Pairs can be created and destroyed with the following singlet operators (singlets, because the two holes are at the same site)

$$\begin{aligned} T_i^+ &= c_{i\downarrow}^\dagger c_{i\uparrow}^\dagger, \\ T_i^- &= c_{i\downarrow} c_{i\uparrow}. \end{aligned} \tag{6.2}$$

Commuting these two equations yields

$$\begin{aligned} [T_i^+, T_i^-] &= 2T_i^z \\ T_i^z &= \frac{1}{2}(n_{i\uparrow} + n_{i\downarrow} - 1). \end{aligned} \tag{6.3}$$

Therefore, T_z is $-\frac{1}{2}$, 0, $\frac{1}{2}$ (empty, one electron, double occupied). The fermionic, single occupied site is always projected out. Therefore, the system is always spin-like, regardless of electron density and forms an $SU(2)$ algebra.

The strong coupling Hamiltonian can be derived using canonical perturbation theory. Observe that virtual hoppings can only occur between nearest-neighbor sites, if one of the sites is empty and the other double occupied. The first possibility is to empty the doubly occupied site and to doubly occupy the empty site.

These processes add terms to the effective Hamiltonian $T_i^- T_{i+d}^+$ with a prefactor $t^2/|U|$. There is a subtle but very important difference compared to super-exchange, In the super-exchange process the electron jumped forth and back, ending up at the site where it started: using complex hoppings $J \approx \frac{tt^*}{U} = \frac{|t|^2}{U}$ and J is always a real quantity. In the attractive case, both electrons move in the same direction and the J is therefore a complex quantity if the t's are complex — this innocent fact will turn out to be responsible for the peculiarities of the superconducting state. Summarizing, the virtual hoppings contribute to the effective Hamiltonian the term,

$$H_{\text{eff}}^{(2b)} = \sum_{i,\delta} \left(\frac{(t_i^\delta)^2}{|U|} T_i^+ T_{i+\delta}^- + \frac{((t_i^\delta)^2)^*}{|U|} T_i^- T_{i+\delta}^+ \right). \tag{6.4}$$

It is also possible for the electron to hop back to the lattice site where it started. These 'stay at home' processes are equivalent to the non-spin reversing processes in the repulsive model, and they turn out to give rise to the same contributions as in the spin case, but now in terms of the Cooper z-axis operators in equation 6.3

$$H_{\text{eff}}^{(2a)} = 2 \sum_{i,\delta} \frac{|t_i^\delta|^2}{|U|} \left(T_i^z T_{i+d}^z - \frac{1}{4} \right). \tag{6.5}$$

Together with equation 6.4, this implies that at half-filling the attractive fermion system is precisely described in terms of a Heisenberg Hamiltonian, with the only difference that the physical meaning of the $SU(2)$ algebra is now different. Hence the system is

completely described in terms of the $SU(2)$ algebra at all fillings. Away from half-filling, one looses the $SU(2)$ global symmetry which characterizes the Hamiltonian in equation 6.4 and 6.5: the 'spin' z-axis becomes inequivalent from the xy-plane. This is because away from half-filling there is no electron-hole symmetry. What remains is the XY symmetry of equation 6.4. This symmetry gets spontaneously broken in the superconducting state as will be shown in the next paragraph. The fundamental symmetry in the charge sector is therefore not $SU(2)$, but instead $U(1)$. Notice that in the presence of longer range interactions it is possible to stabilize either superconducting- or charge density wave order at half-filling: see Micnas, Ranninger and Robaszkiewics [126].

6.1.2 Quantum becomes classical

The Hamiltonian in the preceding equations is a quantum mechanical Hamiltonian in two or three dimensions. The spins are diagonal in z-space with two components, spin $\frac{1}{2}$. The exact solution of this model is difficult. However, this model is equivalent to a classical system (see for example the book by Sachdev [155]). The reason for this is that in general a quantum mechanical system in d dimensions is equal to a classical system in $d+1$ dimensions. This can be proved with a Suzuki-Trotter formula. In the case of quantum spins the resulting classical model is just a replacement of the spins by classical arrows. The Suzuki-Trotter transformation introduces one extra dimension in the problem. This dimension is the imaginary temperature axis. The length in this dimension is equal to the inverse temperature. If the temperature is zero, this extra dimension is infinitely long. However, for finite temperatures, it has a finite length. Thus, at a finite temperature the above quantum Hamiltonian is exactly equivalent to a classical Hamiltonian in $d+$ a finite extra length dimension. For the critical properties, the characteristic length scales go to infinity. Therefore, it is no longer important that there is an extra dimension, thus the model is equivalent to the classical model in d dimensions!

The classical sector of the problem in equations 6.4 and 6.5 can be used to construct the classical limit of a spin-problem. Using the $S = \frac{1}{2}$ spin coherent state, the wave function of the classical state becomes in terms of the fermion operators,

$$|\Phi^0_{Cl}(\{\Omega\})\rangle = \Pi_i (e^{-i\phi_i/2} \sin\theta_i/2 + e^{i\phi_i/2} \cos(\theta_i/2) c^\dagger_{i\uparrow} c^\dagger_{i\downarrow})|\text{vac}\rangle. \tag{6.6}$$

The empty- and doubly occupied sites take the role of the up- and down fermions of the real spin problem. The hopping is parametrized in terms of an absolute value t which is uniform on the lattice and a phase ϕ^δ_i which depends on the bond under consideration,

$$t^\delta_i = t e^{i\phi^\delta_i} \tag{6.7}$$

and the classical energy becomes

$$\begin{aligned} H_{\mathrm{SC}}^{\mathrm{Cl}} &= \langle \Phi_{Cl}^{0}(\{\Omega\}) | H^{0} + H_{eff}^{2a} + \tilde{H}_{eff}^{2b} | \Phi_{Cl}^{0}(\{\tilde{\Omega}\}) \rangle \\ &= -(|U| + 2\mu) \sum_{i} \left(\frac{1}{2} (\cos\theta_i + 1) + \frac{J}{4} \sum_{id} (\cos\theta_i \cos(\theta_{i+d})) \right. \\ &\quad \left. + \sin(\theta_i) \sin(\theta_{i+d}) \cos(2\psi_i^d - \phi_{i+d} + \phi_i) \right). \end{aligned} \tag{6.8}$$

When the system is half-filled ($\mu = -|U|/2$) the external field vanishes and the spins can be chosen to lie along the z-axis. Because the interaction is 'anti-ferromagnetic' this would give rise to a staggering of the T^z component. According to equation 6.3, this state corresponds with a charge density wave: doubly occupied sites on the A sublattice and empty sites on the B sublattice. Going away from half-filling ($\mu \neq |U|/2$) the spins 'flop' to the xy-plane and the effective magnetic field cants the spins uniformly in the (positive or negative) z-direction, just as would be the case for a Heisenberg antiferromagnetic in a real magnetic field. Although the z-component is fixed by the external field, i.e. the number of doubly occupied states is determined by μ, it is still possible to rotate the spins in the xy-plane: the $O(3)$ symmetry is explicitly broken to $O(2)$ (point on a circle), corresponding with the free rotations in the xy-plane, parametrized by the phase angle ϕ_i. This $O(2)$ symmetry gets spontaneously broken. At energies or temperatures much smaller than $||U| + 2\mu|$, the 'diagonal' charge density $\langle T^z \rangle$ does not fluctuate and θ_i takes some uniform value. Therefore the effective problem at low energies is

$$H_{\mathrm{eff}}^{\mathrm{Cl}}(\{\phi_i\}) = J\rho(t, U, \mu) \sum_{i\delta} \cos(2\psi_i^{\delta} - \phi_{i+d} + \phi_i), \tag{6.9}$$

where the effects of the uninteresting z-axis interactions are absorbed in the density ρ. The only important thing is that this quantity is finite. It is directly seen that the classical energy is minimized taking

$$2\psi_i^{\delta} - (\phi_{i+d} - \phi_i) = \pi, \quad \forall i, d. \tag{6.10}$$

The symmetry in the phase channel is spontaneously broken and equation 6.10 is the definition of the *superconducting order parameter*.

This is a classical model, no quantum mechanics is involved. The energy at $T = 0$ is minimized if all the ϕ_i are equal, so all arrows are pointing in the same direction. However, if the temperature is increased, the arrows will start to fluctuate. So, only at $T = 0$ will there be perfect long range order. Now imagine that somehow all the arrows on the left side of the sample are turned over some arbitrary angle and do not apply any force to the other arrows. What will happen at $T = 0$ is that all the other arrows will end up pointing in exactly the same orientation. This also happens to the arrows on the right side of the system. Thus, even without there being any 'transport of arrows' from the left to the right, the local interaction between the arrows has made it possible for the

right side to 'feel' that something changed on the left side. Even if there is for instance a big hole in the system where there are no arrow, the arrows around the hole still will transfer this information to the right[1]. Notice, that in order to transfer this information from the left to the right, there was no need to transport arrows from the left to the right.

6.1.3 Vector potential

What is the relation of all this to superconductivity? Superconductivity involves charged particles in a magnetic field. Therefore the influence of a magnetic field on electrons described by the Schrödinger equation has to be understood. It is more convenient to describe a magnetic field $\vec{B}$ by using the magnetic vector potential $\vec{A}$. The magnetic field and the vector potential are related by $\vec{B} = \nabla \times \vec{\mathbf{A}}$. To include the influence of this vector potential, one has to replace the momentum operator $\frac{h}{i}\nabla$ by $\frac{h}{i}\nabla - q\mathbf{A}$ in the Schrödinger equation. It can be shown that this recipe is exactly equivalent to changing the phase of the hopping amplitude t in the Hubbard model to

$$t_i \rightarrow t_i e^{\frac{iq}{\hbar c}Aa} \tag{6.11}$$

Therefore, the phase of a hopping is related to the vector potential.

Gauge invariance

An extra gradient can be added to A, without influencing B. This is gauge freedom. Because normally only B is measured, all physical properties should not depend on the gradient. If A is replaced by $A' = A + \nabla f$ than the resulting B will be the same. The scalar potential must also change ϕ to $\phi' = \phi - \frac{1}{c}\frac{\partial f}{\partial t}$.

The above discussion of the XY model then leads to

$$A = \phi_{i+\delta} - \phi_i$$

This is approximately equal to

$$\mathbf{A} = \nabla \cdot \phi. \tag{6.12}$$

Thus the spontaneous symmetry breaking in the XY model also leads to a spontaneous breaking of the gauge symmetry. The condensate forces the vector potential to take the form of the gradient of a function, while the function itself is still arbitrary. This is the essential, deep lying phenomena that is at the root of superconductivity.

The physical nature of the order parameter in equation 6.10 is completely different from the normal ordering in magnetism. It is seen that equation 6.10 also amounts to a condition on the *phase of the hopping*: $2\psi_i^{\delta}$ has to be compensated by the difference

[1]For this it is essential that the system is not one-dimensional. In one dimension, a single impurity will disrupt any order.

of the intrinsic phase $\phi_{i+\delta} - \phi_i$: *the phase of the hopping* $2\psi_i^\delta$ *is directly proportional to the vector potential of the electromagnetic field.* The vector potential is usually gauge invariant, but equation 6.10 breaks this gauge invariance. The fact that the ordering of the pseudo-spins also leads to a condition on the magnetic vector potential A leads directly to the Meissner effect. It also explains the superconducting currents.

6.1.4 Phase coherence

Although the gap is very important to show that the BCS mechanism is correct, it is not the essential property that is responsible for the superconductivity. The important thing is that the pairs will have a phase coherent wavefunction. The gap itself is only a manifestation of the underlying physics of pair formation. The characteristic features of superconducting systems, the Meissner effect, zero resistivity, quantized persistent currents in macroscopic rings and quantized flux lines, are the consequences of a long-range ordering process of an essentially quantum nature. This phase coherence can for instance be measured by the quantized magnetic flux through a superconducting ring. The effective unit of charge turns out to be $2e$ rather than e, showing that superconductivity indeed is caused by coherent *pairs*. The long range phase order leads to effects like flux quantization.

6.2 BCS: Small attractive U

The above discussion showed how a model consisting of electrons that are able to move on a lattice, can be shown to be superconducting. The essential part is that the electrons form pairs. However, the above model is also very unrealistic, because the electrons have to be on the same site, which is not very likely because of the Coulomb repulsion between the charged electrons. Electrons repel and do not attract, so the attractive Hubbard model with very strong interaction is not very realistic.

However, the phonons in a crystal can over-screen this repulsion and lead to a *very weak* attractive force between the electrons. Direct evidence that the ionic motion plays a role in establishing superconductivity is provided by the isotope effect discovered in 1950. The attraction can arise from phonons in the following way. As a negatively charged electron moves through a lattice of positive ions, it attracts and locally distorts the lattice in its neighborhood. The residual distortion left in its wake produces a net positive charge that attracts a second electron.

In the large U attractive Hubbard model there are local pairs. In BCS theory there are also pairs. This is based on Cooper's key idea (1956) that two electrons with opposite spins and direction of motion can lower their energy by forming a pair, if there is some sort of effective attractive force between them. He showed that if there is a small attraction between electrons, for instance caused by lattice vibrations, that electrons could

form pairs, not in real space, but in k-space. For this, it is essential that the electrons are fermions, because the other electrons, not in the pair, disallow states lower inside the Fermi sphere.

Pairing Hamiltonian

It can be argued that one should concentrate on these particular interactions in describing the ground state and the low-lying excited states. Phase-space considerations as well as effects due to the antisymmetry of the wave functions show that the $q = 0$ pair state should be macroscopically occupied in cases where the superfluid momentum density is zero (although $\mathbf{v}_s$ need not be zero in the presence of magnetic fields).

The creation and destruction operators for electrons of wavevector $\mathbf{k}$ and z-component of spin s ($\uparrow$ or $\downarrow$) are denoted by $c_{ks}^\dagger$ and c_{ks}, respectively. They satisfy the usual Fermi anti-commutation rules. And the operator $b_k^\dagger$ creates a pair of electrons in the single particle states $k\uparrow$ and $-k\downarrow$, that is,

$$\begin{aligned} b_k^\dagger &= c_{k\uparrow}^\dagger c_{-k\downarrow}^\dagger, \\ b_k &= c_{-k\downarrow} c_{k\uparrow}. \end{aligned} \tag{6.13}$$

This type of Hamiltonian forms the basis of the theory of superconductivity proposed by Bardeen, Cooper and Schrieffer.

The reduced BCS Hamiltonian or pairing Hamiltonian, operating only within the pair subspace (which includes only the configurations having both the Bloch states with opposing spin and momenta occupied or empty; reduced problem of the $q = 0$ pairs), can be written as

$$H = \sum_k \varepsilon_k (c_k^\dagger c_k + c_{-k}^\dagger c_{-k}) - \sum_{kk'} V_{kk'} b_{k'}^\dagger b_k. \tag{6.14}$$

Here $c_k^\dagger$ (c_k) are the creation (annihilation) operator for electrons in Bloch state $(k, \frac{1}{2})$ and the interaction matrix elements $V_{kk'}$ between the *pairs* with moment k and k' is nonzero and attractive only if the energy of both pairs lies within a small shell of thickness $\hbar\omega_D$ (ω_D is the Debye frequency) around the Fermi energy.

It is clear that if V is attractive, the ground state of H_{red} has no state occupied by a single electron. In this case the operator $n_{k\uparrow} + n_{-k\downarrow}$ can be replaced by $2b_k^\dagger b_k$ that is, twice the pair occupation number. The reduced Hamiltonian is then

$$H_{\text{red}}^0 = \sum_k 2\varepsilon_k b_k^\dagger b_k + \sum_{kk'} V_{kk'} b_{k'}^\dagger b_k. \tag{6.15}$$

It should be noted that the pairs are not true Bose particles (but rather pairs of fermions). Therefore one cannot place all bosons in the lowest state. Rather, one finds by direct calculation the commutation relations

$$[b_k, b_{k'}^\dagger] = 0, \qquad \text{for} \quad \mathrm{k} \neq \mathrm{k}',$$

$$[b_k, b_{k'}^\dagger] = 1 - (n_{k\uparrow} + n_{-k\downarrow}), \qquad \text{for} \quad \mathrm{k} = \mathrm{k}', \tag{6.16}$$

and

$$[b_k, b_{k'}] = 0 = [b_k^\dagger, b_{k'}^\dagger]. \tag{6.17}$$

These are not of the form required by Bose-Einstein statistics. The factor $(n_{k\uparrow} + n_{-k\downarrow})$ in the second represents the effect of the Pauli principle acting on the individual electrons forming the pair. The Pauli principle leads to $(b_k^\dagger)^2 = 0 = b_k^2$ for $k = k'$, which ruins a simple Bose gas picture. Instead, they are hard-core Bosons.

6.2.1 Pseudo-spin representation

The normal way to work with the BCS model is to use a variational BCS wavefunction for the ground state with u_k and v_k and the Bogoliubov transformation. It was Anderson [7,8] who first noticed that the commutation relation for b_k are exactly those of hard-core bosons and thus one can write down the pairing Hamiltonian in terms of a pseudo spin Hamiltonian. A simple mean-field solution of this pseudo-spin representation model of the BCS Hamiltonian gives all superconductivity related properties. Anderson has exploited the formal similarity between the commutation relations in equations 6.16 and 6.17 and those for a collection of fictitious Pauli spin operator $\mathbf{S}_k$. The connection between the two sets is

$$\begin{aligned} 2S_{z\mathbf{k}} &= 1 - (n_{k\uparrow} + n_{-k\downarrow}), \\ S_k^x + iS_k^y &= b_k^\dagger, \\ S_k^x - iS_k^y &= b_k. \end{aligned} \tag{6.18}$$

Because they are spins, we also have

$$[S_k^x, S_{k'}^y] = iS_k^z \delta_{kk'}. \tag{6.19}$$

Using this, the reduced Hamiltonian can be written as

$$\begin{aligned} H_{\mathrm{red}}^0 &= \sum_k 2\varepsilon_k (S_k^x + iS_k^y)(S_k^x - iS_k^y) + \sum_{kk'} V_{kk'} (S_k^x + iS_{k'}^y)(S_k^x - iS_k^y) \\ &= \sum_k 2\varepsilon_k (S_k^{x2} + S_k^{y2} - i[S_k^x, S_k^y]) + \sum_{kk'} V_{kk'} (S_{k'}^x S_k^x + S_{k'}^y S_k^y - i[S_{k'}^x, S_k^y]). \end{aligned} \tag{6.20}$$

Now, using $[S_k^x, S_k^y] = iS_k^z$ and $[S_{k'}^x, S_k^y] = 0$ and $\left(S_k^x\right)^2 + \left(S_k^y\right)^2 = 0$ this simplifies to

$$\begin{aligned} H_{\mathrm{red}}^0 &= \sum_k 2\varepsilon_k S_k^z + \sum_{kk'} V_{kk'} (S_{k'}^x S_k^x + S_{k'}^y S_k^y) \\ &= \sum_k 2\varepsilon_k S_k^z + \sum_{kk'} V_{kk'} (S_{k'}^x S_k^x + S_{k'}^y S_k^y). \end{aligned} \tag{6.21}$$

So, this quantum mechanical XY model in a magnetic field is exactly equal to the BCS pair Hamiltonian.

In the pair subspace, eigenvalues of n_k and n_{-k} are the same (1 or 0). In terms of the pseudo-spin operators S^z, S^+ and S^-, defined above, one can easily rewrite the reduced BCS Hamiltonian in equation 6.14 which is the same as a XY model in a transverse magnetic field, written in terms of the pseudo-spin operators.

6.2.2 Solution classical model

Using this approximation, one can reduce the many-body Hamiltonian to a collection of effective (single) spins. They are described by the classical Hamiltonian

$$H = -\sum_k \varepsilon_k S_k^z - \frac{1}{4}\sum_{k',k} V_{k'k}(S_{k'}^x S_k^x + S_{k'}^y S_k^y). \tag{6.22}$$

Note that it contains no S^zS^z terms. An exact solution of this model is still difficult to obtain. However in the ordered state, not too close to the transition temperature, all spins are strongly coupled. Therefore strong fluctuations can be ignored. Then a spin only feels the average influence of its neighbors. Therefore, the above Hamiltonian can be studied using the molecular field theory (see [36]), where the many-particle Hamiltonian is written as the collection of isolated spins in a fictitious magnetic field

$$H = -\sum_k \mathbf{h}_k \cdot \mathbf{S}_k, \tag{6.23}$$

Here $\mathbf{h}_k$ is the effective molecular field at the site i. $\mathbf{h}_k$ and $\mathbf{S}_k$ are treated as classical vectors in the pseudo-spin space and are written as

$$\begin{aligned} \mathbf{h}_k &= \varepsilon_k \hat{z} + \frac{1}{2}\sum_{k'} V_{kk'}(\langle S_{k'}^x\rangle \hat{x} + \langle S_{k'}^y\rangle \hat{y}), \\ \mathbf{S}_k &= S_k^x \hat{x} + S_k^y \hat{y} + S_k^z \hat{z}. \end{aligned} \tag{6.24}$$

Here, $\hat{x}$, $\hat{y}$ and $\hat{z}$ denote unit vectors in the pseudospin space. The effective magnetic field is not oriented along the z-axis, but makes an angle θ with it. Since, at zero temperature, the energy is minimized when S_k is polarized in the direction of the effective molecular field h_k, one can write (with $\langle S_{k'}^y\rangle = 0$),

$$\frac{h_k^x}{h_k^z} = \frac{S_k^x}{S_k^z} = \frac{\frac{1}{2}\sum_{k'} V_{kk'}\langle S_{k'}^x\rangle}{\varepsilon_k} = \tan\theta_k. \tag{6.25}$$

Now using $S_{k'}^x = S\sin\theta_{k'}$ with $S = 1$, a formula for the tangent of θ_k can be derived

$$\tan\theta_k = \frac{1}{2\varepsilon_k}\sum_{k'} V_{kk'}\sin\theta_{k'}. \tag{6.26}$$

This is sometimes called the BCS integral equation. To solve equation 6.26, set $\Delta_k = \frac{1}{2}\sum_{k'} V_{kk'} \sin\theta_{k'} = \varepsilon_k \tan\theta_k$ and using $\sin\theta_{k'} = \cos\theta_{k'}\tan\theta_{k'} = \frac{\tan\theta_{k'}}{\sqrt{1+\tan^2\theta_{k'}}}$, so that

$$\Delta_k = \frac{1}{2}\sum_{k'} V_{kk'} \frac{\Delta_{k'}}{\sqrt{\Delta_{k'}^2 + \varepsilon_{k'}^2}}. \tag{6.27}$$

This equation is called the gap equation. If Δ is assumed to be independent of k, then Δ is a constant. The above formula can be simplified by replacing the summation by an integral over ε from $-\hbar\omega_D$ to $+\hbar\omega_D$. The transformation from k to ε is achieved by using $\int dk = \int N(\varepsilon)d\varepsilon$ where $N(\varepsilon) = \frac{dk}{d\varepsilon}$ is the density of states. Assuming that the attractive potential $V_{kk'}$ is constant in this region and given by $V_{kk'} = V$ and assuming that Δ is independent of k, equation 6.27 reduces to

$$\begin{aligned} 1 &= \frac{V}{2}\int_{-\hbar\omega_D}^{+\hbar\omega_D} d\varepsilon \frac{N(\varepsilon)}{\sqrt{\varepsilon^2+\Delta^2}} \\ &= VN(0)\int_0^{\hbar\omega_D} \frac{d\varepsilon}{\sqrt{\varepsilon^2+\Delta^2}} \\ &= VN(0)\operatorname{arcsinh}\frac{\hbar\omega_D}{\Delta} \end{aligned} \tag{6.28}$$

Inverting the last equation one arrives at the BCS gap equation

$$\Delta = \frac{\hbar\omega_D}{\sinh\frac{1}{N(0)V}} \approx 2\hbar\omega_D e^{-\frac{1}{N(0)V}}, \tag{6.29}$$

where $N(0)$ is the density of states at the Fermi level and it is assumed that $VN(0) \ll 1$. It is clear that the energy gap is positive if the interaction V is positive.

The low T_c follows from the fact that the binding energy is exponentially small and depends in a non-analytic way on the potential energy of attraction.

6.2.3 Finite temperature

At a finite temperature T, there is a probability that $\langle S_i\rangle$ does not point along h, but instead in the opposite direction. Then $E = -\mu_0 H$ or $E = +\mu_0 H$. The probabilities for up and down are $P_\uparrow = e^{\mu_0 H/T}/Z$ and $P_\downarrow = e^{-\mu_0 H/T}/Z$. Thus the average is $\mu_0 P_\uparrow - \mu_0 P_\downarrow = \frac{\mu_0}{Z}(e^{\mu_0 H/T} - e^{-\mu_0 H/T}) = \mu_0 \tanh(\mu_0 H/T)$.

The average magnetization can be written as

$$\langle S_k\rangle = \tanh\beta|h_k|; \quad |h_k| = \sqrt{\varepsilon_k^2 + \Delta^2(T)}. \tag{6.30}$$

The BCS integral equation 6.26 is then modified to (replacing $|h_{k'}|$ with $\tanh\beta|h_{k'}|$).

$$\tan\theta_k = \frac{1}{2\varepsilon_k}\sum_{k'} V_{kk'}\tanh\beta|h_{k'}|\sin\theta_{k'} = \frac{\Delta}{\varepsilon_k}, \tag{6.31}$$

thus

$$\Delta_k = \frac{1}{2}\sum_{k'} V_{kk'} \tanh\beta|h_{k'}| \sin\theta_{k'}. \tag{6.32}$$

This leads to

$$\Delta_k = \frac{1}{2}\sum_{k'} V_{kk'} \frac{\Delta_{k'}}{\sqrt{\Delta_{k'}^2 + \varepsilon_{k'}^2}} \tanh\beta|h_{k'}|. \tag{6.33}$$

Again assuming Δ to be independent of k the result is

$$1 = \sum_{k'} \frac{V_{kk'}}{2} \frac{\tanh\beta|h_{k'}|}{\sqrt{\Delta^2 + \varepsilon_k^2}}, \tag{6.34}$$

or

$$\frac{1}{V} = N(0)\int_0^{\omega_D} d\varepsilon \frac{\tanh\frac{1}{2}\beta\sqrt{\varepsilon^2+\Delta^2}}{\sqrt{\varepsilon^2+\Delta^2}}. \tag{6.35}$$

The phase transition from the superconducting state to the normal state occurs at a temperature T_c given by $\Delta(T_c) = 0$. This leads to $h_k = \varepsilon_k$ and

$$1 = \sum_{k'} \frac{V_{kk'}}{2\varepsilon_{k'}} \tanh\beta\varepsilon_{k'}. \tag{6.36}$$

Thus replacing the summation once again by an integral and performing partial integration,

$$\begin{aligned}
\frac{1}{N(0)V} &= \int_0^{\hbar\omega_D} d\varepsilon \frac{\tanh(\frac{1}{2}\beta\varepsilon)}{\varepsilon} \\
&= \int_0^{\beta_c\hbar\omega_D} d(\ln x)\tanh(\frac{1}{2}x) \\
&= \ln(\beta_c\hbar\omega_D)\tanh(\beta_c\hbar\omega_D/2) - \int_0^{\beta_c\hbar\omega_D} dx \ln(x)\frac{d}{dx}\tanh\frac{1}{2}x.
\end{aligned} \tag{6.37}$$

The integrand of the last term differs only from zero close to $x = 0$. Numerical integration gives $\ln(1.13)$. Therefore

$$\beta_c\omega_D = e^{\frac{1}{N(0)V}} e^{\ln 1.13}. \tag{6.38}$$

Because the Debye temperature is much larger than T_c, the tanh is equal to one. Inverting, one obtains

$$T_c = 1.13\hbar\omega_D e^{-\frac{1}{N(0)V}}, \tag{6.39}$$

for $VN(0) \ll 1$. One can use equation 6.29 in equation 6.39 to obtain the BCS gap equation

$$2\Delta = 3.53T_c. \tag{6.40}$$

This is a universal value, that agrees with the old superconductors. Thus, transforming the reduced BCS Hamiltonian into a XY model in a transverse field, one can obtain the BCS results using simple mean field theory [7, 8, 19, 36, 78].

The BCS theory is very successful and leads to an expression for the total energy, which can be used to calculate for instance the specific heat. Furthermore, BCS theory predicts the outcome of experiments with ultrasonics, infrared spectroscopy, microwaves, sound absorption and nuclear relaxation (de Gennes [53], Schrieffer [159]). The binding energy of a pair is directly measurable with tunneling, where an electron needs an energy larger than the gap. The BCS gap disappears at T_c. If the thermal energy is larger than the binding energy, there will be no superconducting pairs anymore and the system will stop being superconducting.

6.3 Local pairing versus BCS

In three dimensions the negative U Hubbard model has two well understood borderline cases. One is the weak coupling limit $U \ll t$. In this case the model shows superconductivity of mean-field BCS type with a large coherence length of the Cooper pairs. The second well understood case is the limit of strong coupling and low densities $U \gg t$, with n approximately equal to zero. In this case pairs of electrons which now form composite Bosons condense into a two particle bound state and the Fermi surface is destroyed.

In the strong coupling attractive U Hubbard model, there are always pairs. There only is superconductivity if the pseudo-spins order at a lower temperature. The BCS theory is special in the sense that the formation of the pairs and the formation of long-range order take place at the same temperature. As soon as there are pairs, the system has long range order. Thus, although the phenomena of superconductivity is caused by the establishment of long-range coherence, in BCS theory this is equivalent to the formation of the pairs. Therefore, in BCS theory, the binding energy or superconducting gap Δ can be taken as the order parameter of superconductivity, if one takes it as a complex parameter, with both an amplitude and a phase.

The fact that the order parameter and broken symmetry are essentially unchanged when the interactions are changed from weakly attractive in $\mathbf{k}$-space to strongly attractive in real space is actually far from obvious. There could be phase transitions when varying the range and nature of the interaction. As shown in the review article of Micnas, Ranninger and Robaszkiewicz [126], research in the last few years has shown, however, that the cross-over from large Cooper pairs to local pairs is smooth, and that there is no phase transition.

There is a long history associated with this small pair theory. Leggett was the first to propose in 1980 a variational ground state wave function which exhibited a smooth interpolation between the BCS and Bose-Einstein regimes. Nozières and Schmitt-Rink [140] extended Leggett's ideas to non-zero temperature and thereby deduced a transition tem-

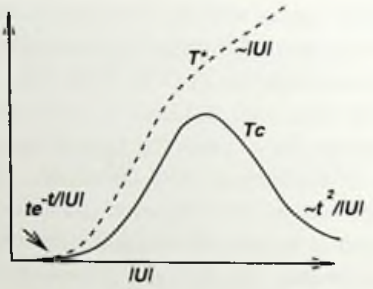

Figure 6.1: Schematic phase diagram of the (half-filled) attractive Hubbard model illustrating the crossover from a BCS superconductor with a Fermi liquid normal state (in the weak coupling $|U|/t \ll 1$ limit) to a condensate of bosons with a normal Bose liquid state above T_c (for $|U|/t \gg 1$). T_c is the transition temperature at which phase coherence is established and T^* is a crossover scale below which pairing correlations become manifest in the normal state. From Randeria [152].

perature T_c which varied continuously with increasing coupling constant g from the BCS exponential dependence on g to the Bose-Einstein asymptote. They offered an illuminating discussion of the problem of transition from weak-coupling to strong-coupling superconductivity. They concluded that at the ground state this transition is smooth (i.e., there is no sharp distinction between superconductivity and pair Bose condensation at $T = 0$K), though the properties of these two limiting cases are in many aspects quite different. They showed that the strong-coupling and the weak-coupling limits of superconductivity are adiabatically connected. The system can be tuned from weak pairing to strong pairing without encountering a phase-transition. In the case of the s-wave superconductor, using the extended Hubbard model with on-site attraction, a continuous evolution from weak coupling to strong coupling limit of the thermodynamic and electromagnetic properties as well as collective modes is obtained. This implies that weak- and strong-coupling superconductivity are qualitatively similar. In the weak-coupling limit, the transition mechanism becomes that of BCS superconductivity, where the Kosterlitz-Thouless transition coincides with the temperature of thermal destruction of composite boson, with a satisfactory description by mean-field equations. See also the work by Denteneer and Van Leeuwen [58, 59, 193].

It is generally agreed that the cuprates are in the short coherence length limit of the pairing state, so that essentially pair "molecules" are first formed and then Bose condensed.

Figure 6.1 shows the phase diagram of the half-filled attractive Hubbard model for a simple cubic lattice for $n = 1$. There are two characteristic temperatures on the diagram, T_c and T_p, denoting the critical temperature for the onset of long range ordering and for the breaking of electronic pairs, respectively. In the region with long-range order the

two-electron excitations from the singlet superconducting state will be gapless, whereas the excitations from the charge density wave state have a gap. In the region of uncorrelated pairs, there is short-range order, and this phase is diamagnetic with a gap of order $|U|$ in a one-electron excitation spectrum.

For weak attraction the superconducting critical temperature T_c follows the BCS theory, increasing with $e^{-|t|/U}$ (although the form of this increase depends on the density of states used), while in the strong-attraction limit it decreases as $t^2/|U|$. In the strong-attraction limit the pairs exist above T_c and they condense below it. This is in contrast tot the BCS-dominated regime, in which electronic pairs are created and condense at the same temperature.

Differences between local pairs and BCS superconductivity

In BCS only a small number of electrons near E_F participate in the Cooper pairing. In real-space pairing non-ordered pairs can exist above T_c, and at T_c they undergo a Bose condensation. In BCS the Cooper pairs are formed and condensed at T_c. In real-space pairing the energy gap in the single-particle spectrum is approximately given by $|U|$ (the binding energy of a local pair). This E_g exists above T_c and at T_c the system goes from singlet superconductivity to a non-metal or a local pair metal. In BCS the gap decreases monotonically with increasing T and at T_c there is a singlet superconductor to metal transition. In real-space pairing the critical behavior can deviate from the classical Ginzburg-Landau type critical behavior of BCS. For BCS the critical region is very narrow and usually inaccessible. The universality class of local pairing is that of $S = \frac{1}{2}$ quantum XY model. This has a large critical regime and a breakdown of mean-field behavior.

6.3.1 Two dimensions

In two dimensions, however the situation is different. Here it has been shown by Schmitt-Rink, Varma and Ruckenstein [158] that for any coupling strength the Fermi surface is lost and Bose condensation (at $T = 0$) takes place. The phase diagram of the negative-U Hubbard model on a two-dimensional square lattice has been studied using the quantum Monte Carlo simulation technique by Scalettar *et al.* [157] and also by Denteneer and Van Leeuwen [58, 59, 193]. They concluded that there $T_c = 0$ at half-filling but with a groundstate having both superconducting and charge density wave long-range orderings. Away from half-filling they found a Kosterlitz-Thouless phase transition at finite temperature into a superconducting state with power-law decay of the pairing correlations. They indicate a smooth transition between weak and strong-coupling regimes. The problem of evolution from weak- to strong-coupling superconductivity at finite temperatures is more involved than in the three-dimensional case, due to the absence of Bose condensation in two-dimensional systems for $T \neq 0$ K.

6.4 BCS for cuprates fails

The preceding sections have shown what BCS is. However, the BCS theory does not work for the cuprates. Seen from the perspective of the BCS model, the properties of the cuprates are considered very strange.

Similarities

The cuprates do display a number of properties that are similar to those of conventional BCS superconductors. They both have a Meissner effect, perfect conductivity, long range phase coherence, show the Josephson effects and can be described by the Ginzburg-Landau equations. In both cases one can define an order parameter which has an amplitude and a phase. Flux quantization, Josephson tunneling experiments, Andreev reflection and NMR Knight-shift measurements have demonstrated that the superconducting state in the cuprates involves electrons that are paired in singlet spin states. Other experiments include observation of the ac-Josephson effect, flux jump measurements, and direct measurements of the magnetic flux quantum ϕ_0 .

Failure of BCS theory for cuprates

On the other hand, a lot of the experimental properties of the new high-T_c superconductors showed that they are not normal BCS superconductors. First, the high value of T_c is very difficult to achieve in BCS theory. In order to increase T_c in BCS theory, the interaction between phonons and electrons would have to become stronger and stronger. However, strong phonons means that the crystal starts to vibrate more and more. This would lead to the melting of the crystal or to a change in crystal structure, killing the superconductivity. Secondly, no isotope effect on T_c has been found, so the involvement of a phonon mechanism seems unlikely. BCS theory also gives a number of universal relationships between among others the correlation lengths, gaps and T_c. The theoretical values for these relationships are completely different from the experimentally determined values in the cuprates. The superconducting coherence length is extremely short: conventional superconductors have coherence lengths of approximately 10^{-6} m, whereas the cuprate superconductors have coherence lengths on the order of 10^{-9} m. For instance, magnetic measurements indicate that in La-Sr-Cu-O compound, $\xi_0 = 20$Å. The small value of the Fermi energy and $\xi_0 k_F \approx 5 - 10$ (for $YBa_2Cu_3O_7$) indicate that all carriers can be involved in pairing and that the size of a pair is on the order of the inter-particle distance, in contrast to the BCS regime, where $\xi_0 k_F \gg 1$. The high-temperature superconductors are "bad metals" for which the concept of a quasiparticle is not well defined. Therefore, phase transitions to a superconducting state or to states with charge or spin order are not consequences of a Fermi surface instability. The poor conductivity of a bad metal also leads to poor screening and to an enhanced role

for the Coulomb interaction. Moreover, the cuprates have an energy gap which shows practically T-independent behavior all the way up to T_c. Another question, crucial for real materials, concerns the coexistence of bound pairs and itinerant electrons and the effects resulting from interactions between these two species. Micnas, Ranninger and Robaszkiewics [126] have written a large overview article comparing local pairing to BCS. Their conclusion is that the cuprates have local pairing.

No Fermi liquid

Another reason for assuming that BCS theory does not apply to the cuprate superconductors is the fact that there is no evidence for quasi-particles in the normal state of the cuprates. This means that Landau's theory of a Fermi liquid is not valid and the whole structure of Cooper pair formation as a Fermi surface instability resulting from an attractive interaction between quasi-particles does not apply. There are many experimental reasons for abandoning Fermi liquid theory for the cuprates. If quasi-particles exist, they should give rise to a peak in the energy spectrum, with that peak growing more narrow as k approaches the Fermi momentum. However, no well defined quasi-particles have been found by ARPES above T_c in the normal state of any of the cuprates. This is unrelated to experimental difficulties, because ARPES has no problem to show the quasi-particle peaks which do exist in the superconducting state. The peaks that are observed have a width which varies linearly with $E - E_F$, whereas the Fermi liquid pictures requires the width to go as $(E - E_F)^2$. According to analysis of resistivity there are no well defined quasi-particles or Fermi surface in the normal state of high temperature superconductors. The temperature dependence of the electrical resistivity in the *ab* plane in the normal phase varies essentially as T rather than as the universal T^2 of the Fermi liquid[2].

Normal state is an insulator

Above T_c the resistance is linear in T for optimally doped cuprates, which means that the resistance increases with temperature. Thus at temperatures above T_c these cuprates are metals. However, it is important to know what would happen at lower temperatures if superconductivity would not intervene. One way to change a sample from superconducting to normal, without doing permanent damage to it, is applying a strong magnetic field. Boebinger *et al.* [12] have shown that when superconductivity in La_2CuO_4 is suppressed by an applied magnetic field, the underdoped superconductors are not metals but insulators. They used a 61 Tesla pulsed magnetic fields to quench the superconductivity, thus revealing the normal state at low temperatures. This again suggests that an

[2]Varma, Nussinov and Van Saarloos [195] have given an overview of theoretical ideas and calculations and the experimental results for systems which depart from Landau Fermi-liquids (the "Non-Fermi" liquids).

instability in a Fermi-liquid is not the way the cuprates become superconducting. The insulator-metal transition is unusual in that all underdoped samples ($x < 0.16$) show low-temperature insulating behavior, even in samples with a linear temperature dependence of the in-plane resistivity above T_c. In every underdoped sample, except at $x = 0.12$, both in-plane (ρ_{ab}) and c-axis resistivity (ρ_c) diverge as the logarithm of the temperature ($\log \frac{1}{T}$). This is unusual and might be related to charge localization. As the carrier concentration is increased in the underdoped regime, the divergence becomes weaker until an insulator-to-metal transition occurs simultaneously in ρ_{ab} and ρ_c at optimal doping ($x \approx 0.16$).

6.5 Other models than BCS

The preceding section has shown that BCS is not applicable. How can this be fixed? A major problem for any mechanism of high temperature superconductivity is how to achieve a high pairing scale in the presence of the repulsive Coulomb interaction, especially in a doped Mott insulator in which there is poor screening. In the high temperature superconductors, the coherence length is no more than a few lattice spacing, so neither retardation nor a long-range attractive interaction is effective in overcoming the bare Coulomb repulsion.

Nevertheless ARPES shows that the major component of the gap function is proportional to $\cos k_x - \cos k_y$. This implies that, in real space, the gap function (and hence in BCS theory the net pairing force) is a maximum for holes separated by one lattice spacing, where the bare Coulomb interaction is very large (0.5 eV, allowing for atomic polarization). It is not easy to find a source of an attraction that is strong enough to overcome the Coulomb force at short distances and achieve a high transition temperature in a natural way by the usual Cooper pairing.

6.5.1 Senthil and Fischer

One intriguing proposal is that of Senthil and Fischer [165]. Superconductivity requires the charge carriers to condense into a single quantum state — and the Pauli exclusion principle means that pairing is usually the only way to achieve this. However, Senthil and Fischer note that superconductivity might even take place without any pairing between charge carriers. They claim that the separation of charge and spin releases the chargons from this restriction, allowing them to condense into a single quantum state without pairing ever taking place. However, recent work by Bonn *et al.* [28] and Kirtley *et al.* [101] seems to cast doubt on this possibility.

6.5.2 The Little model

Little was the first one to consider a non-phonon mechanism for superconductivity [111]. Little's work was also important because it revived the dream of high-T_c. Little considered a polymer with the conduction electrons moving along the main axis. In addition, there are side branches, whose electrons perform oscillatory motion. The main feature of this model is the existence of two groups of electrons. One of the conduction electrons will, by means of the usual Coulomb forces, induce motion of the side-branch electrons. This in turn will affect the state of another conduction electron. In this way, there arises an additional interaction between the electrons on the main branch, brought about by the electrons on the side branches. These side branch electrons take over the role played by the lattice ions in the usual superconductors. They form the auxiliary system that gives rise to pairing of conduction electrons. In this way, a superconducting state develops in the main axis. In the one-dimensional case involving just one conducting chain, there are strong electron density fluctuations which destroy long-range superconducting correlations. However, in a quasi one-dimensional system, like an anisotropic filamentary crystal, the interaction between filaments can suppress the fluctuations. All the principal features and advantages of the Little model remain.

6.5.3 Spin-gap proximity effect

There is one theory for superconductivity related to stripes. Just as in the Little model, a conducting one-dimensional structure is assumed. In this case this is not a polymer, but the stripes in a cuprate. Emery, Kivelson and Zachar [73–75] *assume* that stripes contain mobile holes and that they can be described as one-dimensional *metals*. Normally, for a one-dimensional system to be superconducting, an attractive interaction is needed. A spin gap occurs only if there is an attractive interaction in the spin degrees of freedom. However, the stripes influence the surrounding antiferromagnet. Not because of motion of the electrons or holes on a stripe, but just by being there. Two stripes laterally confine an intervening antiferromagnetic region. Because of this, the AF acquires a spin gap. Only an infinite antiferromagnet has Goldstone modes with zero energy. Therefore, the stripes induce a spin gap in the intervening Mott-insulating regions through spatial confinement by charge stripes. Just as for the Little model, the active environment of the stripe helps the superconductivity.

This spin gap is communicated back to the stripes by pair hopping. The mobile holes on an individual stripe acquire a spin gap via pair hopping between the stripe and its environment. This is a magnetic analog of the usual superconducting proximity effect. This process is the analog of pairing in conventional superconductors. The active environment adds a new element to the picture by allowing the formation of a spin gap with purely repulsive interactions.

At non-vanishing stripe densities Josephson coupling between stripes produces a

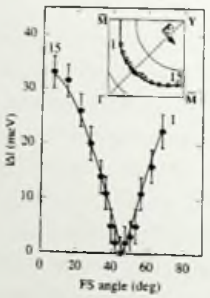

Figure 6.2: ARPES evidence for a d-wave gap from Ding et al. *[64]. The figure shows the Y quadrant energy gap in meV versus angle on the Fermi surface. The solid curve shows fits to the data using a d-wave gap. The inset shows the locations of the data points in the zone as well as the photon polarization direction.*

dimensional crossover to a state with long-range superconducting phase coherence. In contrast to conventional superconductors the superconducting state is characterized by a high density of (spin) pairs, but the phase stiffness which is determined by the density and mobility of holes on the stripe is very low.

There is a local separation of spin and charge on an individual stripe, as in a one-dimensional electron gas. This relation between spin and charge is of central importance for overcoming the Coulomb problem. On a stripe, the objects that form pairs are neutral fermions (spinons), which are not impeded by the Coulomb interaction. The order parameter relies on spin-pairing and does not require the existence of bound pairs of holes. Because of the local separation of spin and charge the spin gap fixed point is stable even in the presence of strong Coulomb interactions, and there is no mass renormalization to depress the onset of phase coherence.

6.6 *d*-wave superconducting gap

In BCS theory, the energy gap is the signature that pair binding is taking place. Because of the large size of a Cooper pair in BCS theory the details of the lattice structure are not very important. Therefore, the electrons in a pair do not have a preferred orientation and this results in a gap that is the same for all directions. This is called *s*-wave pairing. Everything is spherical symmetric.

This however, is not the case in the cuprates. In the cuprates the gap depends strongly on the direction in space. Along the Cu-O-Cu or $(\pi,0)$ direction, the gap is a maximum, while in the diagonal or (π,π) direction there is no gap. The most direct evidence for this

comes from photo-emission experiments. Below T_c there is a sharp quasi-particle peak in the photo-emission spectrum that is shifted away from the Fermi energy for all directions. The value of this gap for the different directions is shown in figure 6.2. Ding *et al.* [63] find a gap function consistent with the form $\cos k_x - \cos k_y$ expected for a d-wave order parameter. They report measurements of the momentum dependence of the superconducting gap in $Bi_2Sr_2CaCu_2O_{8+x}$ with angle-resolved photo-emission spectroscopy using a dense sampling of the Brillouin zone in the vicinity of the Fermi surface. The maximum gap is approximately 35 meV, which is larger than for BCS superconductors. Shen *et al.* [166] were the first to present ARPES data indicating significant momentum anisotropy in the gap function for the two-layer Bi cuprate $Bi_2Sr_2CaCu_2O_8$. Measurements of the gap in $Bi_2Sr_2CaCu_2O_{8+\delta}$ by tunneling and photo-emission indicate that the superconducting gap increases while T_c decreases on the underdoped side.

The pairing symmetry in cuprate superconductors has been reviewed by Tsuei and Kirtley [186]. A number of other types of measurements had been performed earlier that are more indirectly sensitive to the absolute value of the gap as a function of momentum. These type of experiments include the temperature dependence of the penetration depth, microwave surface conductivity, NMR relaxation rate, electronic specific heat, thermal conductivity and Raman scattering. The results of these studies are generally consistent with the above idea of a superconducting state with $d_{x^2-y^2}$ symmetry. Penetration depth measurements on Y-Ba-Cu-O indicate that the gap has line nodes in momentum space. In such a d-wave superconductor the gap vanishes at four points on the (two-dimensional Fermi surface). The quasi-particle excitations at these "nodes" have a linear dispersion, and an associated density of states that vanishes linearly on approaching the Fermi surface. This leads to power law dependence of various physical quantities on temperature.

The momentum dependence of the gap can also be determined by looking at experiments that are sensitive to the phase of $\Delta(k)$. These measurements, all of which involve the Josephson effect, include SQUID interferometry, single junction modulation, tri-crystal ring magnetometry, c-axis Josephson tunneling and grain boundary tunneling. These experiments also indicate that the superconducting order parameter in the $YBa_2Cu_3O_{6+x}$ and TBCCO hole-doped materials has $d_{x^2-y^2}$ symmetry. (Wollman *et al.* [209] and Tsuei and Kirtley [186]).

The symmetry of the gap gives information about the underlying physics of pair formation. Most theories naturally lead to an isotropic gap. However, d-wave pairing is something that follows quite naturally from pairing of electrons in an antiferromagnetic background. Since the Fourier transform of this quantity vanishes unless the distance is one lattice spacing, it follows that the gap (and hence, in BCS theory, the net pairing force) is a maximum for holes separated by one lattice spacing, where the bare Coulomb interaction is very large (≈ 0.5 eV, allowing for atomic polarization).

Still, the superconductivity in the cuprates is caused by electron pairs. This has been shown for instance by flux quantization measurements. From penetration depth

measurements it is known that the correlation length in the cuprates is very short, of the order of a few lattice constants. If the correlation length is assumed to be equal to the average separation between electrons in a pair (as it is in BCS theory), the pairs are very localized in space. Thus, experiments point to an electron only model (no phonons) with *repulsive* Hubbard interactions and end up with something that looks very much like the *attractive* Hubbard model. Although this is a very difficult problem, a possible way to achieve this is by looking at bond-centered stripes.

Results from Poilblanc [145, 147] on two holes in an antiferromagnet show that two holes will bind together in local pairs, a distance of $\sqrt{2}$ apart. He also shows that this configuration is equivalent to d-wave pairing, because of the sign changes related to the embedding antiferromagnet. There is a similar ordered state of short-range hole pairs in stripes in t-J DMRG calculation of White and Scalapino. There are very few explicit models which exhibit real-space hole pairs in an antiferromagnet and for which superconductivity has been demonstrated.

The establishment of d-wave pairing symmetry in high-T_c cuprates does not necessarily specify a high-T_c mechanism. It does impose well-defined constraints on possible models for this mechanism. The BCS pairing interaction is relatively attractive for small momentum transfer q and repulsive for large q. Antiferromagnetic spin fluctuations leads to $d_{x^2-y^2}$ pairing symmetry. It is worth noting that in t-J and Hubbard ladders, d-wave like pairing is the dominant form of pairing observed in both analytic and numerical studies. Scalapino [156] has been very active in making the case that the $d_{x^2-y^2}$ pairing in the cuprate superconductors is caused by holes in an antiferromagnet.

6.7 Pseudogap

The magnitude of the superconducting gap does not go to zero at T_c. In the underdoped cuprate the gap evolves smoothly as the temperature is increased through T_c. ARPES demonstrates that above T_c, but below T^*, the pseudogap is present in the energy dispersion of the normal state electrons. ARPES and scanning tunneling spectroscopy experiments showed a smooth crossover from the pseudo- to superconducting gap. The transition into the true superconducting state at T_c is barely noticeable. Moreover the pseudo- and superconducting gaps also reveal experimentally the same $d_{x^2-y^2}$ wave symmetry vector dependence of the order parameter. They also have the same magnitude. It is clear that the superconducting gap emerges from the normal state pseudogap. The pseudogap and the superconducting energy gap appear to be intimately related to one another, with the former the precursor of the latter. In different experiments the characteristic temperature T^* below which the anomalies attributed to pseudogap appear can somehow change depending on the quantity being measured. T^* does not represent a phase transition, but only determines some characteristic crossover temperature energy scale below which the pseudogap behavior appears.

Photo-emission experiments reveal that the pseudogap is roughly of the same size and has the same type of k-dependence as the d-wave superconducting gap. Furthermore, the gap size is essentially independent of doping x and even increases slightly when T_c is reduced with decreasing x.

Doping dependence

Marshall *et al.* [117] and Ding *et al.* [62] have found that the pseudogap near the Brillouin zone face persist above the superconducting transition temperature and grows in magnitude as doping is reduced. This feature which is also seen in optical conductivity and the "spin gap" effect seen in magnetic resonance, has the momentum dependence expected of a simple d-wave superconductor. The pseudogap disappears at different temperatures for different k. This means that the d-wave node below T_c becomes a gapless arc above T_c which expands in length with temperature, until the entire Fermi surface is recovered at T^*. They is found that the gap increases as the doping concentration is reduced from its optimum value, while at the same time T_c decreases. This results in highly anomalous ratios of $2\Delta/k_BT_c$, which were reported to be able to become larger than 12 in $Bi_2Sr_2CaCu_2O_8$, compared to the weak coupling BCS value of 3.54 (see equation 6.40). ARPES results also indicate that the angular dependence of the gap function on the Fermi surface, which below T_c follows the $\Delta k = \Delta d \cos 2\theta$ shape expected for a $d_{x^2-y^2}$ order parameter, develops extended gapless regions around the nodes above T_c whose size increases with T. As already mentioned, Ding *et al.* [62] find that optimally and overdoped samples exhibit a d-wave gap. They also find that this gap which closes at the same temperature T_c for all k points. They find that T^* scales with the maximum low temperature gap, increasing as the doping is reduced.

Conductivity

Pseudogap formation is clearly seen in the experiments on single-particle tunneling. Below T^* there are deviations from the high temperature linear resistivity, resulting in a clear break in slope at T^*. For the resistivity for instance, as the system becomes more underdoped with decreasing x, the in-plane resistivity deviates from linear behavior at higher temperature at a characteristic temperature T^*, which represents a crossover into the pseudogap state at $T < T^*$. In addition, an excitation gap is also deduced from the suppression of the in-plane scattering rate, measured by infrared reflectivity. Analysis of the Hall coefficient and uniform susceptibility of underdoped samples reveal a temperature scale T^* below which there appears to be a gap. This temperature scale increases very quickly as the samples become more underdoped, with T^* reaching as high as 600 K. The optical data in the far-infrared region, taken on underdoped single-layered high-T_c superconductors show clear evidence of a pseudogap state in both the scattering rate and conductivity along the CuO_2 planes.

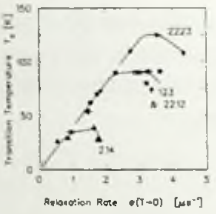

Figure 6.3: The superconducting transition temperature T_c plotted versus low-temperature muon-spin relaxation rate $\sigma(T \to 0)$ measured in 16 different specimens of CuO high-T_c superconductors. The horizontal axis is proportional to $1/\lambda^2$ and consequently to n_s/m^*. From Uemura et al. *[188].*

Explanations for pseudogap

There have been a number of explanations for the pseudogap. Some believe that the electrons separate into spinons and holons; spinons have spin but no charge and holons have charge but no spin. According to some mean-field theory calculations, the spinons form singlet pairs well above the superconducting T_c with superconductivity setting in only when the holes become phase coherent at T_c. In RVB models which incorporate spin-charge separation into spinons with spin $S = \frac{1}{2}$ and charge $q = 0$ and holons with $S = 0$ and $q = +e$, where e is the charge of the electron, the spinons become paired (spin pseudogap) at T^* and coherent pairing of holons (Bose-Einstein condensation) occurs at T_d, resulting in superconductivity. However, this can not explain the continuity of the d-wave symmetry and the experimental fact that there is also a gap in charge excitations above T_c. The most convincing explanation of the pseudogap phase is the idea of precursor formation of pairs above T_c and a phase-coherency transformation at a lower temperature (see the review by Timusk and Statt [177]).

6.8 Proportionality of T_c and superfluid density

That there is a relationship between the superfluid density and the critical temperature has been shown by Uemura *et al.* [188]. They used muon spin resonance (μSR) to determine the magnetic field penetration depth λ which is related to the superconducting carrier concentration n_s through $\frac{1}{\lambda^2} \propto \frac{n_s}{m^*}$, where m^* is the effective mass. They found that the relationship between T_c and $\sigma(T \to 0) \propto n_s/m^*$ is a universal linear relation with increasing carrier doping (see figure 6.3). Samples from different series and different materials with single, double and triple layers of CuO planes in the unit cell all fall on the same line. In heavily doped samples, however, T_c shows saturation and suppression with increasing n_s/m^*. This saturation starts at different values of n_s/m^* for the various series of high-T_c superconductors.

Both T_c and $\sigma(T \to 0)$ represent the experimentally measured quantities. From other experiments it is known that the superfluid density is proportional to the number of holes in the system. Thus T_c is proportional to n_s. This is why T_c is so low [18]. The natural energy scale is much higher. The fraction of particles participating in the condensate determines the superfluid density n_s. Uemura *et al.* show that the energy scale is set by n_s.

6.9 Preformed pairs and phase fluctuations

In the BCS theory of superconductivity, pair formation and phase coherence occur simultaneously, but in the underdoped region the two steps seem to occur at different temperatures. The theoretical interpretation of a number of different experimental facts shows that at a high temperature electron pairs are being formed, but that the pairs do not develop a long-range coherence until a lower temperature. The reason for this is the low superfluid density of the cuprates. It is known that the superfluid density is proportional to the number of holes in the system. This means that for the underdoped samples the superfluid density is very small. This results in large penetration depths, but also in a very small stiffness to fluctuations in the phase of the order parameter. Because in BCS systems the limiting factor is the destruction of pairs, the Ginzburg-Landau theory focuses on the gap. For the high-T_c superconductors, one has to focus instead on the dynamics of the phase. In copper-oxides, the phase stiffness is the weak link, in particular in the underdoped region. This leads to the appearance of two distinct energy scales: the pairing energy scale Δ_o and the phase coherence scale Δ_c, which is equal to T_c observed experimentally. The two energy scales have different dependencies on hole concentration in CuO_2 planes: Δ_p increases linearly with decrease of hole concentration, where as Δ_c has approximately the parabolic dependence on p and scales with T_c as $2\Delta_c/k_BT_c \approx 5.4$.

Superconductivity in metals is the result of two distinct quantum phenomena, pairing and long-range phase coherence. In conventional homogeneous superconductors the phase stiffness is so great that these two phenomena occur simultaneously. On the other hand, in granular superconductors and Josephson junction arrays, pairing occurs at the bulk transition temperature of the constituent metal, while long-range phase coherence occurs, if at all, at a much lower temperature characteristic of the Josephson coupling between superconducting grains. High-temperature superconductivity is hard to achieve, even in theory, because it requires that both scales be elevated simultaneously; yet they are usually incompatible. Consider, for example, the strong-coupling limit of the negative-U Hubbard model. Pairs have a large binding energy but typically, they Bose condense at a very low temperature because of the large effective mass of a tightly bound pair (The effective mass is proportional to $|U|$ in the Hubbard model). A second problem for achieving high-temperature superconductivity is that strong ef-

fective attractions, which might be expected to produce a high pairing scale, typically lead to lattice instabilities, charge- or spin-density wave order, or two-phase (gas-liquid or phase-separated) states. In these models, the superconductivity occurs in the underdoped regime when the phases of the pairs become coherent, not when the pairs are first formed.

However, the phenomenon is quite general and the attractive Hubbard model just serves as an illustration of this. As stressed in particular by Emery and Kivelson [72], superconductivity requires more than just paired charge carriers - it also requires 'phase coherence' between those pairs. As the pseudogap exists almost up to room temperature, it shows that the cuprate structure makes it possible for pairs to form at high temperatures, well above T_c. The onset of superconductivity does not signify the formation of pairs, but the setting in of phase coherence below T_c. The value of T_c is governed by the zero-temperature value of the phase stiffness, which sets the energy scale for the spatial variation of the superconducting phase.

Emery and Kivelson [72] pointed out that in the BCS mean-field theory, an estimate of T_c is give by $T_c = \Delta_0/1.76$, where Δ_0 is the energy gap measured at zero temperature. This is a good approximation for conventional superconductors. However, this criterion does not give a good estimates of T_c for the high temperature superconductors, especially for underdoped materials: $\Delta_0/1.76T_c$ varies with doping and can be much greater than one. If the transition temperature is given by the establishing of phase coherence, than a rough upper bound on T_c is obtained by considering the disordering effects of only the classical phase fluctuations. T_c must than be of the order of $T_\theta = A\rho_s$, where ρ_s is the zero-temperature value of the phase stiffness, which sets the energy scale for the spatial variation of the superconducting phase and A is a number of order unity.

The stiffness ρ_s may be expressed in terms of the superfluid density $n_s(T)$, or equivalently, the experimentally-measured penetration depth $\lambda(T)$ at $T = 0$. For example for Pb, T_θ is about 10^6 Kelvin. The fact that this is much higher than the observed critical temperature explains why BCS theory works so well for conventional metals.

Superconductors with low superconducting carrier density are characterized by a relatively small phase stiffness and poor screening, both of which imply a significantly larger role for phase fluctuations.

Thus, in conventional superconductors, Δ is much smaller than ρ_s, and the destruction of superconductivity is driven by the breakup of electron pairs. In the underdoped cuprates the ordering is apparently reversed, with the phase stiffness now the weaker link. When the temperature exceeds $\approx \rho_s$, thermal agitation will destroy the ability of the superconductor to carry a supercurrent while the pairs continue to exist; thus T_c is bounded above by a pure number times $\rho_s(T = 0)$. Evidently the quasi-particle owes its existence to the phase coherence of the superconducting state, and not the energy gap. T_c marks the destruction of infinite-range phase order. The schematic phase diagram that these considerations suggest is given in figure 6.4.

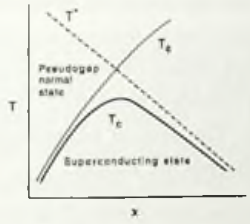

Figure 6.4: Schematic phase diagram from Maple [116] that shows the temperature T^* at which pairs are formed and the critical temperature T_c at which phase coherence is achieved. For underdoped samples there is a large area in phase-space where there are d−wave pairs, but no phase coherence. This is the pseudogap region. For overdoped samples, T_c is limited by the pair-formation.

The above scenario can be made more quantitative in the limit of small phase coherence (doping) with the aid of the classical XY model. The classical phase Hamiltonian is given by an XY model:

$$H = V_0 \sum_{ij} \cos(\theta_i - \theta_j). \tag{6.41}$$

This has a transition to a low-temperature ordered state in three dimensions if $T < T_c$. At a certain temperature, this ordered phase will be destroyed by classical fluctuations. If V_0 is independent of temperature, the phase ordering temperature T_θ is equal to AV_0, where A is a number of order unity. At zero temperature, V_0 is given in terms of the superfluid density $n_s(T = 0)$ or, equivalently, the experimentally measured penetration depth $\lambda(T = 0)$ as:

$$V_0 = \frac{\hbar^2 a}{4m^*} n_s(0) = \frac{(\hbar c)^2 a}{16\pi(e\lambda(0))^2} \tag{6.42}$$

where a is a length scale that depends on the dimensionality of the material. An estimate for T_c is given by the smaller of $\Delta_0/2$ and T_θ (the two lines in figure 6.4). Decreasing x leads to decreasing n_s leads to a decreasing V_0. For underdoped high temperature superconductors, $\Delta_0/2$ is closer to T^* than to T_c, whereas T_θ is very close to T_c itself. In other words, because the high temperature superconductors are doped insulators, $n_s(0) \to 0$ as $x \to 0$ and therefore phase ordering controls T_c.

Because the planes in the cuprates are not completely decoupled, Carlson *et al.* [33] have investigated the XY model in equation 6.41 in the anisotropic three-dimensional case, to model the coupled stacks of superconducting CuO planes. They analyzed an XY model of classical phase fluctuation using a low temperature expansion and Monte Carlo simulations. In agreement with experiment, the value of n_s at temperature $T = 0$

is a quite robust predictor of T_c, and the evolution of n_s with T, including its T-linear behavior at low temperature, is insensitive to microscopic details. The results are not very sensitive to the exact short-distance nature of the interactions. The model yields a $n_s(T)$ curve that looks different from a rounded Kosterlitz-Thouless discontinuity because of the coupling between the planes. The critical phenomena are in the same universality class as the classical three-dimensional XY model.

6.10 Cuprates

The idea that follows from the above line of reasoning is that the underdoped materials are above T_c in a state with a non-zero local amplitude of superconducting pairing. However, this state is not truly superconducting due to thermal fluctuations in the phase of the order parameter. Within such a scenario the transition at T_c is of the Kosterlitz-Thouless type, slightly rounded by the weak coupling between the copper-oxygen planes along the c-axis. In a strictly two-dimensional system the Kosterlitz-Thouless transition is associated with proliferation of unbound vortex-antivortex pairs. Weak coupling between the planes leads to correlated motion between vortices in adjacent planes which form three-dimensional vortex loops close to the critical temperature. The transition to the disordered phase is then characterized by the appearance of vortex loops with arbitrarily large radii [33].

6.10.1 Temperature dependence of penetration depth

Phase fluctuations give a good description of the temperature dependence of the superfluid density below T_c. Hardy *et al.* [84] measured the temperature dependence of the London penetration depth $\lambda(T)$ at low temperatures in $YBa_2Cu_3O_{6.95}$. They demonstrated that when $\rho_s(T)/\rho_s(0)$ (or $\lambda^2(0)/\lambda(T)^2$) is plotted versus T/T_c for various dopant concentrations in $YBa_2Cu_3O_{7-\delta}$, the data collapse onto one curve. T_c increases with the number of planes per unit cell.

In other words, T_c is the one and only energy scale involved in the temperature dependence of $\lambda(T)$ for overdoped, optimally doped, and underdoped samples of $YBa_2Cu_3O_{6+x}$. The entire temperature dependence of $\lambda(T)$ is governed by classical phase fluctuations. Therefore, T_c increases until the two lines cross at an optimal doping. For low T_c superconductors like Pb and Nb_3Sn, the phase fluctuation temp is more than a 1000 times higher than T_c, thus phase fluctuations are not important. However, for the cuprate superconductors, they are roughly the same. This shows that T_c is determined by phase fluctuations.

6.10.2 Superconductivity above T_c

Although the binding of electrons into Cooper pairs is essential in forming the superconducting state, its remarkable properties require phase coherence among the pairs as well. What happens at the transition temperature T_c is that long-range phase coherence is lost. However, pairing remains: there are still pairs above T_c. Together with phase correlations which are finite in space and time. However, they no longer are phase coherent on a long range. However, close to T_c, there still will be short-range phase coherence. It should therefore be possible to find evidence of superconductivity in the material, but only over very short distances or timescales. One way to measure this is to look at the high frequency conductivity. Because of the high frequency, only small length scales will be probed. Two different kind of experiments have been done: high frequency conductivity and the measurement of the Nernst effect.

High frequency conductivity

Tera Hertz optical experiments are a much faster probe than the usual microwave measurements. Because of this, they are sensitive to short-time, short-range phase coherence properties of high-T_c materials above T_c. The recent measurements by Corson *et al.* [45] in underdoped $Bi_2Sr_2CaCu_2O_{8+\delta}$ provides evidence for a phase-fluctuation driven transition from the superconducting normal state. They measured the high frequency conductivity that track the phase-correlation time τ in the normal state of the $Bi_2Sr_2CaCu_2O_{8+\delta}$ family of underdoped copper oxide superconductors. Just above T_c, they find that τ reflects the motion of thermally generated topological defects in the phase (vortices). At low frequency, σ will approach a real constant. At high frequency, they measure the superconducting state. The crossover takes place at the phase-correlation time. The signature of partial phase coherence is that the phase stiffness becomes frequency-dependent above T_c. At very low frequency, ρ_s will be zero, as expected for a normal material. However, if ρ_s were measured at a frequency greater than the de-phasing rate, the superfluid density would tend to a non-zero value proportional to the short-range or *bare* phase stiffness. The frequency dependence of ρ_s can be determined from measurements of the ac conductivity. Their measurements verified that the transition to the normal state takes place when ρ_s is comparable to T_c. A frequency-dependent ρ_s could be detected at a temperature interval of about 10 to 20K above the transition. This shows that phase correlations indeed persist above T_c, but they vanish well below T^*. The crossover to the completely incoherent regime takes place when the de-phasing rate reaches k_BT. They have found phase correlations accompanying pairing in the normal state and they studied how the samples responded to a rapidly alternating electrical field. It shows that Kosterlitz-Thouless type fluctuations are observed near and above T_c. Above T_c they found small vortices regions in which the material become non-superconducting. And the number of these vortices grew with temperature.

Nernst effect

Other evidence for a regime of partial coherence above T_c comes from experiments by Xu *et al.* [211]. They report evidence for vortex-like excitations in $La_{2-x}Sr_xCuO_4$ at temperatures significantly above the critical temperature. Their method consisted of heating one edge of a thin cuprate sample to a higher temperature than the other edge, while applying a magnetic field. This magnetic field creates vortices that are detected by the large transverse electric field produced as they diffuse down the temperature gradient (the Nernst effect).

6.11 Extended pairs $\neq$ superconductivity

The local pair model and the BCS model do not suffice to explain the superconductivity in the high-T_c cuprate superconductors. The problem with both models is that because of the strong Coulomb repulsion the electrons are repelling each other, not attracting. On the contrary, the claim for the high-T_c superconductors is that they are a realization of a strongly *repulsive* Hubbard model.

However, the results from the attractive Hubbard model do not apply in the case of $U \rightarrow \infty$. The problem is that because $U \rightarrow \infty$, the real space pair is extended over at least two sites. Therefore T^+ and T^- have to annihilates and create holes at two different sites. A pair therefore has an orientation in real space: $0-0$ or 8. You do not have this possibility for $U \rightarrow -\infty$ where both electrons of a pair are on one site. The problem this raises is that the creation of $0-0$ does not commute with 8 if one of the two is the same site. The commutator is a diagonal hop, not a T_z. Therefore, the algebra is not closed. The main reason for this serious problem is the fact that we are dealing with a two-dimensional plane, so we can have both vertical and horizontal pairs. This is caused by the simple fact that we cannot have two pairs on the same site, causing the pairs to be extended and thus the holes in the pair have a relative orientation in space. The fact that our algebra is not closed makes it impossible to easily map the electron problem into a model equivalent to the attractive Hubbard model or the BCS model. This problem is not restricted to the repulsive Hubbard model. If one would have an *attractive* Hubbard model with extended pairs (like one would have with pairs having d-wave symmetry), the same problem arises. Therefore, one should take claims for superconductivity in attractive d-wave Hubbard models with a grain of salt as long as they do not explain this fundamental problem with the commutation relations.

One notable example of a model that explains how to get rid of this problem is a model by Van Duin and Zaanen [192], who invented a $\frac{1}{5}$ depleted lattice with Cooper pairs, or dimers, with only spin-spin interactions. Using this strange lattice, they present a model for the strong coupling limit of high-temperature superconductivity. Similar to the strong coupling negative U Hubbard model, the single-electron states are projected

out and one is left with a model of tightly bound Cooper-pairs.

6.12 Conclusion

In this chapter it has been shown that superconductivity is a collective effect. The superconducting phase is the phase where the gauge symmetry is broken and there no longer is charge conservation. The supercurrent is a Goldstone mode, identical to that which follows from an XY model in a magnetic field. There are two known models which are superconducting. The attractive Hubbard model and the BCS model. Both models form pairs which are effective hard-core bosons. This allows both models to be mapped on the XY model in a magnetic field, which assures that they are superconducting. The attractive Hubbard model is easier to understand because it forms real-space Cooper pair. However, because of repulsion that is a very unlikely model. We have also seen that the BCS theory does not apply to the cuprate superconductors. Effects like the pseudogap and the existence of pairing and short-timescale superconductivity above T_c show that there are strongly bound pairs in the cuprates. From this it can be learned that it would be quite promising if one were able to find a theory in a repulsive Hubbard model that forms real-space pairs and maps these hard-core bosons onto an effective XY model in a magnetic field.

Chapter 7

The sublattice parity principle

In the next chapter, an attempt is made to explain why stripes would want to form and why they are build up from real-space pairs. One major assumption in that chapter is that single holes in an antiferromagnet can be considered to be a quasi-particle. That this is the case is not obvious. It is well known that a single hole in an antiferromagnet gives rise to string states and that the movement of single holes is frustrated because of this. In this chapter we look at existing numerical data and show that by looking at second order perturbation theory, it can be seen that a single hole moves through the lattice in steps of two. This *sublattice parity principle* amounts to the assumption that a hole in an antiferromagnet is free and can move to all of its *next* nearest but not to its direct neighbors. This principle is based on and follows from the sublattice structure of antiferromagnetic order. Phenomenological evidence for this assumption will be provided by examining the dispersion relations obtained by existing detailed numerical works.

7.1 Spin flips

It is well known that the Hubbard model for a half-filled system in the large U limit leads to an effective Heisenberg model,

$$H_{\text{Heisenberg}} = \sum_{\langle ij \rangle} \frac{J_\perp}{2}(S_i^+ S_j^- + S_i^- S_j^+) + J_z S_i^z S_j^z, \tag{7.1}$$

with $J_\perp = J_z = J$.

The last (Ising) term of the Heisenberg Hamiltonian wants to make the spins on neighboring lattice sites point in opposite directions. If only this term is present, the groundstate will be a perfect Ising antiferromagnet with long-range (Néel) order: the lattice can be subdivided in an up sublattice and a down sublattice. However, the first (XY)

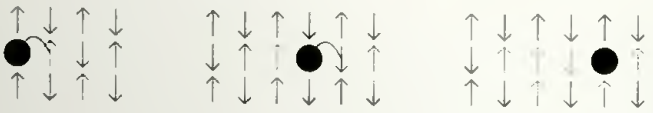

Figure 7.1: If a single hole in an antiferromagnet moves by nearest neighbor hopping of surrounding spins, it cannot move without creating a string of flipped spins. For small values of $J_\perp$, there are no spin flips that can destroy this string. This leads to a linearly increasing confining potential and the eigenfunctions are Airy *wave functions. Because of this string, a single hole cannot easily propagate through an antiferromagnet by nearest neighbor hops.*

term in the Hamiltonian can undo this order by flipping two neighboring, opposite spins. In principle this term can completely destroy the long range order and indeed it does so in one dimension. In dimensions $d \geq 3$ clear sublattice order prevails. A large amount of effort in numerical calculations and the very important analysis of the non-linear sigma model by Chakravarty, Halperin and Nelson [37] have shown that the ground-state of the two-dimensional Heisenberg model (and thus of the undoped Hubbard model) is a long range antiferromagnet for which there exists a two-sublattice structure. The groundstate of the antiferromagnet is not exactly given by the classical Néel state which one would expect from the Ising model. The spin-flip term leads to a finite density of flipped spins (approximately 20%) which give rise to a lowering of the magnetization. It also leads to spin-waves. These spin-waves destroy the long-range antiferromagnetic order at any finite temperature. However, one can define a correlation length and on distances smaller than this length, we can still speak about local antiferromagnetic order. For $T > 0$, we have local order with a correlation length that decreases with increasing temperature. Therefore, thinking in terms of an Ising model is not incorrect as long as one keeps in mind that there is a finite density of flipped spins in the lattice. In the remainder of this chapter we will neglect these spin flips.

A well known argument leads to the conclusion that a single hole cannot propagate freely in an antiferromagnet. As shown in figure 7.1, whenever a non backtracking single hole moves from one sublattice to the other, it creates a string of flipped spins in its wake. This leads to a linear confining potential that strongly inhibits hole motion between different sublattices.

This, however, is not the only process that can take place. Figure 7.2 shows that it is also possible for a hole to move two steps without creating a confining string potential. This is a second order process in perturbation theory. First we create a second hole two sites away from the first hole. We do this by moving that electron one site closer, next to the first hole. This gives rise to a doubly occupied intermediate state with a high energy U. Then, we let the same electron move again, now removing the first hole. The amplitude for the total process is given by $\sigma = \frac{t^2}{U}$, much smaller than t, the first order

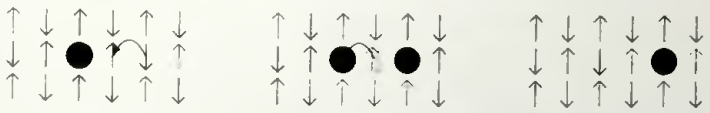

Figure 7.2: A single hole can still move through an antiferromagnet without generating string states by hopping in steps of two. This way it stays on the same sublattice. For this it has to go through an intermediate state with a doubly occupied site. This intermediate state costs an energy U. This leads to movement of the hole on the same sublattice with an amplitude $\propto t^2/U$.

hopping amplitude. However, the final state has exactly the same energy as the starting state. There are eight sites to which a single hole can hop in this fashion. Note that throughout the entire process, the magnetic quantum number in figure 7.2 is preserved, e.g. $S_z^{tot} = \hbar/2$ if perfect Néel order prevails everywhere around the fragment displayed in the figure for a lattice with an even number of sites.

Within the t-J and t-J_z approximations to the Hubbard model, same sublattice hops are more masked. In the t-J model, only a third order process links a hole to one of its next-nearest neighbors on the same sublattice. Albeit holding for models derived from the Hubbard model on bipartite lattices, in many instances the sublattice parity principle becomes much more alive and transparent within the original Hubbard model itself.

7.2 Numerical dispersions

Numerical simulations of the Hubbard and Heisenberg model with a single hole have found a discrete number of sharp peaks in the spectrum which could be identified with string-states [27, 31, 47, 48, 50, 70, 107, 112, 113, 118, 148, 154, 156, 168, 185, 197, 225]. The longer the string, the higher the energy of the peak. Because there is a gap between the first and second peak, we can confine our attention to the lowest peak. This peak has a finite quasi-particle weight. The dispersion of this peak as a function of k, tells us about the effective movement of a hole through an antiferromagnet. A recent numerical result from Louis *et al.* [113] for this dispersion relation in the Hubbard model is shown in figure 7.3. From the above it should come as no surprise that the band-width for single holes in an antiferromagnet is proportional to t^2/U as shown in the inset to figure 7.3.

The central result of numerous investigations is that they all found that a sharp quasi-particle peak appears at the bottom of a broad continuum of the hole spectrum. These quasi-particle poles form a coherent hole band with a width of order of $2J$ over a wide range of J/t, and the coherent propagation is made possible by "healing" a string of flipped spins by quantum fluctuations.

One can easily Fourier transform the numerical low energy hole dispersion relation $\varepsilon(\vec{k})$ to unveil the important real space quasi-particle motions and their respective

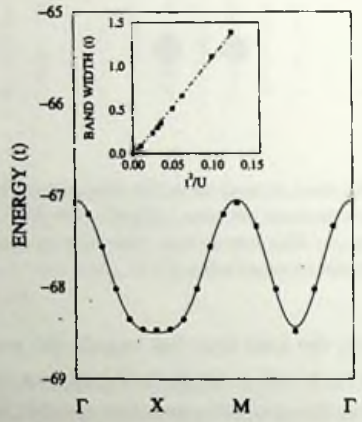

Figure 7.3: Quasi-particle band structure for a single hole on a 12×12 *square lattice with periodic boundary conditions and* $U = 8t$. *The solid line corresponds to the fitted dispersion relation (see text). The inset shows the bandwidth as a function of* t^2/U *for* $U \geq 8t$. *The fitted straight line is* $-0.022t + 11.11t^2/U$. *From Louis, Guinea, López Sancho and Vergés [113].*

amplitudes. If we make the simplifying assumption that the hole is the quasi-particle then we find that essentially all of the low energy weight is distributed among the next-nearest neighbor motions linking the hole to its sublattice. This is a consistent logical outcome of a strong local Néel order fused with the fact that the magnetic moment is a conserved quantum number. That the nearest states on the same sublattice (and those further away) have the highest weight could hardly be surprising. Hopping amplitudes to sites which are further and further away on the same sublattice drops significantly with distance [113].

Stated alternatively, if on the two-dimensional lattice, the hopping amplitude to any of the four co-linear sites (twice (up, down, right or left)) is t_0 and if motion to any of the four diagonal sites has amplitude t_2) then the dispersion relation will read

$$\varepsilon_k = \varepsilon_0 - 4t_2 \cos k_x \cos k_y - 2t_0(\cos 2k_x + \cos 2k_y). \tag{7.2}$$

From lowest order perturbation theory [34], we immediately expect $t_2 = 2t_0 = -O(\frac{t^2}{U})$ where the relative factor of two originates from the two paths by which we may reach diagonal sites by two consecutive hops as compared to the single two-step route to longitudinal next nearest neighbors. As illustrated in figure 7.4, renormalized hopping amplitudes of the same order of magnitude $O(\frac{t^2}{U})$ reproduce the detailed and tedious numerical fits of figure 7.3 remarkably well.

In accordance with expectations from perturbation theory, it is indeed found nu-

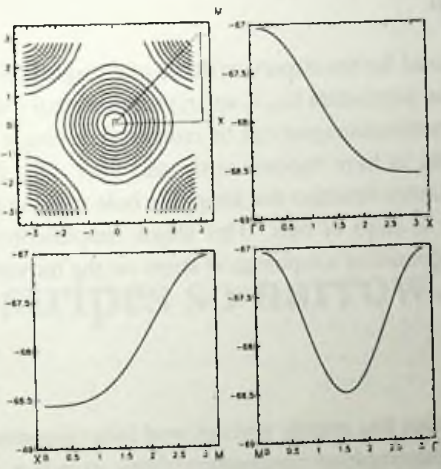

Figure 7.4: Dispersion relation for a single hole in an antiferromagnet according to the simple view that the hole is a quasi-particle that moves on one sublattice by hopping in steps of two (equation 7.2). Here we employ $\varepsilon_0 = -68.15t$, $t_2 = -1.52\frac{t^2}{U}$ *and* $t_0 = -0.70\frac{t^2}{U}$ *with* $U = 8t$.

merically that diagonal (*nodal*) hopping is almost twice as large in amplitude as compared to longitudinal hopping with both amplitudes of order $O(\frac{t^2}{U})$. In figure 7.4, we show the theoretical dispersion curves coming from equation 7.2 for $t_0 = -0.70\frac{t^2}{U}$ and $t_2 = -1.52\frac{t^2}{U}$ and $\varepsilon_0 = -68.15t$. These curves capture all the essential features of the numerical dispersion curve shown in figure 7.3.

The maximum in energy is at Γ and M, where $\varepsilon_{max} = \varepsilon_0 - 4t_2 - 4t_0$. The minimum in energy is the X point with $\varepsilon_{min} = \varepsilon_0 + 4t_2$. Thus the total bandwidth is given by $W = |8t_2 + 4t_0| \approx 12\frac{t^2}{U}$. This is vindicated in the inset of figure 7.3. Note that the influence of the diagonal hops is most important near the X point. This leads to a very flat band in this region. It is obvious that the Brillouin zone has doubled as a result of the fact that the hole is moving in steps of two through the lattice.

Large J means in principle both large J_z and $J_\perp$. A large $J_\perp$ leads to spinflips being relatively important and this will repair the string-states. Increasing the value of J, and thus of $J_\perp$, leads to spin-flips which will restore a string to the normal antiferromagnet. However, the relevant region of the Hubbard model and the t-J model is the region of small values of J. The physical reason for this effect is the difference in time-scales between the t and J processes. For large values of U we are in the small J and thus large t limit. Therefore, the hopping processes (t) are much faster than the string-restoring spin-flips (J).

7.3 Conclusion

The very good fit obtained for the dispersion curve of a single hole in an antiferromagnet by introducing the three parameters (ε_0, t_0 and t_2) suggests that the complicated problem of a single hole in an antiferromagnet can be reduced to a single particle problem. The surrounding spins seem to have become static and their only function is to create a checkerboard like sublattice structure that keeps the hole moving on only one sublattice, by forcing it to move in steps of two. This major simplification is used in the next chapter to study the influence of a topological stripe on the movements of holes.

Chapter 8

Why are stripes so narrow?

In this chapter it is demonstrated how narrow stripes and pairing follow from a single simple principle: a strong antiferromagnetic background forces injected holes to hop in steps of two such that they always remain on the same sublattice. When applied to a domain wall in an antiferromagnet, this simple effect naturally leads to a number of results. First, it is demonstrated that the holes are immediately (exponentially) localized on stripes. Consequently, it will be shown that the holes on a stripe favor the formation of pairs on neighboring rungs or sites. In this way the well known pictures of stripes found by White and Scalapino by numerical Density Matrix Renormalization Group (DMRG) calculations are recovered. Throughout this work much emphasis is placed on the problem of a two-leg ladder immersed in a staggered magnetic field.

8.1 Outline

In the previous chapter, the sublattice principle was introduced, which will form the backbone of this analysis. Invoking the sublattice principle, it will be show in section 8.4 how exponentially localized wavefunctions will be found when it is assumed, self-consistently, that stripes form anti-phase domain walls. From this, it will be found that the transverse stripe scale is of the order of the lattice constant. What drives stripe formation in this picture are not confining magnetic string potentials, but a rather novel kinetic effect which will be termed *dynamical confinement.*

Once it is established, self-consistently, that bond centered stripes form domain walls in the surrounding antiferromagnet, we will move in small steps towards examining further microscopics. As will be explained in section 8.5, we will consider a bond centered stripe engulfed by a surrounding antiferromagnetic region as a two-leg ladder immersed in an external staggered magnetic field. We will then consider the problem of a single electron on a staggered empty two-leg ladder (section 8.6) which will facilitate

the analysis of a single hole on an otherwise full staggered two-leg ladder (section 8.7). Both problems will lead to similar results.

This will be followed by a similar analysis for a two-electron system on an empty staggered ladder and the inverted problem of two holes on a full staggered ladder, in Sections 8.8 and 8.9 respectively. The surprising conclusion is that in this case there is an essential difference between electrons and holes. Numerically, it will be found that for holes, pair states are slightly favored over single hole states although the correlations are very faint. Having shown how narrow bond centered stripes with bound pair states emerge, in section 8.11 all of this chapter's findings will be fused together to reconstruct the real space DMRG pictures of White and Scalapino. In section 8.12, the effects of longer range Coulomb effects and additional longer range kinetic terms are examined to show how much of this self-consistent analysis can easily be fortified by the addition of such terms.

8.2 Sublattice parity principle

The physics of holes and spins in two dimensions is a very complicated subject. In this chapter the simplifying assumption will be invoked that much of the low-energy physics of holes in a strong antiferromagnetic background can be summed up simply as

Holes can only move in steps of two.

This principle is equivalent to the omission of spin-flips, spin-waves, and "magnetic" string states. This sublattice parity principle is, of course, a gross oversimplification — the physics of hole motion in an antiferromagnetic is a fascinating and rich topic. Nonetheless, the low-energy single hole dispersion curves (requiring careful extensive numerical work) coincide very well with those immediately following from this principle.

In recent years, hole dynamics on the stripe has been primarily addressed in terms of spinon-holon excitations, as in the early works of Tchernyshyov and Pryadko [175]. In this chapter it is *not* assumed that the elementary excitations are spinons and holons. This approach is closer in spirit to the work of Chernyshev, White, and Castro Neto [43], which tries to answer the same fundamental questions concerning stripes. Their work examines the elementary excitations within the framework of the t-J_z model. They do this by looking at retraceable paths of a hole out of the stripe into the surrounding antiferromagnet. Much of the same physics is arrived at using the sublattice parity principle as the only guide. These derivations are much more pedestrian yet physically transparent as compared to the detailed Green's function and numerical DMRG analysis carried out by these authors.

Many works place much emphasis on the string states created by hole motion or on kinks [221]. In the analysis of this chapter, there are *no string states*. The role of a

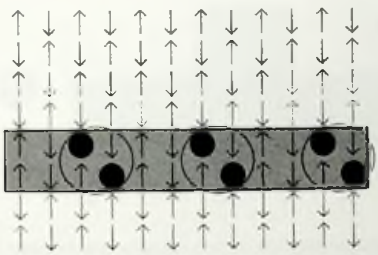

Figure 8.1: Schematic representation of a quarter-filled bond-centered stripe in an antiferromagnet. It is assumed that there are no spin-flips in the antiferromagnet. There is a π-phase shift in the staggered magnetization over the stripe. The cartoon above is not to be taken too literally. In reality, the pairs are smeared along the rungs.

domain wall in an antiferromagnet as an effective attractive potential for holes, simply by its magnetic cost and the careful interplay between string states and transverse and longitudinal hole kinetics, is not what is considered here. A large body of literature complements this chapter's simple asymptotic low-energy analysis.

8.3 Bond-centered stripe in an antiferromagnet

Figure 8.1 shows the system which will be the focus of this chapter. The microscopic anatomy of a bond-centered stripe in an antiferromagnetic background will be examined. As foretold, the spin-flips in this background will be neglected. A perfect Néel antiferromagnet will be assumed. It is also assumed that there is a phase-shift in the staggered antiferromagnetic order parameter across the stripe. This implies that there will be a ferromagnetic bond between spins on the two different legs of the stripe. The ferromagnetic bonds will cost a lot of energy. However, introducing holes into the stripe will reduce this strain. The ferromagnetic bonds will turn out to be essential to explain the stability of stripes against "hole evaporation".

In order to understand why a system would want to form such a stripe, the theoretical assumption is made that the system starts out with an anti-phase boundary as shown in figure 8.2. Theoretically, one can force such a system by imposing suitable boundary conditions. If the system is L sites long, this will entail an energy penalty of, approximately, $2LJ_z$. Introducing holes into this system will reduce the energy of this ferromagnetic seam and ameliorate matters.

Topologically, stripes are not literally domain walls in an antiferromagnet (whose spins $\vec{S}$ are continuous variables and *not* Ising like) but rather excitations known as skyrmions. As noted by Wilczek and Zee [207] and later by others, e.g. Wieg-

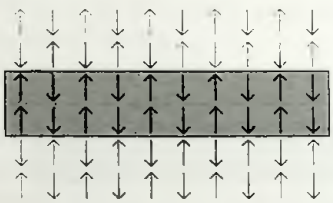

Figure 8.2: The assumption will be made that the system starts out as antiferromagnetic with a "domain wall" *- a skyrmion. It will be analyzed what happens if holes are added to this system.*

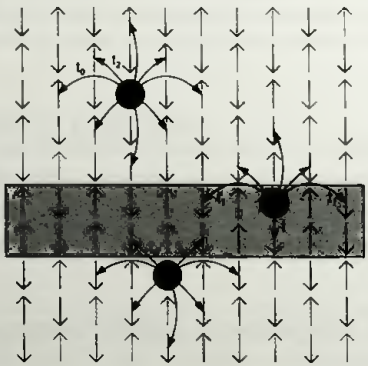

Figure 8.3: A number of holes and an antiferromagnetic domain wall *immersed in the surrounding antiferromagnet. This chapter shows that the holes will automatically end up on the domain wall because of the single step up/down movement with an amplitude t which is possible within the domain wall (the stripe), but not in the surrounding antiferromagnet.*

mann [206], skyrmions in an antiferromagnet are cylindrical domains separating Néel states shifted by half a period. Note that topologically, stripes are identical to skyrmions stretched out to form domain walls of infinite extent. Berry phase effects and the like for domain wall stripes give rise to the exotic statistics possible by skyrmions in $2+1$ dimensions — this can simply be seen and investigated by extending the results of [207] to our domain walls.

8.4 Dynamical confinement (on-stripe hypothesis)

Now examine what happens if a hole is introduced into the antiferromagnet with a domain wall (see figure 8.3). Once again, the major assumption still is that this hole moves

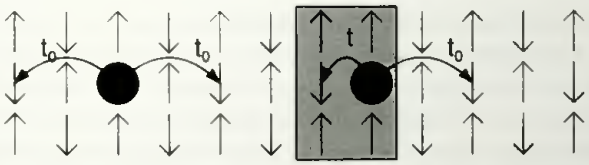

Figure 8.4: One-dimensional example showing the reason for dynamical confinement. *Outside the stripe, the hole moves in steps of two with an amplitude t_0. Inside the stripe it can make a direct hop with amplitude t with $t \gg t_0$.*

in steps of two such that it will always stay on the same sublattice. Note that if the hole is in the antiferromagnet, far away from the stripe, it has eight positions were it can move to (see figure 8.3). If it is sitting next to the boundary (just outside the stripe), it loses one hop, because of the reversed sublattice structure. The remaining seven hops are all the same as if the boundary was not there.

Larger changes happen with a hole located within the stripe. For such a hole there are only six hops left. In figure 8.3, the hole on the stripe cannot move downward left or downward right because of the change in sublattice structure. So, naively, one might come to the conclusion that a hole has more kinetic energy in the antiferromagnet then if it is on or near the boundary/stripe. Naively, confinement of the hole in the stripe would cost kinetic energy. However, this is not the case.

The reason is that within the antiferromagnet the holes can only move in two steps longitudinally with an amplitude t_0 or diagonally with an amplitude t_2 which are of the order of $t^2/U \ll t$. On the stripe the hole can stay on the same spin sublattice by doing a single (instead of double) step up or down with amplitude t. As a consequence, the hole has a much larger kinetic energy if it is situated on the stripe. Therefore the hole automatically moves to the stripe: the amplitude for the ground state wavefunction is a maximum for sites on the stripe and decays exponentially the further the sites are away from the strip (see figure 8.5). Holes are driven by an increase in kinetic energy (not exchange energy) to the domain wall. This mechanism is termed "*dynamical confinement*". The word dynamical is used because it is the motion of the holes on the stripe that lowers the energy. The primary role of kinetic energy in favoring the stripe as a ground state has been discussed many times before, e.g. [32, 43, 175]. Nonetheless, the trivial lowering of the kinetic energy allowed by hole motion along the ferromagnetic rungs on the domain wall seems to have gone unnoticed.

For the two-dimensional problem of a single hole in the vicinity of a full domain wall embedded in a surrounding antiferromagnet (of the variant shown in figure 8.3), one can work in a very much reduced Hilbert space. In effect, the strongly correlated many-particle system reduces to a single particle problem defined on half of the lattice.

As there are, *ab initio*, four possible electronic states on each site (empty, one electron with its spin up, an electron with spin down, and an up and down electronic pair), the Hilbert space of an N site system is a priori, of dimension 4^N. Invoking the sublattice parity principle allows us to reduce the Hilbert space to a mere size of $N/2$. The Hubbard Hamiltonian is then reduced to a purely kinetic model, having an amplitude t for nearest-neighbor direct hops within the stripe, amplitudes t_0 and t_2 for longitudinal and diagonal two-step hops (as depicted in figure 8.4 for the horizontal motions) within the antiferromagnet and an amplitude t_1 for two-step hopping within the stripe along the axis of the ladder.

Before doing a more detailed analysis, let us first get an intuitive feeling of where this section is heading. Looking at figure 8.3, it should be noted that a hole in the bulk disperses with an energy

$$\begin{aligned} \varepsilon_{\text{bulk}} &= \varepsilon_0 - 2t_0(\cos 2k_x + \cos 2k_y) \\ &\quad -2t_2((\cos(k_x + k_y) + \cos(k_x - k_y)). \end{aligned} \tag{8.1}$$

Along the ladder,

$$\varepsilon_{\text{stripe}} = \varepsilon_0 \pm t - 2t_1 \cos 2k_x, \tag{8.2}$$

where the second, $\pm t$, contribution denotes the energies of the bonding/anti-bonding states along the rung. Within this approximation, a sizable finite gap $\Delta \approx t$ separates the minima of both dispersions.

In reality, the hole can hop between the stripe and its surrounding bulk: the stripe states may be connected to the bulk. The low-lying stripe states are however much lower in energy than their counterparts within the bulk; they are localized on the stripe. As $t \gg t^2/U = O(t_0) = O(t_2)$, the on-stripe dispersion is markedly lower in energy than its counterpart for motion within the antiferromagnet. This leads to an exponential decay of the lowest eigenstates states out of the stripe.

We have numerically diagonalized a 12×21 system with a direct nearest-neighbor hopping amplitude $t = 1$, effective longitudinal and diagonal next-nearest neighbor hopping amplitudes $t_0 = t_2 = -0.1$ within the antiferromagnet, and a next-nearest neighbor amplitude along the axis of the stripe (ladder) $t_1 = -0.1$. The groundstate wavefunction is, to good numerical accuracy, given by

$$\psi(x,y) \approx |\frac{t_0}{t}|^y e^{ik_x x}. \tag{8.3}$$

Figure 8.5 depicts this wavefunction along the direction perpendicular to the stripe. This figure is similar to figure 22 from the Chernyshev *et al.* paper [43] who calculated

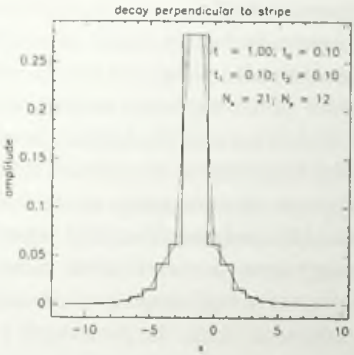

Figure 8.5: Groundstate wavefunction perpendicular to a domain-wall for a single hole in an antiferromagnet. This was calculated using the simple approximation discussed in the main text. The hole prefers to be on the stripe. We find that the wave function $|\psi| \approx |\frac{t_0}{t}|^y$. *The line in the figure just connects the midpoints.* N_x *and* N_y *are the linear extents of the two-dimensional system and the hopping amplitudes* t_0, t_1 *and* t_2 *are as defined in figure 8.3.*

this from a 11×7 t-J_z system employing the numerical DMRG method. Our approach leads directly to this exponential confinement due to the *dynamical confinement*, without the need for complicated numerical calculations. To get an intuitive grip on the physics along with the ability to easily solve an approximate version of the planar problem, the reader can look at a transverse one-dimensional cross-section of the problem. A transverse slice of the stripe and its surrounding environment are shown in figure 8.4.

If we were to allow a hole on the particle to hop to a larger number of neighbors within the bulk (i.e. to artificially enhance kinetic motions and lower confining tendencies), then our system may be mapped into the dynamics of spin-$\frac{1}{2}$ particles in the presence of a transverse magnetic field. The mapping is as follows: let us mark each point within the bulk by its sublattice parity (up/down) number as depicted in figure 8.3. Let us now tile the plane into vertical 2×1 domino blocks lying with their long side parallel to the y axis. Each domino within the bulk contains one up and one down site; the labeling of the up and down sites on the dominoes lying along the rungs of the ladders may be done arbitrarily. Next, let us envision replacing each domino by a single spin-$\frac{1}{2}$ particle: the number of the fictitious spin-$\frac{1}{2}$ particles is equal to half of the number of sites (one sublattice) which from now on are labeled by m and n. For simplicity it will now be assumed that all second order hops are of equal magnitude σ. Let us now consider the Hamiltonian

$$H = -\sigma \sum_{\langle mn \rangle, \sigma} (c^\dagger_{m\sigma} c_{n\sigma} + c^\dagger_{n\sigma} c_{m\sigma}) - \sum_{n \in \text{ladder}} \vec{h}_{ext} \cdot \vec{S}_n, \tag{8.4}$$

with the fictitious external magnetic field $\bar{h}_{ext} = t\sigma_x \hat{e}_x$ oriented along the transverse x-axis, and $\bar{S}_n$ the spin of the pseudo-particle (domino) along the n-th rung of the stripe. In the first term m and n span the entire plane; the sum is performed over all nearest-neighbor sites $\langle mn \rangle$ and on four of the eight next nearest-neighbor sites (such that all same sublattice hoppings of the holes within the bulk are accounted for). For holes not far from the stripe or on it, the Hamiltonian of equation 8.4 introduces additional unphysical motions. These hoppings allow hoppings of the holes off and on the stripes which are disallowed — such additional terms can only enhance delocalization tendencies. Observe that the low-energy dynamics corresponds to the motion of a $|\rightarrow\rangle$ particle polarized along the applied transverse field sensing an attractive confining potential of strength t along the stripe. In physical terms, the pseudospin polarized state $|\rightarrow\rangle$ corresponds to the symmetric low-energy bonding state and its counterpart $|\leftarrow\rangle$ corresponds to the high energy anti-bonding state. The ground state is simply that of a polarized $|\rightarrow\rangle$ particle (symmetric bonding state) sensing a well of infinite extent along one axis and having a finite extent ($2a$ with a the lattice unit) along the transverse direction. As the problem is translationally invariant along the ladder axis, k_x is a good quantum number. The lowest lying wavefunction is translational invariant along the infinite cylindrical axis ($k_x = 0$) and, at long distances, has the transverse profile of a particle of inverse mass $m_{\text{eff}} = \frac{1}{2a}$ on a line subject to the influence of a potential well of depth t and width $(2a)$. This trivially leads to an exponentially decaying amplitude in the direction transverse to the stripe. As $t \gg J$, this confining tendency is much more profound (and physical) than most of the common magnetic bond (J) arguments prevalent in the literature. The reader should bare in mind that our point of departure— the sublattice parity principle— is correct only as low-energy scales (as compared to J). Nonetheless, what drives localization in our picture at low-energy scale are the much more dramatic kinetic effects which overshadow the common bad bond (J) counting arguments.

The problem of an arbitrary stripe configuration may be addressed similarly. In general, the problem of the hole within stripes is equivalent to a kinetic planar problem of a hole coupled by Zeeman couplings to magnetic fields piercing the plane along the stripe trajectories. A multitude of viable self-consistent minima of narrow stripes of various geometries are found. Stripe dynamics is akin to the motion of the fields piercing the plane; these, in turn affect hole dynamics by the Zeeman-like couplings. The evolution of a hole-stripe system may be addressed via such a self-consistent scheme.

Henceforth, our attention will be restricted to systems with the simple rectangular ladder geometry. In our approach, first an antiferromagnetic spin structure with domain walls is created and then the system is doped. Then, if the spin structure is strong enough, the holes will migrate to the walls and will form a charge structure. Hopefully we have convinced the reader that sublattice parity order can indeed drive stripe formation. The energy scale associated with this discrete sublattice parity (Z_2) order [218] can indeed be quite high: the persistence of incommensurate peaks up to at least the high

energy resonance peak in $YBa_2Cu_3O_{6+x}$ might be interpreted as an indication that the stripe persists to be a domain wall up to very high energy scales [21]. Experimentally, charge order is a far greater robust driving force for stripe formation than spin order. The role of sublattice parity (albeit its high energy scales) is not clear at the time of writing. The reader should consider our argument as a self-consistent one in which the creation of the no-hole domain-wall first is a theoretical device that simplifies theoretical discussion. Summarizing, we have seen that once there is a ferromagnetic seam in a very strong antiferromagnet, single holes will automatically move to this seam and be exponentially localized onto them. In the remaining part of this chapter the consequences of this result for more than one hole on the stripe are examined.

8.5 Staggered ladder systems

We have seen that by dynamical confinement we may consider an antiferromagnetic domain wall as a two-leg ladder with staggered boundary conditions. So, once again we can restrict our Hilbert space. Ladder systems have been extensively studied throughout the years. Hundreds of works on standard (unstaggered) ladder systems have been carried. For a well-known review see Dagotto and Rice [49].

However, in our case the influence of the antiferromagnet surrounding the ladder is still there: it effectively gives rise to staggered boundary conditions. Therefore we will look at two-leg ladders with staggered boundary conditions. These staggered boundary conditions are essential. Staggered ladder systems which are enforced by the sublattice parity structure of the surrounding antiferromagnet will be the cornerstone of our analysis from now on. Staggered ladders have not been investigated as intensively as the standard ladder systems.

Krotov, Lee, and Balatsky [104] have examined this situation for the Hubbard model at small U. In this limit, one starts with a non-interacting system and then derives the renormalization group equations. Staggered spin ladders without holes have been studied for instance lately by Wang *et. al* [200]. However, staggered ladder systems with holes in the large U limit have not yet been addressed before as far as we know. This is what we will look at in the next sections.

8.6 A single electron on an empty staggered ladder

To understand the effect of the boundary conditions on the movement of electrons and holes on the ladder we first examine a single electron on an empty ladder immersed in a staggered magnetic field. This is, of course, a hypothetical situation, but it is nevertheless a good starting point for our discussion. If the electron is on the correct sublattice (i.e. if its spin polarization is opposite to that of the applied staggered magnetic field)

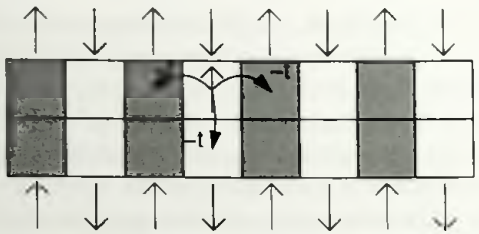

Figure 8.6: Single electron on an empty ladder. In principle the electron can hop to all its nearest neighbors with an amplitude t. However, the ladder is embedded in an antiferromagnetic background (light arrows) that influences the electron on the ladder.

then its magnetic energy will be $\varepsilon_0 = -J$. Being on the wrong sublattice leads to a magnetic energy penalty of $\varepsilon_1 = +J$.

This gives rise to staggered potentials on the ladder. The resulting Hamiltonian for the system as shown in figure 8.6, reads

$$H = \begin{pmatrix}
\varepsilon_1 & -t & -t & & & & & & & \\
-t & \varepsilon_1 & 0 & -t & & & & & & \\
-t & 0 & \varepsilon_0 & -t & -t & & & & 0 & \\
 & -t & -t & \varepsilon_0 & 0 & -t & & & & \\
 & & -t & 0 & \varepsilon_1 & -t & -t & & & \\
 & & & -t & -t & \varepsilon_1 & 0 & -t & & \\
 & & & & -t & 0 & \varepsilon_0 & -t & -t & \\
 & 0 & & & & -t & -t & \varepsilon_0 & 0 & -t \\
 & & & & & & -t & 0 & \varepsilon_1 & -t \\
 & & & & & & & -t & -t & \varepsilon_1
\end{pmatrix}. \tag{8.5}$$

We expressed this Hamiltonian in terms of ordered real-space basis states were we placed the upper and lower sites of each rung adjacent to each other. An electron at any site can always hop to three other sites. Because this is a single particle problem with a translational invariant potential (with unit cell of two), the eigenfunctions of this Hamiltonian can exactly be determined. They are given by

$$\psi = (B, \pm B, Ae^{ik}, \pm Ae^{ik}, Be^{2ik}, \pm Be^{2ik}, Ae^{3ik}, \ldots). \tag{8.6}$$

Here A and B are determined by

$$\begin{aligned} E_k &= \varepsilon_0 \pm t - 2t\frac{B}{A}\cos k \\ E_k &= \varepsilon_1 \pm t - 2t\frac{A}{B}\cos k. \end{aligned} \tag{8.7}$$

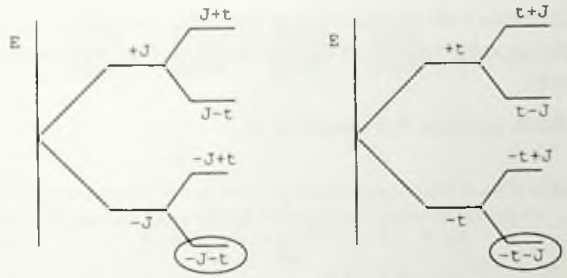

Figure 8.7: Energy diagram for a single electron on an empty staggered ladder. If the staggered potential is large (large J), the splitting J is more important than t. In the lowest state, there are only $N/4$ states. These are the same states as for a single one-dimensional model where an electron moves in steps of two. If $J \ll t$ (right) we still get the same lowest Hubbard sector.

The energy can immediately be obtained from

$$\begin{Vmatrix} \varepsilon_0 \pm t - E_k & -2t\cos k \\ -2t\cos k & \varepsilon_1 \pm t - E_k \end{Vmatrix} = 0, \tag{8.8}$$

leading to

$$\begin{aligned} E_k &= \pm t \pm \sqrt{J^2 + (2t\cos k)^2} \\ &= \pm t \pm \sqrt{J^2 + 2t^2 + 2t^2\cos 2k}. \end{aligned} \tag{8.9}$$

This equation for the energy shows that effectively the electron moves in steps of two, caused by the staggered potential. Fourier transforming the energy shows that because of the symmetry between k and $\pi - k$, only terms which have an even number of steps from the starting point have an appreciable amplitude unequal to zero: only even hops are allowed. In more physical terms, this trivially corresponds to the halving of the period (in k) of the dispersion E_k.

Equation 8.9 shows that, for unphysically large $J \gg t$ (strong influence of the surrounding two-dimensional antiferromagnet), the Hilbert space splits up in four different sectors. First, there is a splitting because of the boundary conditions: half of the sites have the electron on the right sublattice, which leads to a low-energy of $-J$. The other half have the hole on the wrong sublattice, with an energy of $+J$. Because the upper and lower leg of the ladder are exactly equivalent for the electron, it will slosh back and forth between the upper and lower legs. This leads to bonding/anti-bonding linear combinations of the upper and lower sites along each rung, further splitting the Hilbert space again into two additional sectors. The lowest sector, which contains $N/4$ basis states,

consists of wavefunctions with the electron on the right sublattice (e.g. a spin up polarized electron on the up sublattice) with the symmetric linear combination (bonding) of upper and lower sites.

In the large J limit, equation 8.9 simplifies to

$$E_k = -J - t - 2\frac{t^2}{2J} - 2\frac{t^2}{2J}\cos 2k. \tag{8.10}$$

Not surprisingly, we see that we this energy corresponds to the electron populating the correct sublattice ($-J$) and being smeared along the two rungs in a symmetric bonding fashion ($-t$). We can easily read off that the effective hopping is in steps of two from the $\cos 2k$ term. Because we are in the large J limit, the hopping amplitude in second order perturbation theory is given by $\frac{t^2}{2J}$. We have to hop twice (t^2) over an intermediate state with energy $2J$. The extra contribution $-2\frac{t^2}{2J}$ to the energy comes from virtual excitations where the spin moves one position to the left or right and immediately returns back. There are two possible ways of doing this, and the amplitude again is $\frac{t^2}{2J}$. Thus, we can intuitively understand every term in this limit.

There is a gap of $2t$ separating the lowest Hubbard band from the anti-bonding states. Because $2t$ is a very large energy scale (approximately 0.5 eV, or 5000 K), we can neglect the influence of the other sectors and may restrict our attention only to the lowest sector.

Our discussion above hinged on the assumption that J is very big ($J \gg t$). This assumption is not satisfied in the physically relevant region wherein $J \approx 0.25t$. In the physically relevant regime, we still have a splitting of the Hilbert space into four sectors (see figure 8.7). The lowest Hilbert sector is still the same one as the one for the large J limit. For small values of J compared to t, the groundstate properties are still dominated by the $-J$, $-t$ sector. However, the low-lying excitations out of the lowest sector are now to the sector where the electron goes to the wrong sublattice (a single hop) instead of going from a bonding to an anti-bonding state. Such hops will lead to string states. Nevertheless, as long as the width of the lowest Hubbard band is small compared to $2J$ (which itself is also a large energy, of the order of 2400K), we can still think in terms of bonding states on the correct sublattice. Within the lowest Hubbard sector, the electron will only be on the even lattice sites. Effectively, only second order hops are present. Because of the hybridization of up and down sites on a rung, it is sufficient to consider the one-dimensional model shown in figure 8.8.

Just as for the single hole in the two-dimensional antiferromagnet, discussed in the previous chapter, a lone electron on the empty ladder moves as an effective quasiparticle, with a sublattice hopping amplitude σ.

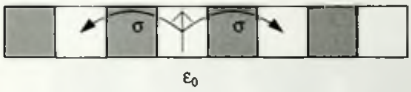

Figure 8.8: Effectively, the electron moves on a one-dimensional chain in steps of two. There are only two effective parameters: the on-site energy ε_0 and the two site hopping amplitude σ.

8.7 One hole on a full staggered ladder

We now examine one hole in an otherwise full ladder immersed in a staggered external magnetic field. The single spin problem was very simple to solve analytically given our assumptions. The single hole problem is exceedingly more difficult because it is a strongly interacting many body problem. For a system of only 6×2 sites, there are already approximately 800,000 states. Systems of this size and larger can be solved by using the Lanczos method of diagonalization, which only finds the lowest eigenstates of a matrix. We employed this method for systems of up to size 8×2. The complicated results that follow from this numerical study can be understood quite easily for large values of J. Though not the physically relevant regime, just as in section VII, both for $J > t$ and $J < t$, the groundstate is in the same sector of Hilbert space.

For large values of J the basic properties are once again those of a single quasi-particle. From the outside, we again assume that the hole cannot leave the stripe. An electron next to the hole can move to the position of the hole, leading to a string-state with one wrong spin. The hole can also move up and down. And it can move in steps of two to the left and right. In addition, we can have spin flips on the ladder. However, just as in the two-dimensional antiferromagnet we neglect the spin-flip processes. For large values of J we find once again a number of Hubbard sectors. The lowest sector has $\frac{N}{2}$ states where the hole is on the right sublattice and an energy of approximately $-2(N-1)J$. Above this lowest Hubbard sector we have the Hubbard sector with a string state of length one. There are $2N$ states in this sector. The gap between this sector and the lowest sector above it is $\Delta = 4J \approx 4800K$. We could ignore this sector if this gap is large with respect to the internal splitting of the lowest Hubbard sector. This bandwidth is given by $4t''$ with $t'' = \frac{t^2}{U+4J} \ll t$. For $U \approx 8t$ we have $t'' \approx 0.1t$: both J and t have approximately the same amplitude. Thus, for the groundstate properties, the relevant properties are those of a single hole moving in steps of two. The band, shifted down by $t^2/2J$ by virtual hopping, has the dispersion of an inverted cosine. In the limit $U, J \gg 1$,

$$\varepsilon_0 = -J - t - 2\frac{t^2}{2J},$$

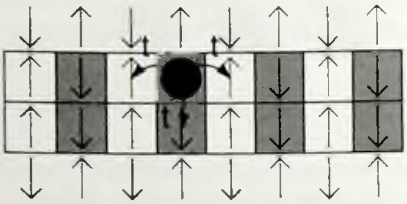

Figure 8.9: We assume a single hole can move on the stripe and cannot leave the stripe. The surrounding antiferromagnet leads to staggered boundary conditions.

$$\sigma = \frac{t^2}{U+2J}. \tag{8.11}$$

where, as before, σis the effective two-step transition amplitude.

The motion of a single hole on a stripe and in a two-dimensional antiferromagnet is identical. The only difference between the parameter sets, is sparked by the presence of the direct hopping term t allowed within the topological domain wall. This is in contrast to one-dimensional effective theories that assume that the hole effectively becomes a holon on a stripe (see for instance Tchernyshyov and Pryadko [175]). Our hole is not a holon in the sense that it will remember if it was injected for a spin up or a spin down electron: they move on different spin sublattices.

We see that we can consider a single hole on a stripe as a quasi-particle, just as a single electron on an empty lattice. They can both be characterized by (different) values for ε_0 and σ. The main difference between a hole on a full ladder and an electron on an empty ladder is that the hole moves more slowly, because it can only move through doubly occupied intermediate states, which costs a lot of energy. Therefore, σ is small for a hole, while it is large for an electron on an empty lattice. *Our main conclusion is that, apart from these differences, a single hole and a single electron are effectively behaving identical.*

8.8 Two electrons on an empty staggered ladder

This equivalence between holes and electrons is no longer true for more than one particle. We will show that the low-energy properties for two electrons are different from two holes. We first consider the problem of two electrons with opposite spin on an empty ladder. Various possible geometries are sketched in figure 8.11. Because only the relative distance is important, we keep the position of the up spin fixed.

The two electrons can be on the same or on opposite legs. Seven amplitudes:

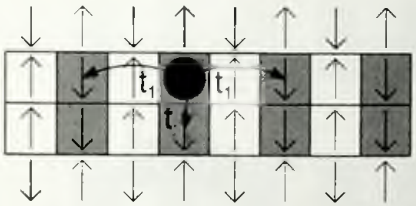

Figure 8.10: For a one-dimensional ladder with strong staggered potentials on the boundaries, a single hole effectively moves in steps of two.

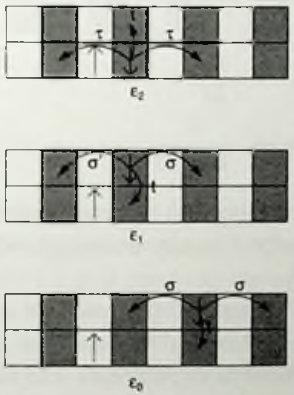

Figure 8.11: Different possible configurations of two spins on a staggered two leg ladder.

$\varepsilon_0, \varepsilon_1, \varepsilon_2, t, \sigma, \sigma'$ and τ, defined in figure 8.11, are of relevance. We notice that the hopping amplitude for the electrons when they are far apart (σ) is much larger than the hopping amplitude when they are next to each other (τ). If they are far apart, they do not notice each other. Two electrons have less kinetic freedom if they are next to each other. In order to move past each other, they have to go through a doubly occupied state.

In the $U, J \gg t$ limit, lowest order perturbation theory yields

$$\begin{aligned} \varepsilon_1 = \varepsilon_0 &= -2J - 4\frac{t^2}{2J}, \\ \varepsilon_2 &= -2J - 2\left(\frac{t^2}{2J} + \frac{t^2}{2J+U}\right), \end{aligned}$$

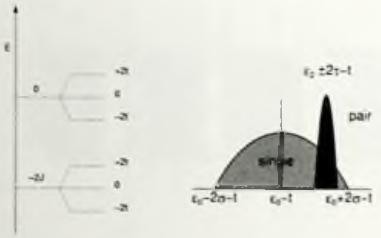

Figure 8.12: Hubbard sectors for two spins on an empty ladder. The lowest Hubbard sector contains both single electrons and pairs of electrons. However, the groundstate consists of single electrons. Pairs are only formed at a higher energy in the lowest Hubbard sector.

$$\begin{aligned} \sigma &= \frac{t^2}{2J}, \\ \tau &= \frac{t^2}{U+2J}. \end{aligned} \tag{8.12}$$

The lowest Hubbard sector contains both electrons separated by a distance and pairs of electrons. However, we have seen that separated single electrons have a larger kinetic energy than pairs.

Therefore, the ground state consists of electrons that are as far apart as possible. Figure 8.12 shows a schematic picture for the density of states. *Only at the higher energies of the lowest Hubbard band do we find pairs.* The pairs have a small bandwidth because of the small hopping amplitude. Once again we find various sectors as shown in figure 8.12.

8.9 Two holes in a full staggered ladder

To see the difference between electrons and holes, we now look at two holes in a filled ladder. When far apart, two holes (quasi-particles) do not notice each other. Just as for two electrons on an empty lattice, there are two states in which they strongly influence each other. The main question we wish to address is whether two holes come together and form a real-space pair, or if they tend to be as far apart as possible.

If the two holes are far apart, they will move independently with amplitude $\sigma = \frac{t^2}{U+2J}$ (see figure 8.13). However, this is different if they are sitting next to each other. In this case no double occupied state is needed. Therefore the hopping amplitude $\tau = \frac{t^2}{2J}$, thus $\tau \gg \sigma$.

It is well known that if the two holes are on the same leg, sitting next to each other (see figure 8.14), they can move together with a much larger amplitude than if they

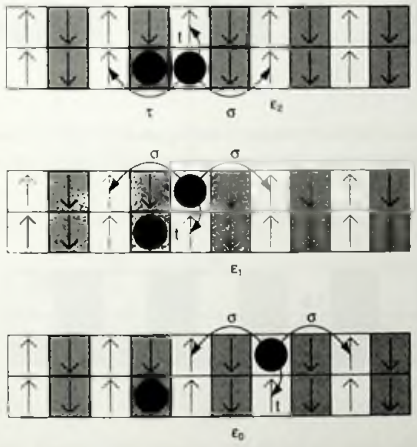

Figure 8.13: Different configurations of two holes on a stripe with the relevant on-site energies and hopping amplitudes.

move separately. In the left subfigure, a spin up electron moves left. The intermediate state in the middle figure has a higher energy of the order of J. From this position, the electron with spin up can move back to the starting position, or it can move on to end up as shown in the right figure. Once it is there, the hole-pair has effectively moved one site to the right. This figure only illustrates one possible hopping sequence, there are also other possible ways of hopping. For discussions of pairing one should be careful with fermionic minus signs sparked by the interchange of identical spins once a pair is made to go around [32, 184]. For the movement of a single hole, there is an intermediate state with an energy of U. However, if the two holes are next to each other then the intermediate state will not have a doubly occupied site, so therefore this energy is only of the order of $4J$. Therefore, σ' is much large than σ. This leads to the formation of pairs on the stripe.

For large U and J, employing the same convention as before, we find in perturbation theory,

$$\begin{aligned}
\varepsilon_0 &= -(N-2)J - 4\frac{t^2}{2J} - (2N-8)\frac{t^2}{U+2J} \\
\varepsilon_1 &= -(N-2)J - 4\frac{t^2}{2J} - (2N-8)\frac{t^2}{U+2J} \\
\varepsilon_2 &= -(N-2)J - 2\frac{t^2}{2J} - (2N-6)\frac{t^2}{U+2J},
\end{aligned} \tag{8.13}$$

Figure 8.14: Two holes can move together without creating an intermediate double occupied state. Therefore, holes want to form real-space pairs. A hole pair can move if a single electron makes two hops.

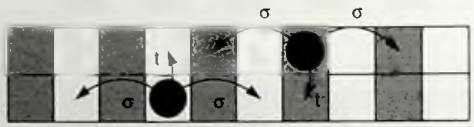

Figure 8.15: We can neglect the spins on the ladder because they cannot change. This is caused by the boundary conditions.

with $N = 2L$ the total number of sites on the two-leg ladder.

The motion of the pairs on a ladder and the motion of single holes is coupled: both are present in the lowest Hubbard sector. If they form disjoint Hilbert spaces, we will find $E = \varepsilon_2 - 2\tau\cos k$ for the real space pair. For two single holes, $E = \varepsilon_0 - 2\sigma\cos k$, within perturbation theory. Because σ is very small, the spectrum for single hole states does not exhibit much dispersion. The dispersion for two holes on a stripe with staggered potentials is suspected to look like that shown in figure 8.16.

The big difference between holes and electrons is that for two electrons the separated electrons have a large bandwidth and the pairs of electrons are a high energy state with a small dispersion. For holes this is reversed: the pairs have the largest bandwidth, while the separated electrons form a low-energy excitation (string states) with a small dispersion.

The lowest state for the pair cosine band is located at $\varepsilon_2 - 2\tau$ and the lowest state for the separated holes is located at $\varepsilon_0 - 2\sigma$. Both are in perturbation theory equal to $-(N-2)J - 4\frac{\gamma^2}{2J} - (2N-8)\frac{t^2}{U+2J}$. However, here we assumed the pairs and separated holes to be independent. But where they overlap in energy, which in this case is the bottom of the band, the wavefunctions will hybridize.

If we think of a hybridization of up and down sites along the rungs, then no possible interchange can be performed between the holes leading to fermionic minus signs that elevate, rather than depress, the pairing energy [32].

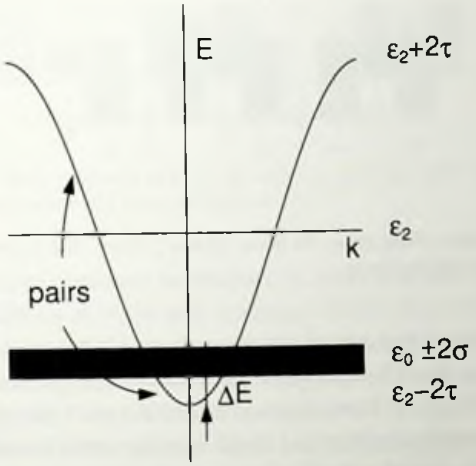

Figure 8.16: Theoretical dispersion relation for two holes in a bond-centered stripe.The groundstate consists of pairs.

8.10 Lanczos calculations

Lowest order perturbation theory for two holes on a staggered ladder leads to the dispersion shown in figure 8.16. The ground state properties cannot be easily determined because of the overlap between separate hole and pair states. To test this situation numerically, we have performed standard Lanczos calculations for the Hubbard model endowed with staggered boundary conditions on a twelve site single chain with staggered boundary conditions. Solving this problem for large two-leg ladders is inhibited by the large Hilbert space. The maximum size which we are able to examine numerically is a 6×2 system for which there are $\approx 650,000$ states. Such a system is too small to observe single hole states and pairs accurately. Because of the strong bonding combination between the upper and lower leg of the ladder, the reduction to a one-dimensional line is physically justified. The results of the Lanczos calculation show that the ground state has the largest amplitude for pair states with only a small admixture of single hole states. Immediately above the ground state, the excited states are predominantly single hole states. There is a finite energy gap separating the ground state and these excited states. Because of the small lattice size, we cannot determine the value of the energy gap ΔE.

Another approach is to assume that $\varepsilon_0, \varepsilon_2$, σ, and τ are adjustable parameters. In that case, we can perform a simplified calculation on a 20×2 ladder having twenty spin up, and twenty spin down sites. This leads to a 400×400 matrix that can be easily

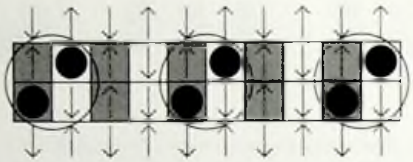

Figure 8.17: For a quarter-filled stripe, the above picture follows. This is the essence of the numerical DMRG results of White and Scalapino.

diagonalized. Using this model it is relatively easy to choose the effective parameters such that the cosine band for the pairs has a lower energy than the states where we have single holes far apart. Our numerical results for the Lanczos method suggest that the gap ΔE separating pair states and single particle states is sufficiently large for the groundstate to consist mostly of pair states.

As the gap separating the single hole and pair states is so small, the pairing physics is very susceptible to the addition of longer range interactions and hopping interactions. Such effects could easily tip the balance between the single hole and pair states (or enhance pairing tendencies).

8.11 DMRG - Putting all of the pieces together

We found that if we assume that somehow the antiferromagnet has a ferromagnetic domain wall, holes will automatically localize on this topological line. Furthermore we looked at the movement of a single hole on this staggered ladder and found that it behaves as a single quasi-particle that moves along the ladder in steps of two. Two electrons on an empty lattice try to be as far apart as possible. Two holes on an otherwise half-filled ladder, however, form a bound pair. Fusing all of these findings together, we obtain the stripes as seen by the DMRG calculations of White and Scalapino [203]. The arguments that we employed throughout were very pedestrian and general. Throughout we invoked the sublattice parity principle and the related staggering potentials. Our findings are further supported by numerical calculations on the t-J model. We give a very simple physical interpretation for the stripes found by DMRG.

A hole is on the stripe will delocalize by the hybridization of the upper and lower leg. If we place a hole on the upper leg, the hole will almost immediately jump to the lower leg and vice verse. In numerical calculations, we will therefore find the linear superposition of a hole and the electron depicted in figure 8.18.

White and Scalapino employed the DMRG technique on the t-J model [203]. Figure 3.6 showed one of their well known results for quarter-filled stripes. We saw that the bond centered stripes are very narrow. They look like a ferromagnetic seam in an

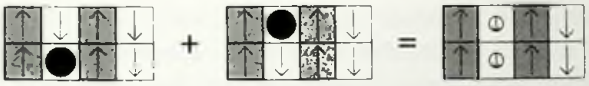

Figure 8.18: The hole has equal amplitude to be on the upper or lower leg of the ladder. Therefore, the groundstate is a linear superposition of a hole and a spin down.

antiferromagnet. The same result can be obtained in mean-field theory (see chapter 3).

The DMRG calculations of White and Scalapino vividly show how spin and charge nestle. White and Scalapino place much emphasis on the fact that again the holes are on next-nearest neighbor sites. On the opposite diagonal, the spins (which are on the same sublattice) have a very strong antiferromagnetic bonding. In effect, the bound pair is creating a flip in the antiferromagnetic lattice. This might also explain why in the exact calculations and the Monte-Carlo results the binding energy would decrease as a function of the lattice size. Basically, the hole-pair is creating an anti-phase boundary, whose energy is increasing as a function of lattice size. That this is indeed a good representation of stripes follows from DMRG calculations by White and Scalapino. The reader is urged to focus on the central part of their picture— the spin and charge texture towards the boundaries are more contorted by the open boundary conditions employed. We claim that figure 8.16 is a useful real-space representation of a quarter-filled stripe. The reason that the mean-field and the DMRG calculation are so similar has to do with the fact that the antiferromagnet is very strongly ordered. The stripes are so narrow because of *dynamical confinement*.

8.12 Longer-range kinetic and Coulomb terms

Let us recapitulate the assumptions that we have invoked, so far, in our analysis:

(i) We assumed, self-consistently, the existence of an anti-phase domain wall having the geometry of a two-leg ladder. Sublattice parity (Z_2) order was assumed to prevail throughout the entire system.

(ii) Albeit the relatively minute energy difference by which the lowest lying pair states were found to be favored over single hole states, we assumed that the stripe was composed entirely of pairs.

It should be noted (especially in the context of assumption (ii)), that the small energy differences we found separating various contending states (as well as those separating, say, bond centered stripes from site centered stripes) are very susceptible to additional terms in the Hamiltonian. The Hubbard model or its t-J truncation is only a model. There are myriad very important effects that it does not include which could easily shift the balance between various nearly degenerate contending states. Coulomb effects

(which are much greater importance here than elsewhere given the poor screening in these materials) enhance and stabilize stripe order: a uniform charge density order is strictly forbidden by the divergent Coulomb penalty that it will incur. This point has been emphasized by Emery, Kivelson, and coworkers [71], [114]. Fourier transforming the action and looking for the minimizing wavenumbers, we are able to see how the charge density modulations will evolve and lead to stripe order [39] once lattice effects are taken into account.

Even if the stripe correlations found by the DMRG calculations of White and Scalapino on the pure t-J model are found to be due to open boundary condition effects, when long range Coulomb interactions are introduced, charge stripe order will be further stabilized. Given the natural coupling between spin and charge [223], this will further enhance the sublattice parity flips across the stripe that we assumed from the outset (assumption (i)). Less emphasized are the role of higher order kinetic terms. These can easily tip the balance too: a next-nearest neighbor hopping increases pairing significantly. Within the pure t-J model (with a vanishing direct diagonal hopping amplitude $t' = 0$) pairing correlations are infinitesimal and are further frustrated by the π phase shift across the domain wall. Numerically, t' which allows holes to move on the same sublattice, enhances pairing dramatically. Furthermore, numerically, a negative t' is seen to favor stripe formation .

8.13 Conclusion

We examined the consequences of hole motion in a strongly ordered antiferromagnet. We showed that holes move to antiferromagnetic domain walls and effectively form two-leg ladders. This *dynamical confinement* of holes onto the stripe is caused by the sublattice structure of the antiferromagnet and the increase in kinetic energy on a domain wall. The effective two-leg ladders still feel the influence of the surrounding antiferromagnet in terms of a staggered boundary potential. As shown by Krotov, Lee, and Balatsky [104], this increases the tendency to superconductivity. The reason for this is that holes on the stripe form real-space pairs. Our results naturally lead to a theoretical description of the numerical results of White and Scalapino. Therefore, our starting assumption about the sublattice parity principle and the neglect of string states appears to have some validity. In the next chapter, we will show that these real-space pairs can be mapped to an effective one-dimensional XXZ model in a transverse field. This will allow us to discuss the filling ratio of the stripes.

Chapter 9

Filling fraction of stripes

This chapter focuses on very general, very large U, doped Mott insulators with arbitrary hopping and interactions. It provides simple testimony to the competition between magnetic and superconducting orders in these systems. By mapping hard-core bosons, spinless, and spinful fermions onto XXZ models, some very simple precise statements are made. The optimal and expected filling fractions of holes within the plane and on stripes are determined in a variety of hole and hole pair geometries. Also the role of attraction and repulsion between hole pairs and single holes is examined. The expected numerical values for filling fractions in various scenarios are provided. The plaquette states seem to naturally provide the correct stripe filling fractions.

9.1 Introduction and outline

This chapter aims to address questions concerning planar and linear (stripe) filling fractions of doped Mott insulators by trying to see how much can be learned by mapping such systems onto spin models. The answers depend greatly on the assumed form of the constituent particles (single holes, pairs) and their various geometries (plaquettes, rungs, bonds). This chapter will demonstrate that plaquette states seem to naturally provide the correct stripe filling fractions. By mapping onto spin models, various competing orders are examined. Among other things in the limit of large on-site repulsions U, magnetic and superconducting orders are shown to always compete.

The outline of this chapter is as follows. Section 9.2 lays out the general standard model of doped Mott Insulators which will form the focus of the discussion. In section 9.3, the problem of spinless and spinful particles in the plane is examined by a mapping onto a spin model. In doing so, another rigorous example of the competition between magnetic and superconducting orders will be shown in a special set of models. Within these spin models that result for large U, the magnetic order as well as the physically

transparent number order (both portrayed by S_z in two different spin representation) compete with the dual superconducting order encapsulated by bilinears in the planar $\vec{S}_\perp$ multiplied by exponentials of a topological nature.

Section 9.4 shows how to map a model of hard core bosons (hole pairs) in non-overlapping plaquettes with arbitrary finite range interactions and hoppings onto a planar XXZ model. If the physics is indeed dominated by such attractive pair states then, within the ground state, the average hole occupancy per site within the optimal doped state may be $\frac{1}{4}$. The large deviation from the observed optimal doping in most doped Mott insulators is hardly surprising and points to the inadequacies of looking at attractive plaquette pairs alone within the plane: not unexpectedly, an analysis of the cuprates based solely on notions of doped Mott insulators and concurrently assuming only Bose pairs of the plaquette size might be flawed.

In section 9.5 the plaquette pairs on bond-centered stripes are examined, and shown to be near $\frac{1}{4}$-filling under a variety of circumstances. The possibility of phase separation or modulation of the hole pairs along the bond centered stripe is discussed. When the condition that diagonal pairs do not have to be in non-overlapping plaquettes is relaxed, in the large hopping amplitude limit a $\frac{1}{3}$-filling fraction of stripes is found. Higher and similar filling fractions are found for pairs on single rungs and legs. From this simple exercise it can be concluded that bond centered stripes cannot be described by simple pairs roaming the stripe axis and that if pairs indeed do dominate the asymptotic low-energy stripe scale physics as was suggested in the previous chapter, then they must be effectively confined to non-overlapping plaquettes in accord with pictures suggested by the DMRG calculations of White and Scalapino [203].

A similar analysis of fermions on bond centered stripes is examined in section 9.7. They lend themselves to $\frac{1}{4}$ filling. This description fortifies earlier work by Nayak and Wilczek [135].

9.2 The model

To describe the physics of the problem, the relatively standard model of doped Mott insulator, the extended Hubbard model, is used:

$$H = -\sum_{\langle ij\rangle\sigma} t_{ij}(c^\dagger_{i\sigma}c_{j\sigma} + c^\dagger_{i\sigma}c_{j\sigma}) + \sum_i U n_{i\uparrow}n_{i\downarrow} + \sum_{ij} V_{ij}n_i n_j, \tag{9.1}$$

where $c^\dagger_{i\sigma}$ creates an electron on-site i with spin σ and j is a nearest neighbor of i. This model contains both the movement of the electrons (hopping) (t, kinetic energy) and the interactions of the electrons if they are on the same site (U, potential energy). The Mott insulating nature is captured by this on-site repulsion which greatly inhibits hole motion. An additional term representing all possible number-number interactions (of all

ranges) is added; these may be the result from a number of interactions — e.g. Coulomb repulsions, interactions mediated by phonons. The number occupancies are defined as

$$\begin{aligned} n_{i\sigma} &= c^{\dagger}_{i\sigma} c_{i\sigma} \\ n_i &= \sum_{\sigma} n_{i\sigma}. \end{aligned} \tag{9.2}$$

At large U, the extended Hubbard model of equation 9.1 may be related to an extended t-J model,

$$H = -\sum_{\langle ij\rangle,\sigma} t_{ij}(c^{\dagger}_{i,\sigma} c_{j,\sigma} + h.c.) + \sum_{\langle ij\rangle} J_{ij} \vec{S}_i \cdot \vec{S}_j + \sum_{ij} V_{ij} n_i n_j, \tag{9.3}$$

where $\vec{S}_i = \sum_{\sigma\sigma'} c^{\dagger}_{i\sigma} \vec{\sigma}_{\sigma,\sigma'} c_{i,\sigma'}$ is the spin of the electron at site i, $\vec{\sigma}$ are the Pauli matrices, and there is a constraint of no double occupancy of any site i ($n_i = \sum_{\sigma} c^{\dagger}_{i,\sigma} c_{i,\sigma}$ has expectation values 0 or 1). The reduction to a Hilbert space where no doubly occupied sites occur (the Gutzwiller projection) will be automatically incorporated in the coming sections.

9.3 Competing orders for fermions in the plane

Spinless fermions

With possible applications to the limit of infinite on-site repulsion U in mind, the competition of charge and superconducting order within the plane has to be examined. In order to highlight the simple similarities between spin and charge when looked at through the prism of the Jordan-Wigner representation of $S = 1$ and $S = \frac{1}{2}$ problems respectively, a slightly longer route is taken. Although not of any use for most practical applications, a high dimensional Jordan Wigner transformation has been devised by Fradkin [79] and later extended by Eliezer and Semenoff [69]. Novel extensions to various spinful cases were recently advanced by Batista and Ortiz [20]. The basic message is that the classic Jordan-Wigner [96] transformation rigidly linking spinless fermions and $S = \frac{1}{2}$ spins in one dimension can, quite naturally, be extended to higher dimensions. The only complication is that now the kink operators that code for the statistics transmutations become high dimensional topological objects. To be more precise, the standard one-dimensional string operator appearing in the usual Jordan-Wigner transformation is replaced by its more general counterpart

$$K_j = \exp[i \sum_{\vec{k}} \theta(\vec{k}, \vec{j}) n_{\vec{k}}], \tag{9.4}$$

with $\theta(\vec{k}, \vec{j})$ the angle between $(\vec{k} - \vec{j})$ and a fixed ray (in the one-dimensional case the "angle of site" θ reduces to either π (for $j < k$) or zero (for $k \geq j$) leading to the standard

string operator). In terms of these new kink operators, the Jordan-Wigner transformation then reads

$$\begin{aligned} S_j^+ &= c_j^\dagger K_j, \\ S_j^- &= K_j^\dagger c_j, \\ S_j^z &= n_j - \frac{1}{2}. \end{aligned} \tag{9.5}$$

The simple pair operator $\Delta_{ij} \equiv c_i^\dagger c_j^\dagger$ may be expressed in terms of the spin variables. The superconducting pairing operator may be expressed as a product of kink variables with the XY components of the spins: $S_i^\pm$ and $S_j^\pm$. The incompatibility of charge (n or S_z) and superconducting phase (descendant from $\vec{S}_\perp$) orders is trivially reflected from the non-vanishing commutator

$$[S^z, S^\pm] = \pm S^\pm. \tag{9.6}$$

Explicitly, inverting all matters to the spin representation,

$$c_i^\dagger = S_i^+ K_i^{-1} = S_i^+ \exp[-i \sum_{\vec{r}} \theta(\vec{r}, \vec{i}) S_r^z], \tag{9.7}$$

the commutator

$$[n_k, \Delta_{ij}] = (\delta_{ik} + \delta_{jk}) \Delta_{ij}, \tag{9.8}$$

which is compatible with $\Delta_{ij} = \exp[i(\phi_i^C + \phi_j^C)]$, and $n_k = -i \frac{\partial}{\partial \phi_k^C}$ with C denoting charge.

If equation 9.1 captured all of the physics, then computing optimal doping would amount to the determination of the value of $\langle S_z \rangle$ when aiming to maximize the topological pairing order parameter Δ.

Spinful fermions

Just as in the spinless case, the simple commutation relations that will be derived next, can be immediately seen by direct computation (no Jordan-Wigner transformations are necessary). Nevertheless, in order to highlight the similarities between the charge and spin sectors as doublet ($S = \frac{1}{2}$) and triplet ($S = 1$) representations of similar entities the Jordan-Wigner representation will once again be employed. Batista and Ortiz [20] extended the Jordan-Wigner transformations to spinful fermions. The operator

$$\bar{c}_{j\sigma}^\dagger = c_{j\sigma}^\dagger (1 - n_{j-\sigma}), \tag{9.9}$$

along with its conjugate, may be transformed into spin $S = 1$ operators in much the same way as for the spinless case. Within the large U limit, $\bar{c}_{j\sigma}^\dagger \to c_{j\sigma}^\dagger$. Any Hamiltonian in

$\{\bar{c}^{\dagger}_{j\sigma}, \bar{c}_{j\sigma}\}$ has the Gutzwiller (no double occupancy) projection automatically built into it. The general t-J Hamiltonian of equation 9.3 will undergo no change when expressed in terms of $\{\bar{c}^{\dagger}_{j\sigma}, \bar{c}_{j\sigma}\}$ instead of $\{c^{\dagger}_{j\sigma}, c_{j\sigma}\}$.

The transverse XY components of the spin may be written as [20]

$$S^{+}_{j} = \sqrt{2}(\bar{c}^{\dagger}_{j,\sigma=+} K_j + K^{\dagger}_j \bar{c}_{j,\sigma=-}). \tag{9.10}$$

The z-component of the spin transforms as the on-site magnetization,

$$S_{jz} = \bar{n}_{j,\sigma=+} - \bar{n}_{j,\sigma=-}, \tag{9.11}$$

with $\bar{n}_{j\sigma} = \bar{c}^{\dagger}_{j\sigma}\bar{c}_{j\sigma}$. As before,

$$K = \exp[i\sum_{\vec{k}} \theta(\vec{k},\vec{j})\bar{n}_k] = \exp[i\sum_{\vec{k}} \theta(\vec{k},\vec{j})(S^{z}_{k})^2], \tag{9.12}$$

where the, new, second equality follows from equation 9.11 and the built-in constraint of no double occupancy. When the inverse transformation is employed, $\Delta_{ij} = c^{\dagger}_{i\sigma}c^{\dagger}_{j-\sigma}$ contains, similar to the case before, the transverse components of the spin $S^{\pm}$ multiplying topological operators K^{-1}, which are simple exponentiated products in $\{(S^{z}_{j})^2\}$. Once again the non-commuting character of the spin components (equation 9.6) disallows concurrent ideal magnetic and superconducting orders. Explicitly,

$$[S^{z}_{k}, \Delta_{ij}] = -\frac{1}{2}(\delta_{ik} - \delta_{jk})\Delta_{ij}. \tag{9.13}$$

This is compatible with

$$\begin{aligned} S^{z}_{k} &= \frac{i}{2}\frac{\partial}{\partial\phi^{M}_{k}}, \\ \Delta_{ij} &= \exp[i(\phi^{M}_{i} - \phi^{M}_{j})], \end{aligned} \tag{9.14}$$

with the superscript M denoting "*Magnetic*". Trivially,

$$[S^{z}(\vec{q}), \Delta(\vec{p})] \neq 0, \tag{9.15}$$

with $\vec{q}$ and $\vec{p}$ arbitrary wavenumbers.

Examining equations 9.8 and 9.13, it should be noted that, apart from an important minus sign, magnetism competes with superconductivity in much the same way as the charge (number) field competes with pairing for spinless fermions. This is, not all too surprising. It is just mentioned to highlight the similarities between the spin and charge sectors as $S = 1$ and $S = \frac{1}{2}$ representations of a similar problem when viewed through the Jordan-Wigner transformation.

All of what was detailed before was for singlet pairing. For a hypothetical triplet pair operator $\Delta_{ij}^{(t)} = c_{i\sigma}^{\dagger} c_{j\sigma}^{\dagger}$ the commutation relations are trivially identical to those of the number and pairing correlations of equation 9.8,

$$[n_k, \Delta_{ij}^{(t)}] = \frac{1}{2}(\delta_{ik} + \delta_{jk})\Delta_{ij}^{(t)}. \tag{9.16}$$

To summarize,

$$[\text{Spin}, \text{Pairing}] \sim [\text{Charge}, \text{Pairing}] \neq 0. \tag{9.17}$$

The charge and spin sectors can be viewed as a doublet $S = \frac{1}{2}$ and triplet $S = 1$ representations of similar entities. The spin component S_z takes on different roles for the two different Jordan-Wigner transformations. This is simply yet another way of viewing matters. The similarity between the two sectors is highlighted in the $SO(5)$ theory of Zhang [226].

9.4 Planar plaquette pair states

Much of the following approach is inspired by the work of Altman and Auerbach [5], who studied the properties of plaquettes (see figure 9.1). Let the operator $\Delta^{\dagger}$ denote the creation operator of a hole pair on a plaquette. The difference between pairs in the cuprates and in conventional BCS superconductors is that within the cuprates the pair size is very small, which makes it possible to consider a reduction to plaquettes. This is also supported by numerical calculations.

Mapping to an XXZ model

Employing the Matsubara-Matsuda transformation [120] (trivially valid in any dimension)

$$\begin{aligned} S_i^z &= n_i - \frac{1}{2}, \\ S_i^+ &= \Delta_i^{\dagger}, \\ S_i^- &= \Delta_i, \end{aligned} \tag{9.18}$$

this may be used to map the most general Hamiltonian describing pair motions and interactions of all ranges

$$\tilde{H}_{\text{eff}} = -\sum_{\langle ij \rangle} t^{ij}(\Delta_i^{\dagger}\Delta_j + \Delta_j^{\dagger}\Delta_i) + \sum_{\langle ij \rangle} V^{ij} n_i n_j + \tilde{J} \sum_i \Delta_i^{\dagger}\Delta_i + \ldots, \tag{9.19}$$

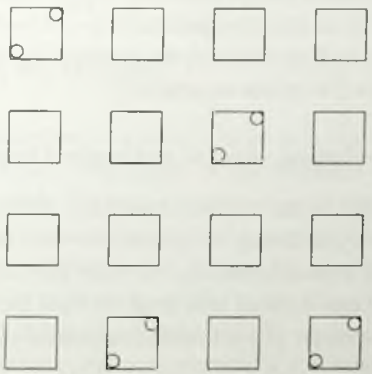

Figure 9.1: In the above picture, holes forming pairs on plaquettes are considered. Following Altman and Auerbach's [5] approach the plane has been tiled with non-overlapping plaquettes. The small circles represent single holes.

to a two-dimensional XXZ model

$$\tilde{H}_{\text{eff}} = -\sum_{\langle ij \rangle} J^{\perp ij}(S_i^+ S_j^- + S_i^- S_j^+) + \sum_{\langle ij \rangle} J^{zij} S_i^z S_j^z - J' \sum_i (S_i^z)^2 - \sum_i h' S_i^z + ..(9.20)$$

with $\tilde{J}^{\perp ij} = 2t^{ij}$, $\tilde{J}^{zij} = V^{ij}$.

The standard nearest neighbor XXZ model can be arrived at by examining the quadratic $O(S^2)$ sector for nearest neighbors ($|i-j|=1$). The XXZ model has two distinct phases: within the Ising limit (large $|J^z|$) the spontaneous breaking of Z_2 symmetry implies phase separation of the bosonic hole pairs. By contrast, for large $|J^{\perp}|$, the system is in the XY limit and the ground state is a superfluid. At the transition between these two phases, the model is $SU(2)$ symmetric. Z_2 order (number order) is dual and conjugate to superconducting order. In the previous chapter, the formation of stripes was arrived at by assuming weak staggered boundary conditions on the real S_z (a Z_2 symmetry order of yet another origin).

Phase separation or not

Whether phase separation of hole pairs will transpire is determined by the sign of the charge-charge interactions V_{ij}.

If the charge-charge interaction is repulsive for all $|i-j|$ (i.e. $V_{ij} > 0$), then in the extended spin model the exchange constants J^z_{ij} will be larger than zero. A positive J^z (a repulsive potential V_{ij}) favors charge neutrality $\langle S^z_{\rm tot}\rangle$ whenever the background charge is taken into account. For an attractive potential $V_{ij} < 0$ leading to $J^z_{ij} < 0$, there is viable ferromagnetic order. In such an instance, the potential V_{ij} allows (and favors) regions of different phase densities (i.e. phase separation).

Superconducting correlations, vortices and optimal doping

Whenever the expectation value $\langle S_z\rangle$ vanishes, there will immediately be half a pair per plaquette or, equivalently, a doping of quarter of a hole per site. In order to make the XXZ model maximally superconducting, the order should be as XY-like as possible to avoid phase separation into bosonic hole pairs. If from the outset the absence of Z_2 like order for the number operator (S_z) is imposed, a quarter of a hole per site is found:

$$\delta_{\rm optimal} = \frac{1}{4}. \tag{9.21}$$

The largest S_z (or number) fluctuations $\langle(S_z - \langle S_z\rangle)^2\rangle$ occur about the symmetric point $\langle S_z\rangle = 0$. This feature is far more generic than assuming a special model of two-dimensional hard core bosons (as was done above). In high enough dimensions, the maximal fluctuations at the symmetry points may diverge signaling a critical point. Large number fluctuations enable well defined superconducting phase (XY) order. A trivial bound on XY order reads

$$\langle \vec{S}^2_\perp\rangle \leq S(S+1) - \langle S_z\rangle^2. \tag{9.22}$$

As the number operator is the dual disorder operator for the phase, in order to have maximal phase ordering, vortex-like number expectation values must be avoided. A finite number density $(n - \frac{1}{2})$, is analogous to a finite vortex density. This, in turn, is equivalent to an imposed external background magnetic flux density in a Josephson junction array. Non-uniformities in the charge order act as frustrating vortices. For maximal phase ordering the appearance of vortices needs to be minimized. This entails lowering the effective magnetic flux background that spontaneously generated vortices must cancel.

Another way of viewing matters at very low finite temperature (like a low temperature classical model) is as follows: If J^z were zero then adding an additional field h' would corrupt the XY order- the previous classical ferromagnetic XY ground state— $\vec{S}_\perp = (\cos\phi, \sin\phi)$ with the phase ϕ uniform over the entire plane. Now imagine turning on J^z and making it negative (attractive interactions among pairs). This will only further corrupt the XY order.

The relatively large deviation of the optimal doping found in the cuprates from $\frac{1}{4}$ suggests that these doped Mott insulators at optimal or near optimal doping may not be

simply viewed as merely composed of pairs of the plaquette size with attractive interactions.

9.5 Plaquette states on stripes

The stripe constitutes a small system coupled to a large bath (the ambient antiferromagnet) from which it can draw holes. Depending on the chemical potential of the stripe, different hole densities will result. For ease a simplifying yet non-essential assumption will be involved: by virtue of the large kinetic scale, the hopping amplitude t is much larger than all potential energy effects, i.e. $\sum_j V_{ij}$ and the magnetic alleviation energy (the energy gained by removing bad ferromagnetic bonds along the seam of the stripe) J. With such assumptions, the chemical potential trivially vanishes. In reality, due to the finite corrections of both effects the chemical potential μ/t is expected to be $\simeq 0$.

As will be shown assuming the constituents of the stripes to be of different geometries and nature (e.g. hole pairs on non overlapping plaquettes, diagonal or parallel hole pairs) different filling fractions will be found at the approximate particle-hole symmetric point $\mu = 0$.

We will now require that every two consecutive rungs of the ladder form a unique plaquette (such that these plaquettes do not overlap) and consider all possible pair states within these plaquettes. If the chemical potential is indeed small by comparison to the kinetic hopping amplitude t, assuming pair states in non-overlapping plaquettes will lead to the "correct" filling fraction. By "correct", we allude to the coincidence, within the large μ/t limit, with the filling fraction attained from an original large U Hubbard Hamiltonian for single fermions augmented by all possible hoppings and interactions among the holes. As shown in section 9.7, starting from the original Hubbard model and allowing holes to do anything that they wish from there (e.g. remain single, pair, phase separate) it is found that the net hole filling fraction is $\frac{1}{4}$. This coincidence suggests that plaquette pair states are indeed viable candidates for the pairs states populating bond centered stripes. Moreover, both numerical [203], and mean field [30] calculations lead to quarter-filling as well as the experimental data [212] (see chapter 5).

These plaquette pair states are indeed the states observed numerically. Moreover, as emphasized by [5] they naturally display d- wave symmetry.

As before, the operator $\Delta^\dagger$ may be used to denote the creation operator of a hole pair on a plaquette and subsequently employ the Matsubara-Matsuda transformation with no change to obtain once again equation 9.19.

As was shown in chapter 3 (see the White and Scalapino bond-centered stripe in figure 3.8), adding a hole pair along the bond centered stripe removes energetic ferromagnetic bonds. Such an effect will only serve as a weak sink favoring more hole pairs to drift into the stripe.

If the charge-charge interaction,

$$\sum_{ij} V_{ij} n_i n_j - 2J \sum_i n_i = \sum_{ij} V_{ij} (n_i - \frac{1}{2})(n_j - \frac{1}{2}) + \sum_i n_i \sum_j V_{ij} - 2J \sum_i n_i, \quad (9.23)$$

is repulsive for all $|i-j|$ (i.e. $V_{ij} > 0$), then in the extended spin model the exchange constant J_{ij}^z will be found to be larger than zero for all $|i-j|$. A positive J^z favors charge neutrality $\langle S_{tot}^z \rangle$ when the background charge of $(-\frac{1}{2})$ (if $\sum_j V_{ij} = 2J$) is taken into account. For an attractive potential $V_{ij} < 0$ leading to $J_{ij}^z < 0$, there is viable ferromagnetic order. The potential V_{ij} allows (and favors) regions of different phase densities (i.e. phase separation).

In the presence of a vanishing electronic chemical potential

$$\mu = \sum_j V_{ij} - 2J, \quad (9.24)$$

or, effectively, an external magnetic field $\tilde{h}$ of a similar magnitude, there is no spontaneous symmetry breaking in the XXZ chain,

$$\langle S_z \rangle = 0, \quad (9.25)$$

and there is an average of one pair per two plaquettes or a quarter of a hole per site. This is indeed in accord with experimental observations [212] and the numerical calculations of White and Scalapino [203], illustrate in figure **5**. In reality, the chemical potential, albeit small compared to t, is not zero and a small deviation from $\frac{1}{4}$ will be found. Nothing is inserted by hand here— the occupancy is dictated by the chemical potential (or magnetic field) which is finite yet may small compared to t by virtue of the various parameters that it includes (i.e. J/t and $\frac{1}{t}\sum_j V_{ij}$). At its very core, the unbroken spin rotational symmetry corresponds to particle-hole symmetry trivially present at $\mu/t = 0$. This symmetry is lightly lifted by a small finite chemical potential shift relative to its vanishing value the particle-hole symmetric point.

Later on, it will be demonstrated that if only symmetrized rung states are assumed for each of the individual holes then no matter how the holes interact and whether they form pairs, phase separate, or not, a bond centered stripe must be nearly quarter-filled when the chemical potential for the insertion of a hole is very small compared to the kinetic hopping scale t.

To conclude, it is expected that

$$\delta_{\text{stripe}} \approx \frac{1}{4}, \quad (9.26)$$

where the approximation sign signifies the relatively small (compared to t) chemical potential shift due to magnetic alleviation energies and hole-hole interactions.

9.6 Non-plaquette pair states

Unless the fundamental pair building blocks are not chosen properly then the hole density may come out to be incorrect (when contrasted with the very general single hole problem for consistency in the large t limit). The filling fraction will be larger than a quarter found for the general hole problem before assuming anything about the possibility of pairing, phase separation etc. among holes. We will now analyze diagonal pairs which may be symmetrized and anti-symmetrized. Apart from some trivial numerical modifications, the considerations that are presented here may be repeated word for word for "vertical" pair states extending along the rungs or "horizontal" pairs extending along the legs. There is a viable link between the correct symmetry of the pair state and its extension over different non-overlapping plaquettes and the anticipated hole density. In order to exhibit this link and point to the viability of plaquette pair physics, the next sections will purposefully focus on a pair state ansatz that will give an incorrect filling fraction in the $\mu/t = 0$ limit. More complicated and comprehensive treatments may employ much of what is known about the two-leg ladders (for instance, the $SO(8)$ symmetry present in their low coupling limit [110]).

Diagonal pairs

We will now write down an effective one-dimensional model for diagonal pairs of two possible chiralities (left/right tilting) as shown in the right and left hand panels of figure 9.2. To give the reader a flavor of where we are heading the general argument may be summarized as follows— we will effectively make an exact projection of the two rung ladder along its axis to produce an effective one-dimensional model. Henceforth the two natural diagonal pair chiralities (or polarizations) will be denoted by a Greek index $\alpha = 1, 2$ and further employ the shorthand

$$\begin{aligned} \Delta_i^{(\alpha=1)} &= c^\dagger_{2,i,\sigma} c^\dagger_{1,i+1,-\sigma} \\ \Delta_i^{(\alpha=1)\dagger} &= c_{1,i+1,-\sigma} c_{2,i,\sigma}. \end{aligned} \tag{9.27}$$

for the hole pair annihilation and creation operators of the diagonal polarization of figure 9.2 ($\alpha = 1$) in terms of the electronic operators. In equation 9.27 the first subscript (which is always one or two) marks the location of the hole on the ladder- on which of the two rungs it is found (upper or lower) while the second (i) denotes the location of the hole along the stripe (ladder) axis. The pair creation operator removes two electrons and the pair annihilation operator creates two electrons. Note that in these operators, there is no spin index symmetrization/anti-symmetrization. The spin polarizations are dictated by the location along the ladder (whether or not i is even). We may conform to the convention that the spin subscript $\sigma = \uparrow$ if i is even and that $\sigma = \downarrow$ along the odd

Figure 9.2: A hole pair advancing along the stripe. To take such motions (either as shown above, or resulting from a higher order hopping process taking the pair in and out of the antiferromagnet surrounding the stripe back to the stripe) into account, overlapping plaquettes must be allowed for. As will be shown, including such possibilities leads to higher filling fractions (i.e. $\delta \geq \frac{1}{3}$ for a nearly vanishing relative chemical potential (μ/t)).

rungs (i.e. the origin $i = 0$ will be chosen in such a way that the spin polarization of both electrons on that rung is $\sigma = \uparrow$). The introduction of each diagonal pair states removes two bad magnetic bonds along the two rungs that it occupies.

The number associated with these hole ("h") pair operators is, as usual,

$$n_{i,h}^{(\alpha)} = [\Delta_i^{(\alpha)}]^\dagger \Delta_i^{(\alpha)}. \tag{9.28}$$

Therefore the most general effective one-dimensional Hamiltonian can be written as

$$\begin{aligned} \tilde{H}_{\text{eff}} &= -\sum_{\langle ij \rangle} t_{\alpha\beta}^{ij} (\Delta_i^{(\alpha)\dagger} \Delta_j^{(\beta)} + \Delta_j^{(\beta)\dagger} \Delta_i^{(\alpha)}) \\ &\quad + \sum_{\langle ij \rangle} V_{\alpha\beta}^{ij} n_{i,h}^{(\alpha)} n_{j,h}^{(\beta)} + \tilde{J}' \sum_{i,\alpha} \Delta_i^{(\alpha)\dagger} \Delta_i^{(\alpha)} + \ldots \end{aligned} \tag{9.29}$$

where the ellipsis denote higher order terms in $\{\Delta_i\}$. All potential terms appear here including ones with infinite long range interactions (e.g. Coulomb effects) in which terms like V_{ij} decay as slowly as desired as a function of the separation $|i - j|$. Note that as a single hole cannot be doubly occupied (or an electron of fixed spin cannot be twice removed), no two diagonal bonds may share the same site; this may formulated in terms of an effective infinite hard core repulsion: $V_{\alpha=1,\beta=2}^{i,i+1} = V_{2,1}^{i,i+1} = \infty$.

Employing the Matsubara-Matsuda transformation once again leads to a flavored version of equation 9.19 where the various spins are dressed by the polarization (diagonal orientation of the pair that they represent). Insofar as commutators are concerned, the two polarization sectors are completely decoupled. Setting, for each α, $\Delta_i = S_i^-$ and $\Delta_i^\dagger = S_i^+$, it can be seen that the pair creation- and annihilation-operators form an $SU(2)$ spin algebra. The effective Hamiltonian is a trivially flavored version of equation 9.19:

$$\tilde{H_{\text{eff}}} = -\sum_{\langle ij \rangle} \tilde{J}_{\alpha\beta}^{\perp ij} (S_i^{x(\alpha)} S_j^{x(\beta)} + S_i^{y(\alpha)} S_j^{y(\beta)}) + \sum_{\langle ij \rangle} \tilde{J}_{\alpha\beta}^{zij} S_i^{z(\alpha)} S_j^{z(\beta)}$$

$$-\bar{J}\sum_{i,\alpha}(S_i^{z(\alpha)})^2-\sum_{i,\alpha}\bar{h}S_i^{z(\alpha)}+\ldots \tag{9.30}$$

where the ellipsis denote higher order spin interactions. As before, to quadratic order, comparison with equation 9.29 shows that equation 9.30 is nothing but an XXZ model with $\tilde{J}_{\alpha\beta}^{\perp ij}=2t_{\alpha\beta}^{ij}$, $\tilde{J}_{\alpha\beta}^{zij}=V_{\alpha\beta}^{ij}$ and $\bar{h}=(2V+J)$ (with J the magnetic alleviation energy), if $V=V_{\alpha\alpha}^{ij}$ is constant for all nearest neighbor links $|i-j|=1$. The only limitation of equations 9.29 and 9.30 is that they only allow for diagonal pairs as the fundamental building blocks (e.g. no single electron excitations are accounted for).

Complete Fock space (Lorentz) algebra

With an eye to things to come, the two diagonal sectors $\alpha=1$ and $\alpha=2$ (corresponding to the left- and right-most real space configurations of figure 9.2 are reshuffled.

By a simple linear transformation

$$\begin{aligned}\vec{\tilde{S}} &= \vec{S}^{(\alpha=1)}+\vec{S}^{(\alpha=2)},\\ \vec{\tilde{A}} &= \vec{S}^{(\alpha=1)}-\vec{S}^{(\alpha=2)},\end{aligned} \tag{9.31}$$

the $SU(2)\otimes SU(2)$ algebra of the two diagonal sectors transforms into a Lorentz $SO(4)$ algebra. Physically,

$$\begin{aligned}\tilde{S}_i^{\pm} &= \Delta_i^1+\Delta_i^2,\\ \tilde{A}_{\pm}^i &= \Delta_i^1-\Delta_i^2,\end{aligned} \tag{9.32}$$

are the creation operators for the symmetric and anti-symmetric rung pair states. The symmetric combination, the angular momentum vector $\vec{S}$ (or $\vec{L}$), forms an $SO(3)$ subgroup: $[\tilde{S}^i,\tilde{S}^j]=i\varepsilon_{ijk}S^k$ with the indices i,j and k now denoting the standard spatial components. The z-component

$$\tilde{S}_i^z = 1-\sum_{\alpha=1,2}n_{i,e}^{(\alpha)}, \tag{9.33}$$

may assume the eigenvalues $\{1,0,-1\}$ corresponding to a 2×2 patch of the ladder being electronically full, having one diagonal hole pair, and two having diagonal hole pairs. The symmetric combinations $\{\vec{\tilde{S}}_i\}$ satisfy $SO(3)$ algebra with spin one. The net number of electrons is given by the total magnetization of the symmetric $\langle\tilde{S}_{tot}^z\rangle$ component.

Restricted symmetric hole pair state basis

We will now make the physical assumption (fortified by the earlier analysis in the previous chapter) that only the low-energy symmetric hole pair bonding states appear at low

energies. Defining, within the restricted symmetric hole pair state basis,

$$\begin{aligned} S_i^- &= \frac{1}{\sqrt{2}}(\Delta_i^1 + \Delta_i^2) \equiv \Delta_i, \\ S_i^+ &= \frac{1}{\sqrt{2}}(\Delta_i^{1\,\dagger} + \Delta_i^{2\,\dagger}) \equiv \Delta_i^\dagger, \\ S_i^z &= \frac{1}{2}[1 - 2n_{i\text{:symm}}], \end{aligned} \tag{9.34}$$

it can be seen that $\vec{S}$ satisfies $SU(2)$ algebra with $S = \frac{1}{2}$ within the restricted symmetric bonding state space $\prod_i (\Delta_i^\dagger)^{r_i}|0\rangle$ with $r_i = 0$ or 1, and where $|0\rangle$ denotes the vacuum state in which no holes are present. The bosonic hole pair states fill up the ladder as the electronic orbital states do the in atomic and molecular systems. This may be regarded as an effective Hund's rule. At low hole filling fractions, only the low-energy bonding states will be occupied. At high hole occupancies (in excess of half a hole per unit site), anti-symmetric anti-bonding states will also appear and the full $SO(4)$ algebra of the full blown unrestricted Fock space will raise its head.

Substituting equations 9.32, 9.33 and 9.34 into equation 9.19 and omitting any terms containing anti-bonding operators (which will take us out of the restricted symmetric pair state subspace) an arbitrarily high polynomial in $\{\vec{S}_i\}$ will result identical to equation 9.19. The hard core repulsion term $V[n_i^{(\alpha=1)} n_{i+1}^{(\alpha=2)} + n_i^{(\alpha=2)} n_{i+1}^{(\alpha=1)}]$ transforms into an analogous hard core term $V S_i^z S_{i+1}^z$ for the z-component of the spins (the distance between up spins cannot be smaller than two).

Such a hard core term may be interpreted from first principles. A state containing nearest neighbor symmetric bonding pairs is not normalized to one. To have normalization the correlated four hole state $\frac{1}{\sqrt{2}} \sum_{\alpha=1,2} \Delta_i^{\alpha\,\dagger} \Delta_{i+1}^{\alpha\,\dagger} |0\rangle$ must be considered. The reduced norm (probability) of the nearest neighbor bonding pairs vis a vis other bonding pairs is similar to having a large potential barrier.

One third doping and beyond

Without the hard core constraint, the model has its ground state at half-filling (i.e. the density of up spins is a half): Whenever an XXZ model has a nearest neighbor hard core constraint (whenever the distance between up spins cannot be smaller than two), the density of up spins is equal to a third within the ground state [4]. A careful counting of the various diagonal pair states reveals that the hole occupancy within the stripe is expected to be $\frac{1}{3}$ in the large t limit. Repeating the same exercise for hole pairs along rungs and legs similar large hole densities are arrived at.

9.7 Single electronic description

Symmetric rung states

The previous chapter numerically obtained the single hole and hole pair energy spectrum on a stripe. Attention will first be restricted to the single electronic description. The states along the various rungs form resonant bonding states. We will now make the physical assumption (fortified by numerics) that only the low-energy symmetric (or anti-symmetric) hole rung bonding states appear at low energies. We will now consider the symmetric (anti-symmetric) smearing of a hole along the two legs of the rung. Defining, within the restricted symmetric hole rung state basis, the two operators

$$c_{i;\pm} \equiv \frac{1}{\sqrt{2}}[c_i^{(\alpha=1)} \pm c_i^{(\alpha=2)}], \tag{9.35}$$

with c the electronic annihilation operator, $\alpha = 1,2$ now a leg index, and i a rung label, it is readily verified that these operators satisfy disjoint canonical Fermi anti-commutation relations: $\{c_{i;\pm}, c^+_{j,\pm}\} = \delta_{ij}$. We will assume that the even parity symmetric bonding hole states are lower in energy and restrict ourselves to that basis. In the problem of physical relevance, $|t_{i=j}^{\alpha=1,\beta=2}|$ is bigger than all other hopping amplitudes and the hole will quickly resonate between the two rungs of the ladder before inching its way along the ladder axis.

Once again, the hole states fill up the ladder as the electronic orbital states do the in atomic and molecular systems. This may be regarded as an effective Hund rule. At low hole filling fractions, only the low-energy bonding states will be occupied. At high hole occupancies (in excess of half a hole per rung of a bond centered stripe or a hole per plaquette in the cuprate plane), anti-symmetric anti-bonding states will also appear and the algebra of the full blown unrestricted Fock space will raise its head. In what will follow shortly, the symmetric rung holes will be treated as spinless fermions. An average density of half a spinless fermion (the particle-hole symmetric point) per rung corresponds to a quarter hole per site. The extended Hubbard model will be considered in the restricted basis of these low lying symmetric rung states.

The ideal spinless Fermi gas

Within the general Hamiltonian equation 9.1 in the limit of infinite on-site repulsion U, the charge degrees of freedom transform into those of a spinless Fermi system. In the bare Hubbard model, at $U = \infty$ the system reduces exactly an ideal (non-interacting) Fermi gas with a dispersion

$$\varepsilon_k = -2t\cos k. \tag{9.36}$$

For a non-interacting Fermi gas, the zero temperature occupancy

$$\langle n_k \rangle = \theta(\mu - \varepsilon_k). \tag{9.37}$$

If inserting a hole leads to no change in the energy balance then the chemical potential, by its very definition, vanishes. The energetics of the chemical potential acts as a Lagrange multiplier enforcing a certain average occupancy. The energy of adding or removing an electron is the same (zero) at a chemical potential $\mu = 0$. By particle-hole symmetry, at $\mu = 0$ the chemical potential lies in the middle of the band and the occupancy of the rung symmetrized spinless Fermi particles is a half- and that of the holes is $\frac{1}{4}$. The particle-hole symmetry of the kinetic energy band is dictated by the hermiticity of the Hamiltonian. In fact, even if the Hamiltonian included arbitrary long range hoppings $\{t_r\}$ and reduced to the general form

$$H = -\sum_{ij} t_{|j-i|}(c_i^\dagger c_j + h.c.), \tag{9.38}$$

in the infinite U limit, then by hermiticity whenever the chemical potential is zero the Hamiltonian will be particle hole symmetric. In that case, the density of rung symmetrized spinless fermions will be a half, and the density of holes along the bond centered stripe will be $\frac{1}{4}$.

If the addition of holes (or removal of electrons) leads to a reduction in the magnetic strain energy along the stripe then the chemical potential for the electrons is reduced (or, equivalently, that for holes, is increased). A removal of a bad bond along the rung leads to a lowering of the magnetic energy by J. Thus the hole chemical potential $\mu = J$ and the net, rung symmetrized, charge occupancy is given by an integral of $\langle n_k \rangle$. The hole density is $\langle (n_k/2) \rangle$. This expectation value (hole occupancy) changes slightly with temperature according to the evolution of the Fermi function.

It is worthwhile viewing this, one last time, in terms of unbroken spin rotational symmetry in an effective $XX(Z)$ model.

Applying the Jordan-Wigner transformation leads to an $XX(Z)$ model. As is well known, the infinite U Hubbard Hamiltonian trivially transforms into

$$H = -2t \sum_i (S_{i,x} S_{i+1,x} + S_{i,y} S_{i+1,y}). \tag{9.39}$$

An infinitesimal chemical potential leads to an additional small magnetic field coupling to σ_z. The absence of spin symmetry breaking in this trivial example (no σ_z interaction appears in H) leads to the conclusion that the band is half-filled (or that the hole density is $\frac{1}{4}$).

This is immediately seen taking note of

$$S_i^z = \frac{1}{2} - c_i^\dagger c_i. \tag{9.40}$$

A vanishing $\langle \sigma_z \rangle$ for the XY Hamiltonian of equation 9.39 leads to $\langle n_j \rangle = \frac{1}{2}$. Related back to the original problem, this implies a quarter empty electronic bond centered stripe. This value is seen here to be dictated by an unbroken particle-hole symmetry. If additional interactions next-nearest neighbor pieces of the Coulomb and other interactions ($\sum_{\langle ij \rangle} V_{ij} n_i n_j$) and the magnetic energy alleviation energy J are added to the Hamiltonian then the Hamiltonian for the spinless symmetrized holes readily transforms to a full blown XXZ model with

$$\begin{aligned} H &= -2t \sum_i (S_{ix} S_{i+1,x} + S_{iy} S_{i+1,y}) \\ &\quad + \sum_{\langle ij \rangle} \frac{V_{ij}}{4} (1 - S_i^z/2)(1 - S_j^z/2) - \frac{J}{2} \sum_i (1 - S_i^z/2) \\ &\equiv \sum_{\langle ij \rangle} [-J_\perp (S^+ S^- + h.c.) + J_z S_i^z S_j^z] + \sum_i h S_i^z. \end{aligned} \tag{9.41}$$

First note that if the electrostatic energy $V_{i,i+1}$ is such that it equals the magnetic alleviation energy J then by the absence of spontaneous symmetry breaking in one dimension, $\langle S^z \rangle = 0$ and the bond centered stripe is quarter-filled. If, hypothetically, S^z would spontaneously develop a nonzero magnetization then this would imply that even if in an ensemble of stripes, the overall density of holes would be a quarter on average, different stripes in the ensemble would exhibit two different densities about that mean. An imbalance between V and J leads to nonzero h and to a finite value of $\langle S^z \rangle \neq 0$—a deviation from quarter-filling on every stripe. In the above both the Coulomb and magnetic alleviation effects were taken into account in one go.

Nayak and Wilczek [135] observed that $\frac{1}{4}$-filling of a doped chain is indeed predicted from the Bethe ansatz solution of Lieb and Wu [108]. Some of the symmetries of the $\frac{1}{4}$-filled point were noted. It must be emphasized that at low chemical potential, quarter-filling not only coincides with symmetries, but is, in fact, a rigorous outcome of symmetry considerations. It should also be noted that a finite magnetic alleviation energy of the holes amounts to a shift in the chemical potential. The approximate calculations employed earlier are not mandatory for the determination of the hole occupancy within the ground state; in order to account for magnetic effects, the hole chemical potential μ may be simply set to J, and subsequently integrate the known ideal spinless Fermi number density $\langle n_\varepsilon \rangle$ up to that energy to obtain an exact result.

Bibliography

[1] E. Abrahams and C. M. Varma. *What angle-resolved photoemission experiments tell us about the microscopic theory for high-temperature superconductors.* Proc. Nat. Aca. Sci. **97** (2000) 5714.

[2] G. Aeppli, T. E. Mason, S. M. Hayden, H. A. Mook and J. Kolda. *Nearly singular magnetic fluctuations in the normal state of a high-T_c cuprate superconductor.* Science **278** (1997) 1432.

[3] S. Alama, A. J. Berlinsky, L. Bronsard and T. Giorgi. *Vortices with antiferromagnetic cores in the $SO(5)$ theory of high temperature superconductivity.* Phys. Rev. B **60** (1999) 6901.

[4] F. C. Alcarez and R. Z. Bariev. *An Exactly Solvable Constrained XXZ Chain.* In *Proceedings of the Conference: Statistical Physics on the Eve of the Twenty-First Century*. World Scientific, 1999.

[5] E. Altman and A. Auerbach. *Plaquette boson-fermion model of cuprates.* Phys. Rev. B **65** (2002) 104508.

[6] G. An and J. M. J. van Leeuwen. *Fixed-node Monte Carlo study of the two-dimensional Hubbard model.* Phys. Rev. B **44** (1991) 9410.

[7] P. W. Anderson. *Coherent Excited States in the theory of superconductivity: Gauge invariance and the Meissner effect.* Physical Review **110** (1958) 827.

[8] P. W. Anderson. *Random-Phase approximation in the theory of superconductivity.* Physical Review **112** (1958) 1900.

[9] P. W. Anderson. *The Resonating Valence Bond State in La_2CuO_4 and Superconductivity.* Science **235** (1987) 1196.

[10] P. W. Anderson. *The theory of High-T_c superconductivity.* Princeton University Press; Princeton, New Jersey, 1997. ISBN 0-691-04365-5.

[11] P. W. Anderson. *How Josephson discovered his effect*. Physics Today (nov 1970) 23.

[12] Y. Ando, G. S. Boebinger, A. Passner, T. Kimura, M. Okuya, J. Shimoyama, K. Kishio, K. Tamasaku, N. Ichikawa and S. Uchida. *Insulator-to-Metal Crossover in the Normal state of $La_{2-x}Sr_xCuO_4$ near optimum doping*. Phys. Rev. Lett. **77** (1996) 5417.

[13] Y. Ando, A. N. Lavrov and K. Segawa. *Magnetoresistance Anomalies in Antiferromagnetic $YBa_2Cu_3O_{6+x}$: Fingerprints of Charged Stripes*. Phys. Rev. Lett. **83** (1999) 2813.

[14] M. Arai, T. Nishijima, Y. Endoh, T. Egami, S. Tajima, K. Tomimoto, Y. Shiohara, M. Takahashi, A. Garrett and S. M. Bennington. *Incommensurate Spin Dynamics of Underdoped Superconductor $YBa_2Cu_3O_{6.7}$*. Phys. Rev. Lett. **83** (1999) 608.

[15] A. Auerbach. *Interacting electrons and quantum magnetism*. Springer, New York, 1994. ISBN 0-387-94286-6. Graduate texts in contempory Physics.

[16] J. D. Axe, A. H. Moudden, D. Hohlwein, D. E. Cox, K. M. Mohanty, A. R. Moodenbaugh and Y. Xu. *Structural phase transformations and superconductivity in $La_{2-x}Ba_xCuO_4$*. Phys. Rev. Lett. **62** (1989) 2751.

[17] A. V. Balatsky and P. Bourges. *Linear Dependence of Peak Width in $\chi(q,\omega)$ vs T_c for $YBa_2Cu_3O_{6+x}$ Superconductors*. Phys. Rev. Lett. **82** (1999) 5337.

[18] A. V. Balatsky and Z.-X. Shen. *Is this why T_c is so low?*. Science **284** (1999) 1137.

[19] J. Bardeen, L. N. Cooper and J. R. Schrieffer. *Theory of Superconductivity*. Physical Review **108** (1957) 1175.

[20] C. D. Batista and G. Ortiz. *Spin-Particle Connections*. Condensed Matter Theories **16** (2001).

[21] C. D. Batista, G. Ortiz and A. V. Balatsky. *Unified description of the resonance peak and incommensuration in high-T_c superconductors*. Phys. Rev. B **64** (2001) 172508.

[22] B. B. Beard, R. J. Birgeneau, M. Greven and U.-J. Wiese. *The Square-Lattice Heisenberg Antiferromagnet at Very Large Correlation Lengths*. Phys. Rev. Lett. **80** (1998) 1742.

[23] F. Becca, L. Capriotti and S. Sorella. *Stripes and spin incommensurabilities are favored by lattice anisotropies*. Phys. Rev. Lett. **87** (2001) 167005.

[24] J. G. Bednorz and K. A. Müller. *Possible high T_c superconductivity in the Ba-La-Cu-O system.* Zeitschrift für Physic B - Condensed Matter **64** (1986) 189.

[25] R. J. Birgeneau, M. Greven, M. A. Kastner, Y. S. Lee, B. O. Wells, Y. Endoh, K. Yamada and G. Shirane. *Instantaneous spin correlations in La_2CuO_4.* Phys. Rev. B **59** (1999) 13788.

[26] G. S. Boebinger, Y. Ando, A. Passner, T. Kimura, M. Okuya, J. Shimoyama, K. Kishio, K. Tamasaku, N. Ichikawa and S. Uchida. *Insulator-to-Metal Crossover in the Normal State of $La_{2-x}Sr_xCuO_4$ Near Optimum Doping.* Phys. Rev. Lett. **77** (1996) 5417.

[27] M. Boninsegni and E. Manousakis. *Quasihole excitation in a quantum antiferromagnet: Variational Monte Carlo calculation.* Phys. Rev. B **43** (1991) 10353.

[28] D. A. Bonn, J. C. Wynn, B. W. Gardner, Y.-J. Lin, R. Liang, W. N. Hardy, J. R. Kirtley and K. A. Moler. *A limit on spin-charge separation in high-T_c superconductors from the absence of a vortex-memory effect.* Nature **414** (2001) 887.

[29] F. Borsa, P. Carretta, J. H. Cho, F. C. Chou, Q. Hu, D. C. Johnston, A. Lascialfari, D. R. Torgeson, R. J. Gooding, N. M. Salem and K. J. E. Vos. *Staggered magnetization in $La_{2-x}Sr_xCuO_4$ from ^{139}La NQR and μSR: Effects of Sr doping in the range $0 < x < 0.02$.* Phys. Rev. B **52** (1995) 7334.

[30] M. Bosch, W. van Saarloos and J. Zaanen. *Shifting Bragg peaks of cuprate stripes as possible indications for fractionally charged kinks.* Phys. Rev. B **63** (2001) 092501.

[31] W. F. Brinkman and T. M. Rice. *Single-particle excitations in magnetic insulators.* Phys. Rev. B **2** (1970) 1324.

[32] E. W. Carlson, V. J. Emery, S. A. Kivelson and D. Orgad. *Concepts in High Temperature Superconductivity.* cond-mat/0206217 (2002). Review chapter to appear in 'The Physics of Conventional and Unconventional Superconductors' ed. by K. H. Bennemann and J. B. Ketterson (Springer-Verlag).

[33] E. W. Carlson, S. A. Kivelson, V. J. Emery and E. Manousakis. *Classical Phase fluctuations in High temperature superconductors.* Phys. Rev. Lett. **83** (1999) 612.

[34] E. W. Carlson, S. A. Kivelson, Z. Nussinov and V. J. Emery. *Doped antiferromagnets in high dimension.* Phys. Rev. B **57** (1998) 14704.

[35] A. H. Castro Neto and D. Hone. *Doped Planar Quantum Antiferromagnets with Striped Phases.* Phys. Rev. Lett. **76** (1996) 2165.

[36] B. K. Chakrabarti, A. Dutta and P. Sen. *Quantum Ising Phases and transitions in Transverse Ising Models*. Springer, Berlin, 1996. ISBN 3-540-61033-2.

[37] S. Chakravarty, B. I. Halperin and D. R. Nelson. *Low-Temperature Behavior of Two-Dimensional Quantum Antiferromagnets*. Phys. Rev. Lett. **60** (1988) 1057.

[38] S. Chakravarty, A. Sudbo, P. W. Anderson and S. Strong. *Interlayer tunneling and gap anisotropy in high-temperature superconductors*. Science **261** (1993) 337.

[39] L. Chayes, V. J. Emery, S. A. Kivelson, Z. Nussinov and G. Tarjus. *Avoided critical behavior in a uniformly frustrated system*. Physica A **225** (1996) 129.

[40] C. H. Chen and S.-W. Cheong. *Commensurate to Incommensurate Charge ordering and its real-space images in* $La_{0.5}Ca_{0.5}MnO_3$. Phys. Rev. Lett. **76** (1996) 4042.

[41] C. H. Chen, S.-W. Cheong and A. S. Cooper. *Charge Modulations in* $La_{2-x}Sr_xNiO_{4+y}$*: Ordering of Polarons*. Phys. Rev. Lett. **71** (1993) 2461.

[42] S.-W. Cheong, G. Aeppli, T. E. Mason, H. Mook, S. M. Hayden, P. C. Canfield, Z. Fisk, K. N. Clausen and J. L. Martinez. *Incommensurate Magnetic Fluctuations in* $La_{2-x}Sr_xCuO_4$. Phys. Rev. Lett. **67** (1991) 1791.

[43] A. L. Chernyshev, S. R. White and A. H. Castro Neto. *Stripes as an effective one-dimensional band of composite excitations*. Phys. Rev. B **65** (2002) 214527.

[44] R. Coldea, S. M. Hayden, G. Aeppli, T. G. Perring, C. D. Frost, T. E. Mason, S.-W. Cheong and Z. Fisk. *Spin waves and electronic interactions in* La_2CuO_4 *excitations*. Phys. Rev. Lett. **86** (2000) 5377.

[45] J. Corson, R. Mallozzi, J. Orenstein, J. N. Eckstrien and I. Bozovic. *Vanishing of phase coherence in underdoped* $Bi_2Sr_2CaCu_2O_{8+\delta}$. Nature **398** (1999) 221.

[46] G. W. Crabtree and D. R. Nelson. *Vortex physics in high-temperature superconductors*. Physics Today (april 1997) 38.

[47] E. Dagotto. *Correlated electrons in high-temperature superconductors*. Rev. Mod. Phys. **66** (1994) 763.

[48] E. Dagotto, R. Joynt, A. Moreo, S. Bacci and E. Gagliano. *Strongly correlated electronic systems with one hole: Dynamical properties*. Phys. Rev. B **41** (1990) 9049.

[49] E. Dagotto and T. M. Rice. *Surprises on the way from one- to two-dimensional quantum magnets: The ladder materials.* Science **271** (1996) 618.

[50] E. Dagotto and J. R. Schrieffer. *Constructing quasiparticle operators in strongly correlated systems.* Phys. Rev. B **43** (1991) 8705.

[51] P. Dai, H. A. Mook and F. Dogan. *Incommensurate magnetic fluctuations in* $YBa_2Cu_3O_{6.6}$. Phys. Rev. Lett. **80** (1998) 1738.

[52] P. Dai, H. A. Mook, R. D. Hunt and F. Dogan. *Evolution of the resonance and incommensurate spin fluctuations in superconducting* $YBa_2Cu_3O_{6+x}$. Phys. Rev. B **63** (2001) 054525.

[53] P.-G. de Gennes. *Superconductivity of Metals and Alloys.* Perseus Publishing, 1999. ISBN 0738201014.

[54] E. Demler, A. J. Berlinsky, C. Kallin, G. B. Arnold and M. R. Beasley. *Proximity Effect and Josephson Coupling in the* $SO(5)$ *Theory of High-*T_c *Superconductivity.* Phys. Rev. Lett. **80** (1998) 2917.

[55] E. Demler, H. Kohno and S.-C. Zhang. *Pi excitation of the t-J model.* Phys. Rev. B **58** (1998) 5719.

[56] E. Demler and S.-C. Zhang. *Theory of the resonant neutron scattering of high-*T_c *superconductors.* Phys. Rev. Lett. **75** (1995) 4126.

[57] M. den Nijs and K. Rommelse. *Preroughening transitions in crystal surfaces and valence-bond phases in quantum spin chains.* Phys. Rev. B **40** (1989) 4709.

[58] P. J. H. Denteneer, G. An and J. M. J. van Leeuwen. *Optimal superconducting critical temperature in the two-dimensional attractive Hubbard model.* Europhysics Letters **16** (1991) 5.

[59] P. J. H. Denteneer, G. An and J. M. J. van Leeuwen. *Helicity modulus in the two-dimensional Hubbard model.* Phys. Rev. B **47** (1993) 6256.

[60] Y. Dimashko and C. Morais Smith. *Superconductor/Insulator Transition in the Striped Phase.* cond-mat/9805027 (1998).

[61] Y. A. Dimashko, C. Morais Smith, N. Hasselmann and A. O. Caldeira. *Dynamics of lattice pinned charge stripes.* Phys. Rev. B **60** (1999) 88.

[62] H. Ding, J. C. Campuzano, M. R. Norman, M. Randeria, T. Yokoya, T. Takahashi, T. Takeuchi, T. Mochiku, K. Kadowaki, P. Guptasarma and D. G. Hinks. *ARPES*

study of the superconducting gap and pseudogap in $Bi_2Sr_2CaCu_2O_{8+x}$. Proceedings of Spectroscopies of Novel Superconductors SNS97, Cape Cod; cond-mat/9712100 (1997).

[63] H. Ding, M. R. Norman, J. C. Campuzano, M. Randeria, A. F. Bellmann, T. Yokoya, T. Takahashi, T. Mochiku and K. Kadowaki. *Angle-resolved photoemission spectroscopy study of the superconducting gap anisotropy in* $Bi_2Sr_2CaCu_2O_{8+x}$. Phys. Rev. B **54** (1996) 9678.

[64] H. Ding, T. Yokoya, J. C. Campuzano, T. Takahashi, M. Randeria, M. R. Norman, T. Mochiku, K. Kadowaki and J. Giapintzakis. *Spectroscopic evidence for a pseudogap in the normal state of underdoped high-*T_c *superconductors.* Nature **382** (1996) 51.

[65] T. Dombre. *Modulated spiral phases in doped quantum antiferromagnets.* J. Phys. France **51** (1990) 847.

[66] R. R. Du, D. C. Tsui, H. L. Stormer, L. N. Pfeiffer, K. W. Baldwin and K. W. West. *Strongly anisotropic transport in higher two-dimensional Landau levels.* Solid State Communications **109** (1999) 389.

[67] M. S. L. du Croo de Jongh. *Density Matrix Renormalisation Group Variants for Spin Systems.* Ph.D. thesis, Instituut-Lorentz, University of Leiden, P.O. Box 9506, 2300 RA Leiden, The Netherlands, Sep. 1999.

[68] R. Eder, A. Dorneich, M. G. Zacher, W. Hanke and S.-C. Zhang. *Dynamics of an* $SO(5)$*-symmetric ladder model.* Phys. Rev. B **59** (1999) 561.

[69] D. Eliezer and G. W. Semenoff. *Intersection Forms and the Geometry of lattice Chern-Simons theory.* Physics Letters B **286** (1992) 118.

[70] V. Elser, D. Huse, B. I. Shraiman and E. D. Siggia. *Ground state of a mobile vacancy in quantum antiferromagnet: Small-cluster study.* Phys. Rev. B **41** (1990) 6715.

[71] V. J. Emery and S. A. Kivelson. *Frustrated electronic phase separation and high-temperature superconductors.* Physica C **209** (1993) 597.

[72] V. J. Emery and S. A. Kivelson. *Importance of phase fluctuations in superconductors with small superfluid density.* Nature **374** (1995) 434.

[73] V. J. Emery and S. A. Kivelson. *Microscopic Theory of High Temperature Superconductivity.* Proceedings of Stripes98; cond-mat/9809083 (1998).

[74] V. J. Emery, S. A. Kivelson and O. Zachar. *Pairing and Phase Coherence in High Temperature Superconductors.* Physica C **282-287** (1997) 174.

[75] V. J. Emery, S. A. Kivelson and O. Zachar. *Spin-gap proximity effect mechanism of high-temperature superconductivity.* Phys. Rev. B **56** (1997) 6120.

[76] Y. Endoh, K. Yamada, R. J. Birgeneau, D. R. Gabbe, H. P. Jensson, M. A. Kastner, C. J. Peters, D. J. Picone, T. R. Thurston, J. M. Tranquada, G. Shirane, Y. Hidaka, M. Oda, Y. Enomoto, M. Suzuki and T. Murakari. *Static and dynamic spin correlations in pure and doped La_2CuO_4.* Phys. Rev. B **37** (1988) 7443.

[77] H. Eskes, R. Grimberg, W. van Saarloos and J. Zaanen. *Quantizing Charged Magnetic Domain Walls: Strings on a Lattice.* Phys. Rev. B **54** (1996) R724.

[78] R. P. Feynman, R. B. Leighton and M. Sands. *The Feynman Lectures on Physics.* Addison-Wesley, 1965. ISBN 81-85015-84-8.

[79] E. Fradkin. *Jordan-Wigner transformation for quantum-spin systems in two dimensions and fractional statistics.* Phys. Rev. Lett. **63** (1989) 322.

[80] E. Fradkin and S. A. Kivelson. *Liquid-crystal phases of quantum Hall systems.* Phys. Rev. B **59** (1999) 8065.

[81] T. Giamarchi and C. Lhuillier. *Variational Monte Carlo study of incommensurate antiferromagnetic phases in the two dimensional Hubbard model.* Phys. Rev. B **42** (1990) 10641.

[82] T. Giamarchi and C. Lhuillier. *Phase diagrams of the two-dimensional Hubbard and t-J models by a variational Monte Carlo method.* Phys. Rev. B **43** (1991) 12943.

[83] F. D. M. Haldane. *General relation of correlation exponents and spectral properties of one-dimensional Fermi systems: Application to the anisotropic $S = \frac{1}{2}$ Heisenberg chain.* Phys. Rev. Lett. **45** (1980) 1358.

[84] W. N. Hardy, D. A. Bonn, D. L. Morgan, R. Liang and K. Zhang. *Precision measurements of the temperature dependence of λ in $YBa_2Cu_3O_{6.95}$: strong evidence for nodes in the gap function.* Phys. Rev. Lett. **70** (1993) 3999.

[85] P. Hasenfratz and F. Niedermayer. *The exact correlation length of the antiferromagnetic $d = 2 + 1$ Heisenberg model at low temperatures.* Phys. Rev. B **268** (1991) 231.

[86] K. C. Hass. *Electronic Structure of Copper-Oxide Superconductors.* Journal of Physics C: Solid State Physics **42** (1989) 213.

[87] R. M. Hazen. *The Breakthrough: The race for the superconductor*. Summit Books, New York, London, Toronto, Sydney, Tokyo, 1988. ISBN 0-671-65829-8.

[88] A. Heeger, S. Kivelson, J. R. Schrieffer and W.-P. Su. *Solitons in conducting polymers*. Rev. Mod. Phys. **60** (1988).

[89] C. S. Hellberg and E. Manousakis. *Phase separation at all interaction strengths in the t-J model*. Phys. Rev. Lett. **78** (1997) 4609.

[90] C. S. Hellberg and E. Manousakis. *Stripes and the t-J model*. Phys. Rev. Lett. **83** (1999) 132.

[91] M. Hervieu, A. Barnabe, C. Martin, A. Maignan, F. Damay and B. Raveau. *Evolution of charge ordering in* $Ca_{1-x}Sm_xMnO_3$ *manganites with* $0.15 \leq x \leq 0.60$. European Journal of Physics B **8** (1999) 31.

[92] K. Hirota. *Neutron scattering studies of Zn-doped* $La_{2-x}Sr_xCuO_4$. cond-mat/0010340 (2000).

[93] A. W. Hunt, P. M. Singer, K. R. Thurber and T. Imai. ^{63}*Cu NQR Measurement of Stripe order parameter in* $La_{2-x}Sr_xCuO_4$. Phys. Rev. Lett. **82** (1999) 4300.

[94] M. Inui and P. B. Littlewood. *Hartree-Fock study of the magnetism in the single-band Hubbard model*. Phys. Rev. B **44** (1991) 4415.

[95] L. B. Ioffe and A. J. Millis. *Cold spots: a new model for transport in high-*T_c *cuprates*. cond-mat/9801092 (1998).

[96] P. Jordan and E. P. Wigner. *About the Pauli Exclusion Principle*. Z. Phys. **47** (1928) 631.

[97] B. D. Josephson. *Supercurrent Through Barriers*. Adv. Phys **14** (1965) 419.

[98] M. A. Kastner, R. J. Birgeneau, G. Shirane and Y. Endoh. *Magnetic, transport and optical properties of monolayer copper oxides*. Rev. Mod. Phys. **70** (1998) 897.

[99] H. Kimura, K. Hirota, H. Matsushita, K. Yamada, Y. Endoh, S.-H. Lee, C. F. Majkrzak, R. Erwin, G. Shirane, M. Greven, Y. S. Lee, M. A. Kastner and R. J. Birgeneau. *Neutron scattering study of static antiferromagnetic correlations in* $La_{2-x}Sr_xCu_{1-y}Zn_yO_4$. Phys. Rev. B **59** (1999) 6517.

[100] H. Kimura, H. Matsushita, K. Kirota, Y. Endoh, K. Yamada, G. Shirane, Y. S. Lee, M. A. Kastner and R. J. Birgeneau. *Neutron scattering study of incommensurate elastic magnetic peaks in* $La_{1.88}Sr_{0.12}CuO_4$. Journal of Physics and Chemistry of Solids **60** (1999) 1067.

[101] J. R. Kirtley, C. C. Tsuei, H. Raffy, Z. Z. Li, V. G. Kogan, J. R. Clem and K. A. Moler. *Direct measurement of single fluxoid dynamics in superconducting rings.* cond-mat/0103474 (2001).

[102] S. A. Kivelson and V. J. Emery. *Topological doping of correlated insulators.* Synthetic Metals **80** (1996) 151.

[103] S. A. Kivelson, E. Fradkin and V. J. Emery. *Electronic liquid-crystal phases of a doped Mott insulator.* Nature **393** (1998) 550.

[104] Y. A. Krotov, D.-H. Lee and A. V. Balatsky. *Superconductivity of a metallic stripe embedded in an antiferromagnet.* Phys. Rev. B **56** (1997) 8367.

[105] H. V. Kruis. *On Hidden Order in Luttinger Liquids.* Ph.D. thesis, Instituut-Lorentz, University of Leiden, P.O. Box 9506, 2300 RA Leiden, The Netherlands, Jun. 2003.

[106] Y. S. Lee, R. J. Birgeneau, M. A. Kastner, Y. Endoh, S. Wakimoto, K. Yamada, R. W. Erwin, S. H. Lee and G. Shirane. *Neutron Scattering Study of Spin Density Wave Order in the Superconducting State of Excess-Oxygen-Doped* La_2CuO_{4+y}. Phys. Rev. B **60** (1999) 3643.

[107] P. W. Leung and R. J. Gooding. *Dynamical properties of the single-hole t-J model on a 32-site square lattice.* Phys. Rev. B **52** (1995) R15711.

[108] E. H. Lieb and F. Y. Wu. *Absence of Mott Transition in an Exact Solution of the Short-Range, One-band Model in One Dimension.* Phys. Rev. Lett. **20** (1968) 1445.

[109] M. P. Lilly, K. B. Cooper, J. P. Eisenstein, L. N. Pfeiffer and K. W. West. *Evidence for an anisotropic state of two-dimensional electrons in high Landau Levels.* Phys. Rev. Lett. **82** (1999) 394.

[110] H. H. Lin, L. Balents and M. P. A. Fisher. *Exact SO(8) Symmetry in the Weakly-Interacting Two-Leg Ladder.* Phys. Rev. B **58** (1998) 1794.

[111] W. A. Little. *Decay of Persistent Currents in Small Superconductors.* Physical Review **156** (1964) 396.

[112] Z. Liu and E. Manousakis. *Spectral function of a hole in the t-J model.* Phys. Rev. B **44** (1991) 2414.

[113] E. Louis, F. Guinea, M. P. López Sancho and J. A. Vergés. *Configuration-interaction approach to hole pairing in the two-dimensional Hubbard model.* Phys. Rev. B **59** (1999) 14005.

[114] U. Löw, V. J. Emery, K. Fabricius and S. A. Kivelson. *Study of an Ising model with competing long- and short-range interactions.* Phys. Rev. Lett. **72** (1994) 1918.

[115] K. Machida. *Magnetism in La_2CuO_4 based compounds.* Physica C **158** (1989) 192.

[116] M. B. Maple. *High Temperature Superconductivity.* cond-mat/9802202 (1998).

[117] D. S. Marshall, D. S. Dessau, A. G. Loeser, C.-H. Park, A. Y. Matsuura, J. N. Eckstein, I. Bozovic, P. Fournier, A. Kapitulnik, W. E. Spicer and Z.-X. Shen. *Unconventional Electronic structure Evolution with Hole Doping in $Bi_2Sr_2CaCu_2O_{8+\delta}$: Angle-Resolved Photoemission Results.* Phys. Rev. Lett. **76** (1996) 4841.

[118] F. Marsiglio, A. E. Ruckenstrein, S. Schmitt-Rink and C. M. Varma. *Spectral function of a single hole in a two-dimensional quantum antiferromagnet.* Phys. Rev. B **43** (1991) 10882.

[119] T. E. Mason. *Neutron Scattering Studies of Spin Fluctuations in High Temperature Superconductors.* In *Handbook on the Physics and Chemistry of Rare Earths, Special Volumes on High Temperature Rare Earth Superconductors.* 1998.

[120] T. Matsubara and H. Matsuda. Prog. Theor. Phys. **36** (1956) 569.

[121] M. Matsuda, M. Fujita, K. Yamada, R. J. Birgeneau, M. A. Kastner, H. Hiraka, Y. Endoh, S. Wakimoto and G. Shirane. *Static and dynamic spin correlations in the spin-glass phase of slightly-doped $La_{2-x}Sr_xCuO_4$.* Phys. Rev. B (2000) 9148.

[122] H. Matsushita, H. Kimura, M. Fujita, K. Yamada, K. Hirota and Y. Endoh. *Sr concentration dependence of incommensurate elastic magnetic peaks in $La_{2-x}Sr_xCuO_4$.* Journal Physics and Chemistry of Solids **60** (1999) 1071.

[123] L. F. Mattheiss. *Electronic Band Properties and Superconductivity in $La_{2-y}X_yCuO_4$.* Phys. Rev. Lett. **58** (1987) 1028.

[124] S. I. Matveenko and S. I. Mukhin. *Analytical stripe phase solution for the Hubbard model.* cond-mat/9912487 (1999).

[125] S. Meixner, W. Hanke, E. Demler and S.-C. Zhang. *Finite-Size Studies on the SO(5) Symmetry of the Hubbard model.* Phys. Rev. Lett. **79** (1997) 4902.

[126] R. Micnas, J. Ranninger and S. Robaszkiewicz. *Superconductivity in narrow-band systems with local nonretarded attractive interactions.* Rev. Mod. Phys. **62** (1990) 113.

[127] A. J. Millis, H. Monien and D. Pines. *Phenomenological model of nuclear relaxation in the normal state of* $YBa_2Cu_3O_7$. Phys. Rev. B **42** (1990) 167.

[128] A. R. Moodenbaugh, Y. Xu, M. Suenaga, T. J. Folkerts and R. N. Shelton. *Superconducting properties of* $La_{2-x}Ba_xCuO_4$. Phys. Rev. B **38** (1988) 4596.

[129] H. A. Mook, P. Dai, S. M. Hayden, G. Aeppli, T. G. Perring and F. Dogan. *Spin fluctuations in* $YBa_2Cu_3O_{6.6}$. Nature **395** (1998) 580.

[130] H. A. Mook, P. Dai, R. D. Hunt and F. Dogan. *Neutron scattering studies of the magnetic fluctuations in* $YBa_2Cu_3O_{7-\delta}$. In *Proceedings of Spectroscopies in Novel Superconductors, Cape Cod, Massachusetts, Sept. 1997.* 1997.

[131] H. A. Mook, P. C. Dai, F. Dogan and R. D. Hunt. *One-dimensional nature of the magnetic fluctuations in* $YBa_2Cu_3O_6$. Nature **404** (2000) 729.

[132] H. A. Mook, F. Dogan and B. C. Chakoumakos. *Magnetic and Charge fluctuations in high-*T_c *superconductors.* cond-mat/9811100 (1998).

[133] S. Mori, C. H. Chen and S.-W. Cheong. *Pairing of charge-ordered stripes in* $(La,Ca)MnO_3$. Nature **392** (1998) 473.

[134] C. Nayak and F. Wilczek. *Possible electronic structure of domain walls in Mott insulators.* International Journal of Modern Physics B **10** (1996) 2125.

[135] C. Nayak and F. Wilczek. *Populated Domain Walls.* Phys. Rev. Lett. **78** (1997) 2465.

[136] C. Niedermayer, C. Bernhard, T. Blasius, A. Golnik, A. Moodenbaugh and J. I. Budnick. *Common Phase Diagram for Antiferromagnetism in* $La_{2-x}Sr_xCuO_4$ *and* $Y_{1-x}Ca_xBa_2Cu_3O_6$ *as seen by Muon Spin Rotation.* Phys. Rev. Lett. **80** (1998) 3843.

[137] T. Niemöller, N. Ichikawa, T. Frello, H. Huennefeld, N. H. Andersen, S. Uchida, J. R. Schneider and J. M. Tranquada. *Charge stripes seen with X-rays in* $La_{1.45}Nd_{0.4}Sr_{0.15}CuO_4$. cond-mat/9904383 (1999).

[138] T. Noda, H. Eisaki and S. Uchida. *Evidence for One-Dimensional Charge Transport in* $La_{2-x-y}Nd_ySr_xCuO_4$. Science **286** (1999) 265.

[139] H. Nowotny and U. Felt. *After the Breakthrough: The emergence of high-temperature superconductivity as a research field*. Cambridge University Press, 1997. ISBN 0-521-56124-8.

[140] P. Nozières and S. Schmitt-Rink. *Bose Condensation in an attractive fermion gas: From weak to strong coupling superconductivity*. Journal of Low temperature physics **59** (1985) 195.

[141] M. Ogata and H. Shiba. *Bethe-Ansatz wave function, momentum distribution, and spin correlation in the one-dimensional strongly correlated Hubbard model*. Phys. Rev. B **41** (1990) 2326.

[142] S. Ortoli and J. Klein. *De uitzonderlijke geschiedenis van de supergeleiding*. Van Gennip, Amsterdam, 1990. ISBN 90-6012-828-1. Original title and edition: Histoire et l'egendes de la supraconduction, Calmann-L'evy, Parijs 1989.

[143] O. Y. Osman. *On Stripe Correlations in Cuprate Superconductors*. Ph.D. thesis, Instituut-Lorentz, University of Leiden, P.O. Box 9506, 2300 RA Leiden, The Netherlands, Oct. 2000.

[144] J. E. Ostenson, S. Bud'ko, M. Breitwisch, D. K. Finnemore, N. Ichikawa and S. Uchida. *Flux expulsion and reversible magnetization in the stripe phase superconductor* $La_{1.45}Nd_{0.40}Sr_{0.15}CuO_4$. Phys. Rev. B **56** (1997) 2820.

[145] D. Poilblanc. *Internal structure of the singlet* $d_{x^2-y^2}$ *hole pair in an antiferromagnet*. Phys. Rev. B **49** (1994) 1477.

[146] D. Poilblanc and T. M. Rice. *Charged solitons in the Hartree-Fock approximation to the large-U Hubbard model*. Phys. Rev. B **39** (1989) 9749.

[147] D. Poilblanc, J. Riera and E. Dagotta. *d-wave bound state of holes in an antiferromagnet*. Phys. Rev. B **49** (1994) 12318.

[148] D. Poilblanc, T. Ziman, H. J. Schultz and E. Dagotto. *Dynamical properties of a single hole in an AF*. Phys. Rev. B **47** (1993) 14267.

[149] P. Prelovsek and X. Zotos. *Hole pairing and clustering in the two-dimensional t-J model*. Phys. Rev. B **47** (1993) 5984.

[150] L. P. Pryadko, S. A. Kivelson, V. J. Emery, Y. B. Bazaliy and E. A. Demler. *Topological doping and the stability of stripe phases*. Phys. Rev. B **60** (1999) 7541.

[151] P. G. Radaelli, D. G. Hinks, A. W. Mitchell, B. A. Hunter, J. L. Wagner, B. Dabrowski, K. G. Vandervoort, H. K. Viswanathan and J. D. Jorgensen. *Structural and superconducting properties of $La_{2-x}Sr_xCuO_4$ as a function of Sr content*. Phys. Rev. B **49** (1994) 4163.

[152] M. Randeria. *Precursor Pairing Correlations and Pseudogaps*. Varenna Lectures, 1997; cond-mat/9710223 (1997).

[153] V. Sachan, D. J. Buttrey, J. M. Tranquada, J. E. Lorenzo and G. Shirane. *Charge and spin ordering in $La_{2-x}Sr_xNiO_{4.00}$ with $x = 0.135$ and 0.20*. Phys. Rev. B **51** (1995) 12742.

[154] S. Sachdev. *Hole motion in a quantum Néel State*. Phys. Rev. B **39** (1989) 12232.

[155] S. Sachdev. *Quantum Phase Transitions*. Cambridge University Press, 1999. ISBN 0-521-58254-7.

[156] D. J. Scalapino. *The case for $d_{x^2-y^2}$ pairing in the cuprate superconductors*. Physics Reports **250** (1995) 329.

[157] R. T. Scalettar, E. Y. Loh, J. E. Gubernatis, A. Moreo, S. R. White, D. J. Scalapino, R. L. Sugar and E. Dagotto. *Phase diagram of the two-dimensional negative-U Hubbard model*. Phys. Rev. Lett. **62** (1989) 1407.

[158] S. Schmitt-Rink, C. M. Varma and A. E. Ruckenstein. *Pairing in two dimensions*. Phys. Rev. Lett. **63** (1989) 445.

[159] J. R. Schrieffer. *Theory of Superconductivity*. Perseus Books; Advanced Book Program, 1964. ISBN 0-7382-0120-0.

[160] J. R. Schrieffer. In F. Bassani, editor, *Proceedings of the International School of Physics Enrico Fermi LXXXIX*. Elsevier, New York, 1985.

[161] H. J. Schulz. *Domain walls in a doped AF*. J. de Physique (Paris) **50** (1989) 2833.

[162] H. J. Schulz. *Incommensurate Antiferromagnetism in the Two-Dimensional Hubbard model*. Phys. Rev. Lett. **64** (1990) 1445.

[163] G. Seibold, C. Castellani, C. Di Castro and M. Grilli. *Striped phases in the two-dimensional Hubbard model with long-range Coulomb interaction*. Phys. Rev. B **58** (1998) 13506.

[164] G. Seibold, E. Sigmund and V. Hizhnyakov. *Unrestricted slave-boson mean-field approximation for the two-dimensional Hubbard model*. Phys. Rev. B **57** (1998) 6937.

[165] T. Senthil and M. P. A. Fischer. *Z_2 gauge theory of electron fractionalization in strongly correlated systems*. Phys. Rev. B **62** (2000) 7850.

[166] Z.-X. Shen, D. S. Dessau, B. O. Wells, D. M. King, W. E. Spicer, A. J. Arko, D. Marshall, L. W. Lombardo, A. Kapitulnik, P. Dickinson, S. Doniach, J. DiCarlo, T. Loeser and C. H. Park. *Anomalously large gap anisotropy in the a-b plane of $Bi_2Sr_2CaCu_2O_{8+\delta}$*. Phys. Rev. Lett. **70** (1993) 1553.

[167] B. I. Shraiman and E. D. Siggia. *Mobile Vacancies in a Quantum Heisenberg Antiferromagnet*. Phys. Rev. Lett. **61** (1988) 467.

[168] B. I. Shraiman and E. D. Siggia. *Mean-field theory for vacancies in a quantum antiferromagnet*. Phys. Rev. B **40** (1989) 9162.

[169] P. M. Singer, A. W. Hunt, A. F. Cederström and T. Imai. *Systematic ^{63}Cu NQR studies of the stripe phase in $La_{1.6-x}Nd_{0.4}Sr_xCuO_4$ for $0.07 \leq x \leq 0.25$*. Phys. Rev. B **60** (1999) 15345.

[170] B. J. Sternlieb, J. M. Tranquada, G. Shirange, M. Sato and S. Shamoto. *Q dependence of the dynamic susceptibility $\chi''(q,\omega)$ in superconducting $YBa_2CuO_3O_{6.6}$ (T_c=46K)*. Phys. Rev. B **50** (1994) 12915.

[171] W. P. Su, J. R. Schrieffer and A. J. Heeger. *Solitons in Polyacetylene*. Phys. Rev. Lett. **42** (1979) 1698.

[172] W. P. Su, J. R. Schrieffer and A. J. Heeger. *Soliton excitations in polyacetylene*. Phys. Rev. B **22** (1980) 2099.

[173] T. Suzuki, T. Goto, K. Chiba, T. Shinoda, T. Fukase, H. Kimura, K. Yamada, M. Ohashi and Y. Yamaguchi. *Observation of modulated magnetic long-range order in $La_{1.88}Sr_{0.12}CuO_4$*. Phys. Rev. B **54** (1996) 7489.

[174] H. Takagi, T. Ido, S. Ishibashi, M. Uota, S. Uchida and Y. Tokura. *Superconductor-to-nonsuperconductor transition in $(La_{1-x}Sr_x)_2CuO_4$ as investigated by transport and magnetic measurements*. Phys. Rev. B **40** (1989) 2254.

[175] O. Tchernyshyov and L. P. Pryadko. *Holons on a meandering stripe: Quantum numbers*. Phys. Rev. B **61** (2000) 12503.

[176] T. R. Thurston, P. M. Gehring, G. Shirane, R. J. Birgeneau, M. A. Kastner, Y. Endoh, M. Matsuda, K. Yamada, H. Kojima and I. Tanaka. *Low-energy incommensurate spin excitations in superconducting $La_{1.85}Sr_{0.15}CuO_4$*. Phys. Rev. B **46** (1992) 9128.

[177] T. Timusk and B. Statt. *The pseudogap in high-temperature superconductors: an experimental overview*. Rep. Prog. Phys. **62** (1999) 61.

[178] J. M. Tranquada, J. D. Axe, N. Ichikawa, A. R. Moodenbaugh, Y. Nakamura and S. Uchida. *Coexistence of, and Competition between, Superconductivity and Charge-Stripe Order in* $La_{1.6-x}Nd_{0.4}Sr_xCuO_4$. Phys. Rev. Lett. **78** (1997) 338.

[179] J. M. Tranquada, D. J. Buttrey and V. Sachan. *Incommensurate stripe order in* $La_{2-x}Sr_xNiO_4$ *with* $x = 0.225$. Phys. Rev. B **54** (1996) 12318.

[180] J. M. Tranquada, D. J. Buttrey, V. Sachan and J. E. Lorenzo. *Simultaneous Ordering of Holes and Spins in* $La_2NiO_{4.125}$. Phys. Rev. Lett. **73** (1994) 1003.

[181] J. M. Tranquada, P. M. Gehring, G. Shirane, S. Shamoto and M. Sato. *Neutron-scattering study of the dynamical spin susceptibility in* $YBa_2Cu_3O_{6.6}$. Phys. Rev. B **46** (1992) 5561.

[182] J. M. Tranquada, J. E. Lorenzo, D. J. Buttey and V. Sachan. *Cooperative ordering of holes and spin in* $La_2NiO_{4.125}$. Phys. Rev. B **52** (1995) 3581.

[183] J. M. Tranquada, B. J. Sternlieb, J. D. Axe, Y. Nakamura and S. Uchida. *Evidence for stripe correlations of spins and holes in copper oxide superconductors*. Nature **375** (1995) 561.

[184] S. A. Trugman. *Interaction of holes in a Hubbard antiferromagnet and high-temperature superconductivity*. Phys. Rev. B **37** (1988) 1597.

[185] S. A. Trugman. *Spectral function of a hole in a Hubbard antiferromagnet*. Phys. Rev. B **41** (1990) 892.

[186] C. C. Tsuei and J. R. Kirtley. *Pairing symmetry in cuprate superconductors*. Rev. Mod. Phys. **72** (2000) 969.

[187] A. A. Tsvetkov, D. van der Marel, K. A. Moler, J. R. Kirtley, J. L. de Boer, A. Meetsma, Z. F. Ren, N. Koleshnikov, D. Dulic, A. Damascelli, M. Grüninger, J. Schützmann, J. W. van der Eb, H. S. Somal and J. H. Wang. *Global and local measures of the intrinsic Josephson coupling in* $Tl_2Ba_2CuO_6$ *as a test of the interlayer tunnelling model*. Nature **395** (1998) 360.

[188] Y. J. Uemura, G. M. Luke, B. J. Sternlieb, J. H. Brewer, J. F. Carolan, W. N. Hardy, R. Kadono, J. R. Kempton, R. F. Kiefl, S. R. Kreitzman, P. Mulhern, T. M. Riseman, D. L. Williams, B. X. Yang, S. Uchida, H. Takagi, J. Gopalakrishnan, A. W. Sleight, M. A. Subramanian, C. L. Chien, M. Z. Cieplak, G. Xiao, V. Y. Lee, B. W. Statt, C. E. Stronach, W. J. Kossler and X. H. Yu. *Universal Correlations*

between T_c and n_s/m^* in High-T_c Cuprate Superconductors. Phys. Rev. B **43** (1991) 6099.

[189] H. J. M. van Bemmel, D. F. B. ten Haaf, W. van Saarloos, J. M. J. van Leeuwen and G. An. *Fixed-Node Quantum Monte Carlo method for lattice fermions.* Phys. Rev. Lett. **72** (1994) 2442.

[190] C. N. A. van Duin. *On Quantum Magnetism in Cuprate Superconductors.* Ph.D. thesis, Instituut-Lorentz, University of Leiden, P.O. Box 9506, 2300 RA Leiden, The Netherlands, 1999.

[191] C. N. A. van Duin and J. Zaanen. *Charge- versus spin-driven stripe order: the role of transversal spin fluctuations.* Phys. Rev. Lett. **80** (1998) 1513.

[192] C. N. A. van Duin and J. Zaanen. *Interplay of superconductivity and magnetism in strong coupling.* Phys. Rev. B **61** (2000) 3676.

[193] J. M. J. van Leeuwen, M. S. L. du Croo de Jongh and P. J. H. Denteneer. *Spin stiffness in the Hubbard model.* Journal of Physics A **29** (1996) 41.

[194] C. M. Varma, P. B. Littlewood, S. Schmitt-Rink, E. Abrahams and A. E. Ruckenstein. *Phenomenology of the Normal State of Cu-O High-Temperature Superconductors.* Phys. Rev. Lett. **63** (1989) 1996.

[195] C. M. Varma, Z. Nussinov and W. van Saarloos. *Non-Fermi liquids.* Physics Reports **361** (2002) 267.

[196] A. Vigliante, M. von Zimmermann, J. R. Schneider, T. Frello, N. H. Anderson, J. Madsen, D. J. Buttrey, D. Gibbs and J. M. Tranquada. *Detection of charge scattering associated with stripe order in $La_{1.775}Sr_{0.225}NiO_4$ by hard X-ray diffraction.* Phys. Rev. B **56** (1997) 8248.

[197] K. J. von Szczepanski, P. Horsch, W. Stephan and M. Ziegler. *Single-particle excitations in quantum antiferromagnet.* Phys. Rev. B **41** (1990) 2017.

[198] M. von Zimmermann, A. Vigliante, T. Niemöller, N. Ichikawa, T. Frello, J. Madsen, P. Wochner, S. Uchida, N. H. Andersen, J. M. Tranquada, D. Gibbs and J. R. Schneider. *Hard-X-ray diffraction study of charge stripe order in $La_{1.48}Nd_{0.4}Sr_{0.12}CuO_4$.* Europhysics Letters **41** (1998) 629.

[199] S. Wakimoto, K. Yamada, S. Ueki, G. Shirane, Y. S. Lee, S. H. Lee, M. A. Kastner, K. Hirota, P. M. Gehring, Y. Endoh and R. J. Birgeneau. *Neutron Scattering Study of Elastic Magnetic Signals in Superconducting $La_{1.94}Sr_{0.06}CuO_4$.* An proceeding of ISSP7 international symposium; cond-mat/9902319 (1999).

[200] Y.-J. Wang, F. H. L. Essler, M. Fabrizio and A. A. Nersesyan. *Quantum criticality in a two-leg antiferromagnetic $S = \frac{1}{2}$ ladder induced by a staggered magnetic field*. Phys. Rev. B **66** (2002) 24412.

[201] S. R. White. *Density Matrix Formulation for Quantum Renormalization Groups*. Phys. Rev. Lett. **69** (1992) 2863.

[202] S. R. White and R. M. Noack. *Real-Space Quantum Renormalization Groups*. Phys. Rev. Lett. **68** (1992) 3487.

[203] S. R. White and D. J. Scalapino. *Density Matrix renormalization group study of the striped phase in the 2D t-J model*. Phys. Rev. Lett. **80** (1998) 1272.

[204] S. R. White and D. J. Scalapino. *Energetics of domain walls in the 2D t-J model*. Phys. Rev. Lett. **81** (1998) 3227.

[205] S. R. White and D. J. Scalapino. *Phase separation and stripe formation in the 2D t-J model: a comparison of numerical results*. Phys. Rev. B **61** (2000) 13424.

[206] P. B. Wiegmann. *Superconductivity in strongly correlated electronic systems and confinement versus deconfinement phenomenon*. Phys. Rev. Lett. **60** (1988) 821.

[207] F. Wilczek and A. Zee. *Linking number, spin and statistics of solitons*. Phys. Rev. Lett. **51** (1983) 2250.

[208] P. Wochner, J. M. Tranquada, D. J. Buttrey and V. Sachan. *Neutron-diffraction study of stripe order in $La_2NiO_{4+\delta}$ with $\delta = \frac{2}{15}$*. Phys. Rev. B **57** (1998) 1066.

[209] D. A. Wollman, D. J. van Harlingen, W. C. Lee, D. M. Ginsberg and A. J. Leggett. *Experimental determination of the Superconducting Pairing State in YBCO from the Phase Coherence of YBCO-Pb dc SQUIDs*. Phys. Rev. Lett. **71** (1993) 2134.

[210] M. K. Wu, J. R. Ashburn, C. J. Torng, P. H. Hor, R. L. Meng, L. Gao, Z. J. Huang, Y. Q. Wang and C. W. Chu. *Superconductivity at 93K in a New Mixed-Phase Y-Ba-Cu-O Compound System at Ambient Pressure*. Phys. Rev. Lett. **58** (1987) 908.

[211] Z. A. Xu, N. P. Ong, Y. Wang, T. Kakeshita and S. Uchida. *Vortex-like excitations and the onset of superconducting phase fluctuation in underdoped $La_{2-x}Sr_xCuO_4$*. Nature **406** (1200) 486.

[212] K. Yamada, C. H. Lee, K. Kurahashi, J. Wada, S. Wakimoto, S. Ueki, H. Kimura, Y. Endoh, S. Hosoya, G. Shirane, R. J. Birgeneau, M. Greven, M. A. Kastner and Y. J. Kim. *Doping dependence of the spatially modulated dynamical spin correlations and the superconducting-transition temperature in $La_{2-x}Sr_xCuO_4$*. Phys. Rev. B **57** (1998) 6165.

[213] C. N. Yang. *Some exact results for the many-body problem in one dimension with repulsive delta-function interaction.* Phys. Rev. Lett. **19** (1967) 1312.

[214] J. Zaanen. *The classical condensates: From crystals to Fermi liquids.* Lecture syllabus No 102, Instituut-Lorentz, University of Leiden, P.O. Box 9506, 2300 RA Leiden, The Netherlands, 1996.

[215] J. Zaanen and O. Gunnarsson. *Charged magnetic domain lines and the magnetism of high-T_c oxides.* Phys. Rev. B **40** (1989) 7391.

[216] J. Zaanen, M. L. Horbach and W. van Saarloos. *Charged domain-wall dynamics in doped antiferromagnets and spin fluctuations in cuprate superconductors.* Phys. Rev. B **53** (1996) 8671.

[217] J. Zaanen and P. B. Littlewood. *Freezing electronic correlations by polaronic instabilities in doped La_2NiO_4.* Phys. Rev. B **50** (1994) 7222.

[218] J. Zaanen and Z. Nussinov. *Stripes and Nodal Fermions as two sides of the same coin.* In J. Bonca, P. Prelovsek, A. Ramask and S. Sarkar, editors, *Open problems in Strongly Correlated Electron Systems, NATO series II*, volume 15, page 129. Dordrecht, 2001.

[219] J. Zaanen and A. M. Oleś. *Striped phase in the cuprates as a semiclassical phenomenon.* Ann. Physik (Leipzig) **5** (1996) 224.

[220] J. Zaanen, O. Y. Osman, H. V. Kruis, Z. Nussinov and J. Tworzydlo. *The geometric order of stripes and Luttinger Liquids.* Philosophical Magzine B **81** (2001) 1485.

[221] J. Zaanen, O. Y. Osman and W. van Saarloos. *Metallic stripes: Separation of spin, charge and string fluctuations.* Phys. Rev. B **58** (1998) R11868.

[222] J. Zaanen and W. van Saarloos. *Dynamical stripe correlations and the spin fluctuations in cuprate superconductors.* Physica C **282-287** (1997) 178.

[223] O. Zachar, S. A. Kivelson and V. J. Emery. *Landau theory of stripe phase in cuprates and nickelates.* Phys. Rev. B **57** (1998) 1422.

[224] F. C. Zhang and T. M. Rice. *Effective Hamiltonian for the superconducting Cu oxides.* Phys. Rev. B **37** (1988) 3759.

[225] N. G. Zhang and C. L. Henley. *Stripes and holes in a two-dimensional model of spinless fermions and hardcore bosons.* Phys. Rev. B **68** (2003) 014506.

[226] S.-C. Zhang. *A Unified Theory Based on SO(5) Symmetry of Superconductivity and Antiferromagnetism.* Science **275** (1997) 1089.

[227] S.-C. Zhang. *A Progress Report on the SO(5) Theory of High T_c Superconductivity.* In *Proceedings of the Grand Finale Taniguchi Symposium on The Physics and Chemistry of Transition Metal Oxides.* Springer Verlag, 1998.

[228] X. J. Zhou, P. Bogdanov, S. A. Kellar, T. Noda, H. Eisaki, S. Uchida, Z. Hussain and Z.-X. Shen. *One Dimensional Electronic Structure and Suppression of d-Wave Node State in $La_{1.28}Nd_{0.6}Sr_{0.12})CuO_4$.* Science **286** (1999) 268.

Summary

This thesis, called *"Stripes and Cuprate High-T_c Superconductors"*, is about a new theory to describe the properties of cuprate superconductors. This thesis explains what stripes are, how and why they exist and what their relationship with high temperature superconductivity in cuprate superconductors is. Stripes are related to the position of electrons in the crystal-lattice. The new cuprate superconductors are built up from atomic layers of copper and oxygen. Chapter 1 shows that this fact simplifies the problem because it makes it possible to model the system as a two-dimensional square lattice, where on every lattice point there is effectively one electron. Every electron has in addition to a negative charge also a spin. One can visualize this spin as an arrow that can point in two directions: up or down. Because of the Pauli principle, neighboring electrons want to have an opposing spin. This causes the system to become an antiferromagnet. Superconductivity only happens when more than 5% of the electrons is removed from this antiferromagnet. By removing the electrons, holes are formed. To describe the properties of the holes, the simplest assumption would be that they distribute themselves randomly over the lattice. However, because of the interaction between the electrons this is not what happens. In reality the holes concentrate themselves on one-dimensional lines, called stripes. Because these stripes have a charge, they for instance influence the lattice constants and crystal structures. They also influence de surrounding antiferromagnet by disrupting the periodicity of the antiferromagnet. Because of the changed periodicity, the peak in the Fourier-transformed spin-spin correlation function moves from (π, π) to four nearby incommensurate positions. This effect has led to the experimental discovery of stripes by John Tranquada in 1995, who measured these incommensurate peaks by using neutron-diffraction. After this initial discovery, the existence of stripes has been shown experimentally in many other ways (X-ray diffraction, muon-resonance, photo-emission experiments). Because of this, the existence of stripes is now generally accepted. The relationship with superconductivity however is still a very much discussed topic.

Since it has already been more than 15 years that high-T_c superconductors were discovered, there have been many articles and theories to describe the properties of the cuprates. To relate the new results of this thesis to previous work, relatively much attention is paid to a description of earlier work by other researchers. Chapter 1 gives an

introduction to the physical properties of cuprate superconductors, such as the antiferromagnetic properties and the phase diagram. It also shortly describes the Hubbard model and a number of theories to describe the properties of the cuprates.

Chapter 2 discusses the experimental evidence for the existence of stripes in the cuprate superconductors and in some other systems. Also, the fact that stripes are quarter-filled and the coexistence of superconductivity and stripes is discussed.

The actual theoretical work on stripes starts in chapter 3. There the mean-field or Hartree-Fock approximation of the Hubbard model is used to determine a number of properties of half-filled and quarter-filled stripes. For small values of the interaction parameter U the charge and staggered magnetization distributions are smooth curves. Although there sometimes is some doubt on the value of mean-field calculations, a comparison with variational Monte Carlo calculations shows that the qualitative features of mean-field theory are correct in this case. For large values of the interaction energy, the stripes are strongly localized. In that case, the stripes are effectively only one or two lattice constants wide. This is also a necessity, because at a doping concentration of 12.5% the stripes are only four lattice constants apart. The results of the mean-field calculation for quarter-filled stripes are almost identical to those of very time consuming calculations with the advanced DMRG method.

The numerical methods from chapter 3 are used in chapter 4 to look at kinks and fluctuating stripes. For small values of the interaction energy, the binding to the lattice can be neglected. The stripes can then be seen as freely fluctuating strings and can be described by a classical theory. For large values of the interaction the influence of the lattice is, however, very large. Stripes that are not completely straight have localized kinks. In this case a half-filled stripe can be described as a quantum mechanical lattice string. By using a mapping to a spin-1 model the different phases of this model can be investigated.

Chapter 5 takes the idea of kinks a step further by looking at kinks in quarter-filled stripes. For quarter-filled stripes there is an additional degree of freedom compared to half-filled stripes: the distribution of charge on the stripe. This can for instance be like 0.0.0.0. *etc.* (a $4k_F$ stripe) or as 00..00..00.. (a $2k_F$ stripe). Just as is the case with half-filled stripes, localized kinks are formed in this system. In this case, it is however possible to put an extra charge at the position of the kinks. In the case of a $2k_F$ stripe it can be shown that this charge has a fractional value of $\frac{1}{2}e$. The chapter makes a theoretical prediction of the relationship between the kink charge (and thus the on-stripe charge distribution) and the position of the incommensurate neutron peaks. The effect of kink-doping also explains why at a doping of more than $\frac{1}{8}$ the distance between the stripes does not decrease anymore: the minimum distance between the stripes stays at four lattice constants, without the stripe becoming charge compressible. Experimentally, around a doping of $\frac{1}{8}$ a displacement of peaks has indeed been found. The quality of the data at the moment however does not allow to determine whether the stripes have a $2k_F$

or $4k_F$ charge distribution.

The previous chapters have shown that there is a large amount of evidence that stripes do exist. To be able to investigate the relationship between superconductivity and stripes, chapter 6 focuses on the theory of superconductivity. The BCS theory has been discussed in many books and articles before. To give the reader a clear physical insight into the *"Zen"* of superconductivity, a somewhat different road is taken: an intuitive description is given why the attractive Hubbard model is superconducting. The physical reason for this is the fact that in the attractive Hubbard model the electrons want to form pairs. Because of this, the model can be mapped into a pseudo-spin model using a projective renormalization. This XY model has a phase-transition: below a critical temperature the pseudo-spins are ordered. At this ordering the angle between the pseudo-spins gets fixed. The essence of superconductivity is that the angle between the pseudo-spins is influenced by the vector potential. Therefore the phase-transformation leads to restrictions on the possible values of the vectorpotential: this is the essence of the Meissner effect and of superconductivity.

Using the same approach, the BCS model can also be mapped to a pseudo-spin representation. The solution of this pseudo-spin model using a mean-field approach leads to exactly the same results as the standard BCS approach. Thus, both in the limit of local pairs (attractive Hubbard model) and in the weakly coupled pairs limit (the BCS model) it is possible to discuss superconductivity by mapping the model to a pseudo-spin model.

This chapter also shows that in the cuprates the pairs are not weakly coupled as in the BCS model. Instead, there are strong suggestions that local pairs are already formed at very high temperature. Because of phase fluctuations the pair-formation temperature is not equal to T_c: this is called the pseudogap phenomena. However, at very short time- and space scales it has been shown that there is superconductivity even above T_c. This situation resembles strongly a number of effects of the attractive Hubbard model: local pairs, that have a finite temperature phase ordering transition, related to the XY model. However, there are also some clear differences: in the cuprates the electrons *repel* instead of attract each other. Also in the attractive Hubbard model, both electrons of a pair are localized on the same site, while in the cuprates this is impossible, because there is only a possibility for one hole per site. In practice, the pairs therefore have to be extended.

As a preparation for chapter 8, in chapter 7 a simplified description for the movement of holes in an antiferromagnet is constructed. This is a non-trivial task, because of effects such a *string states* that play a role. However, in some cases it is possible to describe the movement of a hole in an antiferromagnet as that of a particle moving in steps of two through the lattice. This is called the *sublattice parity principle*: a hole stays on its own sublattice. This can be compared to a chessboard, where a bishop always ends up on the same-colored square. With this simplification it is very well possible to describe the

lowest energy states of the dispersion relation of a single hole in an antiferromagnet.

In chapter 8, the central chapter of this thesis, the sublattice parity principle is used to look at the influence of a topological jump in the antiferromagnetic order on these holes. It is assumed that for some unknown reason the antiferromagnetic order in part of the lattice has been flipped. The boundary between two of these areas can be characterized as an empty stripe. The surprising effect is that holes prefer to stay on this boundary instead of in the antiferromagnet. In the antiferromagnet the holes have to move in steps of two. The probability amplitude for this is relatively small. However, on a stripe the hole can move from one part of the boundary to the other side. This leads to a lowering of the kinetic energy. This effect leads to a majority of the holes willing to concentrate on the boundary and thus forming a real stripe. A same kind of analysis shows that it is more favorable for holes to form pairs (a $2k_F$ stripe) than to stay apart as far as possible (a $4k_F$ stripe). This line of reasoning finally leads to a physical explanation of the DMRG results for quarter-filled stripes, as discussed in chapter 3. In this case, it is not an attractive force that brings the holes together, but more a kind of repulsion by the antiferromagnet. Kinetic energy is in this case more important than potential energy.

The last chapter finally tries, just as in chapter 6, to map the resulting theory of pairs onto an XY model of pseudo-spins. With this mapping it is possible to discuss the filling fraction of stripes: are they half-filled, quarter-filled or maybe even $\frac{1}{3}$-filled in certain cases?

Samenvatting

De vertaling van de titel van dit proefschrift naar het Nederlands luidt "*Stripes en cuprate hoge-T_c supergeleiders*". Voor veel mensen zal deze vertaling nog steeds niet echt duidelijk maken waar dit proefschrift nu precies over gaat. Daarom volgt hier een korte uitleg van deze titel. Het onderwerp van dit proefschrift is de theorie van supergeleiders. Supergeleiders zijn materialen waardoor bij lage temperaturen electrische stroom kan lopen zonder enige weerstand te ondervinden. Er zijn niet veel van dit soort materialen bekend. Heike Kamerlingh Onnes ontdekte in 1911 in Leiden het eerste voorbeeld van een supergeleider: kwik. Hij zag dat de weerstand exact nul werd bij een temperatuur van ongeveer $-270°$C. Boven deze temperatuur is er sprake van een normaal weerstandseffect. De temperatuur waarbij de sprong naar een weerstandsloze toestand optreedt wordt de kritische temperatuur of T_c genoemd. Zeer lange tijd was de hoogst bekende T_c gelijk aan ongeveer $-240°$C. Doordat deze temperatuur zo laag is, merk je in de dagelijkse praktijk vrijwel niets van het verschijnsel van supergeleiding. De meest bekende praktische toepassing van supergeleiders zijn de MRI-machines in het ziekenhuis. Hiermee worden dwarsdoorsnedes van een menselijk lichaam gemaak. Hierbij wordt gebruik gemaakt van zeer sterke magneetvelden die opgewekt worden door sterke electrische stromen die door supergeleidende draden stromen. Naast een beperkt aantal gespecialiseerde onderzoekstoepassingen, zoals zeer nauwkeurige magneetveld meters (SQUIDS), wordt supergeleiding in de praktijk verder niet toegepast. De belangrijkste reden hiervoor is dat T_c zo laag is dat het enorm veel moeite kost om de materialen af te koelen.

In 1986 ontdekten George Bednorz and Alex Müller echter een nieuw materiaal, La-Ba-Cu-O, dat supergeleidend werd bij een hogere temperatuur. Vlak hierna werd het materiaal Y-Ba-Cu-O ontdekt, dat al supergeleidend werd bij een temperatuur van ongeveer $-180°$C. Hoewel dit nog steeds zeer koud is, is het warmer dan bijvoorbeeld de temperatuur van vloeibaar stikstof. Dus door een draadje van Y-Ba-Cu-O onder te dompelen in vloeibaar stikstof is het mogelijk om supergeleiding te verkrijgen. Een visueel bewijs hiervoor kan worden geleverd door een blokje Y-Ba-Cu-O op een permanente magneet te leggen. Door het blokje af te koelen met vloeibaar stikstof, wordt het opeens magnetisch (een neveneffect van supergeleiding, dat het Meissner effect wordt

genoemd) en gaat zweven boven de permanente magneet wegens het feit dat magneten elkaar afstoten.

Na deze ontdekkingen ontstond er een ware stormloop binnen de natuurkunde om andere materialen te ontdekken die een nog hogere T_c hadden. Het grote doel hierbij was om supergeleiding bij kamertemperatuur te vinden. Dit zou het namelijk mogelijk maken om bijvoorbeeld zweeftreinen te bouwen of om energie op te slaan in grote spoelen. Hoewel er in de loop van de volgende jaren wel steeds nieuwe materialen gevonden werden, met steeds iets hogere T_c's, is de zoektocht intussen vrijwel gestaakt. Het is namelijk gebleken dat het merendeel van deze nieuwe supergeleiders bestaan uit lagen van koper (Cu) en zuurstof (O). In het Engels worden deze materialen ook wel *cuprates* genoemd. Het nadeel van dit soort materialen is dat het geen metalen zijn, maar zogenaamde keramische materialen, net zoals bijvoorbeeld porselein. En zoals bekend is porselein nogal breekbaar. Hierdoor is het niet mogelijk gebleken om eenvoudig lange kabels te maken voor electrische draden. Hierdoor zijn toepassingen op grote schaal niet mogelijk. Het bovenstaande verhaal verklaart het "*cuprate hoge-T_c supergeleiders*" gedeelte uit de titel.

Theoretische uitdaging

De uitdaging voor natuurkundigen zit hem op dit moment dus eigenlijk niet meer in het vinden van nieuwe materialen die supergeleidend zijn (alhoewel dat natuurlijk altijd mooi meegenomen is). De uitdaging zit op dit moment vooral aan de theoretische kant van het verhaal. Het heeft heel veel moeite gekost om de eerste proeven van Kamerlingh Onnes theoretisch te kunnen verklaren. Dit gebeurde pas op een afdoende manier in 1957 door John Bardeen, Leon N. Cooper en John R. Schrieffer met de naar hen genoemde BCS theorie. Deze beschrijving bevat elementen uit de Quantum Mechanica, zoals het Pauli principe en Fermi oppervlakken en gebruikt statistische mechanica van veel-deeltjes systemen en hun fase overgangen om de overgang naar de supergeleidende toestand te beschrijven. Ook de invloed van de trillingen van het kristalrooster is voor deze theorie zeer belangrijk. Nadat de BCS theorie ontwikkeld was, bleek het vrijwel alle toen bekende supergeleiders uitstekend te beschrijven. Het is om allerlei redenen (zie bijvoorbeeld hoofdstuk 6 van dit proefschrift) echter niet mogelijk gebleken om de nieuwe supergeleiders met behulp van de BCS theorie te beschrijven. Er zijn in de afgelopen jaren vele alternatieve theoriën opgesteld. Geen enkele hiervan wordt op dit moment echter algemeen geaccepteerd als *de* verklaring van hoge-T_c supergeleiding. Dit proefschrift gaat over een relatief nieuw idee om de *cuprates* te beschrijven: de *stripes*. *Stripes* zijn het hoofdonderwerk van dit proefschrift en verklaren het eerste gedeelte van de titel van dit proefschrift.

Dit proefschrift gaat dus over wat *stripes* precies zijn, hoe en waarom ze ontstaan en hun relatie met hoge temperatuur supergeleiding in de cuprate supergeleiders.

Stripes

Stripes hebben te maken met de positie van de electronen in het kristalrooster van de materialen. De nieuwe *cuprate* supergeleiders blijken uit atomaire lagen van koper en zuurstof te bestaan. Hoofdstuk 1 laat zien dat dit feit het probleem simplificeert doordat het hierdoor mogelijk is om het systeem te modelleren als een twee-dimensionaal vierkant rooster, waarbij zich op elk roosterpunt effectief een electron bevindt. Elk electron heeft naast een negatieve lading ook een *spin*. Deze *spin* kan voorgesteld worden als een pijltje dat in twee richtingen kan wijzen: omhoog of omlaag. Door een Quantum Mechanisch effect dat het Pauli principe wordt genoemd willen nabij gelegen electronen een tegengestelde *spin* hebben. Dit leidt ertoe dat het systeem een antiferromagneet vormt. Supergeleiding treedt pas op als er een percentage van 5% of meer aan electronen uit deze antiferromagneet verwijderd wordt. Door het verwijderen van electronen ontstaan er gaten in de antiferromagneet. Een beschrijving van de supergeleiding moet zich dus bezighouden met gaten in een antiferromagneet. De meest simpele aanname zou zijn dat deze gaten zich random zouden verdelen over het rooster. Door de interactie tussen de electronen is dit echter niet wat er gebeurt. In werkelijkheid gaan de gaten zich concentreren op één-dimensionale lijnen. Deze lijnen worden *stripes* genoemd. Deze *stripes* hebben een lading, waardoor ze invloed hebben op bijvoorbeeld roosterconstantes en kristalstructuren. Ook verstoren ze de periodiciteit van de antiferromagneet. Door de veranderde periodiciteit verschuift de piek in Fourier-getransformeerde *spin-spin* correlatie functie van (π,π) naar vier nabijgelegen *incommensurabele* posities. Dit effect heeft geleidt tot de experimentele ontdekking van *stripes* door John Tranquada in 1995, die deze *incommensurabele* pieken heeft gemeten met behulp van neutronen-verstrooiing. Hierna is op vele andere manieren (Röntgen-verstrooiing, muon-resonanties, photo-emissie experimenten) het bestaan van *stripes* bevestigd. Hierdoor is het bestaan van *stripes* nu algemeen geaccepteerd. De relatie met supergeleiding is echter nog zeer omstreden.

Inhoud van dit proefschrift

Aangezien het al weer meer dan 15 jaar geleden is dat de hoge temperatuur supergeleiders ontdekt zijn, zijn er al vele artikelen geschreven en theoriën bedacht om de eigenschappen van de *cuprates* te beschrijven. Om de nieuwe resultaten in dit proefschrift te relateren aan het voorgaande werk wordt relatief veel aandacht besteed aan een beschrijving van eerder werk van anderen. Hoofdstuk 1 geeft een introductie tot de fysische eigenschappen van de cuprate supergeleiders, zoals de antiferromagnetische eigenschappen en het fase diagram. Tevens wordt kort ingegaan op het Hubbard model en een aantal theoriën ter beschrijving van de eigenschappen van de *cuprates*.

In hoofdstuk 2 wordt ingegaan op het experimentele bewijs voor het bestaan van *stripes* in de cuprate supergeleiders en in sommige andere systemen. Ook wordt hier in-

gegaan op het feit dat *stripes* kwart-gevuld zijn en op de coexistentie van supergeleiding en *stripes*.

Het eigenlijke theoretische werk aan *stripes* start in hoofdstuk 3. Daar wordt de *mean-field* of Hartree-Fock benadering van het Hubbard model gebruikt om een aantal eigenschappen van half-gevulde en kwart-gevulde *stripes* te bepalen. Zo blijken voor kleine waarden van de interactie parameter U de ladingsverdeling en de *gestaggerde* magnetisatie vloeiende curves te zijn. Hoewel er wel eens getwijfeld wordt aan de waarde van *mean-field* berekeningen, laat een vergelijking met variationele Monte Carlo berekeningen zien dat de kwalitatieve resultaten van *mean-field* theorie in dit geval juist zijn. Voor grote waarden van de interactie-energie ten opzichte van de bewegingsenergie van de electronen blijkt dat de *stripes* zeer gelokaliseerd zijn. Dit is de situatie zoals die zich in de praktijk voordoet. De *stripes* zijn in dat geval effectief maar één tot twee rooster constantes breed. Dit is ook noodzakelijk, aangezien bij een doping concentratie van 12,5% de *stripes* zich maar vier rooster constantes uit elkaar bevinden. De resultaten die de *mean-field* berekeningen voor kwart-gevulde *stripes* opleveren zijn vrijwel identiek aan die van zeer langdurige berekeningen met de geavanceerde DMRG methode.

De numerieke methoden uit hoofdstuk 3 worden in hoofdstuk 4 gebruikt om te kunnen kijken naar kinks en fluctuerende *stripes*. Voor kleine waarden van de interactie energie is de binding aan het rooster vrijwel te verwaarlozen. De *stripes* kunnen dan gezien worden als vrij fluctuerende touwtjes: ze kunnen beschreven worden met een klassieke theorie. Voor grote waarden van de interactie is de invloed van het rooster echter zeer groot. *Stripes* die niet geheel rechtdoor lopen hebben hierdoor gelokaliseerde kinks. Hierdoor kan een half-gevulde *stripe* beschreven worden als een Quantum Mechanische roosterketting. Met behulp van een mapping op een *spin*-1 model kunnen de verschillende fases van dit model onderzocht worden.

Hoofdstuk 5 neemt het idee van kinks een stap verder door te kijken naar kinks in kwart-gevulde *stripes*. Voor kwart-gevulde *stripes* is er een extra vrijheidsgraad ten opzichte van halfgevulde *stripes*: de verdeling van de lading over een *stripe*. Dit kan bijvoorbeeld als 0.0.0.0. etc. (een $4k_F$ *stripe*) of als bijvoorbeeld 00..00..00.. (een $2k_F$ *stripe*). Net als bij de half-gevulde *stripes* ontstaan in dit systeem gelocaliseerde kinks. In dit geval is het echter mogelijk om extra lading te stoppen op de positie van de kink. In het geval van de $2k_F$ *stripe* wordt aangetoond dat deze lading een *fractionele* waarde van een $\frac{1}{2}e$ heeft. Het hoofdstuk doet een experimentele voorspelling over het verband tussen de kink-lading (en dus de *on-stripe* ladingsverdeling) en de positie van de *incommensurabele* neutronenpieken. Tevens verklaard dit effect van kink-doping waarom na een doping van $\frac{1}{8}$ de afstand tussen de *stripes* niet meer afneemt: de minimale afstand tussen de *stripes* blijft vier roosterconstantes, zonder dat de *stripe* ladings compressibel wordt. Experimenteel zijn er rond een doping van $\frac{1}{8}$ inderdaad een aantal van deze verplaatste pieken gevonden. De kwaliteit van de data laat echter nog niet toe om een uitspraak te doen over het feit of *stripes* een $2k_F$ of een $4k_F$ ladingsverdeling hebben.

De voorgaande hoofdstukken hebben laten zien dat er onontkoombaar bewijs is dat *stripes* bestaan. Om de eventuele relatie met supergeleiding te kunnen onderzoeken, wordt in hoofdstuk 6 ingegaan op de theorie van supergeleiding. De BCS theorie is al in vele leerboeken en dictaten uitgewerkt. Om de lezer echter een duidelijk fysisch inzicht te geven in de "*Zen*" van supergeleiding wordt niet de standaard weg bewandeld. In plaats daarvan wordt op een inzichtelijke wijze aangegeven waarom het attractieve Hubbard model supergeleidend is. De fysische reden is het feit dat in het attractieve Hubbard model de electronen paren willen vormen. Hierdoor kan het model door een projectieve renormalisatie afgebeeld worden op een *pseudo-spin* model. Dit XY model ondergaat een fase-transformatie: beneden een kritische temperatuur zijn de *pseudo-spins* geordend. Bij deze ordening komt de hoek tussen de *pseudo-spins* dus vast te liggen. De essentie van supergeleiding is nu dat de hoek tussen de *pseudo-spins* beïnvloedt wordt door de magnetische vectorpotentiaal. Hierdoor legt de fase-transformatie dus opeens voorwaarden op aan de mogelijke waarden van de vectorpotentiaal: dit is de essentie van het Meissner effect en van supergeleiding. Op eenzelfde manier is ook het BCS model voor electronen rechtstreeks om te schrijven in een *pseudo-spin* representatie. De oplossing van dit *pseudo-spin* model met behulp van een *mean-field* benadering leidt tot exact dezelfde resultaten als de standaard BCS benadering. Dus zowel in de limiet van lokale paren (attractief Hubbard model) als dat van zwak gekoppelde paren (het BCS model) is het door middel van het mappen op een *pseudo-spin* model mogelijk om supergeleiding te bespreken.

Dit hoofdstuk laat ook zien dat er bij de *cuprates* geen sprake is van zwak gekoppelde paren zoals in de BCS theorie. Er zijn juist sterke aanwijzingen dat al op zeer hoge temperatuur lokale paren worden gevormd. Vanwege fase fluctuaties is de paarvorming temperatuur echter niet gelijk aan de T_c. Dit wordt het pseudogap effect genoemd. Echter, op zeer korte tijd- en ruimte schalen blijkt er ook boven T_c sprake te kunnen zijn van supergeleiding. Deze situatie lijkt heel sterk op een aantal effecten van het attractieve Hubbard model: lokale paren, waarbij bij een eindige temperatuur fase coherentie ontstaat, gerelateerd aan het XY model. Er zijn echter ook duidelijke verschillen: in de *cuprates* is er sprake van sterke afstoting tussen de electronen, in plaats van aantrekking. Ook zijn in het attractieve Hubbard model de beide electronen van een paar gelokaliseerd op dezelfde site, terwijl dat in de *cuprates* niet mogelijk is omdat er maar één gat per site mogelijk is. Hierdoor zijn de paren in de praktijk dus *extended*.

Ter voorbereiding van hoofdstuk 8 wordt in hoofdstuk 7 geprobeerd om een eenvoudige beschrijving van de beweging van gaten in een antiferromagneet te maken. Dit is niet triviaal, aangezien er allerlei effecten zoals *string states* een rol spelen. Het blijkt echter in sommige gevallen mogelijk om de beweging van een gat in een antiferromagneet te zien als dat van een deeltje dat in stappen van twee over het rooster beweegt. Dit wordt het *sublattice parity principe* genoemd: een gat blijft op zijn eigen subrooster. Dit kan vergeleken worden met een schaakbord, waarbij een loper steeds op dezelfde

kleur uitkomt. Met deze vereenvoudiging blijkt het zeer goed mogelijk om de laagste energie toestanden uit de dispersie relatie van een gat in een antiferromagneet te kunnen beschrijven.

In hoofdstuk 8, het centrale hoofdstuk van dit proefschrift, wordt met behulp van dit *sublattice parity principe* gekeken naar wat de invloed van een topologische sprong in de antiferromagnetische orde is op deze gaten. Er wordt aangenomen dat om onbekende redenen de antiferromagnetische order in één helft van het rooster omgeslagen is. De overgang tussen twee van deze gebieden kan gekarakteriseerd worden als een lege *stripe*. Het verrassende effect is nu dat gaten zich veel liever op deze *stripe* bevinden dan in de antiferromagneet. In de antiferromagneet moeten de gaten zich voortbewegen in stappen van twee. De waarschijnlijkheid (of amplitude) hiervoor is relatief klein. Op de *stripe* kan het gat zich echter ook van de ene kant naar de andere kant van de grens bewegen. Dit leidt tot een verlaging van de kinetische energie. Dit effect leidt ertoe dat het merendeel van de gaten zich dus zal willen concentreren in het grensgebied en dus een echte *stripe* wil vormen. Eenzelfde soort analyse laat ook zien dat het vervolgens voordeliger is om paren te vormen (een $2k_F$ *stripe*) dan om de gaten zover mogelijk uit elkaar te halen (een $4k_F$ *stripe*). Deze redenatie leidt uiteindelijk tot een fysische verklaring voor het in hoofdstuk 3 besproken DMRG resultaat voor kwart-gevulde *stripes*. Het is in dit geval dus niet een aantrekkende kracht die de gaten naar elkaar toe brengt, maar juist een soort afstoting uit de antiferromagneet. Kinetische energie is in dit geval belangrijker dan potentiële energie.

Het laatste hoofdstuk probeert vervolgens om net als in hoofdstuk 6 de resulterende theorie van ruimtelijk uitgebreide paren af te beelden op een XY model. Met deze mapping is het onder andere mogelijk om de *filling fraction* van *stripes* te bepalen: zijn ze half-gevuld, kwart-gevuld of misschien zelfs $\frac{1}{3}$-gevuld in bepaalde gevallen?

Dankwoord

Het dagelijkse leven van een promovendus in de theoretische natuurkunde bestaat voor een groot deel uit het proberen te begrijpen van de grote hoeveelheid specialistische literatuur die dagelijks op *cond-mat* verschijnt. Zonder hulp van de postdocs en medepromovendi van het Instituut-Lorentz zou dit een eenzame taak zijn geweest. Over het specifieke onderwerp van *stripes* heb ik vooral van gedachten kunnen wisselen met de mensen van de "*stripe-club*" uit Leiden. Ik heb veel steun gehad aan een groot aantal discussies met Armando Gama Goicochea en Zohar Nussinov. Over *stripes* en andere onderwerpen heb ik ook vele interessante discussies gehad met Herman Kruis, Babak Hosseinkhani, Osman Y. Osman, Coen van Duin en Koert van Bemmel. Michael Patra wil ik bedanken voor zijn hulp met de vele computer en Linux gerelateerde uitdagingen. Een speciaal woord van dank voor Zohar Nussinov: zonder zijn enthousiaste aanmoedigingen zouden de laatste twee hoofdstukken van dit proefschrift misschien nooit geschreven zijn. Bij al deze werkzaamheden was Jan Zaanen een grote bron van inspiratie.

Publications

- *Shifting Bragg peaks of cuprate stripes as possible indications for fractionally charged kinks*, Marco Bosch, Wim van Saarloos, and Jan Zaanen, Physical Review B **63**, 092501 (2001). cond-mat/0003236.
- *Why Are Stripes So Narrow? Confinement of Holes and Pairing On a Stripe*, Marco Bosch and Zohar Nussinov, cond-mat/0208383. Submitted to Physical Review B.
- *Planar and Stripe Orders of Doped Mott Insulators in Dual Spin Models*, Marco Bosch and Zohar Nussinov, cond-mat/0208600. Submitted to Physical Review B.

Curriculum vitæ

Op 15 november 1972 ben ik geboren te Eindhoven. Van 1985 tot en met 1990 genoot ik voorbereidend wetenschappelijk onderwijs aan het Strabrecht college te Geldrop. In 1990 nam ik deel aan de Nederlandse Natuurkunde Olympiade. In datzelfde jaar begon ik mijn studie Technische Natuurkunde aan de Technische Universiteit Eindhoven. In juni 1991 behaalde ik de propaedeuse. Tijdens mijn studie heb ik een studentassistentschap bekleed bij de faculteit Techniek en Maatschappij. Mijn eerste stage bij de vakgroep halfgeleiderfysica behelsde de simulatie van de groei van gallium-arsenide halfgeleider kristallen tijdens de zogenaamde Molecular Beam Epitaxy techniek. Mijn tweede stage was bij de vakgroep Coöperatieve Verschijnselen en bestond uit het maken van een overzicht van theoriën ter verklaring van het Reuze Magnetoweerstands effect. Mijn afstudeeronderzoek naar de magnetische eigenschappen van kleine clusters van rhodium atomen heb ik verricht in de vakgroep Theorie van de Gecondenseerde materie onder begeleiding van dr. Peter Bobbert. In februari 1997 slaagde ik met lof voor het Ingenieursexamen.

In maart 1997 trad ik in dienst van de Stichting voor Fundamenteel Onderzoek der Materie (FOM) om als Onderzoeker In Opleiding promotieonderzoek te verrichten bij prof. dr. ir. Wim van Saarloos op het gebied van de theorie van de gecondenseerde materie. Dit werk werd verricht op het Instituut-Lorentz voor theoretische natuurkunde aan de Universiteit Leiden. De resultaten van dit onderzoek staan beschreven in dit proefschrift. Ik heb mijn onderzoeksresultaten gepresenteerd op nationale en internationale conferenties. Gedurende mijn promotie-periode heb ik verschillende congressen en scholen bezocht. Verder heb ik werkcolleges gegeven voor de vakken Statistische Fysica 2 en Quantumtheorie 1.

Sinds maart 2002 ben ik als researcher in dienst bij Corus Research, Development en Technology in IJmuiden (het voormalige Hoogovens).

Stellingen

Behorende bij het proefschrift

"STRIPES IN CUPRATE HIGH-T_c SUPERCONDUCTORS"

door Marco Bosch

1. In tegenstelling tot hetgeen Emery en Kivelson aannemen, zijn er goede argumenten om te concluderen dat *stripes* lokaal isolerend zijn en niet metallisch.

   Dit proefschrift, hoofdstuk 2.
   V. Emery, S. Kivelson en O. Zachar, Physical Review B **56** *(1997), blz 6120.*

2. De Hartree-Fock benadering van het Hubbard model geeft een goede kwalitatieve beschrijving van de fysica van kwart gevulde *stripes*.

   Dit proefschrift, hoofdstuk 3.

3. Kinks in *stripes* kunnen *fractionale lading* hebben; deze kinks leiden tot meetbare veranderingen in de Fourier getransformeerde spin-spin correlatie functie, waardoor het mogelijk is om met behulp van neutronenverstrooiing de *on-stripe* ladingsverdeling ($2k_F$ of $4k_F$) te bepalen.

   Dit proefschrift, hoofdstuk 5.

4. De vorming van paren in cuprate supergeleiders wordt niet veroorzaakt door een dynamisch mechanisme, zoals fononuitwisseling, maar is het gevolg van een verlaging van de kinetische energie.

   Dit proefschrift, hoofdstuk 8.

5. Bethe Ansatz oplossingen van het Hubbard model in éérdimensie moeten vooral gezien worden als een efficiënt numeriek algoritme om grote één-dimensionale systemen te kunnen bestuderen.

6. Lokale paren met *d-wave* symmetrie in een twee-dimensionaal Hubbard model zijn niet automatisch supergeleidend. Claims van supergeleiding in het attractieve *d-wave* Hubbard model moeten daarom met een korrel zout genomen worden zolang niet wordt uitgelegd hoe het fundamentele probleem met de commutatierelaties wordt opgelost.

   C.N.A. van Duin en J. Zaanen, Physical Review B ***61*** *(2000), blz 3676.*

7. De publikatiedruk, die versterkt wordt door een afnemend aantal permanente posities voor jonge onderzoekers, is mede verantwoordelijk voor een toename van het aantal falsificaties in artikelen, zoals bijvoorbeeld in de Schön-af faire.

8. Dat supergeleiding sociologisch gezien een speciale plek inneemt binnen de natuurkunde blijkt onder andere uit het feit dat dit jaar al voor de vijfde keer een Nobelprijs in de natuurkunde wordt toegekend aan onderzoekers die direct werkzaam zijn in dit gebied.

9. Patenten op software en business-practices belemmeren vooruitgang van software ontwikkeling en zijn daarmee een gevaar voor de economische groei.

10. Computerprogramma's worden groter, uitgebreider en duurder totdat ze voor de modale burger niet meer legaal te verkrijgen zijn.

11. Het veronderstelde gebrek aan innovatie in Nederland wordt niet veroorzaakt door kennisgebrek, maar door een gedwongen fixatie van het management op de beurskoersen, wat leidt tot korte termijn oplossingen voor fundamentelere problemen.

12. Het getuigt van een ambtelijke paradox dat enerzijds Parijse politie agenten op skates verplicht zijn om een vuurwapen te dragen, maar dat het anderzijds niet toegestaan is om dit vuurwapen te gebruiken zolang ze zich op skates bevinden.

Marco Bosch
Leiden, 10 december 2003